Thermal analysis of a ventilated facade with phase change materials (PCM)

Alvaro de Gracia Cuesta

Dipòsit Legal: L.698-2013
http://hdl.handle.net/10803/117144

PhD Thesis

Thermal analysis of a ventilated facade with phase change materials (PCM)

Author

Alvaro de Gracia Cuesta

Directors of the PhD thesis

Dr. Luisa F. Cabeza (University of Lleida, Spain)

Dr. Albert Castell (University of Lleida, Spain)

Departament d'Informàtica i Enginyeria Industrial

Escola Politècnica Superior

Universitat de Lleida

Thermal analysis of a ventilated facade with phase change materials (PCM)

Memòria presentada per optar al grau de Doctor per la Universitat de Lleida redactada segons els criteris establerts en l'Acord núm. 19/2002 de la Junta de Govern del 26 de febrer de 2002 per la presentació de la tesis doctoral en format d'articles.

Programa de doctorat: Enginyeria i Tecnologies de la Informació
Directors de la Tesis: Dra. Luisa F. Cabeza i Dr. Albert Castell

La Dra. Luisa F. Cabeza, Catedràtica de l'Escola Politècnica Superior de la Universitat de Lleida i el Dr. Albert Castell, professor agregat de l'Escola Politècnica Superior de la Universitat de Lleida.

CERTIFIQUEN:

Que la memòria "Thermal analysis of a ventilated facade with phase change material (PCM)" presentada per Alvaro de Gracia Cuesta per optar al grau de Doctor s'ha realitzat sota la seva supervisió.

Lleida, 4 de març de 2013

Acknowledgements

I would like to thank Dr. Luisa F. Cabeza and Dr. Albert Castell not only for the opportunity they gave me four years ago, but also for the support, dedication, tools and knowledge that I received throughout the whole path.

I would like to thank the national projects with reference ENE2008-06687-C02-01/CON, ENE2011-28269-C03-01, ULLE10-4E-1305, to the project “MECLIDE-Soluciones estructurales con materiales especiales para la climatización de edificios”, to COST Action TU0802 for the funding during these years, to the Catalan Government 2009 SGR 534, and to the City hall of Puigverd de Lleida.

A sincere thanks to my colleagues in GREA to help and guide me when the road became winding. Especially to those with whom I shared motivation, codes and trips to Puigverd.

I would like to thank Dr. Mohammed M. Farid for his influence and his wise guidance at the beginning of my research career.

How can I not mention the brothers I grew up with? Now we drink good Dry Gin together while we remember that the bird is the word.

And finally, last but not least, I would like to thank my parents and Maria, for their patience, understanding, continuous lessons and love.

Resum

L'alt consum energètic en el sector de l'edificació, especialment en l'àmbit de calefacció i refrigeració ha promogut noves i més restrictives polítiques energètiques arreu del món, tals com la nova directiva europea 2010/31/EU sobre el consum energètic dels edificis. La millora i estudi de nous tipus de tancaments dels edificis presenta un alt potencial per reduir la demanda de calefacció i refrigeració.

L'ús de façanes ventilades s'està estenent en els últims anys en el sector de l'edificació. Aquests sistemes constructius es basen en un tipus especial de tancament, on una segona pell (transparent o opaca) s'instal·la davant de la façana habitual de l'edifici. L'espai d'aire entremig, anomenat canal, pot ser ventilat mecànica o naturalment. Aquests tipus de façanes, si estan ben dissenyades, poden reduir el consum energètic anual de l'edifici absorbint radiació solar durant els períodes de calefacció i evitant el sobreescalfament durant l'estiu. A més, aquests sistemes poden ser implementats no solament en obra nova, sino que la seva naturalesa els fa òptims per a rehabilitació d'edificis ja existents.

L'objectiu d'aquesta tesis és el d'analitzar el comportament tèrmic d'una façana ventilada amb material de canvi de fase macro encapsulat en el seu canal d'aire. L'ús de materials de canvi de fase incrementa la capacitat d'emmagatzematge d'energia tèrmica en la solució constructiva proposada, i intensifica l'emmagatzematge i l'operació de la façana ventilada en un rang de temperatures desitjat.

El rendiment energètic d'aquest nou tipus de façana ventilada s'estudia de forma experimental per veure el seu potencial en reduir els consums energètics tant de calefacció com de refrigeració. Posteriorment, s'estudia mitjançant l'anàlisi de cicle de vida, quin és l'impacte mediambiental que suposa la manufactura i operació d'aquest sistema. Finalment, es desenvolupa un model numèric per optimitzar el funcionament i disseny d'aquesta façana. Aquest model numèric utilitza una nova correlació empírica del nombre de Nusselt per al càlcul dels coeficients de transferència de calor entre el material de canvi de fase i el flux d'aire circulant pel canal.

Resumen

El alto consumo energético en el sector de la edificación, especialmente en el ámbito de calefacción y refrigeración ha promovido nuevas y más restrictivas políticas energéticas en todo el mundo, tales como la nueva directiva europea 2010/31/EU sobre el consumo energético de edificios. La mejora y estudio de nuevos tipos de envolventes de edificios presenta un alto potencial en reducir la demanda de calefacción y refrigeración.

El uso de fachadas ventiladas se está extendiendo en los últimos años en el sector de la edificación. Estos sistemas constructivos se basan en un tipo especial de envolvente, donde una segunda piel (transparente u opaca) se instala frente a la fachada habitual del edificio. El espacio de aire intermedio, llamado canal, puede ser ventilado mecánica o naturalmente. Estos tipos de fachadas, si están bien diseñadas, pueden reducir el consumo energético anual del edificio absorbiendo radiación solar durante los períodos de calefacción y evitando el sobrecalentamiento durante el verano. Además, estos sistemas pueden ser implementados no sólo en obra nueva, sino que su naturaleza los hace óptimos para rehabilitación de edificios ya existentes.

El objetivo de esta tesis es el de analizar el comportamiento térmico de una fachada ventilada con material de cambio de fase macro encapsulado en su canal de aire. El uso de materiales de cambio de fase aumenta la capacidad de almacenamiento de energía térmica en la solución constructiva propuesta, e intensifica el almacenamiento y la operación de la fachada ventilada en un rango de temperaturas deseado.

El rendimiento energético de este nuevo tipo de fachada ventilada se estudia experimentalmente para ver su potencial en reducir los consumos energéticos tanto de calefacción como de refrigeración. Posteriormente, se estudia mediante el análisis de ciclo de vida, el impacto medioambiental que supone la manufactura y operación de este sistema. Finalmente, se desarrolla un modelo numérico que optimiza el funcionamiento y diseño de esta fachada. Este modelo numérico utiliza una nueva correlación empírica del número de Nusselt para el cálculo de los coeficientes de transferencia de calor entre el material de cambio de fase y el flujo de aire circulando por el canal.

Summary

The high energy consumption in the building sector, especially for heating and cooling, has promoted new and more restrictive energetic policies around the world, such as the new European directive 2010/31/EU on the energy consumption of buildings. The improvement and study of new types of building envelopes has a high potential to reduce the energy demand for both heating and cooling.

The use of ventilated facades has recently become more popular in the building sector. These constructive systems are based on a special type of envelope, where a second skin (transparent or opaque) is installed in front of the regular building facade. The intermediate air space, called channel, can be mechanically or naturally ventilated. These types of facades, if well designed, can reduce the overall energy consumption of the building by absorbing solar radiation during heating periods and can avoid overheating in summer. In addition, these systems can be implemented not only in new buildings, but their nature makes them optimal for refurbishing of existing buildings, as well.

The objective of this thesis is to analyse the thermal behaviour of a ventilated facade with macro-encapsulated phase change material in its air channel. The use of phase change materials increases the ability of thermal energy storage in the proposed constructive system, and enhances the storage and operation of the ventilated facade in a desired temperature range.

The energy efficiency of this new type of ventilated facade is experimentally studied to determine its potential in reducing the energy consumption both for heating and cooling. Hereafter, the environmental impact of the manufacture and operation of this system is studied by a life cycle analysis. Finally, a numerical model is developed to optimize the operation and design of this facade. This numerical model uses a new empirical correlation for the Nusselt number to calculate the convective heat transfer coefficients between the phase change material and the air flow circulating in the chamber.

Nomenclature

CFD	Computational fluid dynamics
HVAC	Heating Ventilation and Air Conditioning
LCA	Life cycle assessment
PCM	Phase change materials
TES	Thermal energy storage
VDSF	Ventilated double skin facade

Contents

List of Figures

1 Introduction

1.1 Energy consumption in the building sector

The building sector, including both the residential and services sub-sectors, consumes approximately 32% of global final energy use, making it responsible for almost 15% of total direct energy-related CO_2 emissions from final energy consumers. According to the ETP 2012 [1], these emissions must be reduced over 60% by 2050.

The total energy consumed in the building sector reached 115 exajoules (EJ) in 2009. The source of around 60% of this energy was renewable and electricity, as shown in Figure 1. Moreover, this total energy consumption has been growing 1.8% per year since 1971. As shown in Figure 2, the residential sector accounts for 75% of these consumptions and has experimented a continuous and substantial increment.

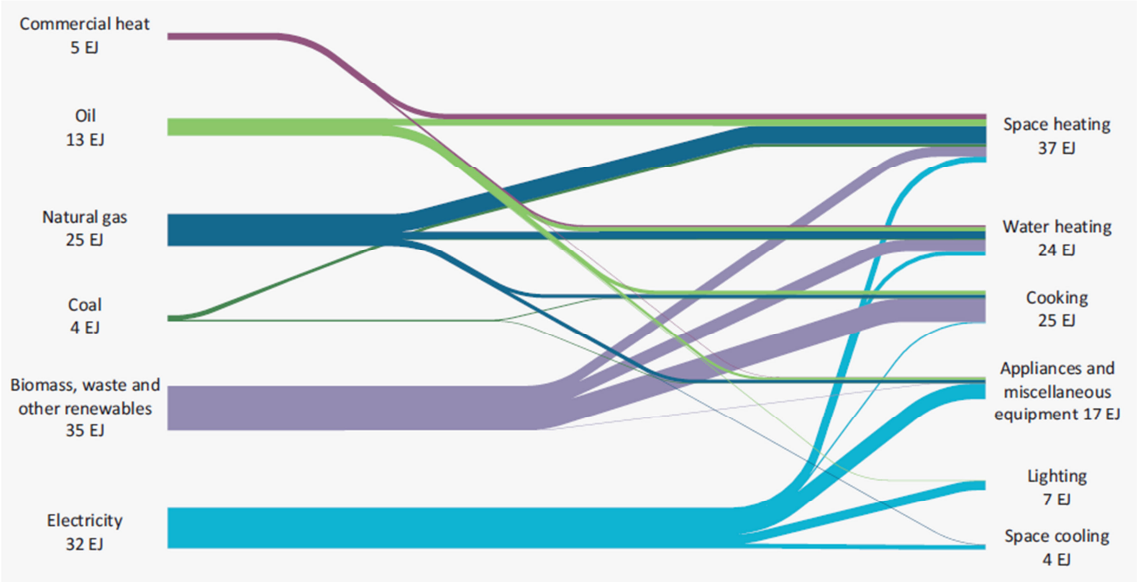

Figure 1. Energy consumption flow in the building sector, 2009 [1].

Apart from enforce stringent building codes that include minimum energy consumption for new and refurbished buildings, the ETP 2012 highlights the necessity of using highly-efficient technologies in the envelopes, equipment and new strategies to address the high energy consumption of the sector. Moreover, policies are required to promote the research and development of these highly-efficient technologies.

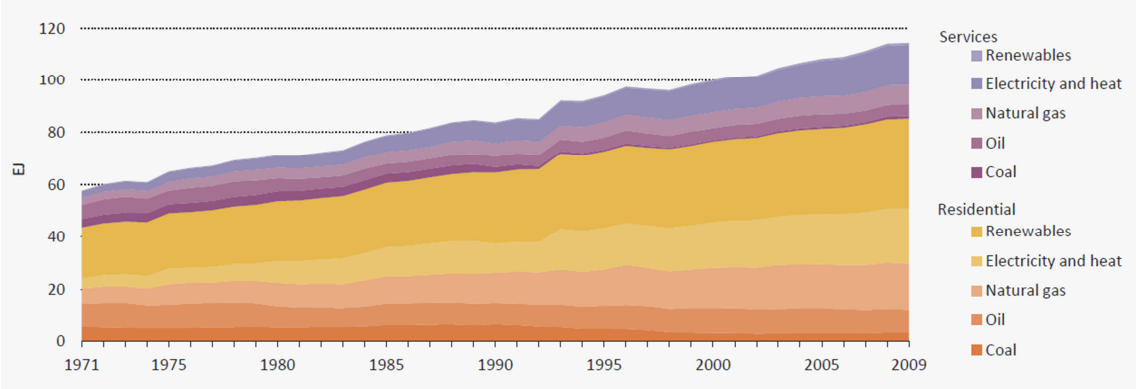

Figure 2. World buildings energy consumption by energy source [1].

The improvements in buildings envelopes have high potential in energy demand reduction and consequently in energy savings [2]. Within this context, the use of ventilated double skin facades (VDSF) in the building sector has recently become more popular.

1.2 Ventilated double skin facades

VDSF are becoming an important and widely used architectural element in office buildings, as they can contribute to numerous advantages apart from their good aesthetics [3]. These systems can provide ventilation to the building under different modes depending on the energetic requirements and weather conditions (Figure 3). Moreover, the use of VDSF can improve the acoustic characteristics and day lighting inside the building, as well as provide greater thermal insulation due to the outer skin both in winter and summer [4].

The VDSF are based on a special type of envelope, where a second skin, usually a transparent glazing, is placed in front of a regular building facade. The air space in between (the channel) can be mechanically or naturally ventilated to improve the thermal performance of the building [5]. Those facades, if well designed, can efficiently reduce the overall HVAC consumption in buildings by using part of the solar radiation during winter, and preventing overheating during warm periods [4].

On the other hand, Poirazis [6] stated that the main disadvantages of these systems are their higher construction costs, the additional maintenance and operational costs, fire protection problems and possible overheating if not properly designed.

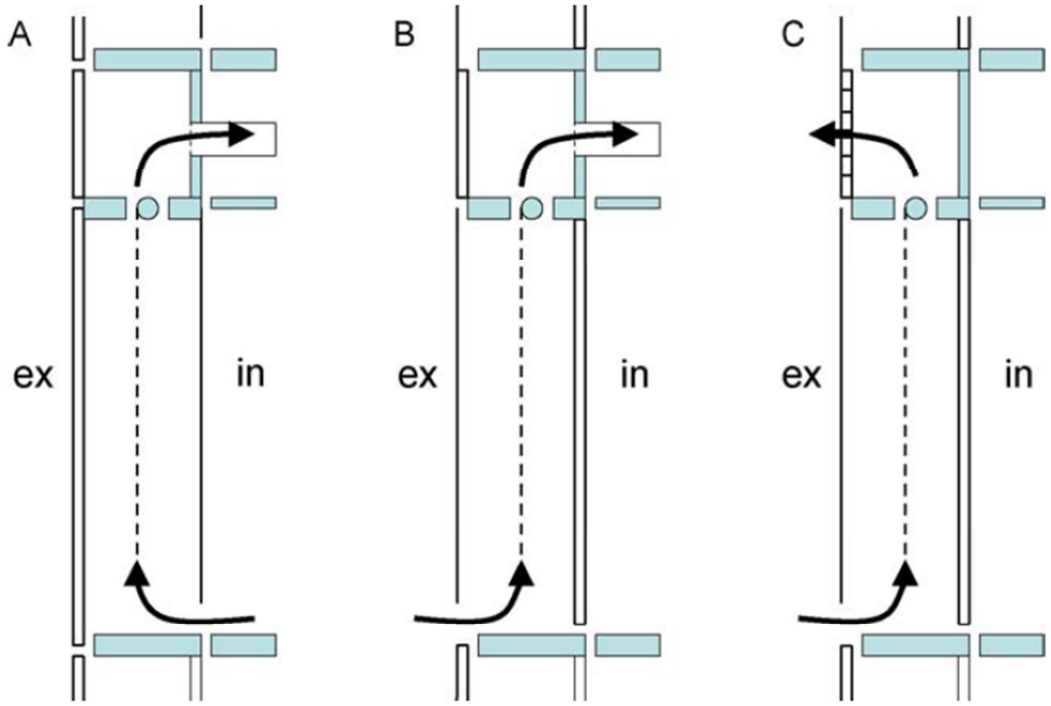

Figure 3. Schematic representation of the working modes for ventilated double-skin facades [7].

According to Ruiz-Pardo [8] the operating principle and design of double skin envelopes can be classified depending on the morphology of the outer and inner skin:

- Glazed outer skin / opaque inner skin: These systems are used when the heating demand is dominant due to climate and operative conditions. The well-known Trombe wall belongs to this category. It takes benefits from the solar radiation by heating up the air from the inner environment usually with natural ventilation. Solar walls also present this morphology, however, no recirculation of air is produced in them.
- Glazed outer skin / Glazed inner skin: This combination is used when a glazes aspect of the facade is required. Even though the building can present important heating loads, the cooling loads are usually higher. The outer skin is made by a clear glass, while a double or absorbent glass is used in the inner skin. The use

of venetian blinds or shading devices is advised in order to adapt the heating, cooling and day lighting requirements (Figure 4).

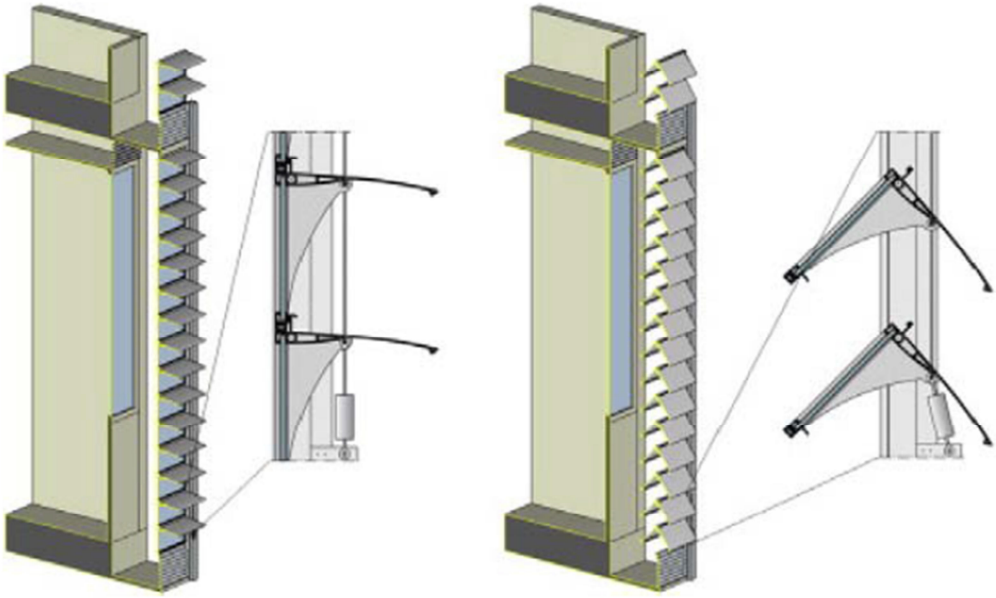

Figure 4. Integrated movable shading system in winter and summer configurations [9].

- Opaque outer skin / Opaque inner skin: These systems can be divided into sealed cavity and open-joint ventilated facades. The ventilation is produced with upper and lower openings in the sealed cavity or through the open-joints. Several operative options can be found within this morphology, such as the use of PV panels in the outer skin [10] (Figure 5).

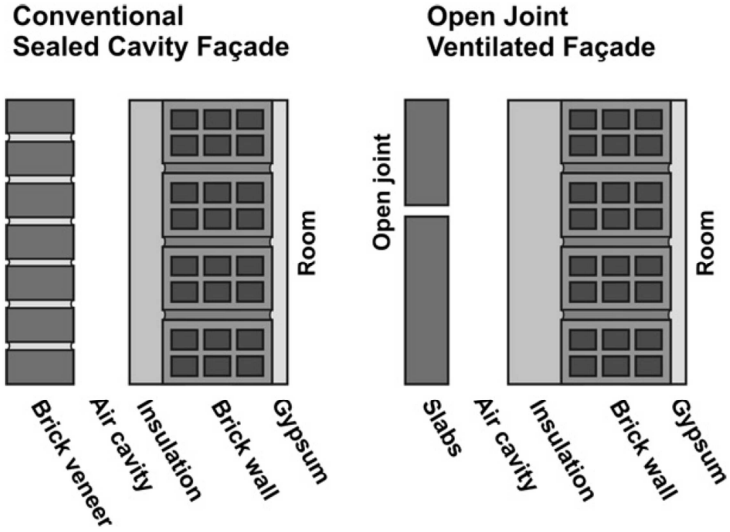

Figure 5. Cross section of a sealed cavity and an open-joint ventilated facade [11].

The geometrical partition of the air cavity can define the thermal performance and operational mode of the VDSF. Depending on the facade configuration [12], the VDSF can be classified as:

- Buffer: In this configuration the air within the cavity acts as a thermal buffer. The cavity is connected to the outdoor air for pressure balance purposes.
- Box-window (Figure 6a): The facade is divided both vertically and horizontally, forming a box. The air is entering from outdoors at every storey level and is released in the same corridor or in a contiguous one.
- Shaft-box (Figure 6b): This configuration is similar to the box-window, except that the shaft-box might discharge exhaust air through a lateral building-height opening as well as to the front openings.
- Corridor (Figure 6c): The VDSF is horizontally divided, forming a storey level corridor. Inlet and outlet openings are placed in such a way that the mixing of exhaust air and supply air to the above storey is avoided.
- Multi-storey (Figure 6d): This system has no cavity partitions. Louvered facades are a particular case of multi-storey facades, in which the external skin is composed of louvers that can be moved from a closed to an open position. In the open position, they no longer act as a second skin.

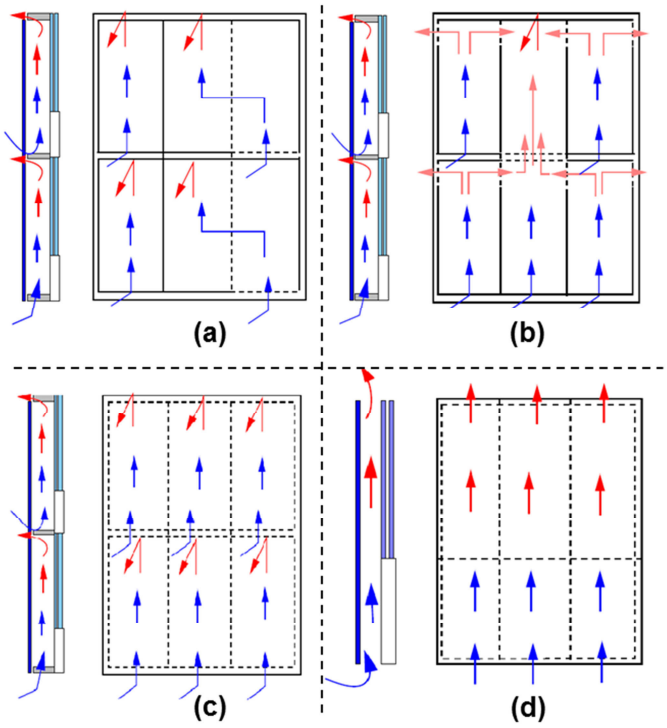

Figure 6. Schematic working conditions of the different VDSF configuration [13].

1.3 Thermal energy storage

It is well known that the use of adequate thermal energy storage (TES) systems in the building and industrial sector presents high potential in energy conservation [14,15]. The use of TES can overcome the lack of coincidence between the energy supply and its demand; its application in active and passive systems allows the use of waste energy, peak load shifting strategies, and rational use of thermal energy.

Passive TES systems can enhance effectively the naturally available heat energy sources in order to maintain the comfort conditions in buildings and minimize the use of mechanically assisted heating or cooling systems [16]. These systems include increased use of ventilated facades [17], thermal mass [18,19], shading effect using blinds [20], coated glazing elements [21], and solar heating and free cooling (night ventilation) techniques [22].

On the other hand, the use of active TES systems provides a high degree of control of the indoor conditions and improves the way of storing heat energy. These systems are usually integrated in buildings to shift the thermal load from on-peak to off-peak

conditions in several applications, such as domestic hot water applications [23] or HVAC systems [24,25].

High energy storage density and high power capacity for charging and discharging are desirable properties of any storage system. It is well known that there are three methods of TES: sensible, latent and thermochemical energy storage.

1.3.1 Sensible energy storage

Sensible heat storage materials are defined as a group of materials that undergo no phase change in the temperature range of the storage process. The ability to store sensible heat for a given material strongly depends on the value of its energy density, that is the heat capacity per unit volume or $\rho \cdot C_P$. For a material to be useful in a TES application, it must be inexpensive and have good thermal conductivity [26]. The sensible energy stored in any material can be calculated using the following equation:

$$Q_{sensible} = \int_{T_1}^{T_2} C_p \cdot dT$$

where $Q_{sensible}$ is the sensible energy stored per mass unit, C_p is the specific heat of the material, and dT is the temperature change. The temperature change ($\Delta T=T_2-T_1$) depends on the application and is limited by the heat source and by the storage system.

1.3.2 Latent energy storage

The latent energy is the energy needed for the phase change of a material and presents higher energy density than sensible energy. Three different phase changes are possible: solid-solid, solid-liquid, and liquid-gas. The phase change liquid-gas is the one with higher energy density. However, serious problems in pressure control are found due to the volume expansion of the process [27]. Solid-solid phase change presents low energy density, hence the phase change between solid-liquid is presented as the most suitable due to the high energy density and the lack of problems related to volume expansions.

The energy density is drastically increased when phase change materials (PCM) are used. Having a phase change within the temperature range of the storage ($\Delta T=T_2-T_1$) the stored energy in a PCM can be calculated as follows:

$$Q_{latent} = \int_{T_1}^{T_{pc}} C_{p,s} \cdot dT + \Delta H_{pc} + \int_{T_{pc}}^{T_2} C_{p,l} \cdot dT$$

where Q_{latent} is the sensible and latent energy stored and ΔH_{PC} is the heat of fusion at the phase change temperature T_{PC}.

The use of latent energy storage systems in buildings has been a topic of great interest in the literature [28,29] both in active and passive systems.

The use of PCM in the envelopes smoothes the daily temperature fluctuations and can absorb solar radiation and internal thermal loads [30]. Within this context, Xu et al. [31] implemented PCM in the floor in order to absorb the solar radiation energy in the daytime and release the heat at night in winter. Moreover, Castell et al. [18] registered experimentally important electrical energy savings during the cooling season due to the use of macro-encapsulated PCM in the building envelope. Furthermore, the use of PCM has been also used to enhance the cooling loads of a building by using cold storage from the night. The free-cooling system (Figure 7) solidifies the PCM during the night time, when lower temperatures are available, and uses this cold stored to cool down the inlet air to the building.

These systems are usually based on PCM-air heat exchangers. The use of PCM is suitable because of small temperature difference between day indoors and night outdoors. Zalba et al. [32] conducted a viability analysis of a real installation (Figure 8 [33]), which demonstrated that this type of system is not only technically feasible, but also economically advantageous in comparison to existing cooling systems, as well. Furthermore, Vakilaltojjar and Saman [34] developed three computer models to optimize the design of these PCM-air heat exchangers. They conclude that the better performance can be obtained by using small air gaps and thin PCM slabs, even though

this increases the number of PCM containers, which might lead to higher pressure drop across the storage system. Similarly, Hed and Bellander [35] studied numerically the thermal performance of a PCM air heat exchanger and pointed out how the shape of the heat capacity vs. temperature function affects the cooling power of the system.

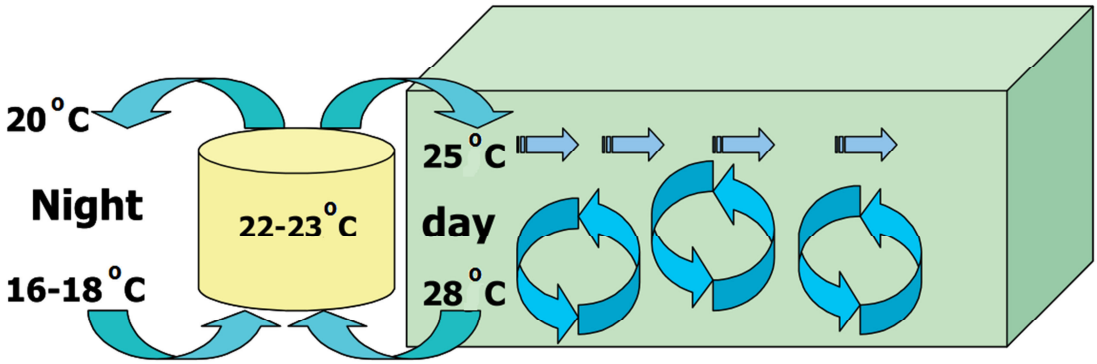

Figure 7. Concept of free-cooling [32].

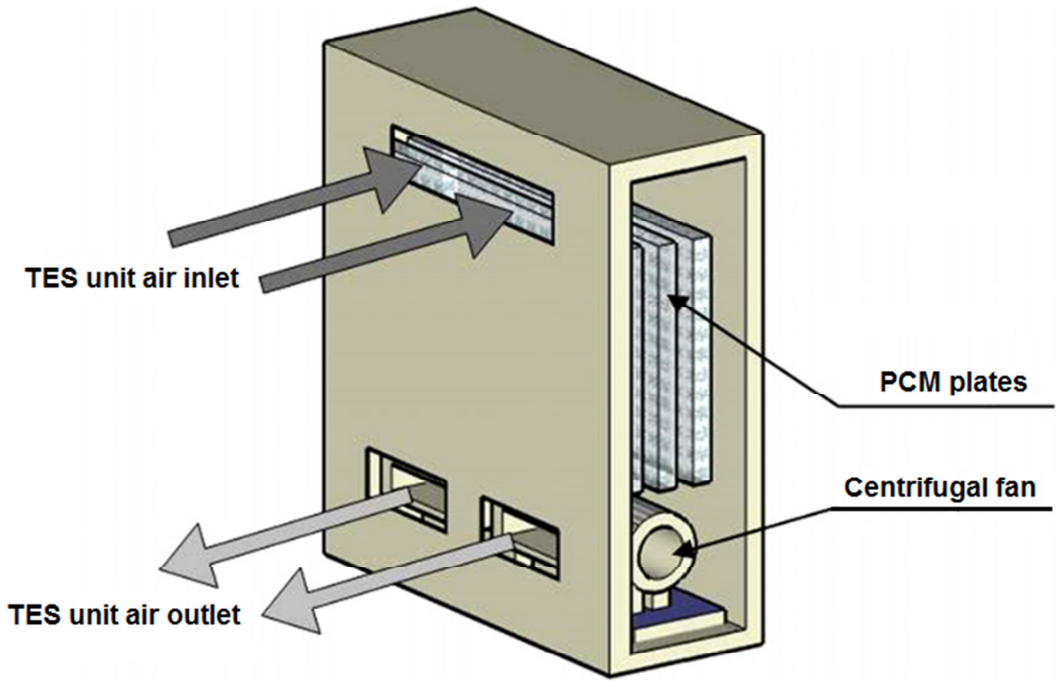

Figure 8. Air flow through the storage unit [33].

On the other hand, latent energy storage system can be implemented as a part of the building both for cooling or heating purposes. Stirith and Butala [36] studied experimentally and numerically the ceiling and floor free-cooling systems (Figure 9). The results showed a reduction of the peak temperatures leading to smaller room temperature fluctuations and a reduction of the cooling demand. The air temperatures, heat fluxes and heat as a function of time were given for different air velocities and inlet temperatures [37]. Saman et al. [38] implemented latent energy storage into a roof integrated solar heating system. They used several layers of PCM slabs with a melting temperature of 29 ºC. The stored heat is utilised to heat ambient air before being admitted to a living space. The possibility of integrating storage intro buildings should be simplified by using prefabricated assemblies or module-type constructions [39].

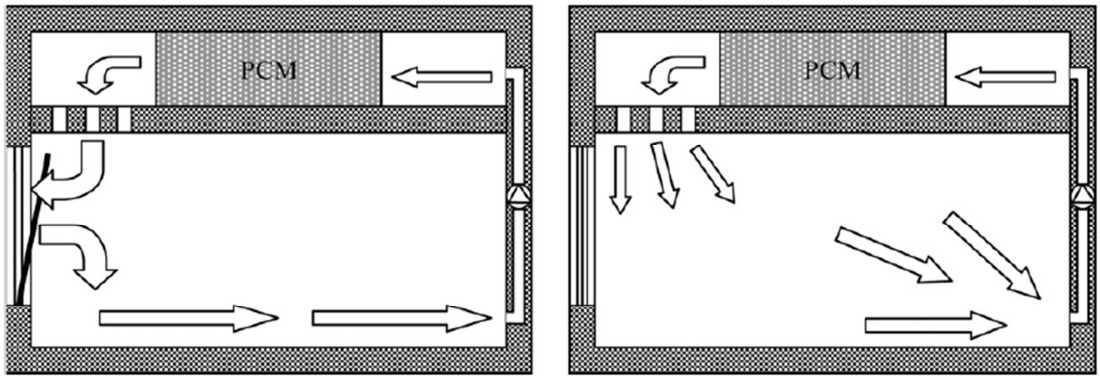

Figure 9. Principal function of PCM "free-cooling system": (left) cooling of PCM at night, (right) cooling of building during the day [37].

Moreover, Cabeza et al. [40] have reviewed the different materials used as PCM for thermal energy storage application in the building sector. Furthermore, Zalba et al. [41] stated that PCM must have high latent heat and high thermal conductivity. They should have a melting/freezing temperature lying in the practical range of operation, melt/freeze congruently within minimum subcooling and be chemically stable, low in cost, nontoxic and non-corrosive.

Abhat [42] classified the substances used for thermal energy storage (Figure 10).

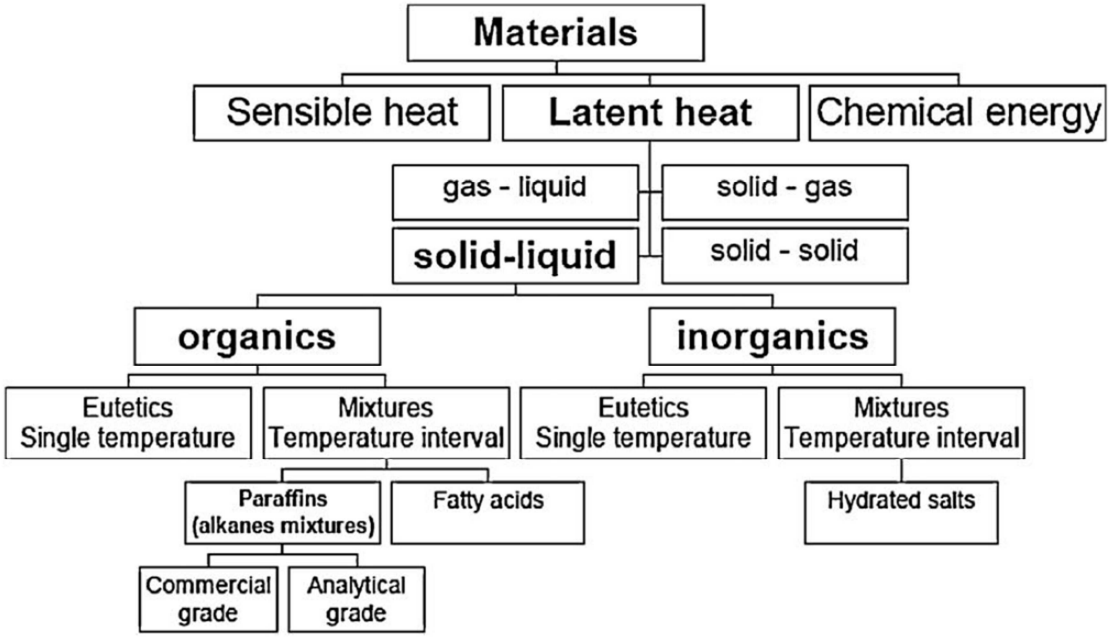

Figure 10. Families of phase change heat storage materials [42].

Salt hydrates are suitable for their application in the building sector for their low cost, availability, and lack of fire risk hazards. However, some problems such as subcooling, segregation and hysteresis can modify their thermal performance. On the other hand, although organic substances present a more stable thermal behaviour, their high cost and fire hazards limits their application in buildings [43].

1.3.3 Thermochemical energy reactions

From all the thermal energy storage processes, chemical sorption and chemical reactions based on solid-gas systems show the highest potential for energy savings and CO_2 mitigation [44]. The heat is not stored directly as sensible or latent heat but by a reversible chemical process or reaction, as follows:

$$A + HEAT \leftrightarrow B + C$$

First, in the charging period, heat is absorbed to transform the chemical A into two new chemicals, B and C. Hereafter, the two new chemicals must be stored in separate vessels at ambient temperature. Whenever the heat is required, chemical B reacts with chemical C to form the original chemical A and the stored heat is released.

The research for short or long term thermal storage using this technology is in the early stage, only few experimental have been carried out for short discharging periods.

1.4 Use of PCM in ventilated facades

In this PhD, the use of PCM is combined with the VDSF constructive system. The combination of these two technologies has been briefly addressed in the literature.

Bourdeau [45] has implemented PCM (calcium chloride hexahydrate with a melting point of 29 ºC) in Trombe walls and found out that an 8 cm PCM wall has slightly better performance than a 40 cm thick masonry wall. Ghoneim et al. [46] also investigated the reliability of PCM as a Trombe wall. They used sodium sulphate decahydrate as phase change material in a South facing Trombe wall. The conclusions were also that PCM wall with smaller thickness were more desirable than traditional masonry for providing efficient thermal energy storage. Using a similar configuration, Stritih and Novak [47] tested numerically the operation of the wall during the heating season. The high efficiency of converting solar energy into latent heat (79 %) was remarked. The numerical analysis for the heating season gave an optimum melting point a few degrees above room temperature. In addition, Eiamworawutthikul et al. [48] presented the results of simple simulations of a Trombe wall improved with the incorporation of PCM. The calculations were carried out using typical winter climate data from the Raleigh-Durham location in North Carolina. Three types of wall were evaluated. Two normal concrete walls, one having a thickness of 30 cm and the other of 10 cm, and the other one having 20 % by weight of paraffin homogeneously mixed with the concrete wall material. The configuration of the test model is shown in Figure 11. The results showed that the thermal energy storage capacity of the PCM wall is much better than the concrete wall having the same thickness, and it is slightly better than the thick concrete wall.

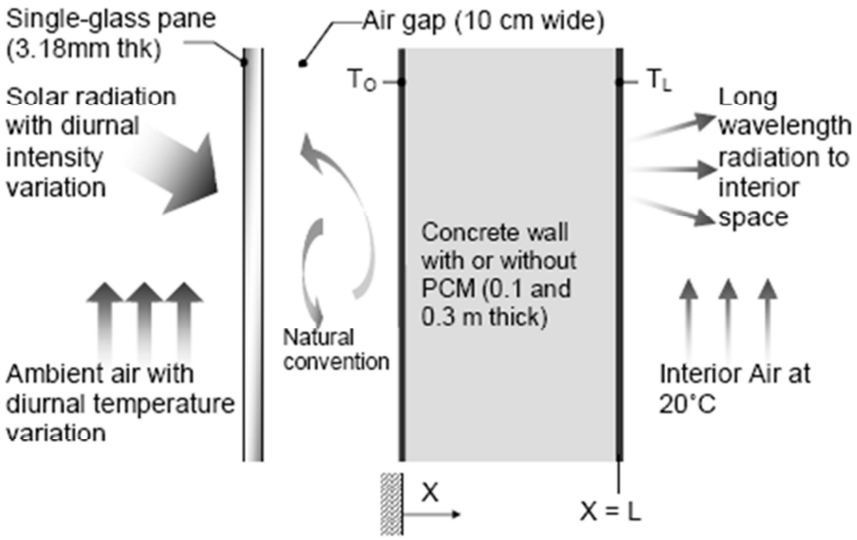

Figure 11. Configuration of a Trombe wall with PCM [48].

Moreover, Costa el al. [49] developed eight prototypes to evaluate experimentally the thermal performance of VDSF in different European climates (Southern, Central and Northern climates). In one prototype (M3) a PCM layer was included in the inner skin; however, due to the small amount of PCM (4 cm), no significant improvements were found due to its use (Figure 12).

In addition, the use of PCM and transparent insulation materials (TIM) in VDSF systems has been numerically studied by Heim [50] (Figure 13). The modelling and simulations were carried out using ESP-r. This was adapted to describe the physical elements of the PCM model using ESP-r zones and network elements, and the effective heat capacity method to describe the phase change phenomena. The results showed that the effect of the PCM reduces the temperature fluctuations during winter time (December and January). Furthermore, in spring and autumn the influence of PCM on the thermal behaviour of the wall is noticeable.

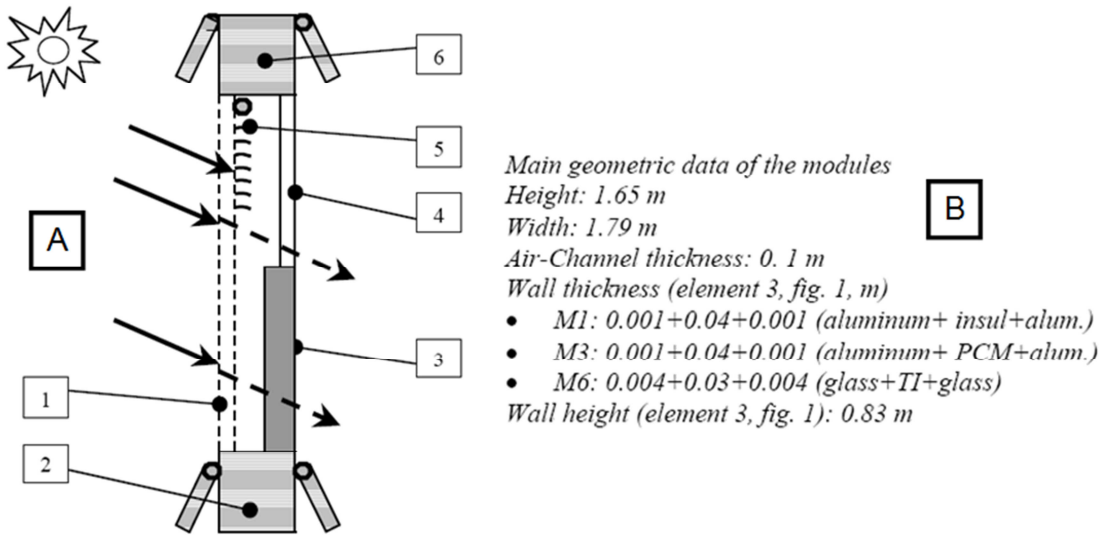

Figure 12. (A) South prototypes sketch. 1 outdoor glass, 2 lower damper box & ventilators, 3 indoor wall, 4 double indoor glass, 5 blind, 6 upper damper box. (B) Main geometric data of the modules (M1, M3 and M6), [49].

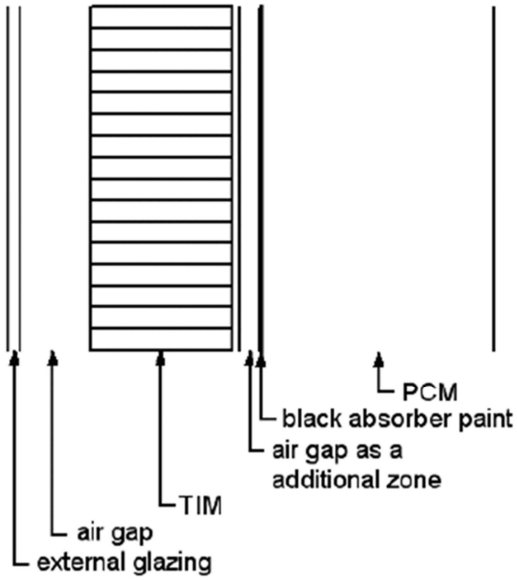

Figure 13. Cross section of a VDSF with TIM-PCM wall [50].

Even though the studies regarding the use of PCM in VDSF are very limited and focused mainly on passive solar techniques (use of PCM to replace the masonry in a Trombe wall), they demonstrated the potential of these special envelopes to enhance the thermal efficiency of the buildings. In this PhD the use of PCM in the VDSF system is not only focused in absorbing the solar radiation and use it for heating purposes during the winter season, but to use the PCM as a cold storage system during the summer

season and hence reduce the HVAC energy consumption, as well. An innovative and versatile VDSF with macro-encapsulated PCM in its air chamber is designed and presented as a suitable tool to reduce both heating and cooling demands making an intensive use of the PCM.

2 Objectives

The main objective of this PhD thesis is to analyse the thermal performance of an active ventilated facade with macro-encapsulated PCM in its air chamber and to study its potential in reducing both heating and cooling energetic consumption. To accomplish the aforementioned objective, several specific objectives were specified:

- To study experimentally the energetic performance of the new facade and to determine its potential in reducing the heating demand during winter period.

- To study experimentally the potential of the ventilated facade with PCM in its air chamber to be used as a cold storage system during the summer period and hence reduce the cooling loads.

- To evaluate the environmental impact due to the manufacturing and operation of this new ventilated facade through its whole life cycle.

- To review and compare the different numerical methods which are available in the literature to study numerically the thermal performance of a ventilated double skin facade.

- To develop an empirical correlation to determine the convective heat transfer coefficient between a PCM flat plate and an air flow.

- To optimize, using numerical tools, the operational schedule and design of the ventilated facade when used for cooling purposes.

3 PhD thesis structure

The PhD thesis is based on six papers; three of them have been already published in SCI journals while the other three have been submitted.

The first step which has been done in order to study the new ventilated facade with PCM, was its design and construction in an experimental set-up, which enables to test experimentally the thermal performance of this new system under winter and summer Mediterranean climate conditions.

During the heating season, the ventilated facade could absorb and use an important amount of the incident solar radiation and registered important net energy savings. On the other hand, according to the experimental results during the summer season, no net electrical energy savings were achieved due to an excessive use of the fans during the solidification process.

The energetic results from the winter and summer experimental campaign were used to evaluate the environmental impact of the ventilated facade with PCM. A life cycle assessment based on the Eco-Indicator99 methodology is used to determine the environmental payback of this system.

As it was previously said, no net energy savings were registered during the summer period, hence, numerical tools were required to optimize the design of the system and minimize the use of fans for cooling purposes.

This requirement leaded the PhD candidate to study, review and compare which methods have been used in the literature to study numerically the performance of ventilated double skin facades.

Moreover, it was noticed that the convective heat transfer coefficient between the PCM panels and the air flow was critical to determine the capacity of the system in storing and releasing the heat or cold stored in the PCM. In the literature, the existing heat transfer correlations for the flow between parallel plates are for constant and equal wall

temperatures or heat fluxes. Therefore, no correlation has been built for the specific case of an air flow over PCM plates, so a new correlation was developed which takes into account the perturbation in the Nusselt evolution due to the phase change process.

Finally, this new Nusselt correlation was implemented in a numerical model, based on the control volume approach, to study numerically under which operational schedule and climate conditions the ventilated facade could achieve net energy savings during the cooling season.

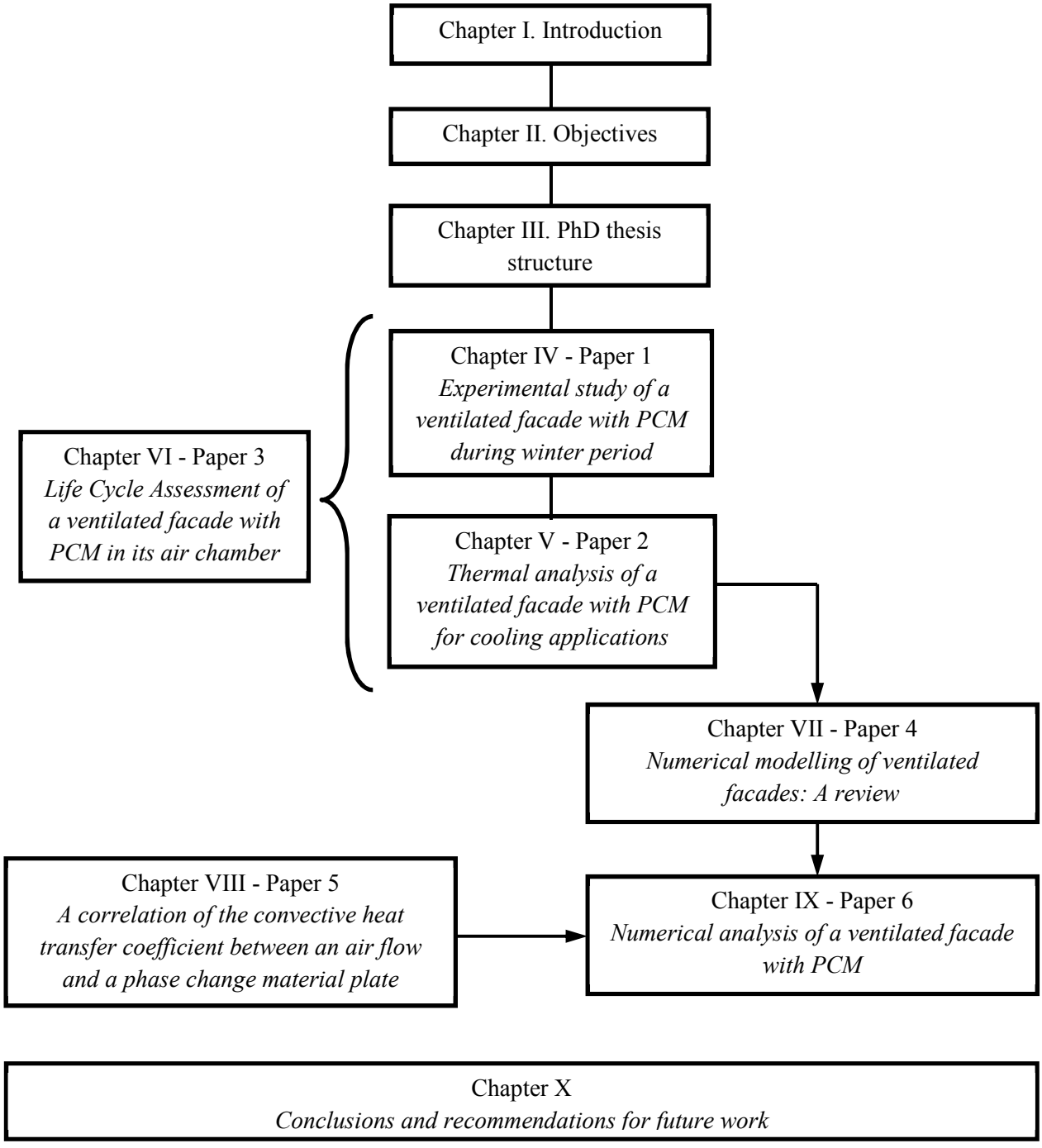
Chapter I. Introduction
Chapter II. Objectives
Chapter III. PhD thesis structure
Chapter IV - Paper 1
Experimental study of a ventilated facade with PCM during winter period
Chapter V - Paper 2
Thermal analysis of a ventilated facade with PCM for cooling applications
Chapter VI - Paper 3
Life Cycle Assessment of a ventilated facade with PCM in its air chamber
Chapter VII - Paper 4
Numerical modelling of ventilated facades: A review
Chapter VIII - Paper 5
A correlation of the convective heat transfer coefficient between an air flow and a phase change material plate
Chapter IX - Paper 6
Numerical analysis of a ventilated facade with PCM
Chapter X
Conclusions and recommendations for future work

4 Experimental study of a ventilated facade with PCM during winter period

4.1 Introduction

It is well known that ventilated double skin facades (VDSF), if well designed, can efficiently reduce the heating HVAC energy consumption of buildings by absorbing part of the solar radiation during winter period [4]. Moreover, the use of PCM in the building sector has been widely researched to increase the thermal inertia of the building envelopes [29,40], and its influence in reducing the cooling loads during the summer season has been demonstrated experimentally [18,51]. However, the high cost of these materials makes them non-attractive to market purposes if designed specifically for cooling and not for helping to cover also heating demands. This becomes a critical aspect in areas of the planet with higher energetic consumption for heating than for cooling, such as the location of the experimental set-up used in this PhD [1].

In this study the use of PCM is combined with the VDSF technology in order to reduce the heating demand during the winter season. The VDSF acts as a solar collector during the sunny hours and once the PCM is melted and the solar energy is needed by the building heating demand, the heat stored is discharged to the inner environment as a heating supply.

The scope of the work was to test experimentally the thermal performance of the VDSF with PCM under different weather conditions, energetic requirements and ventilation modes. An experimental set-up consisting of two identical house-like cubicles (2.4 m x 2.4 m x 5.1 m indoor dimensions) was built in Puigverd de Lleid (Spain). The only difference between these two cubicles is that in one of them a VDSF with macro-encapsulated PCM was constructed in the south wall (Figure 14).

Figure 14. Experimental set-up: Ventilated facade and reference cubicles during heating season

4.2 Contributions to the state-of-the-art

A new VDSF with macro-encapsulated panels of PCM in its air chamber has been experimentally tested for heating purposes. This research is described in the following publication:

- A. de Gracia, L. Navarro, A. Castell, A. Ruiz-Pardo, S. Álvarez, L.F. Cabeza. Experimental study of a ventilated facade with PCM during winter period. Energy and Buildings 58 (2013) 324-332.

This VDSF is equipped with three fans at the inlet of the channel which can provide mechanical ventilation if needed. Six openings allow the air to flow through the facade from outdoor or indoor, or to operate with no ventilation. The innovative design and versatility of this VDSF allows the system to operate as a heating supply. The operating principle and sequence of operation of the VDSF is shown in Figure 15. The ventilated facade acts as a solar collector during the sunny hours (Figure 15.a). Once the PCM is melted and a heating supply is required, the heat discharge period starts (Figure 15b). This heating supply is performed until no more thermal energy is needed o can be

provided by the system. Hereafter, the system closes all its openings to reduce heat losses to the environment (Figure 15c).

The experimental results demonstrated the high potential of this new VDSF in reducing the electrical energy consumption of the HVAC systems of a building during the winter season. These savings depend strongly on the mode of operation and the weather conditions, being under severe winter conditions 19% and 26% depending on the HVAC set point (21 ºC and 19 ºC, respectively). Moreover, with and appropriate operational schedule the system could achieve net energy savings of 86.2% during the mild winter season.

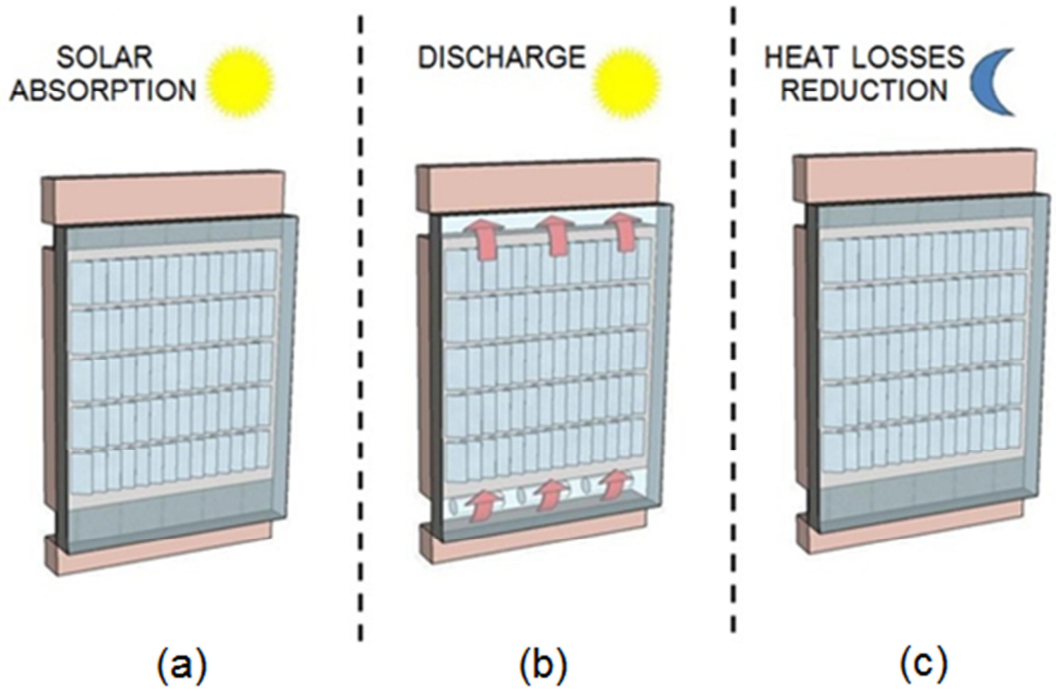

Figure 15. Sequence of operation of the ventilated facade

Moreover, the heat injection efficiency, defined as the ratio between the amount of heat that the system is able to pump and the amount of solar heat absorbed by the facade, is very sensitive to the operational schedule of the VF. This efficiency is around 40% when the system supplies heat to the inner environment during the sunny hours. On the other hand, this value is significantly reduced (19%) when the use of the solar energy (heating supply) does not match with its production.

In addition, the measured electrical energy consumption of the heat pumps and fans demonstrated that the use of mechanical ventilation in this system is unnecessary unless a fast heating supply is needed.

Finally, the experimental results also showed that the use of SP-22 provides almost no thermal benefits, since its solidification process starts below 20 ºC, which limits strongly the possibility of injecting the stored latent heat to the indoor environment.

4.3 Journal paper

Energy and Buildings 58 (2013) 324–332

Contents lists available at SciVerse ScienceDirect

Energy and Buildings

journal homepage: www.elsevier.com/locate/enbuild

Experimental study of a ventilated facade with PCM during winter period

Alvaro de Gracia[a,1], Lidia Navarro[a,1], Albert Castell[a,1], Álvaro Ruiz-Pardo[b,2], Servando Alvárez[b,2], Luisa F. Cabeza[a,*,1]

[a] GREA Innovació Concurrent, Universitat de Lleida, Edifici CREA, Pere de Cabrera s/n, 25001, Lleida, Spain
[b] Grupo de Termotécnia, Universidad de Sevilla, Escuela de Ingenieros Camino de los Descubrimientos s/n, 41092, Seville, Spain

Energy and Buildings 58 (2013) 324–332

Contents lists available at SciVerse ScienceDirect

Energy and Buildings

journal homepage: www.elsevier.com/locate/enbuild

Experimental study of a ventilated facade with PCM during winter period

Alvaro de Gracia[a,1], Lidia Navarro[a,1], Albert Castell[a,1], Álvaro Ruiz-Pardo[b,2], Servando Alvárez[b,2], Luisa F. Cabeza[a,*,1]

[a] GREA Innovació Concurrent, Universitat de Lleida, Edifici CREA, Pere de Cabrera s/n, 25001, Lleida, Spain
[b] Grupo de Termotécnia, Universidad de Sevilla, Escuela de Ingenieros Camino de los Descubrimientos s/n, 41092, Seville, Spain

ARTICLE INFO

Article history:
Received 8 October 2012
Accepted 13 October 2012

Keywords:
Double skin facades (DSF)
Phase change materials (PCM)
Buildings
Experimental measurements

ABSTRACT

The aim of this article is to test experimentally the thermal performance of a ventilated double skin facade (DSF) with phase change material (PCM) in its air channel, during the heating season in the Mediterranean climate. Two identical house-like cubicles located in Puigverd de Lleida (Spain) were monitored during winter 2012, and in one of them, a ventilated facade with PCM was located in the south wall. This ventilated facade can operate under mechanical or natural ventilation mode and its thermal control depends on the weather conditions and the energetic demand of the building. Hence, three different tests were performed: free floating, controlled temperature and demand profile conditions. The experimental results conclude that the use of the ventilated facade with PCM improves significantly the thermal behaviour of the whole building (working as a heat supplier in free floating tests and reducing significantly the electrical consumption of the HVAC systems). However, these improvements might be increased if thermal control is used. Moreover, the measured electrical energy consumption of the heat pumps and fans indicates that the use of mechanical ventilation in this system is not justified; unless a fast heating supply is needed.

1. Introduction

New policies are being promoted all over the world to reduce the energetic demand of the HVAC systems used in the building sector, and hence reduce the CO_2 emissions. In the world, the building sector (residential and commercial) is consuming around 40% of the final energy [1]. In order to reduce this high energy demand, the European directive on the energy performance of buildings [2] dictates that all the EU member states must approve energetic policies to promote the inclusion of very low and even close to zero energy buildings.

The high potential of the building envelopes in the energy demand reduction and consequently in electrical energy savings has been widely proved [3–5]. The main effort in this topic was focused in increasing the thermal resistance of the envelopes by improving the insulation [6,7]. However, a lot of research also evaluated its thermal energy storage capacity. Within this context, many latent heat storage applications in buildings have been studied [8–10], since the use of phase change materials (PCM) in the envelopes smoothes the daily temperature fluctuations and can absorb solar radiation and internal thermal loads [11].

In addition, the use of ventilated double skin facades (DSF) in the building sector has recently become more popular. Those facades, if well designed, can efficiently reduce the overall HVAC energy consumption of buildings by absorbing part of the solar radiation during winter and preventing overheating during warm periods [12]. Those constructive systems are based on a special type of envelope, where a second skin, usually a transparent glazing, is placed in front of a regular building facade. The air space in between (the channel) can be mechanically or naturally ventilated to improve the thermal performance of the building [13]. Ventilated facades can operate under different modes (Trombe wall, internal and/or external ventilation) depending on the air flow path, as shown in Fig. 1.

In this study, the use of PCM is combined with the ventilated facade constructive system. Macro-encapsulated PCM panels were installed inside the air chamber of a ventilated facade, and its thermal performance was experimentally studied and compared against a conventional constructive system. Two identical house-like cubicles were monitored, and in one of them, a ventilated facade with PCM was located in the south wall.

The PCM inside the air cavity will not only increase the solar energy absorption capacity during winter but it might be used as a cold storage system during warm periods, as well. This ventilated facade with PCM in the air chamber might reduce both heating

* Corresponding author. Tel.: +34 973 003576.
E-mail addresses: arp@esi.us.es (Á. Ruiz-Pardo), lcabeza@diei.udl.cat (L.F. Cabeza).
[1] Tel.: +34 973 00 35 77.
[2] Tel.: +34 954487471.

0378-7788/$ – see front matter © 2012 Elsevier B.V. All rights reserved.
http://dx.doi.org/10.1016/j.enbuild.2012.10.026

Nomenclature

$A_{channel}$	*Cross sectional area of the ventilated facade cavity [m²]*
A_{solar}	Effective solar absorption area [m²]
CP_{air}	Air heat capacity [J kg^{-1} K^{-1}]
Q_{fac}	Total injected heat supplied from the facade [J]
$Q_{load\_reduction}$	Thermal load difference between the REF and the FAC cubicle [J]
Q_{sol}	Total solar radiation incident in the DSF [J]
Q_{glob_rad}	Incident vertical global solar radiation [W/m²]
T_{inlet}	Temperature at the inlet of the DSF channel [K]
T_{outlet}	Temperature at the outlet of the DSF channel [K]
t	Time [s]
v_{air}	Air velocity [m/s]

Greek symbols

ρ_{air}	Air density [kg m^{-3}]
η_{load}	Load reduction efficiency
η_{sol}	Heat injection efficiency

and cooling demands of the building. However, this paper fully describes the available experimental set-up, focusing in the potential of using this special building envelope to reduce the heating demand during winter period.

2. Experimental set-up

In order to test the improvement in the thermal performance of a building due to the use of a ventilated DSF with PCM in its air cavity, two real cubicles with the same inner dimensions (2.4 m × 2.4 m × 5.1 m) were monitored in the experimental set-up located in Puigverd de Lleida, Spain. The constructive system used in the walls of both cubicles is based on alveolar bricks (30 cm × 19 cm × 29 cm) with an external cement mortar and inner plaster coating. The only difference between the two cubicles is that one of them has a ventilated facade with PCM inside its air chamber in the south wall, while the other cubicle keeps the basic constructive system (Fig. 2). Both roofs were made using concrete pre-cast beams, 3 cm of polyurethane and 5 cm of concrete slab. The polyurethane is placed over the concrete and it is protected with a cement mortar roof with an inclination of 3%, a double asphalt membrane and 5 cm of gravel [5].

A metallic structure is used to build the ventilated facade with an air cavity of 15 cm thick, which represents 0.36 m² of channel area ($A_{channel}$). The inner layer is based on the alveolar brick constructive system while the outer envelope is made by a glass layer.

The ventilated facade has an effective solar absorption area of 6.4 m² (A_{solar}) and it is equipped with three fans (FCL 133 Airtecnics) in the inlet of the air channel to provide mechanical ventilation when needed. Moreover, in order to control the operational mode of the facade, six automatized gates (Fig. 3) were installed at the different openings of the channel. Hence, the air can flow through the facade from outdoor or indoor, or operate as a Trombe wall. Those gates are controlled by ST450N linear spindle actuators. A system to control the fans and gates is programmed in a Microchip 18F45J10.

The PCM used in this application was the macro-encapsulated salt hydrate SP-22 from Rubitherm. The selection of this PCM (melting temperature at 22 °C) allows the ventilated facade to store high quantities of solar energy during winter periods, and to be used as a cold storage system during summer periods using the night free cooling effect. A total of 112 PCM panels are distributed over the facade creating 14 air flow channels as shown in Fig. 4. The use of this thin air flow channels maximizes the heat transfer area between the air flow and the PCM.

Both cubicles were fully instrumented and the following data was registered at 5 min intervals to evaluate their thermal performance:

Internal wall temperatures (east, west, north, south, roof and floor) measured with Pt-100 DIN B.

Indoor air temperature and humidity (at a height of 1.5 m and 4.5 m) measured with ELEKTRONIK EE21.

Electrical consumption of the HVAC systems using an electrical network analyser (MK-30-LCD).

Moreover, in order to analyze the behaviour of the ventilated facade with PCM, the following data was also measured:

Air temperature of the cavity at different heights and locations (10 Pt-100 with an irradiative cover).

Air velocity of the cavity at different heights and locations (4 hot wire sensors KIMO CTV 210).

Pressure drop across the air cavity (KIMO CP 200).

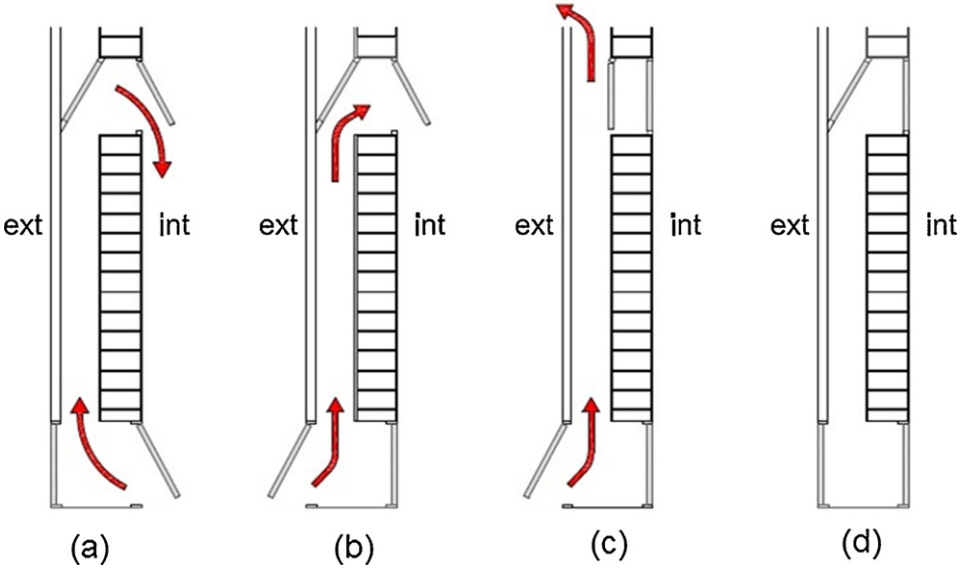

Fig. 1. Different operational modes of a ventilated DSF.

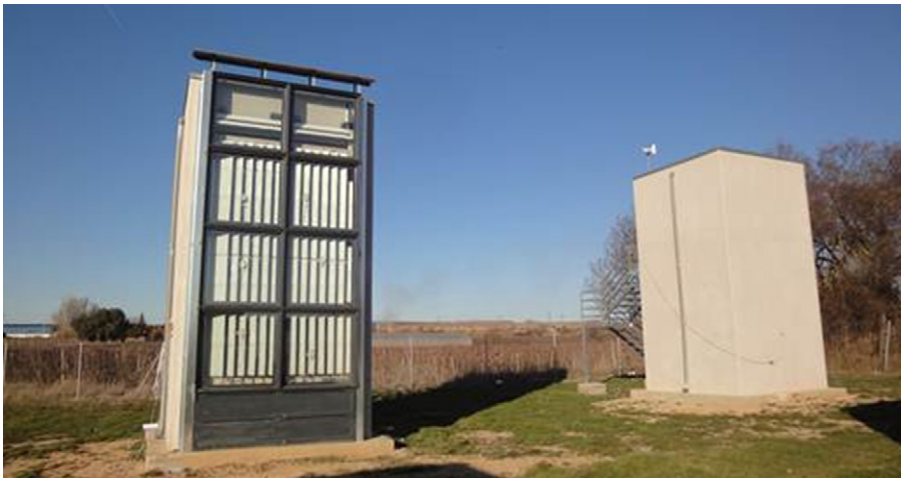

Fig. 2. Experimental set-up: reference and ventilated facade cubicles.

Outer and inner skin surface temperature (glass and alveolar brick, respectively) at different heights and locations (6 Pt-100 each).

External surface temperature at different heights and locations (6 Pt-100).

Heat flux transferred to indoor (2 HUKSEFLUX HFP01).

Heat flux transferred to the front and back surface of a PCM panel (2 HUKSEFLUX HFP01).

Temperature of the PCM at three different heights (3 Thermocouples Type T, 0.5 mm thick inserted in the PCM panels).

Front and back surface temperature of the PCM panels (2 Thermocouples Type T).

In addition, the weather data was also registered every 5 min. Two Middleton Solar pyranometers SK08 were used to capture the horizontal and vertical global solar radiation, the outer air temperature and humidity were measured using an ELEKTRONIK EE21 with a metallic shield to be protected against radiation, and finally the wind speed and direction was provided by a DNA 024 anemometer.

The experimental set-up offers the possibility to perform two kinds of indoor conditions: free floating temperature and fixed controlled temperature. Both cubicles are provided by two heat pumps (Fujitsu Inverter ASHA07LCC), located at different heights (3 and 5 m).

3. Methodology

In this paper, the thermal performance of the ventilated facade is experimentally tested under different weather conditions (severe and mild Mediterranean winter), thermal control (free floating and controlled temperature conditions) and ventilation mode

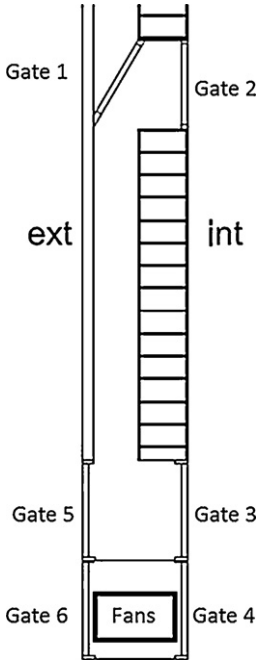

Fig. 3. Automatized gates and fan distribution along the facade.

Fig. 4. PCM distribution inside the air chamber.

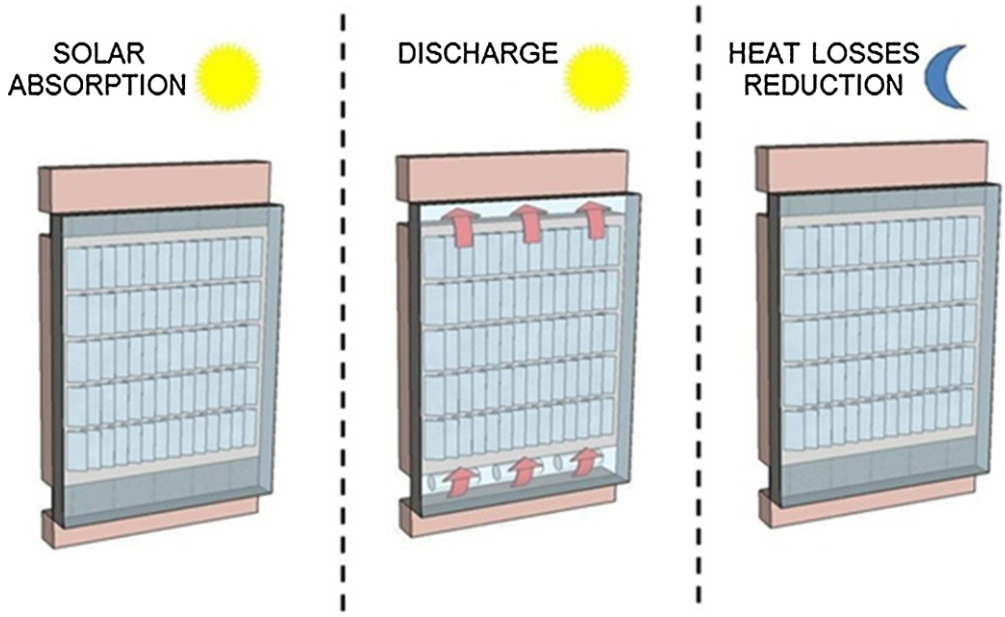

Fig. 5. Sequence of operation of the ventilated facade.

(mechanically and naturally ventilated facade). The different tests under severe winter (SW) conditions were performed from 9th to 22nd of February 2012, which were clear sunny days (global solar radiation peaks of 1200 W/m^2) with an outer temperature oscillating from around 12 °C to −4 °C. On the other hand, the mild winter (MW) conditions experiments were tested from 1st to 29th of March 2012, with similar solar radiation than in the previous experiments (global solar radiation peaks of 1100 W/m^2) but with outer temperatures varying from 24 °C to 4 °C.

The sequence of operation of all the experiments is similar and is shown in Fig. 4. The ventilated facade acts as a solar collector during the solar absorption period (Fig. 5a). Once the PCM is melted and the solar energy is needed by the heating demand, the heat discharge period starts. During this period the openings drive the air flowing from indoor to the facade cavity, where it is heated up by the PCM panels and sent it back into the cubicle (Fig. 5b). This discharge period is performed until no more thermal energy is needed or can be provided by the facade; hereafter the system closes all the openings, acting as a Trombe wall, to minimize the heat losses to the environment (Fig. 5c). The different weather conditions and energetic demand scenarios define the timing of this mode of operation as well as the ventilation mode.

As it was previously said, the thermal control of the ventilated facade depends on the weather conditions and the energetic demand of the building, for that purpose three different experiments were performed:

- Free floating (FF): During these experiments no HVAC system is used, hence the thermal response of the building is evaluated by its indoor air temperature. This experiment is presented in the mechanically ventilated mode for severe and mild winter weather conditions. During the experiments under severe winter conditions, the system discharges the absorbed solar heat from 12:00 to 18:00 h, while during the mild winter test, the discharge period is programmed from 18:00 to 23:00 h.
- Controlled temperature (CT): The indoor temperature of each cubicle is fixed by using the heat pumps. The electrical energy consumed by each heat pump is measured and compared. This experiment was performed in the mechanically and naturally ventilated mode for severe and mild winter weather conditions. Moreover, different temperatures set points were analyzed. Similarly as in the FF experiment, the heat discharge schedule varies depending on the weather conditions (from 12:00 to 18:00 h during severe winter conditions and from 12:00 to 23:00 h in the mild period).
- Demand profile (DP): In the mild season, the HVAC systems were controlled by a timer, so they operate altogether with the facade from 18:00 to 23:00 h, simulating the demand profile of a conventional house. This experiment is presented with the facade operating as a Trombe wall, and in the mechanically and naturally ventilated mode.

In order to analyze the thermal performance of the system two parameters are introduced. The heat injection efficiency (η_{sol}) is calculated as the ratio between the amount of heat that the system is able to pump to the inner environment (Q_{fac}), by the amount of solar heat absorbed by the facade (Q_{sol}), as shown in Eq. (1).

$$\eta_{sol} = \frac{Q_{fac}}{Q_{sol}} \tag{1}$$

where,

$$Q_{sol} = \int \dot{Q}_{glob\_rad} \cdot A_{solar} \cdot dt \tag{2}$$

$$Q_{fac} = A_{channel} \cdot \rho_{air} \cdot Cp_{air} \cdot \int v_{air} \cdot (T_{outlet} - T_{inlet}) \cdot dt \tag{3}$$

The second parameter is the load reduction efficiency (η_{load}), which is used in the controlled temperature and demand profile experiments and is defined as the ratio between the thermal energy saved in the heat pump ($Q_{load\_reduction}$), by the amount of heat injected by the facade (Q_{fac}). The electrical energy savings measured from the heat pumps installed in the reference and ventilated facade cubicles are multiplied by the COP (4.55 kW/kW) of these heat pumps in order to calculate the $Q_{load\_reduction}$.

$$\eta_{load} = \frac{Q_{load\_reduction}}{Q_{fac}} \tag{4}$$

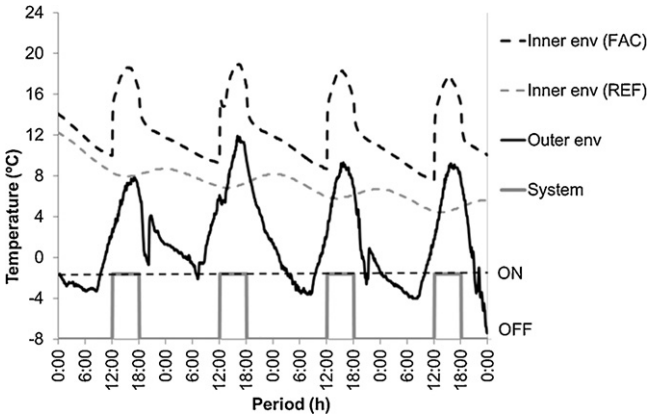

Fig. 6. FF severe winter inner temperature evolution.

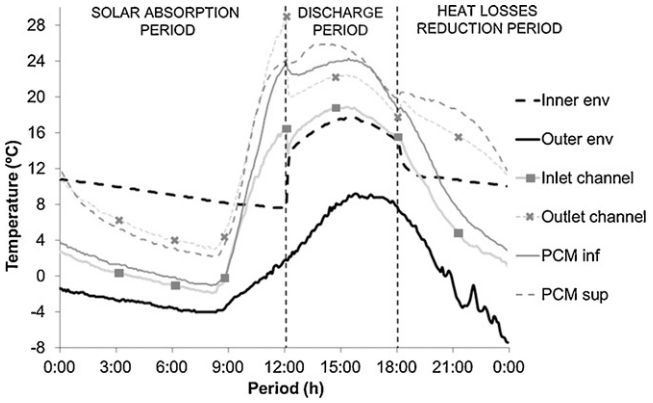

Fig. 7. Thermal profiles of PCM, air flow, and inner and outer environment on 12th of February 2012.

4. Results

4.1. Free floating (FF)

4.1.1. FF under severe winter (FF SW)

The free floating experiments were tested under severe and mild winter conditions. The severe winter experiment was performed from 9th to 12th of February 2012. During these four days, the measured outdoor temperature oscillated from 8 to −4 °C, and the global radiation on vertical surface was 99.6 MJ/m^2, giving a total radiation incident on the facade of 159.37 MJ/day (Eq. (2)). A fraction of the absorbed heat is pumped to the interior of the cubicle from 12:00 to 18:00 using the fans at a fixed air flow rate of 2600 m^3/h. The heat injected from the facade to the inner environment was 57.2 MJ/day (Eq. (3)), hence the system has an efficiency of pumping the absorbed solar heat of 36% (Eq. (1)). The amount of solar heat which was not pumped to the interior regards to heat losses to the environment and the reflection of solar radiation occurring in the outer skin. Moreover, it is important to highlight that the temperature of the overall thermal mass of the facade at the end of the discharge is much higher (around 20 °C) than the temperature at the beginning of the solar absorption period (around 0 °C). Hence, part of the solar heat is also used to cover this difference.

The indoor temperatures of both cubicles are presented in Fig. 6. The indoor temperature of the reference cubicle (REF) drops daily due to the tendency of the outdoor temperature, while the use of the ventilated facade with PCM (FAC) makes the temperature increase every day from 9 °C to 18 °C. The discharge period of the system is also shown in Fig. 6.

The thermal profiles of the PCM and the air flow at the inlet and outlet of the channel are presented in Fig. 7 altogether with the indoor and outdoor environmental temperatures of the ventilated facade cubicle during 12th of February 2012. This figure shows that the system does not use the whole available latent heat, stored in the PCM, since after the discharge (18.00 h) the PCM in the upper part of the facade is just starting its solidification process. Hence, the discharge might have been prolonged in order to take advantage of the stored latent heat. Thus indicates the necessity of using a thermal control system which can be programmed depending on the energy demand, production and storage, and not only using the time as controlling parameter.

The PCM and air flow temperature drops to values close to 0 °C during night time. However, the temperatures of the whole ventilated facade increase fast with the solar radiation due to the greenhouse effect, achieving its maximum just before the discharge. A vertical thermal gradient was measured in the airflow during the solar absorption period (12 °C) indicating an important air stratification in the air channel.

It is important to highlight that the system is still absorbing solar radiation during the discharge period, when working under these operational mode. This is why the PCM and air flow temperatures increase until 15:00 even though part of the solar heat is being used and injected to the interior of the cubicle.

Fig. 7 also shows that the inlet temperature of the channel is not equal to the indoor temperature, which coincides with the measurements and simulations performed by Saelens et al. [14]. This research stated that in order to estimate the inlet temperature entering in a ventilated facade, the heating and cooling due to contact with the bounding surfaces must be taken into account, as well as the heating due to solar radiation.

4.1.2. FF under mild winter (FF MW)

The free floating experiment under mild winter weather conditions was tested on 16th and 17th of March 2012. The solar radiation incident to the facade during these two days was 163.2 MJ/day (Eq. (2)). The system discharges this solar heat from 18:00 to 23:00, injecting to the indoor environment 31.6 MJ/day, which produces a η_{sol} = 19.4%. It can be seen that the efficiency of pumping the absorbed solar heat has been reduced in comparison to the previous experiment (FF under severe conditions). This occurs because in the experiment described in Fig. 6 the heat is being discharged at the same time as it is being absorbed. On the other hand, in the experiment presented in Fig. 8 the absorbed solar energy is stored for later uses and hence exposed during more time to the heat losses to the environment. The measurements under these climatic conditions proved that the ventilated facade improves strongly the thermal performance of the cubicle, making the use of HVAC system almost not necessary, since the indoor temperature is nearly all the time inside the thermal comfort range.

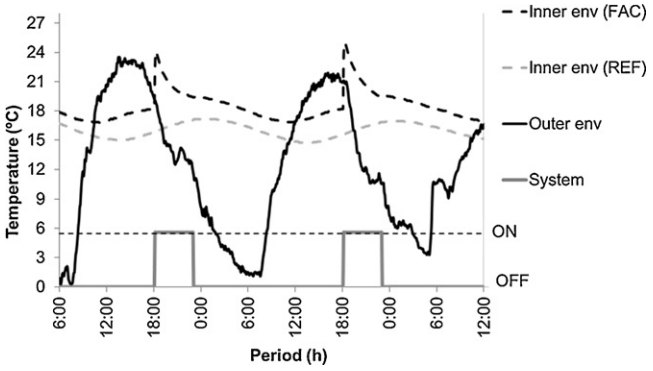

Fig. 8. FF mild winter inner temperature evolution.

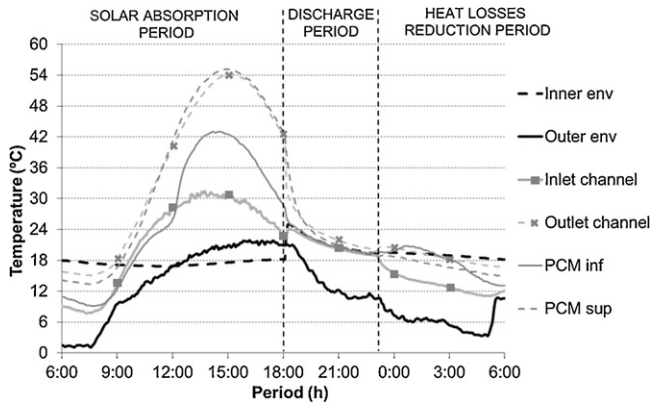

Fig. 9. Thermal profiles of PCM, air flow, and inner and outer environment during 17th of March2012.

During this experiment, since the discharge was programmed after the whole solar energy was absorbed, the PCM at the upper part of the facade achieved 55 °C (Fig. 9). Looking at the PCM curve, both melting and solidification process can be easily identified, showing an important hysteresis between the phase change temperatures during heating (23 °C) and cooling (20 °C). Furthermore, it can be also seen that the latent heat is only partially used and the discharge process might have been prolonged.

Finally, special attention on the PCM temperature peak must be taken into account in order to avoid melting of the nucleants included in the PCM, which will lead to stronger subcooling effects and the malfunction of the system.

4.2. Controlled temperature (CT)

4.2.1. CT 21 °C Mechanically Ventilated under severe winter (CT MV SW 21)

As previously said, during the controlled temperature experiments, two heat pumps were used in each cubicle and their electrical energy consumption was registered. The first CT experiment was tested from 15th to 17th of February 2012 with the heat pumps working the whole day at a set point of 21 °C and the fans pumping air from 12:00 to 18:00 h. The solar heat incident to the facade during this period was 169.6 MJ/day (Eq. (2)) and the heat injected from the facade to the indoor environment was 60.56 MJ/day, giving an efficiency η_{sol} of 35.7%. Note that this efficiency is similar to the value in the free floating experiment under the same climatic conditions and time schedule of discharge (36%).

Fig. 10 shows that the heat pumps in the reference cubicle were working all the time, while in the FAC cubicle the heat pumps did not need to heat up the indoor air during the discharge period. Thus, produces a significant difference in the electrical energy consumption of the HVAC system of the REF cubicle (40.58 MJ/day) and the FAC cubicle (30.76 MJ/day). In addition, in the mechanically ventilated experiments it is important to take into account the electrical energy consumption of the fans (120 W). The fans consumed 2.59 MJ/day, hence the use of the ventilated facade operating under the described conditions achieved a net electrical energy reduction of the HVAC system of 7.77 MJ/day (19.14% in comparison to the reference). These energy savings would have been higher if the system had used the stored latent heat in the discharge period. However, it could not be used since the set point of the HVAC system was set to 21 °C and the solidification process of the PCM SP-22 was at 20 °C.

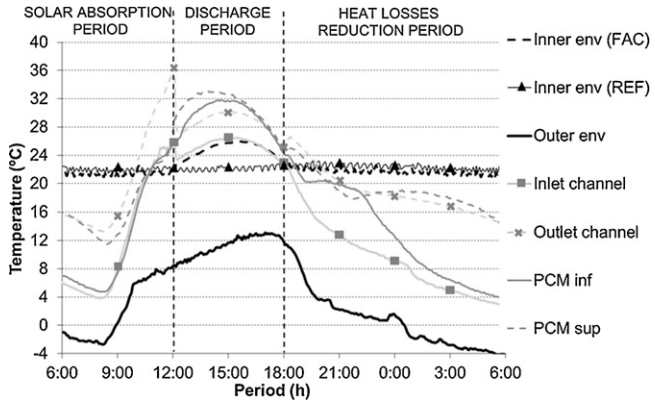

Fig. 10. Thermal profiles of PCM, air flow, and inner and outer environment during 17th of February 2012.

Furthermore, the 9.82 MJ/day of electrical energy savings registered from the heat pumps corresponds to 44.681 MJ/day of thermal energy savings, since the COP of the heat pumps is 4.55 kW/kW. Hence, the system operating under these conditions presents a load reduction efficiency η_{load} of 73.7% (Eq. (4)). It is important to highlight that not all the heat injected by the facade can be directly used to reduce the heating load of the cubicle, since the FAC cubicle presented an important stratification of the air inside (the hot air is pumped inside from the upper part of the facade), and overheating of the indoor environment above the set point temperature, which increases the heat losses to the outer environment in comparison to the REF cubicle.

4.2.2. CT 19 °C mechanically ventilated under severe winter (CT MV SW 19)

As it was discussed, in the previous experiment the PCM did not release its latent heat during the discharge period, since its phase change temperature during the solidification process was below the HVAC set point (19 °C and 21 °C, respectively). Therefore, the previous experiment was repeated with a set point of 19 °C during 18th and 19th of February 2012. However, the latent heat could not have been injected to the indoor environment during this experiment since, once the discharge period was finished, the PCM was still above the phase change range.

Nevertheless, the experiment was useful to determine how the set point of the HVAC system influences the efficiency of the ventilated facade. The solar heat incident to the facade during this period was 163.9 MJ/day (Eq. (1)) and the heat injected from the facade to the indoor environment was 52.73 MJ/day (η_{sol} of 32.2%). Moreover, the ventilated facade presents a load reduction efficiency (η_{load}) of 92.3%, which involves an electrical energy reduction of 34% in the FAC cubicle compared to the REF one.

4.2.3. CT 21 °C naturally ventilated under severe winter (CT NV SW 21)

From 21st to 23rd of February 2012 the system was programmed to discharge the absorbed solar radiation from 12:00 to 18:00 without the use of fans. The registered thermal profiles during this experiment are presented in Fig. 11, showing how the indoor environmental temperature did not vary abruptly once the naturally ventilated discharge started. The system operating under this mode reduced the electrical energy consumption of the HVAC in 7.79 MJ/day (18.7% in comparison to the reference cubicle), which is similar to the electrical energy savings achieved in the analogue experiment with the facade using the fans (CT MV SW 21). However, it is important to highlight that the HVAC system was operating due to insufficient temperature at the beginning of the discharge, while it did not operate during the whole discharge in the mechanically ventilated test. Thus, the use of fans is unnecessary in this system, unless the energetic demand of the indoor environment needs a fast response.

The heat injection efficiency η_{sol} was 35.2%, close to the one in mechanically ventilated test. This high value might not be expected

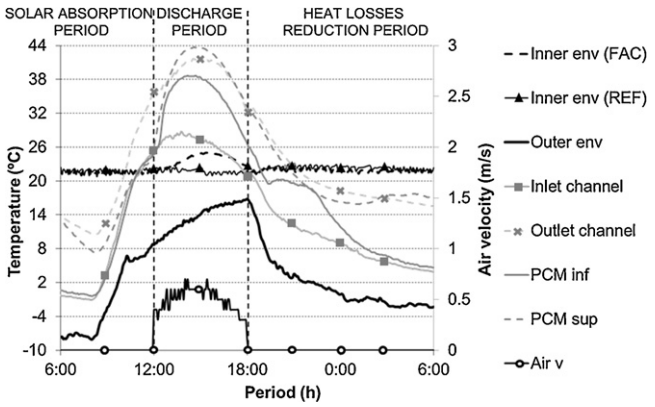

Fig. 11. Thermal profiles of PCM, air flow, and inner and outer environment during 23rd of February 2012.

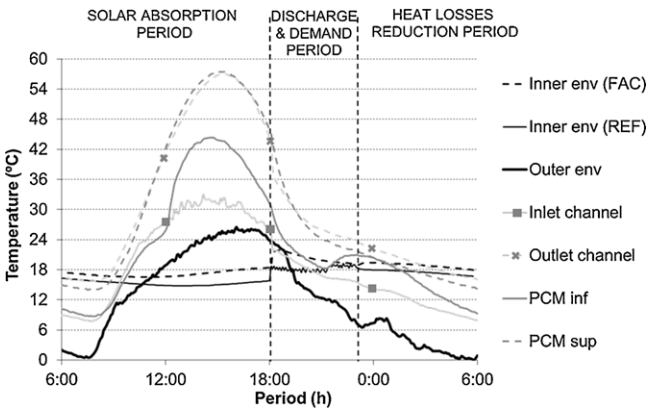

Fig. 13. Thermal profiles of PCM, air flow, and inner and outer environment during 15th of March 2012.

because of the difference in the air velocities, 1.9 m/s in the MV tests and less than 0.7 m/s when NV, as it can be seen in Fig. 11. However, it is justified by the high thermal gradient between the inlet and outlet of the channel, being more than 12 °C when naturally ventilated, while this value was less than 4 °C in the mechanically ventilated operational mode.

The latent heat stored in the PCM could not be used during the heat discharge of this experiment, since the temperature at which the heat pumps are set (21 °C), is higher than the phase change temperature (20 °C).

4.2.4. CT 19 °C mechanically ventilated under mild winter (CT MV MW 19)

The mild winter conditions allow the system to discharge the absorbed solar heat from 12:00 to 23:00. Thus, altogether with the low set point of the heat pumps (19 °C) enables the use of part of the stored latent heat in the PCM during its solidification process, as seen in Fig. 12. In the experiment performed from 1st to 3rd of March 2012, the HVAC system of the FAC cubicle did not need to provide heat during the discharge period, as well as, during several hours after the discharge had finished. Hence, the discharge period might have been prolonged and/or started earlier, which highlights again the necessity of using a programmable thermal control system.

The facade injected 62.85 MJ/day, being the 40% of the incident solar radiation. Although the heat injection is useful and makes the use of HVAC unnecessary during the whole discharge, this is more significant during the first 6 h, when the thermal gradient between the inlet and outlet channel achieves 4 °C. Moreover, this injected heat increases the indoor temperature up to 28 °C, producing overheating and underlining the critical necessity of a thermal control system.

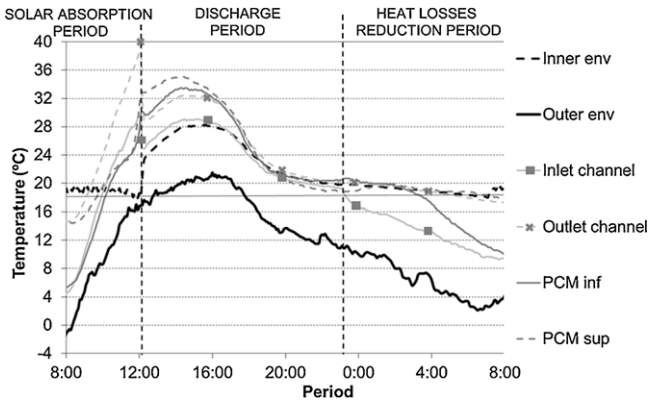

Fig. 12. Thermal profiles of PCM, air flow, and inner and outer environment during 1st of March 2012.

The use of the ventilated facade under this operational mode reduces a 57% the electrical energy consumption of the HVAC in comparison to the REF cubicle. However, it must be taken into account that from 8.443 MJ/day saved by the system, the fans consumed 4.75 MJ/day. It is important to highlight the energy consumption difference in the REF depending on the weather conditions. It consumed 14.673 MJ/day and 31.3 MJ/day during mild and severe winter conditions, respectively.

4.3. Demand profile (DP)

4.3.1. DP 19 °C naturally ventilated under mild winter (DP NV MW 19)

During the demand profile experiments, the HVAC system was only connected from 18:00 to 23.00, simulating a real domestic thermal demand. In the FAC cubicle, the ventilated facade discharged the stored heat during this demand period. The system operating in naturally ventilated mode reduced the electrical energy consumption of the HVAC from 2.565 MJ/day (REF) to 0.353 MJ/day (FAC), being the use of an active heating system under mild winter conditions almost unnecessary. Furthermore, as shown in Fig. 13, the PCM releases part of its stored latent heat, and the indoor temperature of the FAC cubicle is inside the thermal comfort range almost during the whole demand period.

The thermal profile of the PCM close to the inlet of the channel shows clearly the melting and solidification process occurring from 10:30 to 12:00 h and from 20:30 to 1:00 h, respectively. The solidification process of the PCM shows a clear hysteresis in the phase change temperature when compared against the melting (fusion at 23 °C and solidification at 20 °C). Moreover, this process is clearly affected by subcooling. Even though the phase change temperature during the solidification is at 20 °C, the PCM temperature falls down to 18 °C without starting the solidification process, hereafter, once the crystallization starts, the PCM returns to 20 °C where phase change occurs.

4.3.2. DP 19 °C mechanically ventilated under mild winter (DP MV MW 19)

The ventilated facade operating with mechanical ventilation under mild winter conditions reduces the electrical energy consumption of the HVAC from 4.625 MJ/day (REF) to 1.976 MJ/day (FAC). However, this 2.65 MJ/day of electrical energy savings does not balance the energy consumed by the fans during the experiment (4.75 MJ/day), which supports the idea that the fans must be only used when a fast thermal heating is demanded in the cubicle.

Table 1
Thermal performance of the facade under the CT and DP experiments.

	η_{sol} (%)	η_{load} (%)	HVAC FAC (MJ/day)	HVAC REF (MJ/day)	Net energy savings (MJ/day)	% Energy savings
CT MV SW 21	35.7	73.8	30.76	40.58	7.77	19.1
CT MV SW 19	32.2	92.9	20.53	31.30	8.18	26.1
CT NV SW 21	35.3	60.8	33.79	41.58	7.79	18.7
CT MV MW 19	40.0	61.12	6.23	14.67	3.69	25.2
DP MV MW 19	19.0	39.2	1.98	4.63	−2.1	−45.4
DP NV MW 19	10.9	58.3	0.35	2.57	2.212	86.2
DP TW MW 18	–	–	0.44	1.82	1.38	75.6

4.3.3. DP 18 °C Trombe Wall under mild winter (DP TW MW 18)

As previously discussed, after the heat discharge period, the ventilated facade can operate as a Trombe Wall, and hence reduce the heat losses through the southern facade as well as acting as a solar collector. In the experiment performed from 27th to 29th of March 2012 (mild winter conditions), the HVAC system was programmed to operate from 18:00 to 23:00 h with a set point at 18 °C. The Trombe wall, by limiting the heat losses, decreases the electrical energy consumption from 1.82 MJ/day (REF) to 0.44 MJ/day (FAC), which implies a reduction of more than 75%, without any ventilation system under these climatic conditions and thermal demand.

5. Discussion

A summary of the main results extracted from the CT and DP experiments is presented in Table 1. The heat injection efficiency (η_{sol}) is very sensitive to the operational schedule, being around 35% when the system discharges the absorbed solar radiation from 12:00 to 18:00 h (severe winter experiments), 40% when this discharge period is extended until 23:00 h. This heat injection efficiency is reduced significantly for the demand profile experiments, since the use of the solar energy (from 18:00 to 23:00) does not match with its production. During these experiments, a significant difference was measured between the mechanically ventilated (19%) and the naturally ventilated (10.9%) operational mode, which is justified since the use of fans supplies the stored heat faster, limiting the heat losses.

Moreover, the heat injected to the facade does not directly reduce the electrical energy consumption of the HVAC system, since higher heat losses due to overheating above the set point and air stratification occur in the FAC cubicle. The facade presents the higher load reduction efficiency (η_{load}) when operating with the fans from 12:00 to 18:00 h and with the set point at 19 °C.

As shown in Table 1, the use of the facade under the mechanically ventilated mode is unnecessary; unless a fast heating supply is needed. This is justified by looking at the net energy savings that the system can achieve when operating under severe winter conditions at 21 °C (7.77 MJ/day and 7.79 MJ/day for MV and NV, respectively). Furthermore, the use of fans implies an extra energetic cost to the system when used under mild winter conditions, since the energy savings measured in the HVAC do not compensate the electrical energy spent in the fans (2.65 MJ/day and 4.75 MJ/day, respectively).

It is important to highlight the difference of energetic requirements depending on the weather conditions. This difference strongly influences the percentage of energy savings and must be taken into account when comparing operational modes.

6. Conclusions

The thermal behaviour of a ventilated facade with macro-encapsulated PCM in its air cavity is experimentally evaluated and presented in this paper. The experimental set-up consists of two identical house-like cubicles (2.4 m × 2.4 m × 5.1 m indoor dimensions). The only difference between the two cubicles is that in one of them a ventilated facade with macro-encapsulated PCM (SP 22) inside its air chamber is constructed in the south wall. The ventilated facade acts as a solar collector during the solar absorption period, until the solar energy is demanded and can be discharged to the indoor environment.

Three different sets of experiments were presented in order to test the thermal performance of the system operating under severe and mild winter conditions: free floating, controlled temperature, and demand profile experiments.

The thermal performance of the whole cubicle is improved by the use of this ventilated facade under free floating conditions. While the indoor temperature of the reference cubicle drops daily due to the oscillation of the outer temperature, the use of the ventilated facade with PCM increases the temperature every day from 9 °C to 18 °C under severe winter conditions. Moreover, the free floating experiments demonstrated that the use of HVAC system is almost not necessary during the mild winter period.

The use of the ventilated facade reduces significantly the electrical energy consumptions of the installed HVAC systems. These savings depend strongly on the mode of operation and the weather conditions. The authors want to highlight the energy savings registered during the experiments under severe winter, being 19% and 26% depending on the HVAC set point (21 °C and 19 °C, respectively). It is expected that those values would have been even higher if a thermal control system would have been programmed depending on the energy demand, production and storage.

The measured electrical energy consumption of the heat pumps and fans demonstrated that the use of mechanical ventilation in this system is unnecessary unless a fast heating supply is needed. Furthermore, the experimental results showed that the use of mechanical ventilation during low heating demands periods can produce higher electrical consumption of the overall system, since the energy saved by the HVAC systems does not compensate the electrical energy consumed by the fans.

Moreover, the use of SP-22 as PCM provides almost no thermal benefits in this system, since its phase change temperature during the solidification process is very low (20 °C) to be used in this facade, and only in some operational modes, a part of the stored latent heat is injected to the indoor environment. Hence it must be highlighted that if the system would have used the whole latent heat stored in the PCM, it would have provided even higher thermal benefits.

Acknowledgements

This work was supported by the "Corporación Tecnológica de Andalucía" by means of the project "MECLIDE-Soluciones estructurales con materiales especiales para la climatización diferida de edificios" with the collaboration of DETEA. The work partially funded by the Spanish government (ENE2011-28269-C03-02 and ULLE10-4E-1305) and the European Union (COST Action COST TU0802). The authors would like to thank the Catalan Government for the quality accreditation given to their research group (2009 SGR 534).

References

[1] J. Laustsen, Energy efficiency requirements in building codes, energy efficiency policies for new buildings, International Energy Agency (2008).

[2] Directive 2010/31/eu of the European parliament and of the council of 19 May 2010 on the energy performance of buildings. Available from: http://www.epbd-ca.eu

[3] C. Balaras, K. Droutsa, E. Dascalaki, S. Kontoyiannidis, Heating energy consumption and resulting environmental impact of European apartment buildings, Energy and Buildings 37 (1995) 429–442.

[4] M.M. Farid, S. Behzadi, Energy storage for efficient energy utilization in buildings, in: 1st International High Performance Buildings Conference 12–15 July, Purdue University, USA, 2010.

[5] A. de Gracia, A. Castell, M. Medrano, L.F. Cabeza, Dynamic thermal performance of alveolar brick construction system, Energy Conversion and Management 52 (2011) 2495–2500.

[6] L.F. Cabeza, A. Castell, M. Medrano, I. Martorell, G. Pérez, A.I. Fernández, Experimental study on the performance of insulation materials in Mediterranean construction, Energy and Buildings 42 (2010) 630–636.

[7] T. Soubdhan, T. Feuillard, F. Bade, Experimental evaluation of insulation material in roofing system under tropical climate, Solar Energy 79 (2005) 311–320.

[8] L.F. Cabeza, A. Castell, C. Barreneche, A. de Gracia, A.I. Fernández, Materials used as PCM in thermal energy storage in buildings: a review, Renewable & Sustainable Energy Reviews 15 (2011) 1675–1695.

[9] F. Kuznik, J. Virgone, K. Johannes, In-situ study of thermal comfort enhancement in a renovated building equipped with phase change material wallboard, Renewable Energy 36 (2011) 1458–1462.

[10] A.M. Khudhair, M.M. Farid, A review on energy conservation in building applications with thermal storage by latent heat using phase change materials, Energy Conversion and Management 45 (2004) 263–275.

[11] D. David, F. Kuznik, J. Roux, Numerical study of the influence of the convective heat transfer on the dynamical behavior of a phase change material wall, Applied Thermal Engineering 31 (2011) 3117–3124.

[12] M.A. Shameri, M.A. Alghoul, K. Spoian, M. Fauzi, M. Zain, O. Elayeb, Perspectives of double skin facade systems in buildings and energy savings, Renewable & Sustainable Energy Reviews 15 (2011) 468–1475.

[13] N. Safer, M. Woloszyn, J.J. Roux, Three-dimensional simulation with a CFD tool of the airflow phenomena in single floor double-skin façade equipped with a Venetian blind, Solar Energy 79 (2005) 193–203.

[14] D. Saelens, S. Roels, H. Hens, The inlet temperature as a boundary condition for multiple-skin facade modelling, Energy and Buildings 36 (2004) 825–835.

5 Thermal analysis of a ventilated facade with PCM for cooling applications

5.1 Introduction

The importance of avoiding overheating during the summer season is highlighted in the European Directive 2010/31/EU [52]. One of the most important methods to reduce the energetic demand of a building is by carefully designing its facade. In this sense, ventilated facades have been presented as an interesting constructive system to improve the energy efficiency of new and refurbished buildings [3] . Xu and Ojima [53] have registered experimentally a reduction in the cooling loads of 10-15% due to the use of a double skin facade in a two-story house in Japan.

Those constructive systems are based on a special type of envelope, where a second skin, usually a transparent glazing, is placed in front of a regular building facade. The air space in between (the channel) can be mechanically or naturally ventilated to improve the thermal performance of the building [5]. The ventilation of the channel and the use of shading devices are critical to avoid undesirable overheating during summer months when peak outside air temperatures coincide with high solar gains [54,55].

The ventilated facade with PCM previously described could be also used to reduce the cooling demand of a building. In order to address this requirement, an extra opaque insulating layer was installed in the outer skin of the facade (Figure 16). This opaque layer covers the transparent glazing during the summer period and avoids solar radiation inside the cavity.

Figure 16. Experimental set-up: Ventilated facade and reference cubicles during cooling season

5.2 Contribution to the state-of-the-art

The versatility of the VDSF allows the system to operate as a cold storage or a night free cooling system. When used as a cold storage system and in order to solidify the PCM, the air is pumped by the fans to the channel from the outer environment during night time (Figure 17a). The outer temperature must be lower than the phase change temperature during this step. Hereafter, the VDSF closes all its openings and stores the PCM solidified until a cooling supply is needed by the energetic demand of the building. The air is cooled down by the PCM and is pumped to the inner environment (Figure 17b). After all the cold stored in the PCM has been released to the air, the system lets the air flow from outdoors to outdoors due to buoyancy forces avoiding the overheating effect in the air chamber (Figure 17c). Moreover, the system can also provide a night free cooling effect after the heat stored in the PCM is released to the outer environment. During this operational mode, the air from the outside is injected mechanically to the inside (Figure 17d).

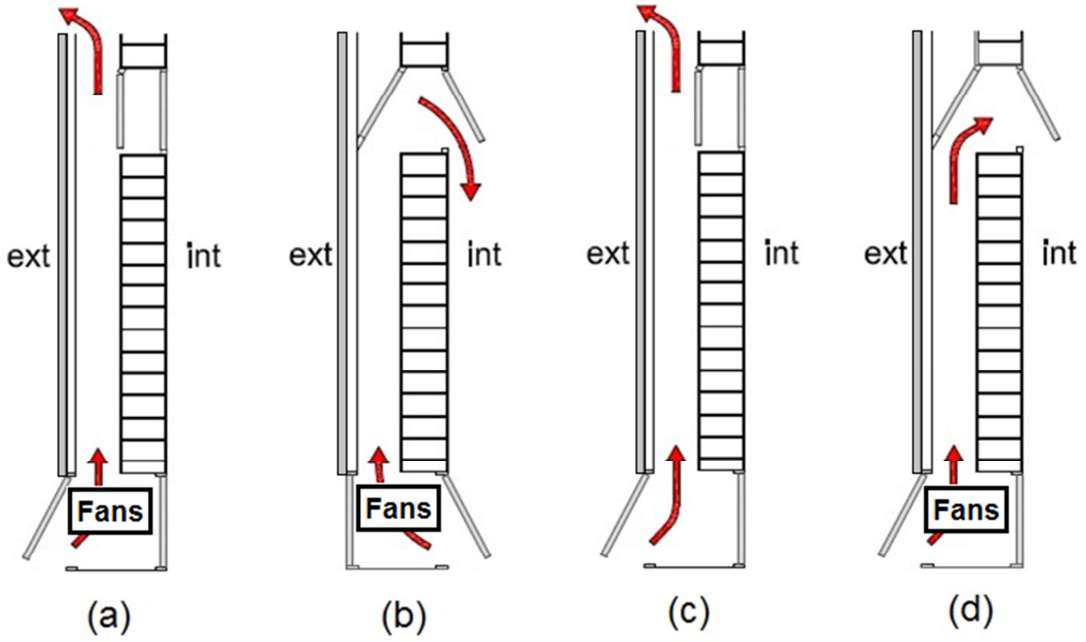

Figure 17. Modes of operation of the ventilated facade

The experimental results which evaluate the thermal performance of the ventilated facade with PCM in its air chamber during the summer season are presented and discussed in the following publication:

- A. de Gracia, L. Navarro, A. Castell, A. Ruiz-Pardo, S. Álvarez, L.F. Cabeza. Thermal analysis of a ventilated facade with PCM for cooling applications. Energy and Buildings, submitted ENB-S-12-01723

The experimental results demonstrated the high potential of the night free cooling effect in reducing the cooling loads of a building. This operational mode could inject air at a temperature below the set point under both severe and mild summer conditions (34.9 MJ/day and 42.8 MJ/day, respectively).

On the other hand, when operating with the cold storage sequence, the system presents low energy storage efficiency in all cases due to important heat gains through the outer skin. Moreover, the cold storage capacity of the system is very sensitive to the outer night temperature, being limited under severe summer conditions. Under these weather

conditions, minimum night temperatures of 18 ºC are registered, which unable the PCM to fully solidify due to its subcooling and hysteresis.

The ventilated facade with PCM does not provide any net energetic savings if the energy consumed by the fans are taken into account. This is because the fans are pumping air not only during cooling supply (11 to 13 h), but during the whole night period (0 to 8 h), as well. The excessive use of fans must be avoided and some key design aspects must be optimized. Moreover, the use of natural night ventilation is suggested as a future solution to reduce the high electrical energy consumed by the fans.

5.3 Journal paper

Elsevier Editorial System(tm) for Energy and Buildings
Manuscript Draft

Manuscript Number:

Title: Thermal analysis of a ventilated double skin facade with PCM for cooling applications

Article Type: Full Length Article

Keywords: Double skin facades (DSF); phase change materials (PCM); buildings; experimental measurements; cooling applications; energy efficiency

Corresponding Author: Prof Luisa F. Cabeza, PhD

Corresponding Author's Institution: University of Lleida

First Author: Alvaro de Gracia, Engineer

Order of Authors: Alvaro de Gracia, Engineer; Lidia Navarro, Engineer; Albert Castell, PhD; Alvaro Ruiz-Pardo, PhD; Servando Alvarez, PhD; Luisa F. Cabeza, PhD

Thermal analysis of a ventilated facade with PCM for cooling applications

Alvaro de Gracia[1], Lidia Navarro[1], Albert Castell[1], Álvaro Ruiz-Pardo[2], Servando Alvárez[2], Luisa F. Cabeza[1]

[1]GREA Innovació Concurrent, Universitat de Lleida, Edifici CREA, Pere de Cabrera s/n, 25001, Lleida, Spain. Tel: +34.973.00.35.77. Email: lcabeza@diei.udl.cat
[2]Grupo de Termotécnia, Universidad de Sevilla, Escuela de Ingenieros Camino de los Descubrimientos s/n. 41092, Seville, Spain, Phone: 34-954487471, Email: arp@esi.us.es

Abstract

A new type of ventilated facade (VF) with macro-encapsulated phase change material (PCM) in its air cavity is presented in this paper. The thermal performance of this special building envelope is experimentally tested to analyse its potential in reducing the cooling demand during the summer season in the Continental Mediterranean climate. Two identical house-like cubicles located in Puigverd de Lleida (Spain) were monitored during summer 2012, and in one of them, a ventilated facade with PCM was located in the south wall. Six automatized gates were installed at the different openings of the channel in order to control the operational mode of the facade. This versatility allows the system to be used as a cold storage unit, as an overheating protection system or as a night free cooling application. The experimental results point out the night free cooling effect as the most promising operational sequence to reduce the cooling load of the cubicle. On the other hand, the thermal resistance of the outer skin of the facade must be increased; otherwise the cold storage system cannot be used efficiently.

Key-words: Ventilated facade (VF), phase change materials (PCM), buildings, experimental measurements, cooling applications, energy efficiency.

1. Introduction

The high energetic demand in the building sector is becoming a critical issue worldwide. The European Directive 2010/31/EU [1] stands that by 2020 the new buildings in the EU must consume "nearly zero" energy and highlights the importance of stimulating the transformation of refurbished buildings into very low energy buildings. Within this context, the study of the energetic design of buildings and their envelopes has become an important issue for the scientific community. Moreover, the importance to avoid overheating during the summer season is also highlighted in the European Directive 2010/31/EU as an important goal for the future buildings, not only in warm climate countries, but in all Europe.

One of the most important methods of reducing the energetic demand of a building is by carefully designing its facade. In this sense, a ventilated facade with phase change material (PCM) in its air cavity is presented in this research. PCM have been intensively studied for building applications [2,3] and their potential to reduce the energy consumed in buildings have been demonstrated both for passive [4,5] and active systems [6,7].

Moreover, ventilated facades (VF) have been presented as interesting constructive systems to match the energetic restrictions required by the European Directive, and as a suitable tool to improve the energetic efficiency of refurbished buildings. According to Shameri et al. [8] VF systems have great potential for decrease energy consumption in wide ranges of research areas. These facades are special types of envelopes, where a second skin is placed in front of a regular building facade, creating an air space in between, named the channel [9].

Thermal benefits of using double skin facades and ventilation aspects have been studied numerically and experimentally over the last 20 years. The high costs of these constructive systems have caused that numerical studies have been more popular and abundant in the literature. The existing numerical methods used to predict the thermal performance of ventilated facades can be grouped as analytical and lumped models [10,11], non-dimensional analysis [12], network models [13-15], control volume [16-18], zonal approach [19], and Computational Fluid Dynamics (CFD) [20,21].

Nevertheless, other than the numerical studies, important effort has also been done in the experimental field for better understanding these systems and to provide data and tools which might be used to improve its thermal design. Many aspects have been investigated experimentally, such as, the effect of different angle of the solar shading device [22], the influence of the wind and speed direction [23], and the natural ventilation in a narrow double-skin facade cavity [24].

The overall thermal performance of the double skin facade has been also experimentally evaluated. Huckemann et al. [25] presented a long-term monitoring of 28 different buildings with and without VF. In order to analyse the thermal comfort inside those buildings, the measured data is discussed simultaneously with a questionnaire given to office users. It was concluded from the measured data and the questionnaires that the buildings with double skin facades have slightly better thermal performance than the single skin facade buildings. Moreover, Xu and Ojima [26] performed a set of experiments under different weather conditions in a double skin facade of a two-story house in Japan. It was measured that the stack effect in the channel during summer reduces the cooling loads in a 10-15% and increases the thermal lag between solar radiation and inner room temperature (3-4 hours). Moreover, the green-house effect during winter saves 20-30% of the energy consumed for space heating, and natural ventilation and sun shading modes are proposed for intermediate weather seasons.

The present paper evaluates experimentally the thermal performance of a ventilated facade with phase change material (PCM) in its channel. The same experimental facility has been used to test a similar ventilated facade but with an outer glassed skin for heating purposes under winter conditions by de Gracia et al. [27], registering between 19% and 26% of energy savings, depending on the HVAC set point. It was also demonstrated that the PCM inside the air cavity increases the heat storage capacity of the system.

This paper presents the set of experiments performed during summer 2012 in Puigverd de Lleida (Spain) to evaluate the potential of this constructive system to reduce the cooling loads of a single family house. Moreover, the inclusion of this technology in real buildings might be specifically analyzed for each case using simulation tools. This

paper provides useful experimental data which might be used to validate numerical models.

2. Experimental set-up

The experimental facilities used to evaluate the thermal performance of a ventilated facade with PCM during summer period consist of two identical house-like cubicles with the same inner dimensions (2.4 m x 2.4 m x 5.1 m). The cubicles were designed so they are big enough to be representative of a room but small enough to present an achievable cost.

The only difference between the two cubicles is that one of them is equipped in the south wall with a ventilated facade with PCM inside its air chamber, while the other cubicle keeps the basic constructive system. Both cubicle, reference (REF) and ventilated facade (VF) are shown in Figure 1.

The ventilated facade presents an air channel of 15 cm thick which represents 0.36 m^2 of channel area ($A_{channel}$). The inner layer is based on the alveolar brick constructive system [28,29] while the outer envelope is made by a glass layer. An extra outer layer of expanded polyurethane panels was placed to cover the transparent glazing during the summer period since solar radiation inside the cavity must be avoided for cooling purposes. Both roofs were made using concrete pre-cast beams, 8 cm of polystyrene and 5 cm of concrete slab. The polystyrene is placed over the concrete and it is protected with a cement mortar roof with an inclination of 3%, a double asphalt membrane and 5 cm of gravel. The constructive system used in both cubicles is presented in Figure 2. Moreover, the thermo-physical properties of the used materials are detailed in Table 1.

Six automatized gates (Figure 3) were installed at the different openings of the channel in order to control the operational mode of the facade. These gates are controlled by ST450N linear spindle actuators. Moreover, three fans (FCL 133 Airtecnics), of 40 W each, were placed at the inlet of the air channel to provide mechanical ventilation when needed. The system which controls the fans and gates is programmed in a Microchip 18F45J10, and allows the system to operate under the following modes:

- PCM solidification period (Figure 4a): During the night time, the air enters to the channel from the outer environment, solidifies the PCM and is pumped outdoors. This mode uses the fans (mechanical ventilation) to ensure the complete solidification of all the PCM. The use of this system in different regions is mainly restricted by the night outer temperatures. Since the PCM has to be fully solidified during night time, the outer temperature must be lower than the phase change temperature during this period
- PCM melting period (Figure 4b): The air is cooled down by the PCM and is pumped to the inner environment.
- Overheating prevention period (Figure 4c): After the cold stored in the PCM has been released to the air, the system lets the air flow from outdoors to outdoors due to the buoyancy forces. This mode prevents the overheating effect in the air channel.
- Night ventilation (Figure 4d): The air is pumped from outdoors to indoors through the VF and is removed from the inner environment to achieve a free cooling effect, using a one-way ventilation grid installed in the door of the cubicle. The high thermal mass of the alveolar brick constructive system produces a high thermal lag between the outer heat flux and the inner one. Hence, the night ventilation can deal with the peak load and reduce significantly the use of HVAC. Note that the "PCM solidification period" must be finished before the night ventilation can start, otherwise the melted PCM would heat up the air and produce an extra cooling load. The authors want to clarify that this effect is not exclusive of the described constructive system. However, the versatility of the ventilated facade allows to test this effect and to control its timing.

The PCM used inside the air channel was the macro-encapsulated CSM panels of salt hydrate SP-22 from Rubitherm. This PCM present a heat storage capacity of 150 kJ/kg in a temperature range from 15ºC to 30ºC. The selection of this PCM (melting and solidification temperature at 22 ºC and 18 ºC, respectively) allows the ventilated facade to be used as a cold storage system during summer periods using the night free cooling effect. A total of 112 PCM panels (1.4 kg of SP-22 each) were distributed over the

facade creating 14 air flow channels as shown in Figure 5. More detailed information about the thermo-physical properties and safety requirements can be found in [30].

Both cubicles were fully instrumented and the following data was registered at 5 min intervals to evaluate their thermal performance:

- Internal wall temperatures (east, west, north, south, roof and floor) measured with Pt-100 DIN B with a maximum error of ±0.3ºC.
- Indoor air temperature and humidity (at a height of 1.5 m and 4.5 m) measured with ELEKTRONIK EE21 with a maximum error of ±0.3ºC.
- Electrical consumption of the HVAC systems using an electrical network analyser (MK-30-LCD). Each cubicle is equipped with two heat pumps (Fujitsu Inverter ASHA07LCC), located at different heights (3 and 5 m).

Moreover, in order to analyse the behaviour of the ventilated facade with PCM, the following data was also measured:

- Air temperature of the cavity at different heights and locations (10 Pt-100 with an irradiative cover) with a maximum error of ±0.1ºC.
- Air velocity of the cavity at different heights and locations (4 hot wire sensors KIMO CTV 210) with an accuracy of 3% of the reading.
- Pressure drop across the air cavity (KIMO CP 200) with an accuracy of 1% of the reading.
- Outer and inner skin surface temperature (polyurethane panel and alveolar brick, respectively) at different heights and locations (4 Pt-100 each) with a maximum error of ±0.3ºC.
- External surface temperature at different heights and locations (6 Pt-100) with a maximum error of ±0.3ºC.
- Heat flux transferred to indoor (2 HUKSEFLUX HFP01) with an accuracy of 5% of the reading.
- Heat flux transferred to the front and back surface of a PCM panel (2 HUKSEFLUX HFP01).
- Temperature of the PCM at three different heights (3 Thermocouples Type T, 0.5 mm thick inserted in the PCM panels) with an accuracy of 0.75% of the reading.

- Front and back surface temperature of the PCM panels (2 Thermocouples Type T).

In addition, the weather data was also registered every 5 minutes:

- Two Middleton Solar pyranometers SK08 were used to capture the horizontal and vertical global solar radiation with an accuracy of 5% of the reading.
- The outer air temperature and humidity were measured using an ELEKTRONIK EE21 with a metallic shield to be protected against radiation.
- Wind speed and direction was provided by a DNA 024 anemometer.

3. Methodology

A set of experiments were carried out during summer 2012 period in order to test the thermal performance of the previously described ventilated facade for cooling purposes under different weather and operational conditions. Five experiments are analysed in this paper to highlight how the use of this system could reduce the electrical energy consumption of the installed heat pumps.

The different weather conditions analysed in this work were grouped as severe and mild summer. The experiments under severe summer conditions were tested during the months of July and August, with an outer temperature oscillating from around 18 ºC to 34 ºC. On the other hand, the mild summer conditions tests were performed during the months of June and September 2012, with an outer thermal oscillation of 14 ºC to 32 ºC. The authors have discerned between these two periods for the thermal analysis of the whole system because it is very important to ensure that the PCM can be completely solidified every cycle. The PCM can be fully solidified only when the outer temperature during the night time drops below 18ºC.

Moreover, in order to take advantage of the versatility of the ventilated facade, two different sequences of operation were tested:

- Cold storage sequence: First the PCM is solidified during night time using the "PCM solidification period" mode with mechanical ventilation, as shown on Figure 4a. This mode is typically programmed from 2 to 8 a.m. (see Table 2 for

details). Hereafter, the cold is stored inside the VF until is needed and all the openings of the VF are closed to minimize the heat gains from the outer environment. Once the demand requires a cooling supply, the cold is released to the air with mechanical ventilation as shown on Figure 4b (typically from 11 to 13 hours). After all the available cooling has been pumped to the inside, the VF starts the "overheating prevention period", where using the natural ventilation mechanism reduces the overheating effect (Figure 4c).

- Night free cooling sequence: During these experiments, the cold storage sequence is also programmed, but with one difference. During the night time, after the heat stored in the PCM is released to the outer environment, air from the outside is injected mechanically to the inside (Figure 4d), producing a night free cooling effect (typically from 4 to 8 a.m).

The set of experiments which are discussed in this paper are detailed in Table 2.

In order to analyse the potential of the cold storage sequence operating under different modes, and the potential of the night free cooling effect, some parameters were defined. The cold storage efficiency (ε_C) is given as the ratio between the amount of cold released to the inner environment (Q_r), by the amount of cold that the system stores during the night time (Q_{st}), as shown in Equation 1. The average velocity vair is considered to be 0.85 times the maximum velocity at the centre of the channel, since the flow is in turbulent regime [31].

$$\varepsilon_C = \frac{Q_r}{Q_{st}} \quad \text{(Eq.1)}$$

where,

$$Q_r = A_{channel} \cdot \rho_{air} \cdot Cp_{air} \cdot \int_{t_i}^{t_e} v_{air} \cdot (T_{inlet} - T_{outlet}) dt \quad \text{(Eq.2)}$$

$$Q_{st} = A_{channel} \cdot \rho_{air} \cdot Cp_{air} \cdot \int_{t_i}^{t_e} v_{air} \cdot (T_{outlet} - T_{inlet}) dt \quad \text{(Eq.3)}$$

The experimental values of Q_r and Q_{st} have a relative error of 4% due to the propagation of error in the measurement devices.

The amount of useful cold injected to the cubicle due to the night free cooling effect is also quantified (also with a relative error of 4%). It is calculated using the enthalpy gradient between the injected air from the facade at T_{outlet} and the air inside the cubicle at a certain set point temperature of the HVAC ($T_{S.P.}$) which is removed to the outer environment, as shown in Eq. 4:

$$Q_{vent} = A_{channel} \cdot \rho_{air} \cdot Cp_{air} \cdot \int_{t_i}^{t_e} v_{air} \cdot (T_{outlet} - T_{S.P.}) dt \qquad \text{(Eq.4)}$$

Note that the reference temperature used to calculate the useful cold injected is not the temperature of the inner environment. This is because the air can only reduce the cooling load if injected at lower temperature than set point.

4. Results and Discussion

4.1 Experiment 1

The first experiment was performed from 25th to 27th of May 2012 under mild summer weather conditions. The outer temperature oscillated from 32 ºC to 13 ºC and solar radiation daily peaks of around 1000 W/m^2 were registered. The set point of both cubicles (VF and REF) was fixed at 23 ºC during the whole experiment. The electrical network analyser installed at each heat pump showed that the heat pump of the cubicle with the ventilated facade have consumed 10.76 MJ to keep the inner environment at the set point, while the ones of the reference cubicle have only consumed 6.94 MJ. This increment in the energy consumed by the VF cubicle is due to an inefficient use of the ventilated facade. Figure 6 will be used to explain the reasons why the ventilated facade has increased instead of reduced the cooling load of the cubicle. The figure shows the thermal evolution of the outer and both inner environments (VF and REF cubicles), the air at the inlet and outlet of the channel and the temperature inside a PCM panel located at the outlet of the channel.

First, it can be seen from the air channel temperature that the period when the PCM releases the cold stored to the air was programmed too late (it starts at 14 h), and hence the cold stored in the PCM was too long exposed to thermal heat gains from the outer environment. Note that even though the PCM and air inside of the channel drop to 13 ºC during the "PCM solidification period", its temperature raises up to 20 ºC and 26 ºC, respectively, before its use. Therefore, the first injection of air inside the cubicle was warmer than the set point (23ºC), producing an extra cooling load and making the heat pump of the VF cubicle start up, while the other heat pump (REF) did not need to cool down the inside environment. Moreover, the PCM is not fully melted during the "PCM melting period", since the set point of the heat pumps was programmed at 23 ºC, which was inside the phase change thermal range. Thus makes the use of the available latent heat useless for cooling purposes.

This inefficient operational mode makes the facade give an average cold release of 2.03 MJ/day (Q_r), although it has stored 32.4 MJ/day (Q_{st}), which makes a cold storage efficiency ε_C of 6.2%.

In addition, Figure 6 also shows that the inlet temperature of the channel is not equal to neither the indoor temperature nor the outdoor, which coincides with the measurements and simulations performed by Saelens et al. [32]. This research stated that in order to estimate the inlet temperature entering in a ventilated facade, the heating and cooling due to contact with the bounding surfaces must be taken into account, as well as the heating due to solar radiation.

4.2 Experiment 2

This experiment was tested from 25th to 28th of July 2012 under severe summer weather conditions and the set point of the heat pumps was programmed at 25 ºC. The outer temperature oscillated from 36 ºC to 18 ºC and vertical solar radiation daily peaks of around 900 W/m^2 were registered.

The electrical energy consumed by the heat pump installed at the VF cubicle presents during this experiment a reduction of 16 % in comparison to the reference, and the

average cold storage efficiency ε_C was 10.86 %. Figure 7 shows the temperature evolution of the PCM panels located at the outlet of the facade, the air channel and the inner and outer environments during the 26th of July. The heat gains from the outer environment before the "PCM melting period" (11 to 13 h) have been significantly reduced, since only 2 ºC were increased in the PCM. However, even though the PCM starts to release the cold stored at 20 ºC, it is in liquid state, and hence it cannot release any cold energy through its melting process. The PCM is in liquid state, because not only the solidification process of SP22 starts at 18ºC, but an important subcooling of 2 ºC has been also measured in previous experiments with SP-22 [27]. This lack of the phase change strongly limits the capacity of the system in keeping the air injected to the room below the set point. That is the reason why the heat pump of the VF cubicle has to cool down the air in the last part of the period when the PCM release the cold stored to the air. The authors want also to highlight that the period between the PCM melting and solidification periods (from 13 h to 2 h) is not only preventing successfully the overheating effect, but it keeps the air temperature inside the cavity lower than the outer environmental temperature. Hence the cubicle is exposed to less heat gains through this envelope, which produces a reduction in the energy consumed by the heat pump during the period.

4.3 Experiment 3

The experiment 3 was also tested under severe summer weather conditions (25th to 28th of August 2012) and the set point of the heat pumps was programmed at 25 ºC. As it can be seen in Figure 8 the outer temperature was never below 18 ºC, hence no solidification process of the PCM occurred. The cold storage system has not been efficiently used during this period, and only during the second day of experiment it could inject cold during part of the "PCM melting period". Note that during the first and the third day, the system produced an extra cooling load since the air was injected at a temperature above the set point. The air flowing through the facade during the first and third day was also exposed to heat gains from the outer skin since high outer temperatures during the cold discharge (28-30 ºC) were registered.

However, the night free cooling effect has worked properly during the first and second nights since the PCM has been already cooled enough before the night ventilation starts (2 a.m.). On the other hand, during the third night, the PCM was still at 23 ºC due to high outer temperatures, limiting the potential of the night free cooling effect in reducing the electrical energy consumed by the heat pumps (it does stop cooling down the air at 4:20 a.m.). Although the cold storage system has been almost useless and the night free cooling was not optimized, the use of this ventilated facade reduced the electrical energy consumption of the heat pumps in a 23.1% during this experiment. This reduction is mainly due to the night free cooling effect injecting air below the set point, with an average of 34.9 MJ/day.

4.4 Experiment 4

The potential of the cold storage system and the night free cooling effect was also tested under mild summer weather conditions. From the 6th to 10th of September 2012, the outer temperature varied from 34 ºC to 14 ºC. This low value of minimum daily temperatures allowed the PCM to solidify, at least partially. Figure 9 presents the thermal profiles of the inner and outer environments during the whole experiment as well as the air temperature at the outlet of the channel. Both, the cold storage system and the night free cooling effect worked efficiently all the days, which reports in a 50.2 % of electrical energy savings of the heat pumps. Although most of the energy savings were produced due to the night free cooling (38.9 MJ/day (Q_{vent}), Figure 9), the cold storage system injects an average of 2.1 MJ/day (Q_r). The cold storage system only presents a storage efficiency of ε_C = 6.2 % because of the important heat gains through the outer skin. Even though the PCM could be partially solidified during the night period, and is still at low temperatures during the cold release, the metallic structure of the ventilated facade (Figure 5) acts as an important thermal bridge and limits drastically the potential of the cold storage system.

4.5 Experiment 5

This experiment was performed from 18th to 25th of September 2012 and demonstrated that the system is able to improve the thermal performance of the building in spite of the

weather variations occurring during the last summer weeks. As shown in Figure 10, the heat pump installed in the cubicle with the ventilated facade did not need to cool down the air at any time during the whole week to preserve the thermal requirements, while the one in the reference cubicle (REF) has consumed 12.66 MJ in the last four days. The cold storage system has been able to inject an average of 2.8 MJ/day (Q_r), except during the first and sixth cold discharges because of high night temperatures. Moreover, night free cooling has been also clearly affected during these two days. However, the system could inject an average Q_{vent} of 46.7 MJ/day.

Table 3 presents a summary of the main results extracted from the set of experiments performed during summer 2012. The thermal performance of the ventilated facade with PCM as well as the cooling demand depends strongly on the outer weather conditions and each experiment should be analysed separately, as it has been already done. However, some general comments related to the system and its operational mode can be given:

- The cold storage capacity of the system is very sensitive to the outer night temperature, being limited under severe summer conditions (Experiments 2 and 3). As it was previously discussed during this hot period, with minimum night temperatures of 18 ºC, the PCM could not be solidified due to the subcooling (2ºC) and its solidification range (typically 18–19ºC).
- Q_r should be maximized in order to take advantage of the cold storage system. However, the cold has to be delivered at a temperature below the set point of the heat pumps. Otherwise, the cold discharge supposes an extra heat gain to the cubicle (Experiment 1).
- The night free cooling effect has been proven to be an efficient operational sequence to reduce the cooling load of the cubicle. Its potential is, at least, 20 times higher than the potential of the cold storage system.
- The authors want to highlight that the energy consumptions presented in Table 3 do only refer to the heat pumps. If the electrical energy consumed by the fans is taken into account (120 W), the system with the ventilated facade presents in any case, the highest overall energy consumption. This is because the fans are pumping air not only during the "PCM melting period" (11 to 13 h), but during

the whole night period (0 to 8 h), as well. The authors suggest using natural night ventilation as a future solution to reduce the high electrical energy consumed by the fans. However, the system operating under natural ventilation might present different thermal performance and energy efficiency.

5. Conclusions

The thermal performance of a ventilated facade with macro-encapsulated PCM in its air channel is experimentally evaluated under summer conditions in this paper.

The experimental set-up consists of two identical house-like cubicles (2.4 x 2.4 x 5.1 m indoor dimensions), in which in one of them, a ventilated facade with macro-encapsulated PCM (SP 22) inside its air chamber is constructed in the south wall. The versatility of the ventilated facade allows the system not only to be programmed as a cold storage unit, but to use the night free cooling effect, as well. Five different experiments have been carried out in order to highlight the potential of these different sequences in reducing the electrical energy consumption of the installed heat pumps.

The experimental results demonstrated the high potential of the night free cooling effect in reducing the cooling loads of a building. This operation mode could inject air at a temperature below the set point under both severe and mild summer conditions (34.9 MJ/day and 42.8 MJ/day, respectively).

Regarding the potential of the cold storage sequence, the system presents low energy storage efficiency in all cases due to important heat gains through the outer skin. Moreover, the air temperature at the outlet of the channel must be monitored in order to prevent hot air injections, which might produce extra cooling loads. The set of experiments demonstrated that the cold storage system is almost useless unless the PCM has been fully solidified during the night period. Also, there is a necessity of improving the thermal resistance of the outer skin by supressing, when possible, the thermal bridges occurring through the metallic structural frame.

The system can prevent successfully the overheating effect between the PCM solidification and melting periods, being the air inside the cavity lower even lower than the outer environmental temperature during the peak load. Therefore, the cubicle is exposed to less heat gains through this envelope, which produces a reduction in the energy consumed by the heat pump during the period.

The thermal performance of this system is very sensitive to the weather conditions and the cooling demand of the final users, which makes essential the use of a programmable thermal control system in order to use efficiently the ventilated facade for cooling purposes.

Acknowledgements

This work was supported by the "Corporación Tecnológica de Andalucía" by means of the project "MECLIDE-Soluciones estructurales con materiales especiales para la climatización diferida de edificios" with the collaboration of DETEA. The work partially funded by the Spanish government (ENE2011-28269-C03-02 and ULLE10-4E-1305) and the European Union (COST Action COST TU0802). The authors would like to thank the Catalan Government for the quality accreditation given to their research group (2009 SGR 534).

References

[1] Directive 2010/31/EU of the European parliament and of the council of 19 May 2010 on the energy performance of buildings. Available from: http://www.epbd-ca.eu.

[2] L.F. Cabeza, A. Castell, C. Barreneche, A. de Gracia, A.I. Fernández, Materials used as PCM in thermal energy storage in buildings: A review, Renewable and Sustainable Energy Reviews 15 (2011) 1675-1695.

[3] A.M. Khudhair, M.M. Farid, A review on energy conservation in building applications with thermal storage by latent heat using phase change materials, Energy conversion and Management 45 (2004) 263-275.

[4] M.M. Farid, S. Behzadi, Energy storage for efficient energy utilization in buildings,

in: 1st International High Performance Buildings Conference, 12–15 July, Purdue University, USA, 2010.

[5] A. Castell, I. Martorell, M. Medrano, G. Perez, L.F. Cabeza, Experimental study of using PCM in brick constructive solutions for passive cooling, Energy and Buildings 42 (2010) 534–540.

[6] M. Koschenz, B. Lehmann, Development of a thermally activated ceiling panel with PCM for application in lightweight and retrofitted buildings, Energy and Buildings 36 (2004) 567-578.

[7] J.R. Turnpenny, D.W. Etheridge, D.A. Reay, Novel ventilation cooling system for reducing air conditioning in buildings. Part I: testing and theoretical modelling, Applied Thermal Engineering 20 (2000) 1019-1037.

[8] M.A. Shameri, M.A. Alghoul, K. Sopian, M. Fauzi, M.Zain, O. Elayeb, Perspectives of double skin façade systems in buildings and energy saving, Renewable and Sustainable Energy Reviews 15 (2011) 1468-1475.

[9] N. Safer, M. Woloszyn, J.J. Roux, Three-dimensional simulation with a CFD tool of the airflow phenomena in single floor double-skin façade equipped with a Venetian blind, Solar Energy 79 (2005) 193-203.

[10] J. von Grabe, A prediction tool for the temperature field of double facades, Energy and Buildings 34 (2002) 891-899.

[11] C. Park, G. Augenbroe, T. Messadi, M. Thitisawat, N. Sadegh, Calibration of a lumped simulation model for double-skin façade systems, Energy and Buildings 36 (2004) 1117-1130.

[12] C. Balocco, M. Colombari, Thermal behavior of interactive mechanically ventilated double glazed façade: Non-dimensional analysis, Energy and Buildings 38 (2006) 1-7.

[13] J. Hensen, M. Bartak, F. Drkal, Modeling and simulation of a double-skin façade system, ASHRAE Transactions 108 (2002) 1251-1259.

[14] W. Stec, D. van Paassen, Symbiosis of the double skin façade with the HVAC system, Energy and Buildings 37 (2005) 461-469.

[15] E. Gratia, A. De Herde, Optimal operation of a south double-skin façade, Energy and Buildings 36 (2004) 41-60.

[16] D. Faggembau, M. Costa, M. Soria, A. Oliva, Numerical analysis of the thermal behaviour of ventilated glazed facades in Mediterranean climates. Part I: development and validation of a numerical model, Solar Energy 75 (2003) 217-228.

[17] D. Saelens, J. Carmeliet, H. Hens, Energy Performance Assessment of Multiple-Skin Facades, HVAC&R Research 9 (2003) 167-185.
[18] P. Seferis, P. Strachan, A. Dimoudi, A. Androutsopoulos, Investigation of the performance of a ventilated wall, Energy and Buildings 43 (2001) 2167-2178.
[19] T.E. Jiru, F. Haghighat, Modeling ventilated double skin façade – A zonal approach, Energy and Buildings 40 (2008) 1567-1576.
[20] H. Manz, A. Schaelin, H. Simmler, Airflow patterns and thermal behavior of mechanically ventilated glass double façades, Building and Environment 39 (2004) 1023-1033.
[21] F. Patania, A. Gagliano, F. Nocera, A. Ferlito, A. Galesi, Thermofluid-dynamic analysis of ventilated facades, Energy and Buildings 42 (2010) 1148-1155.
[22] V. Gavan, M. Woloszyn, F. Kuznik, J.J. Roux, Experimental study of a mechanically ventilated double-skin façade with venetian sun-shading device: A full scale investigation in controlled environment, Solar Energy 84 (2010) 183-195.
[23] T. Pasquay, Natural ventilation in high-rise buildings with double facades, saving or waste of energy, Energy and Buildings 36 (2004) 381-389.
[24] N. Mingotti, T. Chenvidyakarn, A.W. Woods, The fluid mechanics of the natural ventilation of a narrow-cavity double-skin façade, Building and Environment 46 (2011) 807-823.
[25] V. Huckemann, E. Kuchen, M. Leão, E.F.T.B. Leão, Empirical thermal comfort evaluation of single and double skin façades, Building and Environment 45 (2010) 976-982.
[26] L. Xu, T. Ojima, Field experiments on natural energy utilization in a residential house with a double skin façade system, Building and Environment 42 (2007) 2014-2023.
[27] A. de Gracia, L. Navarro, A. Castell, A. Ruiz-Pardo, S. Álvarez, L.F. Cabeza, Experimental study of a ventilated facade with PCM during winter period, Energy and Buildings 10.1016/j.enbuild.2012.10.026.
[28] A.de Gracia, A. Castell, M. Medrano, L.F. Cabeza, Dynamic thermal performance of alveolar brick construction system, Energy Conversion and Management 52 (2011) 2495-2500.
[29] A. Castell, I. Martorell, M. Medrano, G. Pérez, L.F. Cabeza, Experimental study of using PCM in brick constructive solutions for passive cooling, Energy and Buildings 42 (2010) 534-540.

[30] Rubitherm Technologies GmbH. http//www.rubitherm.com

[31] G.S. Sawhney, Fundamentals of fluid mechanics, I.K. International Publishing House (2011), New Delhi.

[32] D. Saelens, S. Roels, H. Hens, The inlet temperature as a boundary condition for multiple-skin facade modelling, Energy and Buildings 36 (2004) 825-835.

Nomenclature

$A_{channel}$	Cross sectional area of the ventilated facade cavity [m2]
Cp_{air}	Air heat capacity [J kg-1 K-1]
Q_r	Cold energy released to the inner environment [J]
Q_{st}	Cold energy stored during the night period [J]
Q_{vent}	Cold energy injected to the inner environment during the night free cooling period [J]
t_i	Time at the beginning of the process (Table 2) [s]
t_e	Time at the end of the process (Table 2) [s]
T_{inlet}	Temperature at the inlet of the VF channel [K]
T_{outlet}	Temperature at the outlet of the VF channel [K]
$T_{S.P.}$	Set point temperature of the HVAC [K]
T	Time [s]
v_{air}	Developed flow air velocity [m/s]

Greek symbols

ρ_{air}	Air density [kg m^{-3}]
ε_C	Cold storage efficiency

Figure captions

Figure 1. Experimental set-up: reference (right) and ventilated facade (left) cubicles

Figure 2. Alveolar brick constructive system used in both cubicles

Figure 3: Automatized gates and fan distribution along the facade

Figure 4: Modes of operation of the ventilated facade

Figure 5: PCM distribution inside the air chamber.

Figure 6. Thermal profiles of PCM, air flow and inner and outer environment during 25th of May 2012

Figure 7. Thermal profiles of PCM, air flow and inner and outer environment during 26th of July 2012

Figure 8. Thermal profiles of PCM, air flow and inner and outer environment from 25th to 28th of August 2012. (CD) Cold discharge period, (NFC) Night free cooling period.

Figure 9. Thermal profiles of outlet air flow and inner and outer environment from 6th to 10th of September 2012. (CD) Cold discharge period, (NFC) Night free cooling period.

Figure 10. Thermal profiles of the outlet air flow and inner and outer environment from 18th to 25th of September 2012.

Table(s) with Caption(s)

Table 1: Thermo-physical properties of the used materials

	Material	Thermal conductivity (W/m·K)	Density (kg/m^3)	Specific Heat (J/kg·K)
Wall system	Cement mortar	0.7	1350	840
	Alveolar brick	0.27	1080	900
	Plastering	0.57	1150	900
Roof system	Polyurethane	0.034	35	1000
	Concrete precast beam	0.472	760	960
	Concrete	1.650	2150	960
	Double asphalt membrane	0.7	2100	920
	Crushed stones	2.0	1450	1050
Ventilated facade	Glass	0.053	1300	840
	Opaque insulation panel	0.034	35	1000

Table 2: Set of experiments description

Exp	Date	Fans flow rate	Heat Pumps Set point	PCM discharge period	Preventing overheating period	PCM charge period	Free cooling period
1	May 2012	0.9 m^3/s	23 ºC	14 to 19 h	19 to 3 h	3 to 8 h	-
2	July 2012	0.6 m^3/s	25 ºC	11 to 13 h	13 to 2 h	2 to 8 h	-
3	August 2012	0.6 m^3/s	25 ºC	11 to 13 h	13 to 0 h	0 to 2 h	2 to 7 h
4	September 2012	0.6 m^3/s	25 ºC	11 to 13 h	13 to 0 h	0 to 4 h	4 to 8 h
5	September 2012	0.6 m^3/s	25 ºC	11 to 13 h	13 to 0 h	0 to 4 h	4 to 8 h

Table 3: Summary of the main experimental results

	Q_{st} (MJ/day)	Q_r (MJ/day)	ε_C (%)	Q_{vent} (MJ/day)	HVAC DSF (MJ/day)	HVAC REF (MJ/day)	% HVAC Energy savings
Exp 1	32.40	2.03	6.20	-	3.44	2.31	- 48.9
Exp 2	20.25	2.20	10.86	-	10.07	12.29	18.06
Exp 3	25.93	0.10	0.39	34.90	6.43	8.37	23.2
Exp 4	33.62	2.12	6.31	38.94	1.53	3.07	50.16
Exp 5	29.85	1.85	6.20	46.67	0	1.81	100

Figure(s)
Click here to download high resolution image

Figure 1

Figure(s)
Click here to download high resolution image

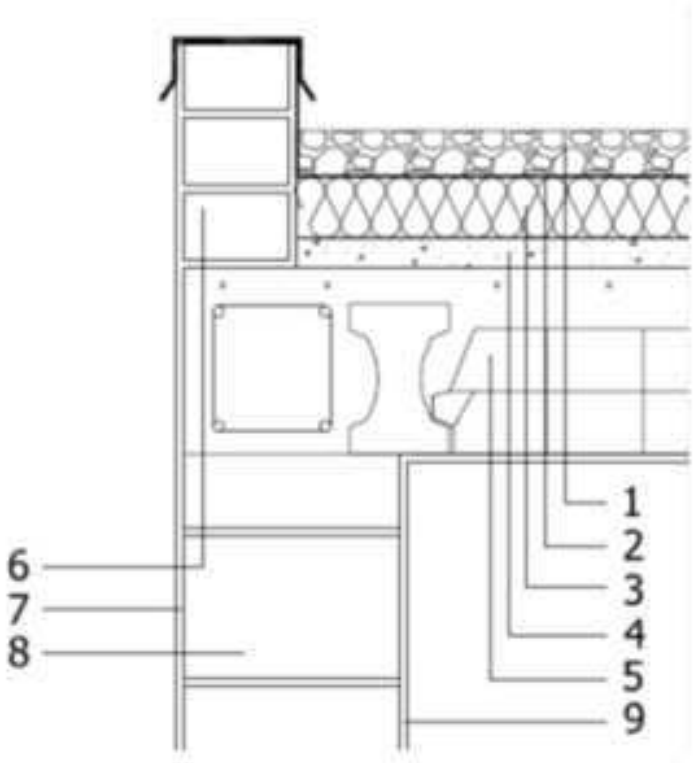

1. Gravel
2. Double asphaltic membrane
3. Polystyrene 8 cm
4. Cement mortar, flat roof 3% inclined
5. Concrete precast beams + 5 cm concrete slab
6. Hollow brick wall
7. Cement mortar finish
8. Alveolar brick wall 30x19x29 cm
9. Plaster plastering

Figure 2

Figure(s)
Click here to download high resolution image

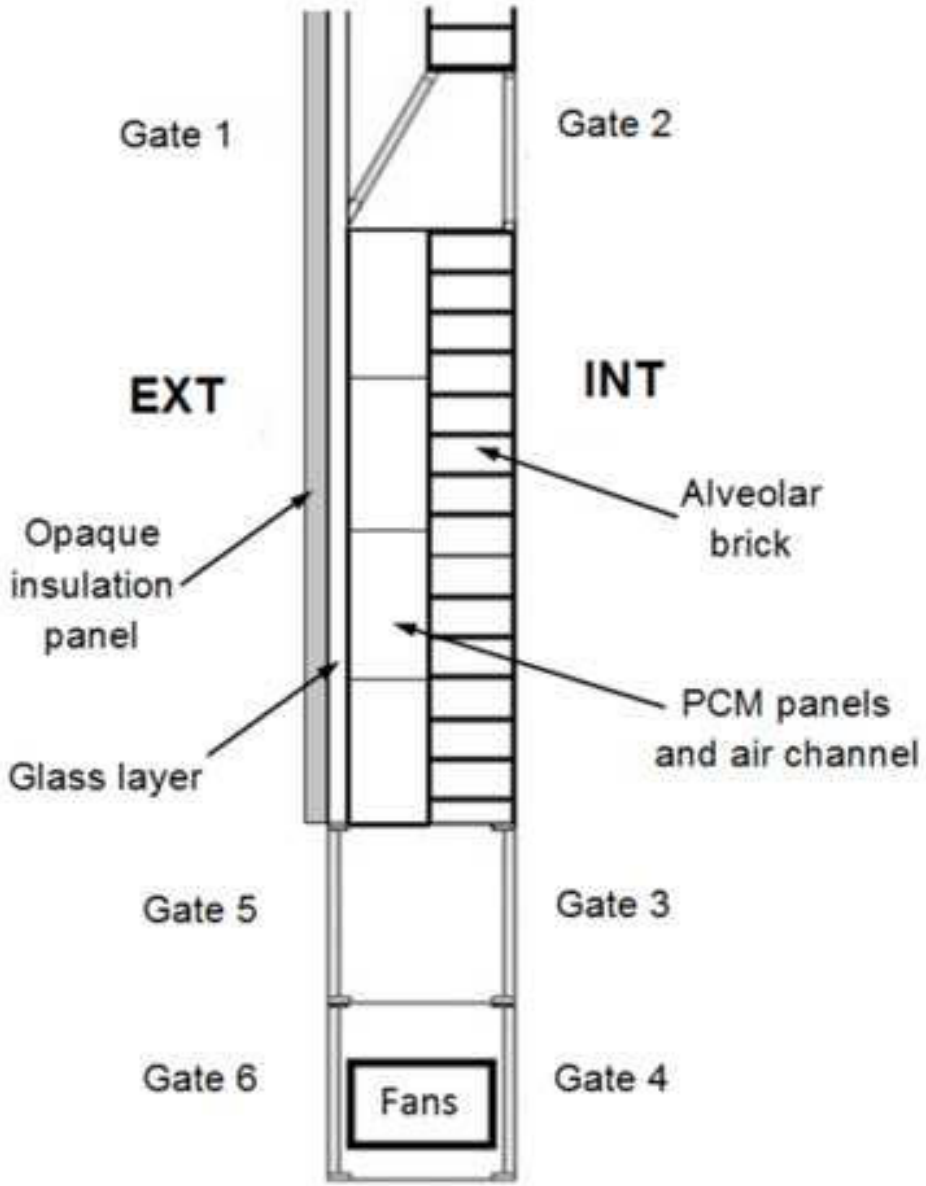

Figure 3

Figure(s)
Click here to download high resolution image

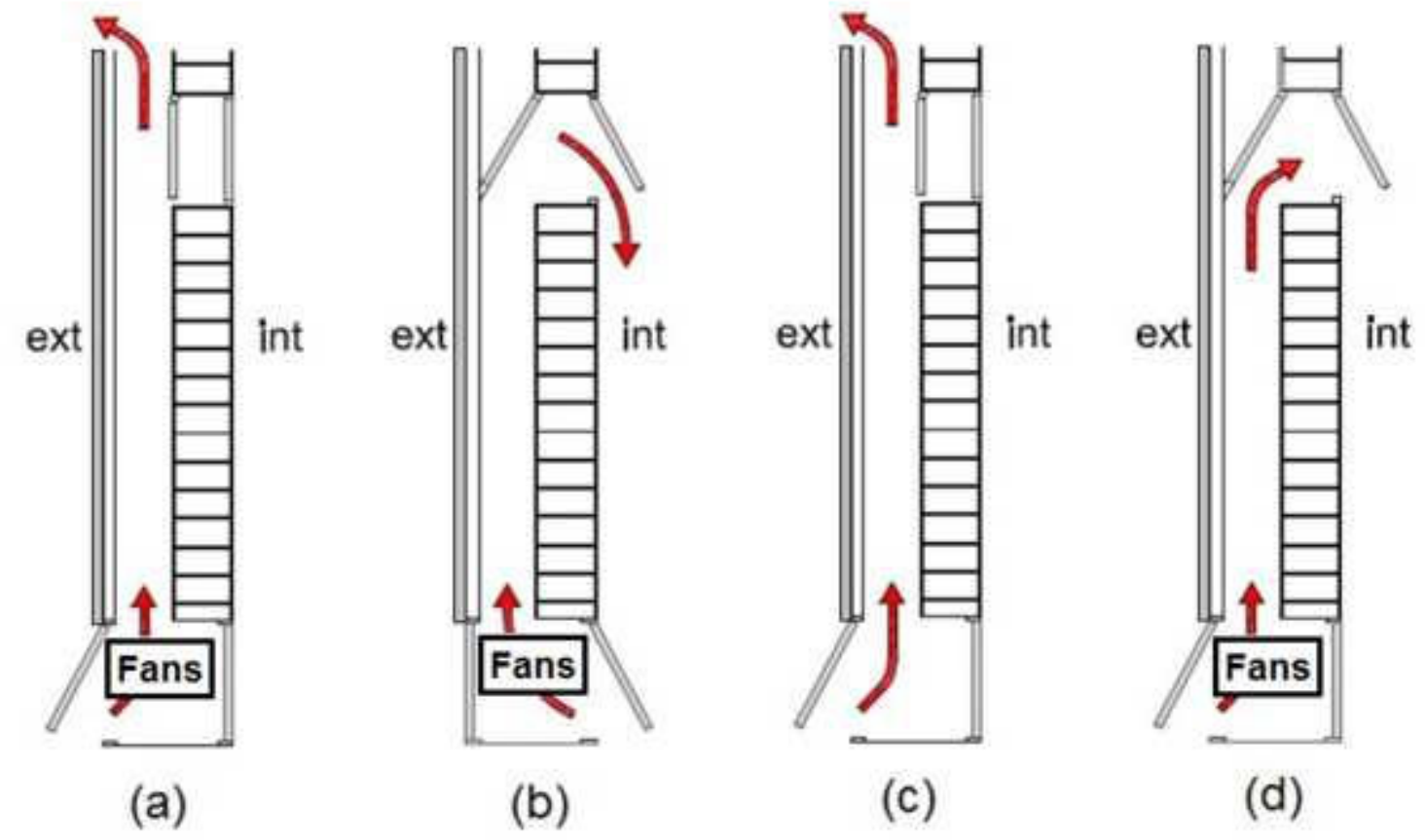

Figure 4

Figure(s)
Click here to download high resolution image

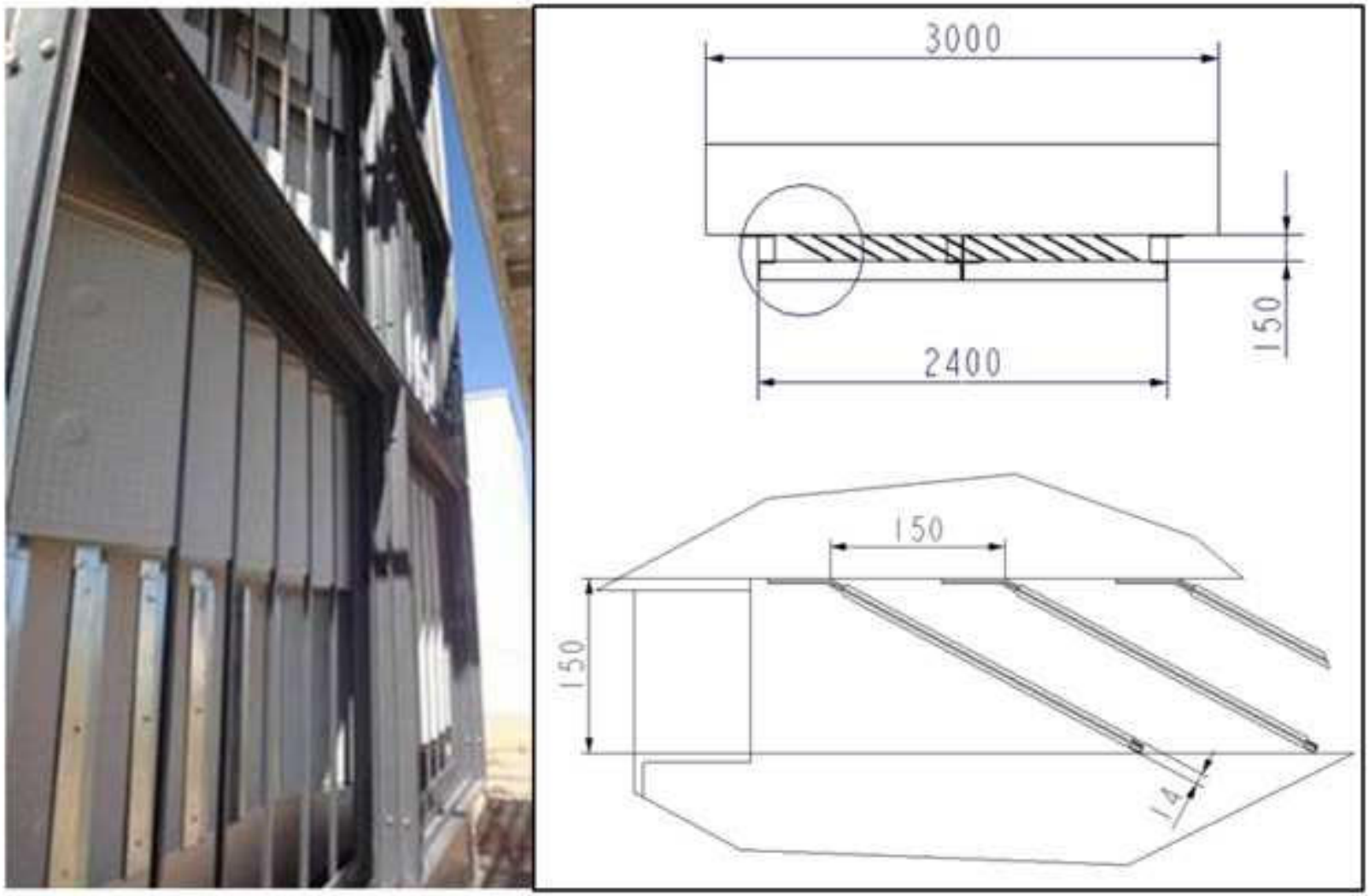

Figure 5

Figure(s)
Click here to download high resolution image

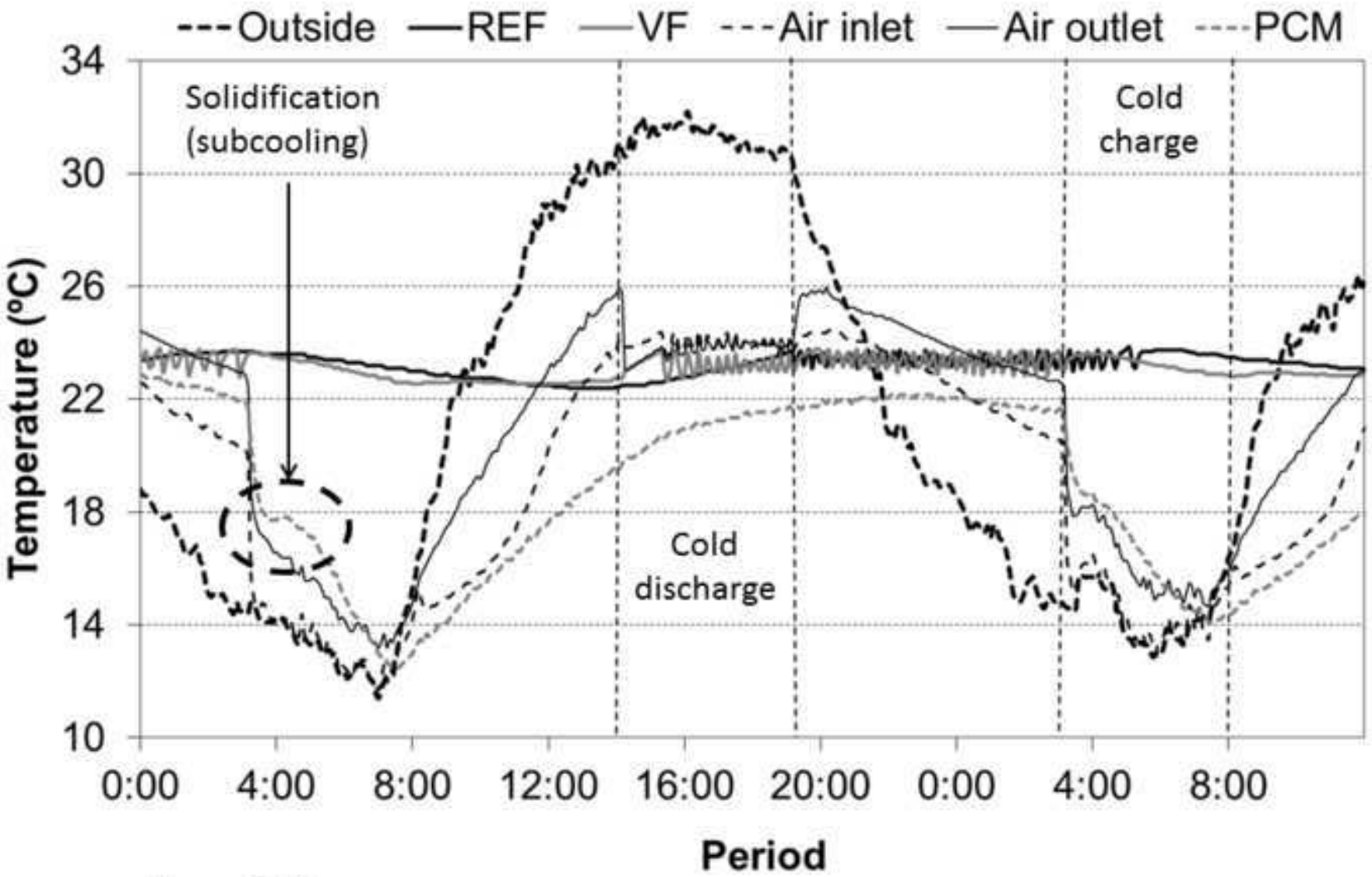

Figure 6 b/w

Figure(s)
Click here to download high resolution image

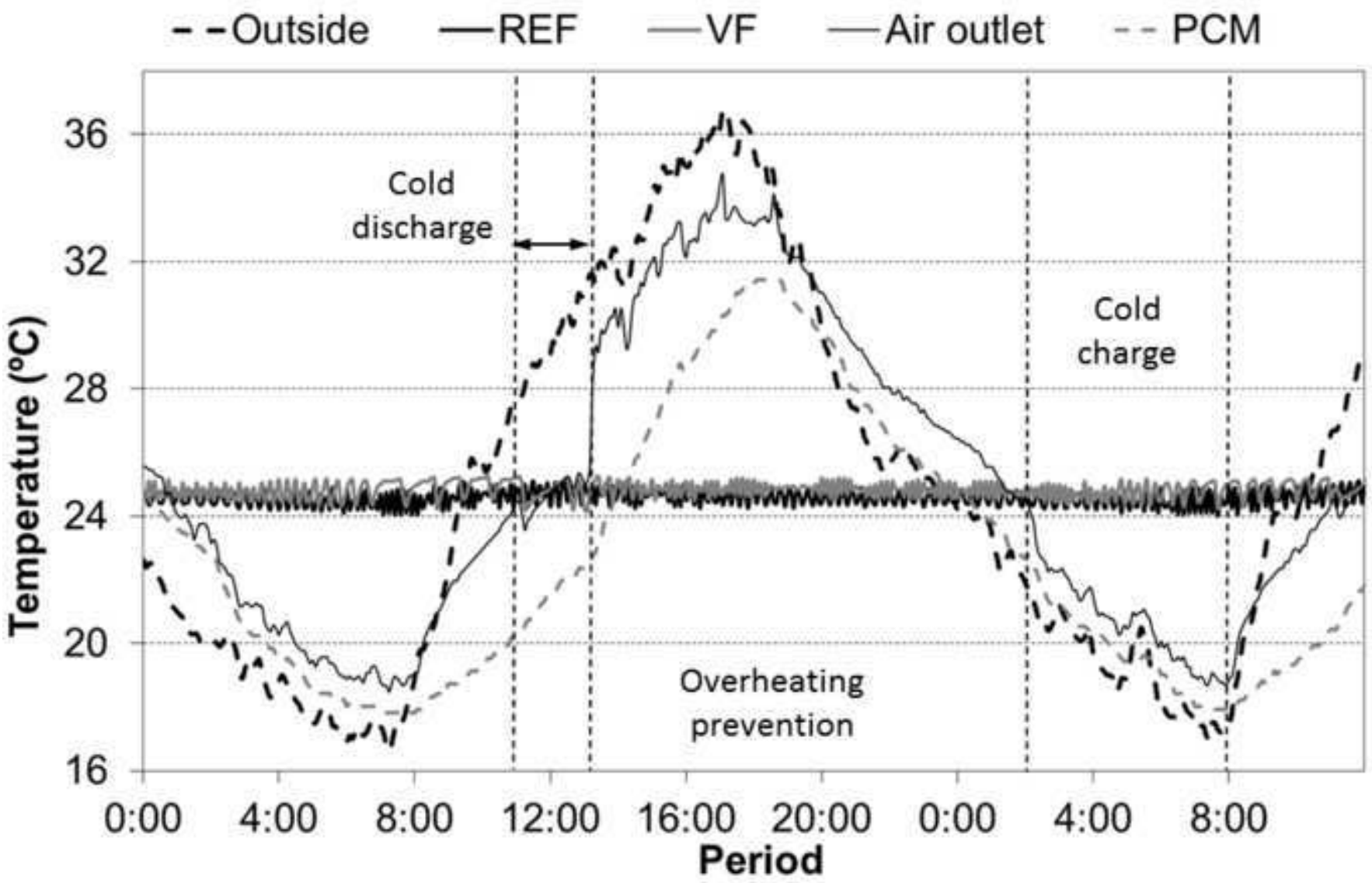

Figure 7 b/w

Figure(s)
Click here to download high resolution image

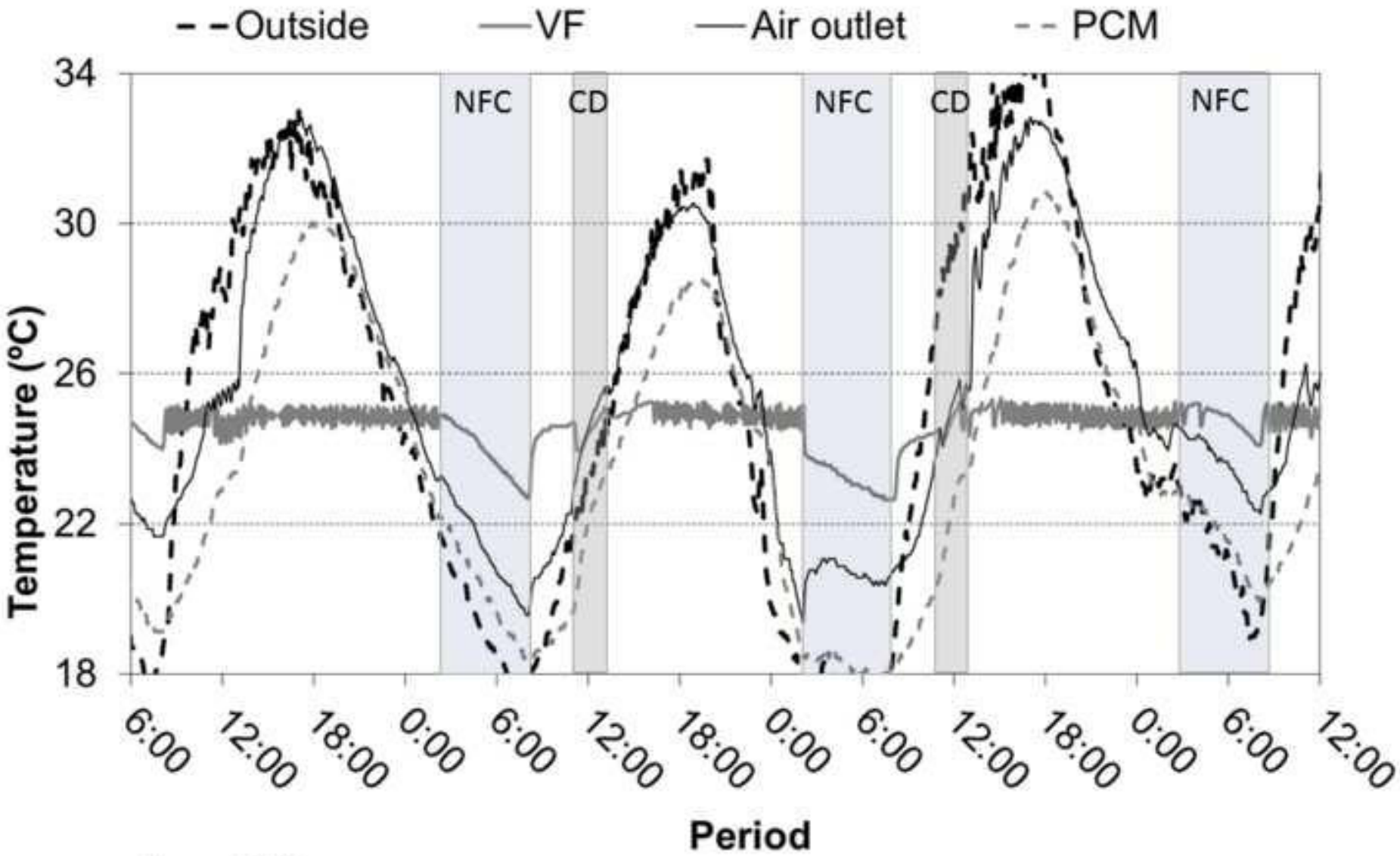

Figure 8 b/w

Figure(s)
Click here to download high resolution image

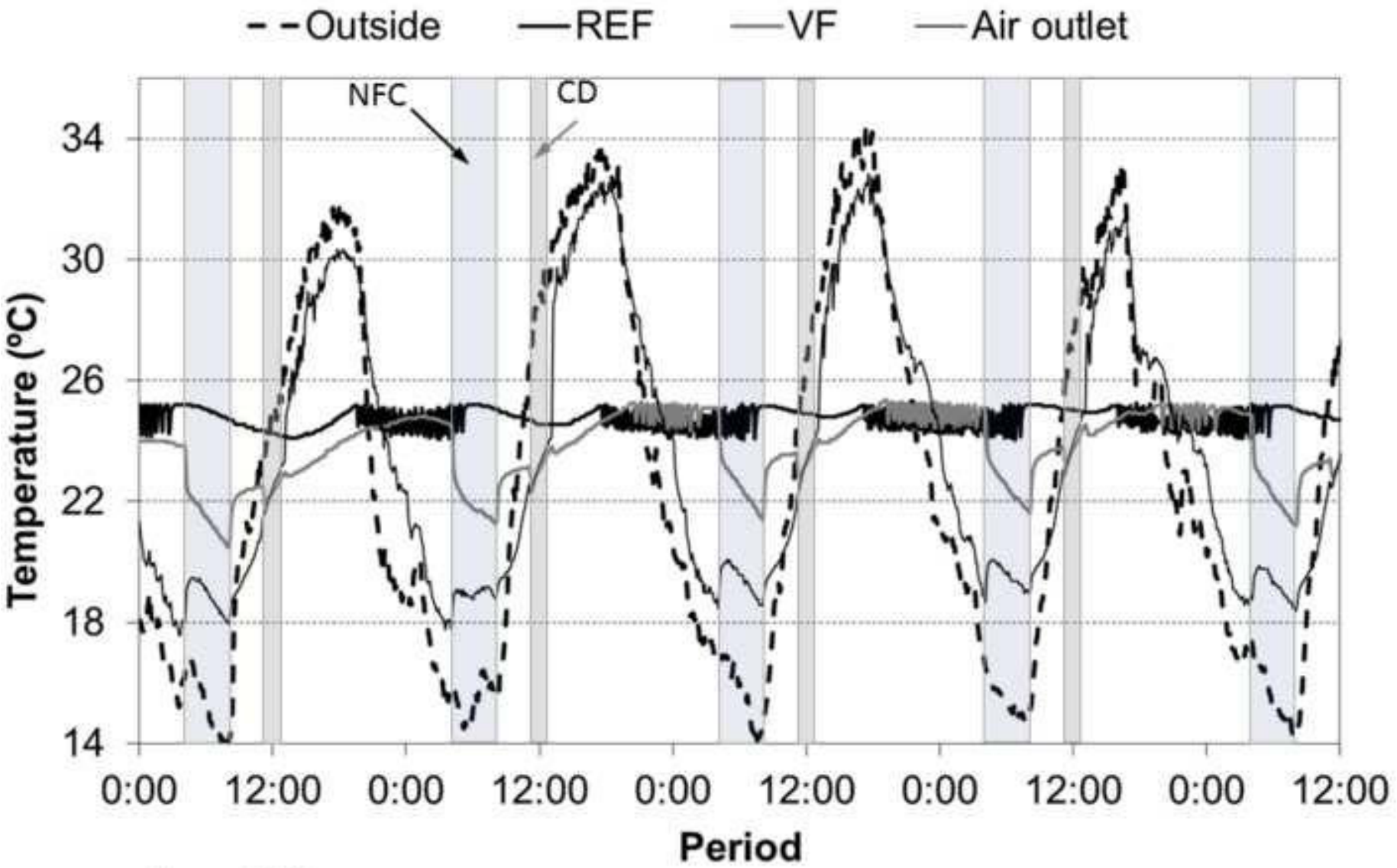

Figure 9 b/w

Figure(s)
Click here to download high resolution image

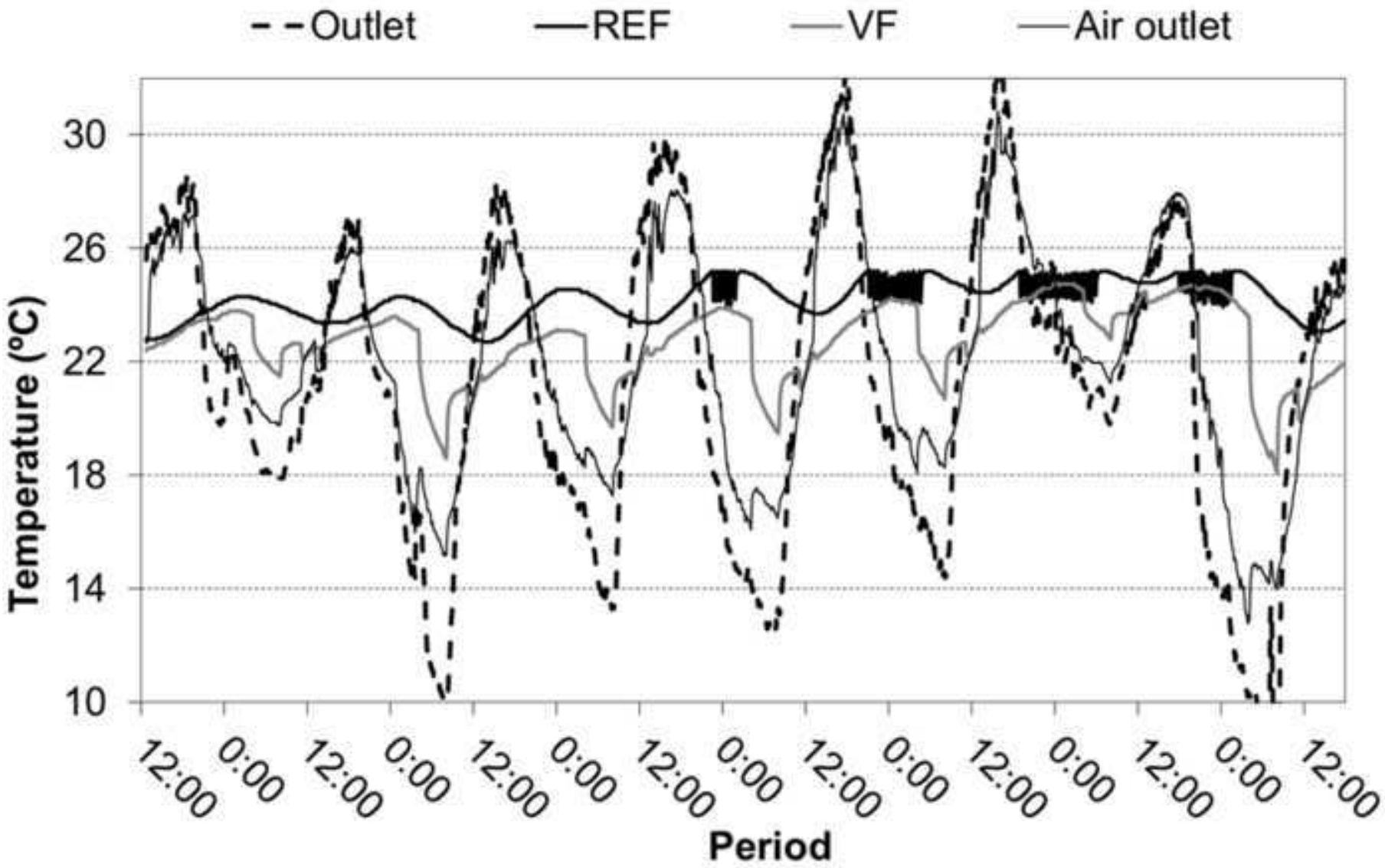

Figure 10 b/w

6 Life Cycle Assessment of a ventilated facade with PCM in its air chamber

6.1 Introduction

The potential of the ventilated facade with PCM in reducing the energetic consumption of a building has been experimentally demonstrated. The reduction of the heating and cooling demands helps strongly to reduce the environmental impact of the buildings during their operational phase. However, the use of this new constructive system could lead to high energy consumptions during the manufacturing and dismantling phase of the building.

LCE studies are useful to determine the energetic balance of a building during its whole lifetime [56,57]. However, they do not take into account important environmental aspects, such as how the operation, construction, dismantling and maintenance of the building affect the human health, the eco-system quality, or the use of the available fossil resources. The process to quantify and evaluate this environmental balance is known as life cycle assessment (LCA).

This methodology has been already used to evaluate the environmental consequences due to possible improvements in building envelopes, such as the use of different insulating materials [58,59], or the implementation of PCM as passive system to increase the thermal energy storage capacity [60-62]. The results regarding the use of PCM as passive systems, demonstrated that the inclusion of paraffin or salts hydrates did not improve significantly the environmental impact, since these PCM were only designed to reduce the cooling demand of the cubicles. Therefore, they were not used during most part of the year.

6.2 Contribution to the state-of-the-art

In order to determine the potential in reducing the environmental impact of the whole building by using PCM in active systems, this paper presents an LCA study which is carried out based on the impact assessment method EcoIndicator 99 [63,64].

- A. de Gracia, L. Navarro, A. Castell, D. Boer, L.F. Cabeza. Life cycle assessment of a ventilated facade with PCM in its air chamber. Solar Energy, submitted SE-S-2013-00328

The ventilated facade with PCM in its air cavity causes an important increment in the environmental impact during the manufacturing/dismantling phase of the building. Taken into account that the whole DSF system increases 196.9 impact points the manufacturing/dismantling environmental cost, it is important to highlight that the steel used in the DSF is responsible of more than 55% of this increment (110.5 impact points).

On the other hand, the efficient use of the ventilated facade leads to a significant reduction of the electrical energy consumption of the HVAC system both for heating and cooling purposes. These energetic reductions cause environmental savings during the operational phase.

The overall analysis shows that the use of the DSF with PCM in its air chamber reduces by 7.7 % the environmental impact when operating during 50 years. As shown in Figure 18, the environmental payback of the system is 30 years.

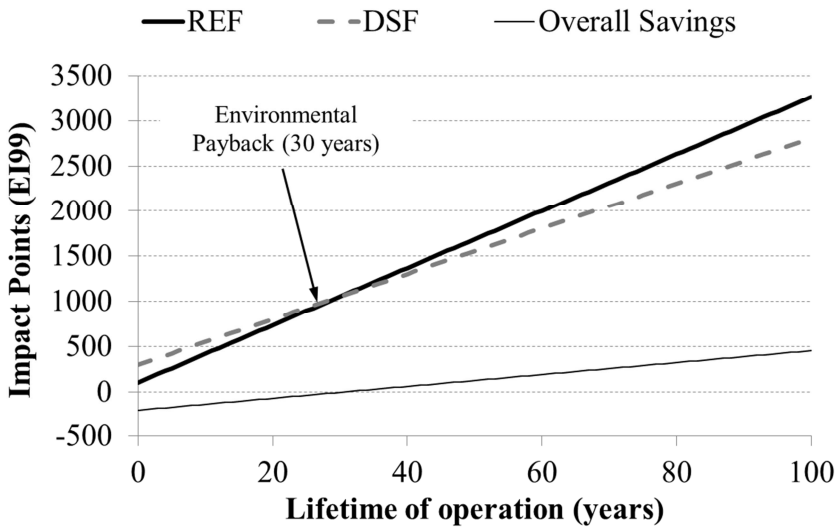

Figure 18. Overall impact points evolution depending on the lifetime of operation

As it was previously pointed out, more than half of the impact points during the manufacturing phase are due to the use of a metallic structure. The environmental payback of the system with a wooden structure instead of the metallic one, would be reduced to 6 years.

6.3 Journal paper

Elsevier Editorial System(tm) for Solar Energy
Manuscript Draft

Manuscript Number:

Title: Life Cycle Assessment of a Ventilated Facade with PCM in its air chamber

Article Type: Special Issue: Solar Heating & Cooling

Keywords: Life cycle assessment (LCA); Ventilated double skin facades (VDSF); Phase change materials (PCM); Energy efficiency

Corresponding Author: Prof. Luisa F. Cabeza, PhD

Corresponding Author's Institution: Universitat de Lleida

First Author: Alvaro de Gracia, Engineer

Order of Authors: Alvaro de Gracia, Engineer; Lidia Navarro, Engineer; Albert Castell, PhD; Dieter Boer, PhD; Luisa F. Cabeza, PhD

Life Cycle Assessment of a Ventilated Facade with PCM in its air chamber

Alvaro de Gracia[1], Lidia Navarro[1], Albert Castell[1], Dieter Boer[2], Luisa F. Cabeza[1]

[1]GREA Innovació Concurrent, Universitat de Lleida, Edifici CREA, Pere de Cabrera s/n, 25001, Lleida, Spain. Tel: +34.973.00.35.77. Email: lcabeza@diei.udl.cat

[2]Department of Mechanical Engineering, Universitat Rovira i Virgili, Av. Paisos Catalans 26, 43007, Tarragona, Spain.

Abstract

In the buildings sector, the use of ventilate double skin facades in order to reduce the energy demand and the environmental impact of the building during its operational phase has grown significantly. However, the use of this constructive system could lead to high environmental costs during the manufacturing and dismantling phase of the building. This paper presents a life cycle assessment (LCA) study based on the EcoIndicator 99 of a ventilated facade with PCM in its air chamber. Two cubicles were built in an experimental set-up located in Puigverd de Lleida (Spain), one with this ventilated facade system and the other without. The differences in the electrical energy consumption of the HVAC systems were registered and used to determine the environmental savings produced during the operational phase of each building. The results of the LCA show that considering a lifetime of 50 years, the use of this particular ventilated facade reduces by 7.7% the overall environmental impact of the whole building. It also highlights that the environmental payback of this active system is significantly lower than other systems which use PCM in the building envelopes. The environmental payback of the system is 30 years, which can be reduced to only 6 years if instead steel wood would have been used in the structure.

Key-words: Life cycle assessment (LCA); Ventilated double skin facades (VDSF); Phase change materials (PCM); Buildings; Energy efficiency.

1. Introduction

In the building sector, the high energy consumption and CO_2 emissions for heating and cooling purposes have become an important issue worldwide, and has induced new energy policies. The European directive on the energy performance of buildings (Directive 2010/31/EU) dictates that all the EU member states must approve energetic policies to promote the inclusion of very low and even close to zero energy buildings.

In order to reduce this high energy demand both for heating and cooling, several research efforts have been done in improving the thermal resistance of the building envelopes and roofs (Cabeza et al., 2010 and Soubdhan et al., 2005), and its thermal inertia by the use of sensible heat storage (de Gracia et al., 2011) or latent heat systems (Cabeza et al., 2011 and Castell et al., 2010). Moreover, within this context the use of ventilated double skin facades (VDSF) has recently become more popular. These facades, if well designed, can efficiently reduce the overall HVAC energy consumption of buildings by absorbing part of the solar radiation during the winter and preventing overheating during warm periods (Shameri et al., 2011).

The reduction of the heating and cooling demands helps strongly to reduce the environmental impact of the buildings during their operational phase. However, the use of more insulation or heavy materials, or the inclusion of a new constructive system such as the VDSF, could lead to high energy consumptions during the manufacturing and dismantling phase of the building. Life cycle energy (LCE) studies take into account not only the operation and maintenance energetic cost of the building but the embodied energy of the used materials, as well. Ramesh et al. (2012) studied the life cycle energy analysis of a residential building with different envelopes operating under five different climatic zones in India. The authors concluded that there is a limit for the thickness of insulation that can be applied in roofs and walls, which are 10 cm for hot and dry, warm and humid, and cold climates, and 5 cm for moderate climates. Moreover, Dodoo et al. (2012) studied the effect of thermal mass for space heating by comparing the LCE of a concrete and a wood-frame building. They demonstrated that the benefits of a high thermal mass (concrete) are balanced by the lower production primary energy use in the wood-frame system.

LCE studies are useful to determine the energetic balance of a building during its whole lifetime. However, they do not take into account important environmental aspects, such as how the operation, construction, dismantling and maintenance of the building affect the human health, the eco-system quality or the use of the available fossil resources. The process to quantify and evaluate this environmental balance is known as life-cycle assessment (LCA). LCA is a tool to evaluate the environmental impact of a product through analysing the corresponding life cycle phases from cradle to grave. Cabeza et al. (2012) have reviewed the LCA and LCE studies available in the literature.

Several studies have analysed the environmental impact of the buildings using different indicators. Ortiz et al. (2010) have used the LCA approach to evaluate the environmental impacts of two dwellings located in Spain and Colombia and its operational activities, such as HVAC, domestic hot water, electrical appliances, cooking and illumination. The study showed that the adequate combination of energy supplies leads to reduce environmental impacts during the operational phase. Kofoworola and Gheewala (2008) have used LCA to evaluate the environmental impact of a typical commercial office building in Thailand. The authors verified that the operational stage is the predominant in case of commercial buildings.

In addition, Ardente et al. (2008) presented a LCA of the use of kenaf-fibre insulation board into residential buildings. The results demonstrated that these fibres reduce significantly the environmental impact in comparison to the employment of synthetic insulation material. However, the study showed that the best environmental solution is achieved using mineral wools. Moreover, Pappadopoulos and Giama (2007) have also evaluated the environmental impact of using different insulation materials in the building envelope, and highlighted the importance of the environmental performance evaluation (EPE) as a decision management tool.

Apart from the selection of different insulation materials, the LCA methodology has been also applied to quantify the environmental benefits of using phase change materials in building envelopes in order to increase their thermal energy storage capacity (de Gracia et al., 2010, Castell et al., 2012 and Menoufi et al., 2012). These LCA studies compared the overall environmental impact of different cubicles which

were built using typical Mediterranean constructive systems. The results pointed out that considering a 50 years lifetime of the cubicles, the inclusion of paraffin or salts hydrates did not improve significantly the environmental impact, since these PCM were only designed to reduce the cooling demand of the cubicles. Therefore, they were not used during most part of the year.

In order to determine the potential in reducing the environmental impact of the whole building by using PCM in active systems, the present paper studies the environmental impact of using a ventilated facade with PCM in its air chamber in a Mediterranean-climate region. An LCA study is carried out based on the impact assessment method EcoIndicator 99 (EI99) (Pré-Consultants, 2000, and Ecoinvent Center, 2000).

2. Methodology

2.1 Description of the constructive system

The thermal performance of two different cubicles has been tested under winter (de Gracia et al., 2012) and summer conditions (de Gracia et al., 2013); one of them is equipped in the south wall with a ventilated facade with PCM in its air channel (Figure 1). The constructive system used in the walls of both cubicles is based on alveolar bricks (30 x 19 x 29 cm) with an external cement mortar and inner plaster coating. Both roofs were made using concrete pre-cast beams, 8 cm of polystyrene and 5 cm of concrete slab. The polyurethane is placed over the concrete and it is protected with a cement mortar roof with an inclination of 3 %, a double asphalt membrane and 5 cm of gravel (Castell et al., 2010). A total of 112 PCM panels (SP-22 from Rubitherm) are distributed over the facade creating 14 air flow channels as shown in Figure 2. A total mass of 156,8 kg of PCM are distributed over the facade

A metallic structure is used to build the ventilated facade with an air cavity of 15 cm thickness. The inner layer is based on the alveolar brick constructive system while the outer envelope is made by a glass layer. An extra outer layer of expanded polyurethane panels was placed to cover the transparent glazing during the summer period since solar radiation inside the cavity must be avoided for cooling purposes.

The ventilated facade is equipped with three fans (FCL 133 Airtecnics) in the inlet of the air channel to provide mechanical ventilation when needed. Moreover, six automatized gates were installed at the different openings of the channel to control the operational mode of the facade. Those gates are controlled by ST450N linear spindle actuators.

2.2 Experimental set-up characteristics

The experimental set-up offers the possibility to perform two types of indoor conditions: free floating temperature and fixed controlled temperature. Both cubicles are provided by two heat pumps (Fujitsu Inverter ASHA07LCC), located at different heights (3 and 5 m), and their electrical energy consumption is registered every five minutes with an electrical network analyser (MK-30-LCD).

The system which controls the fans and gates is programmed in a Microchip 18F45J10, and allows the system to operate under the different modes during summer and winter period.

2.2.1. Operational modes of the system during summer period

The operational modes of the system during the summer period following described:

- PCM charge period (Figure 3a): During the night time, the air enters to the channel from the outer environment, solidifies the PCM and is pumped outdoors. This mode uses the fans (mechanical ventilation) to ensure the complete solidification of all the PCM.
- Night ventilation (Figure 3b): The air is pumped from outdoors to indoors through the VDSF and is removed from the inner environment to achieve a free cooling effect, using a one-way ventilation grid installed in the door of the cubicle. The high thermal mass of the alveolar brick constructive system produces a high thermal lag between the outer heat flux and the inner one. Hence, the night ventilation can deal with the peak load and reduce significantly the use of HVAC. Note that the PCM charge period must be finished before the night ventilation can start, otherwise the melted PCM would heat up the air and produce an extra cooling load.

- PCM discharge period (Figure 3c): The cold stored in the PCM is pumped by the fans to the inner environment to supply a cooling demand.
- Overheating prevention period (Figure 3d): After the cold discharge, the system lets the air flow from outdoors to outdoors due to the buoyancy forces. This mode prevents the overheating effect in the air channel.

2.2.2. Operational modes of the system during winter period

Furthermore, the sequence of operation during the winter period is shown in Figure 4. The ventilated facade acts as a solar collector during the solar absorption period (Figure 4a). Once the PCM is melted and the solar energy is needed by the heating demand, the heat discharge period starts. During this period the openings drive the air flowing from indoor to the facade cavity, where it is heated up by the PCM panels and sent back into the cubicle (Figure 4b). This discharge period is performed until no more thermal energy is needed or can be provided by the facade; hereafter the system closes all the openings, acting as a Trombe wall, to minimize the heat losses to the environment (Figure 4c).

More information related to the experimental set-up and its different modes of operation can be found in de Gracia et al. (2012, 2013).

2.3 Life Cycle Assessment (LCA)

The ISO 14040-43 standard series (1998, 2000a, 2000b and 2006) recommends the following steps in an LCA study:

- Definition of goal and scope
- Inventory analysis
- Impact assessment
- Interpretation of results

The methodology used for performing the LCA study in this article is based on the impact assessment methodology Eco-Indicator 99 (EI99) (Pré consultants, 2000) using the database EcoInvent 2009 (Ecoinvent center, 2000). The selection of products and

services to be analysed mainly relies on the marked (and consumption) situation in Europe (RER) and Switzerland (CH) in the year 2000. More information about the EI99 methodology will be detailed in the following subsections. The LCA steps recommended by the ISO 14040-43 standard series are to be applied in the following subsections.

2.3.1. Goal and scope definition

The aim of this study is to evaluate the environmental impact of using a VDSF with PCM in a location with continental-Mediterranean weather conditions. The life cycle phases considered are the manufacturing, dismantling and operational phases. The use of this new constructive system has been proved to provide important energy savings on the HVAC electrical consumptions (de Gracia et al. 2012). Hence, the high environmental investment of the cubicle with the VDSF during its manufacturing phase will be compensated after certain period during the operational phase.

The general conditions assumed for applying the LCA in the two studied cubicles are as follows:

- The considered lifetime for a cubicle is 50 years.
- The lifespan of the installed fans is 150,000 hours, which corresponds to more than 111 years, since they are used 1350 hours/year.
- The maintenance operations of the cubicles and the HVAC systems are considered equal for the REF and VDSF cubicles. Hence they do not produce any difference in the overall global impact, and are neglected.
- The electricity used considers the production mix corresponding to the Spanish energy production system.
- No data is available in the EcoInvent database about the disposal of salt hydrates. Its value is estimated considering the same percentage for all the other used components to the total impact. This estimation method has been used in (de Gracia et al. 2010) to calculate the disposal impact of PCM and does not affect significantly the LCA study, since the disposal of the PCM represents less than the 0.01% of the whole impact during the manufacturing and dismantling phase.

- The results of the manufacturing and dismantling phases are aggregated into one phase (manufacturing/dismantling phase).
- As detailed in subsection 2.2, to evaluate the operational phase impact, the measured energy consumption values from the cubicles are used. Within this context, five different periods per year are defined:
    - Severe winter period: 2 months with similar heating demand to the third week of February 2012. Comfort conditions are achieved using the heat pumps with a set point of 21 ºC (de Gracia et al. 2012).
    - Mild winter period: 3 months with similar heating demand to the first week of March 2012. Comfort conditions are achieved using the heat pumps with a set point of 21 ºC (de Gracia et al. 2012).
    - Severe summer period: 2 months with similar cooling demand to the fourth week of August 2012. Comfort conditions are achieved using a heat pump with a set point of 25 ºC (de Gracia et al. 2013). Since no net electrical energy savings could be achieved in the VDSF cubicle due to the excessive use of fans during this experiment, the electrical consumption of both cubicles is considered equal.
    - Mild summer period: 3 months with similar cooling demand to the second week of September 2012. Comfort conditions are achieved using a heat pump with a set point of 25 ºC (de Gracia et al. 2013). The electrical consumption of both cubicles is considered equal.
    - No need of HVAC period: 2 months without temperature control.

LCA is accomplished for extended lifetimes of the cubicles: some studies consider buildings lifetime to be between 50 and 100 years (Mithraratne and Vale, 2004, and Gustavsson and Joelsson, 2010). Therefore, a parametric study considering 75 and 100 years lifetime for the cubicles is also presented.

2.3.2 Inventory analysis

In this step, the inventory list of all the materials used in the manufacturing/dismantling phase of the cubicles is shown. The correlation between the cubicle components used in the manufacturing/dismantling phase and the EcoInvent data base is shown in Table 1. The energy consumption rates of the studied cubicles are quantified as well. The

measured energy consumption values for heating and cooling are shown in Table 2. The electricity used considers the production mix corresponding to the Spanish energy production System (#674 in the EcoInvent data base).

2.3.3 Impact assessment

According to the EI99 methodology and the requirements of this study, the environmental impact is evaluated and expressed through ten damage categories (acidification & eutrophication, ecotoxicity, land occupation, carcinogenics, climate change, ionising radiation, ozone layer depletion, respiratory effects, fossil fuels, and mineral extraction). Those damage categories are further aggregated into three areas of protection that express the main aspects of environmental and societal concern: human health, eco-system quality and natural resources. After extracting the inventory data needed from the data base, the evaluation of each impact category is given by:

$$IMP_j = \sum_k d_{k,j} \cdot LCI_k \qquad \text{(Eq.1)}$$

where IMP_j is the j damage category, d_{kj} is the coefficient of damage extracted from the considered data base (Ecoinvent center, 2000) associated with the component k and damage j, and finally the LCI_k is the life cycle inventory entry (i.e. kg of polyurethane). These results are single score indicators representing the potential impact on the environment through different damage categories. The coefficient of damage for the natural resources damage category is expressed in MJ of surplus energy needed for future extraction. For the ecosystem quality damage category, the coefficient of damage stands for the loss of species over a certain area, during a certain time (% plant, species / $m^2 \cdot$year, Potentially Disappeared Fraction PDF). Finally, the damage to human health is expressed as the number of years life lost and the number of years lived disabled (disability adjusted life years, DALYs).

One point of the EI99 represents one thousandth of the environmental load of one average European inhabitant during one year. But in the context of our work the absolute value of these points is not very relevant as the main purpose is to compare relative differences between products. Lower impact score results mean lower impact on

the environment and hence mean that the product associated with the results is more environmentally friendly. These single score indicators from the EI99 methodology are convenient for the case studies of this article, as the impact of the cubicles and their relevant components on the environment can be easily interpreted and demonstrated (Goedkoop and Spriensma, 2001).

3. Results and discussion

In this section, the results of the impact assessment phase are evaluated. The environmental impacts caused during the operational and manufacturing/dismantling phase of each cubicle are studied separately. Finally, the overall environmental impacts of the cubicle with and without the ventilated double skin facade are compared in order to determine the global environmental benefits of using this constructive system.

3.1 Manufacturing/dismantling phase

The impact of each damage category during the manufacturing/dismantling phase is shown in Table 3. The use of the VDSF with PCM increases in 186.4 % the environmental impact of the cubicle during its construction and disposal period. The authors want to highlight that the fossil fuels damage category is the most affected due to the use of the VDSF. Moreover, the damage categories of ecotoxicity, carcinogenics, climate change, respiratory effects, and mineral extraction are also significantly increased.

In order to better understand the origin of these environmental impacts, a list of all materials used in the construction of both cubicles and the impact associated with them during the manufacturing and dismantling phase is shown in Table 4. The materials used in the construction of the ventilated facade do not have to be inventoried for the reference cubicle; hence, these components are marked with (*). Taken into account that the whole VDSF system increases 196.939 impact points the manufacturing/dismantling environmental cost, note that the steel used in the VDSF is responsible of more than 55% of this increment (110.49 impact points). Almost all the steel needed in the VDSF is used for the structure of the system; hence the use of a wooden structure for the

VDSF is expected to reduce significantly the manufacturing impact of the whole system.

3.2 Operational phase

The energy consumed for heating and cooling purposes of each cubicle has been measured in the previously described experimental set-up (Figure 1). The measured electrical energy consumptions of heat pumps and fans were registered during winter 2012 (de Gracia et al. 2012) and summer 2012 (de Gracia et al. 2013) and are used to determine the impact during the operational phase of the cubicles (Table 2). Since the electrical consumption of the fans is not compensated by the energy savings from the heat pumps during summer, the electrical energy consumption of the VDSF cubicle is considered equal to the consumption of the reference during this period. Nevertheless, note that this is the worst electrical consumption scenario for the VDSF cubicle, since the system could at least reduce the daily cooling demand during the overheating prevention period. It is important to highlight that even though the system is only useful during winter, the heating demand is more than 4 times higher than the cooling demand (Table 2).

The impact points of each damage category during the operational phase of the VDSF and REF cubicles, for a lifetime of 50 years, are shown in Table 5. The use of this VDSF system only during the winter period reduces by 20.7% the environmental impact during the operational phase. The environmental savings were produced mainly in the respiratory effects and fossil fuels damage category.

3.3 Global results

The overall environmental impact of the two analysed cubicles is presented in Figure 5. The impact produced during both the manufacturing/dismantling and operational phases is considered. The results extracted from the LCA demonstrated that the use of the VDSF with PCM in its air chamber reduces 7.7 % the environmental impact when operating during 50 years. The higher impact during the manufacturing phase is balanced by the electrical energy savings of the HVAC system during its lifetime. The environmental payback of the system is 30 years. Moreover, it can be seen that the

environmental savings due to the use of the VDSF system are almost fully produced in the human health damage category.

The authors want to highlight that this environmental savings were calculated only considering the reduction of the electrical demand during the heating season (de Gracia et al. 2012), while the system has a high potential in reducing also the cooling demand by being used as a night free cooling or cold storage system, and by preventing the overheating effect. These reductions in the cooling demand could lead to electrical energy savings in the case of an efficient use of the provided mechanical ventilation.

Moreover, as it was previously said, the use of a wooden structure instead of the built metallic VDSF is expected to decrease drastically the environmental impact during the manufacturing/dismantling phase of the VDSF system. In order to study the impact of using wooden structure instead of the steel the following eco-indicators are used:

- Roundwood, paraná pine (SFM), under bark, u=50%, at forest road [m^3] (#10208).
- Disposal, building, waste wood, chrome preserved, to final disposal [kg] (#2051).

This new eco-indicators substitute the ones for the steel:

- Reinforcing steel, at plant [kg] (#1141).
- Disposal, building, reinforcement steel, to final disposal [kg[(#2048).

The manufacturing/dismantling environmental cost of the whole facade is then reduced from 302.59 impact points to 185.253 by only replacing the material used in the structure of the DSF. Moreover, considering a lifetime of 50 years, the overall environmental impact of using this system decreases 14.67 % in comparison to the reference cubicle without the VDSF. In addition, the use of a wooden structure would increase the thermal resistance of the outer skin, and hence increase the efficiency of the system. However, this effect is not taken into account to calculate the environmental savings.

3.4 Extension of the cubicles lifetime

As it was previously discussed, the VDSF system presents higher environmental impact during the manufacturing/dismantling phase. However, the use of this system represents an important electrical energy reduction of the HVAC system during the heating period, which reduces the environmental impact during the operational phase. A sensitive analysis of the lifetime of the building is shown in Figure 6. It can be clearly seen that the system is environmentally efficient if used at least during 30 years. This value is similar to the environmental payback of using salt hydrates as passive system in the building envelopes (25 years), and significantly lower than that of using paraffins (61 years). Moreover, the environmental payback of the system using a wooden structure decreases to 6 years.

After the environmental payback, the overall environmental impact of the cubicle with the VDSF system is always lower in comparison to the reference cubicle, being the rate of impact reduction 6.3 impact points/year of operation. As it was previously said, the use of the VDSF with PCM reduces the overall environmental impact 7.7 % if operating during 50 years. This value is increased to 11.84 % and 13.99 % if the system is used 75 and 100 years, respectively.

4. Conclusions

The environmental impact of a ventilated double skin facade with phase change material in its air channel is evaluated by a life cycle assessment study using the Eco-Indicator 99 methodology.

This particular system causes an important increment in the environmental impact during the manufacturing/dismantling phase of the building. On the other hand, the efficient use of this system leads to a significant reduction of the electrical energy consumption of the HVAC system both for heating and cooling purposes. These energy reductions cause environmental savings during the operational phase.

Considering a building lifetime of 50 years, the LCA study demonstrated that the use of this particular ventilated facade reduces 7.7 % the overall environmental impact. Moreover, the environmental payback of the system is 30 years.

The authors want to highlight that 56% of the environmental impact produced during the manufacturing/dismantling phase of the system belongs to the construction and disposal of the structural steel; hence important environmental savings could be achieve replacing the structure with wood profiles. The environmental payback of the system with a wooden structure is reduced to 6 years.

Acknowledgments

This work was supported by the "Corporación Tecnológica de Andalucía" by means of the project "MECLIDE-Soluciones estructurales con materiales especiales para la climatización diferida de edificios" with the collaboration of DETEA. The work was partially funded by the Spanish government (ENE2011-28269-C03-02 and ULLE10-4E-1305) and the European Union (COST Action COST TU0802). The authors would like to thank the Catalan Government for the quality accreditation given to their research group (2009 SGR 534).

References

Ardente F., Beccale M., Cellura M., Mistretta M., 2008. Building energy performance: A LCA case study of kenaf-fibres insulation board. Energ Buildings. 40, 1-10.

Cabeza, L.F., Castell, A., Medrano, M., Martorell, I., Pérez, G., Fernández, A.I., 2010. Experimental study on the performance of insulation materials in Mediterranean construction. Energ Buildings. 42, 630-636.

Cabeza, L.F., Castell, A., Barreneche, C., de Gracia, A., 2011. Materials used as PCM in thermal energy storage in buildings: A review. Renew Sust Energ Rev. 45, 1675-1695.

Cabeza, L.F., Rincón, L., Vilariño, V., Pérez, G., Castell, A., 2012.Life cycle assessment (LCA) and life cycle energy analysis (LCEA) of buildings and the building sector: a review. Submitted to Journal of Cleaner Production.

Castell, A., Martorell, I., Medrano, M., Pérez, G., Cabeza, L.F., 2010. Experimental study of using PCM in brick constructive solutions for passive cooling. Energ Buildings. 42, 534-540.

Castell, A., Menoufi, K., de Gracia, A., Rincón, L., Boer, D., Cabeza, L.F., 2012. Life Cycle Assessment of alveolar brick construction system incorporating phase change materials (PCMs). Appl Energ. dx.doi.org/10.1016/j.apenergy.2012.06.066.

de Gracia, A., Rincón, L., Castell, A., Jiménez, M., Boer, D., Medrano, M., Cabeza, L.F., 2010. Life Cycle Assessment of the inclusion of phase change materials (PCM) in experimental buildings. Energ Buildings. 42, 1517–1523.

de Gracia, A., Castell, A., Medrano, M., Cabeza, L.F., 2011. Dynamic thermal performance of alveolar brick construction system. Energ Convers Manage. 52, 2495–2500.

de Gracia, A., Navarro, L., Castell, A., Ruiz-Pardo, A., Álvarez, S., Cabeza, L.F., 2012. Experimental study of a ventilated facade with PCM during Winter period. Energ Buildings. 58, 324-332.

de Gracia, A., Navarro, L., Castell, A., Ruiz-Pardo, A., Álvarez, S., Cabeza, L.F., 2013. Thermal analysis of a ventilated double skin facade with PCM for cooling applications. Energ Buildings.

Directive 2010/31/eu of the European parliament and of the council of 19 May 2010 on the energy performance of buildings. Available from: http://www.epbd-ca.eu.

Dodoo, A., Gustavsson, L., Sathre, R., 2012. Effect of thermal mass on life cycle primary energy balances of a concrete- and a wood-frame building. Appl Energ. 92, 462-472.

Goedkoop M., Spriensma R., 2001. Eco-indicator 99, a damage oriented method for life cycle impact assessment, methodology report, Third edition. Ministry of Housing, Spatial planning and the Environment, The Netherlands.

Gustavsson, L., Joelsson, A., 2010. Life cycle primary energy analysis of residential buildings. Energ Buildings. 42, 210-220.

ISO International Standard 14041:1998. Environmental Management – Life cycle assessment. Goal and scope definition and Inventory analysis. International Organisation for Standardisation (ISO).

ISO International Standard 14042:2000a. Environmental Management – Life cycle assessment. Life cycle Impact assessment. International Organisation for Standardisation (ISO).

ISO International Standard 14043:2000b. Environmental Management – Life cycle assessment. Life cycle Interpretation. International Organisation for Standardisation (ISO). ISO International Standard 14040:2006. Environmental Management – Life cycle assessment. Principles and framework. International Organisation for Standardisation (ISO).

Kofoworola, O.F., Gheewala, S.H., 2008. Environmental life cycle assessment of a commercial office building in Thailand. International J Life Cycle Ass. 13, 498–511.

Menoufi, K., Castell, A., Navarro, L., Pérez, G., Boer, D., Cabeza, L.F., 2012. Evaluation of the environmental impact of experimental cubicles using Life Cycle Assessment: A highlight on the manufacturing phase. Appl Energ. 92, 534-544.

Mithraratne, N., Vale, B., 2004. Life cycle analysis model for New Zealand houses. Build Environ. 39, 483-492.

Ortiz, O., Castells, F., Sonnemann, G., 2010. Operational energy in the life cycle of residential dwellings: The experience of Spain and Colombia. Appl Energ, 87, 673-680.

Papadoppoulos A.M., Giama E., 2007. Environmental performance evaluation of thermal insulation materials and its impact on the building. Build Environ. 42, 2178–2187.

PRé-Consultants, 2000. The Eco-indicator 99. A damage oriented method for life cycle impact assessment. Methodology report and manual for designers. Technical Report, PRé Consultants, Amersfoort. The Netherlands.

Ramesh, T., Prakash, R., Shukla, K.K., 2012. Life cycle energy analysis of a residential building with different envelopes and climates in Indian context. Appl Energ. 89, 193-202.

Soubdhan, T., Feuillard, T., Bade, F., 2005. Experimental evaluation of insulation material in roofing system under tropical climate. Sol Energy. 79, 311-320.

Shameri, M.A., Alghoul, M.A., Spoian, K., Fauzi, M., Zain, M., Elayeb, O., 2011. Perspectives of double skin facade systems in buildings and energy savings. Renew Sust Energ Rev. 15, 468-1475.

The ecoinvent Center. A competence centre of ETH; PSI;Empa & ART; http://www.ecoinvent.ch/. Ecoinvent data v2.1.

Figure captions

Table 1. Components relation with EI99 data base [18]

Component	Name in the data base Eco Invent corresponding to the component
Alveolar Brick	brick, at plant, RER, [kg] (#495)
Base Plaster	base plaster, at plant, CH, [kg] (#536)
Cement mortar	cement mortar, at plant, CH, [kg] (#537)
Steel Bars	section bar rolling, steel, RER, [kg] (#1170)
Concrete	concrete, normal, at plant, CH, [m^3] (#504)
In-floor bricks	concrete roof tile, at plant, CH, [kg] (#9244)
Asphalt	mastic asphalt, at plant, CH, [kg] (#9245)
Glass	glazing, double (2-IV), U<1.1 W/m^2K, laminated safety glass, at plant [m^2] (#7141)
XPS	polystyrene, extruded (XPS), at plant [kg] (#7126)
PU	polyurethane, rigid foam, at plant, RER, [kg] (#1839)
Fans 40 W	pump 40W, at plant [unit] (#1865)
Steel in VDSF	reinforcing steel, at plant [kg] (#1141)
Aluminium	powder coating, aluminum sheet, RER, [m^2] (#1166)
Hydrated Salts	calcium chloride, $CaCl_2$, at regional storage, CH, [kg] (#260)
Disposal Alveolar bricks	disposal, building, brick, to final disposal, CH, [kg] (#2005)
Dispoal plaster	disposal, building, mineral plaster, to final disposal, CH, [kg] (#2021)
Disposal mortar	disposal, building, cement (in concrete) and mortar, to final disposal, CH, [kg] (#2007)
Disposal concrete +steel bars	disposal, building, reinforced concrete, to final disposal, CH, [kg] (#2045)
Disposal In-floor bricks	disposal, building, concrete, not reinforced, to final disposal, CH, [kg] (#2010)
Disposal asphalt	disposal, asphalt, 0.1% water, to sanitary landfill, CH, [kg] (#2216)
Disposal PU	disposal, building, polyurethane foam, to final disposal, CH, [kg] (#2040)
Disposal steel	disposal, building, reinforcement steel, to final disposal [kg] (#2048)
Disposal XPS	disposal, building, polystyrene isolation, flame-retardant, to final disposal [kg] (#2039)
Disposal aluminium	disposal, aluminum, 0% water, to sanitary landfill, CH, [kg] (#2215)
Disposal hydrated salts	disposal, hydrated salts, to final disposal, CH, [kg] (calc)

Table 2. Annual electric energy consumption (kWh) for each cubicle during 2012 [20,21]

Annual electric energy consumption (kWh)	REF	VDSF
Mild Summer period (3 months)	76.74	76.74
Severe Summer period (2 months)	139.50	139.50
Mild Winter period (3 months)	366.75	274.50
Severe Winter period (2 months)	521.66	385.34
Total for a whole year	1104.65	876.08

Table 3. EI99 Impact points in each damage category during the manufacturing/dismantling phase

	Damage Category	REF	VDSF
Eco system quality	acidification & eutrophication	2.312	5.962
	ecotoxicity	1.304	11.098
	land occupation	1.490	3.324
Human health	carciogenics	1.316	15.794
	climate change	12.354	25.760
	ionising radiation	0.132	0.405
	ozone layer depletion	0.104	0.140
	respiratory effects	30.019	102.909
Resources	fossil fuels	55.817	123.436
	mineral extraction	0.802	13.759
TOTAL		105.649	302.588

Table 4. Life Cycle Inventory and impact during manufacturing and dismantling phase.

Component	Quantity used	EI99 Impact points
Alveolar Brick	3616 kg	39.721
Base Plaster	890.1 kg	5.265
Cement mortar	869.4 kg	4.569
Steel Bars	262.2 kg	2.209
Concrete	0.516 m^3	3.263
In-floor bricks	1770 kg	12.823
Asphalt	153.1 kg	3.871
Glass (*)	11.52 m^2	33.280
XPS	29.45 kg	11.57
PU	9.8 kg	3.58
Fans 40 W (*)	3 units	5.220
Steel in VDSF (*)	1010.3 kg	110.492
Aluminium (*)	21.49 m^2	4.814
Hydrated Salts (*)	68.2 kg	3.922
Polyurethane (*)	45.794 kg	16.729
Disposal Alveolar bricks	3616 kg	8.782
Dispoal plaster	890.1 kg	1.842
Disposal mortar	869.4 kg	2.179
Disposal concrete +steel bars	1491.6 kg	4.000
Disposal In-floor bricks	1770 kg	4.437
Disposal asfalt	153.1 kg	0.252
Disposal steel (*)	1010.3 kg	7.530
Disposal XPS	29.45 kg	0.72
Disposal aluminium (*)	58.023 kg	3.523
Disposal PU	9.8 kg	0.252
Disposal hydrated salts (*)	68.2 kg	0.025

Table 5. EI99 impact points of each damage category during the operational phase

Damage Category		Summer period		Winter period		Total period	
		REF	VDSF	REF	VDSF	REF	VDSF
Eco system quality	acidification & eutrophication	11.19	11.19	45.97	34.14	57.16	45.33
	ecotoxicity	3.24	3.24	13.31	9.89	16.55	13.13
	land occupation	3.39	3.39	13.95	10.36	17.34	13.75
Human health	carcinogenics	9.63	9.63	39.55	29.38	49.18	39.00
	climate change	29.80	29.80	122.43	90.93	152.23	120.73
	ionising radiation	1.70	1.70	6.97	5.17	8.66	6.87
	ozone layer depletion	0.01	0.01	0.03	0.02	0.04	0.03
	respiratory effects	134.53	134.53	552.72	410.52	687.26	545.05
Resources	fossil fuels	115.08	115.08	472.81	351.17	587.89	466.25
	mineral extraction	0.52	0.52	2.14	1.59	2.66	2.11
Total		309.09	309.09	1269.90	943.18	1578.99	1252.27

Figure
Click here to download high resolution image

Figure 1

Figure
Click here to download high resolution image

Figure 2

Figure
Click here to download high resolution image

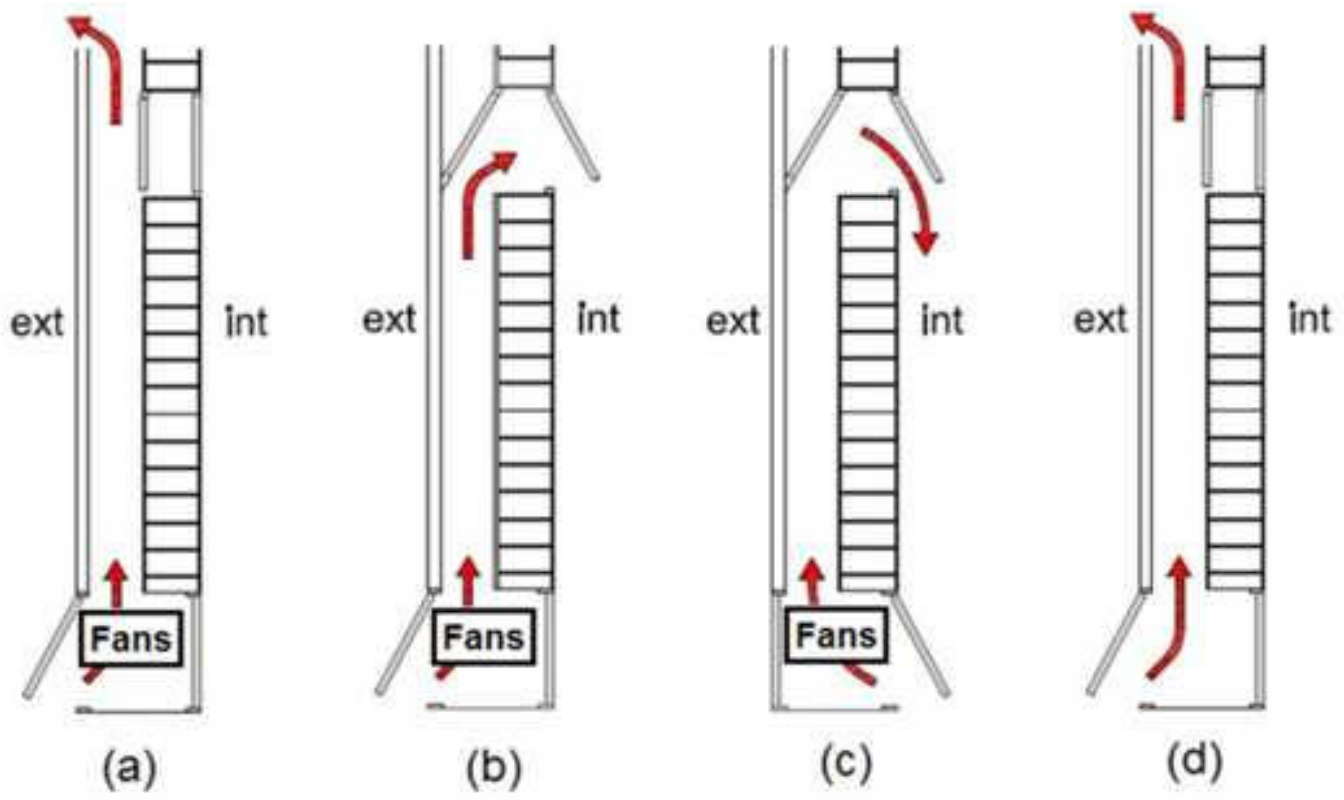

Figure 3

Figure
Click here to download high resolution image

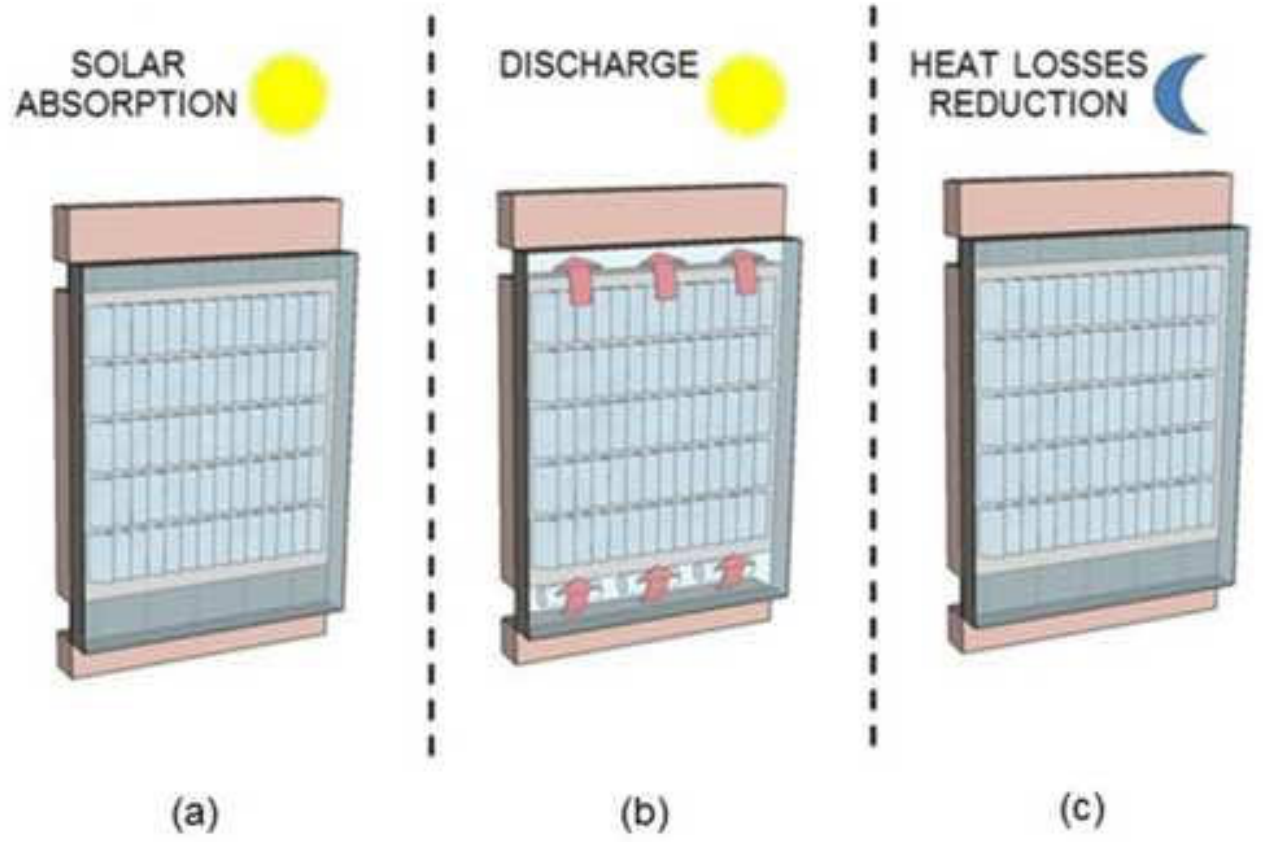

Figure 4

Figure
Click here to download high resolution image

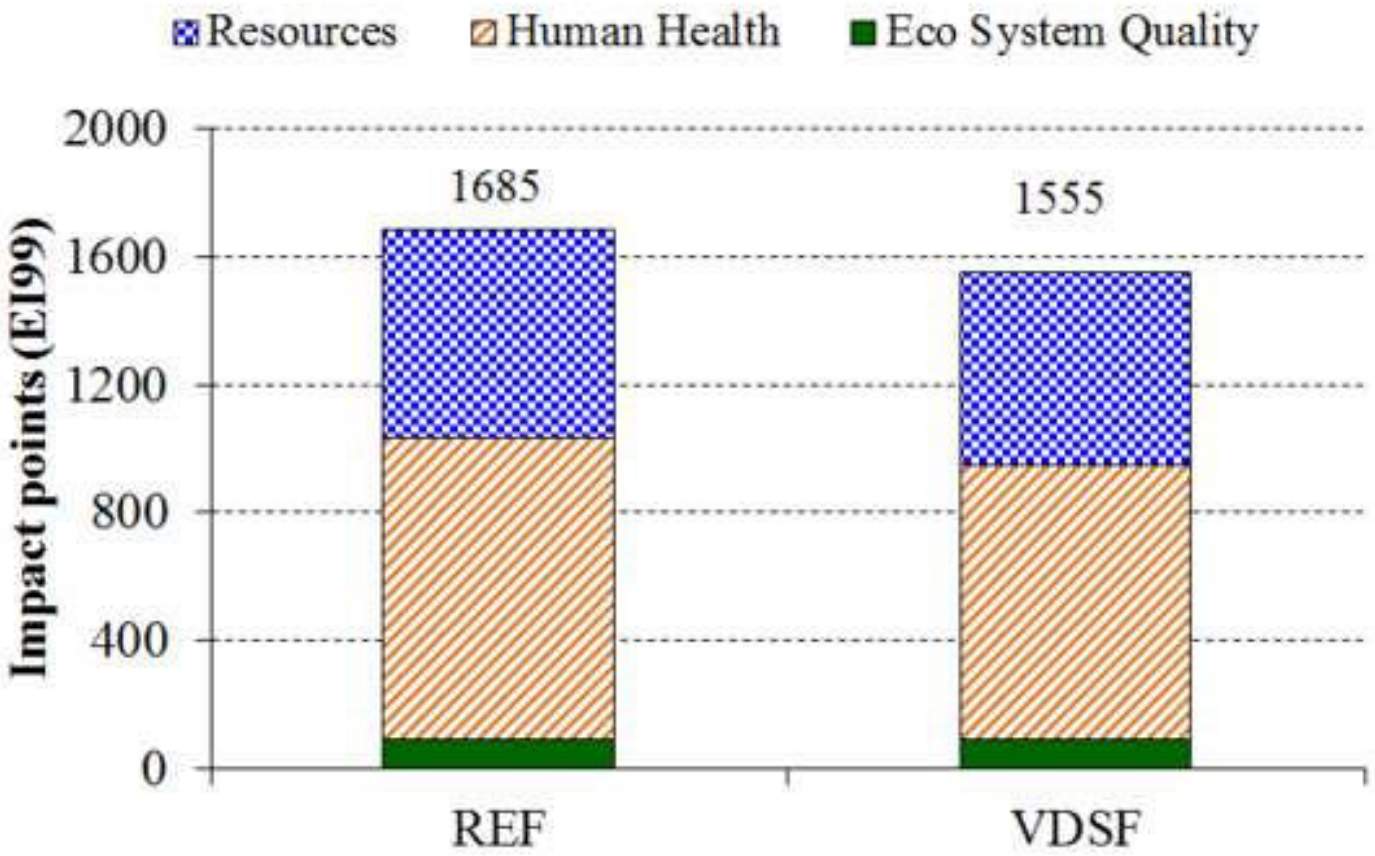

Figure 5

Figure
Click here to download high resolution image

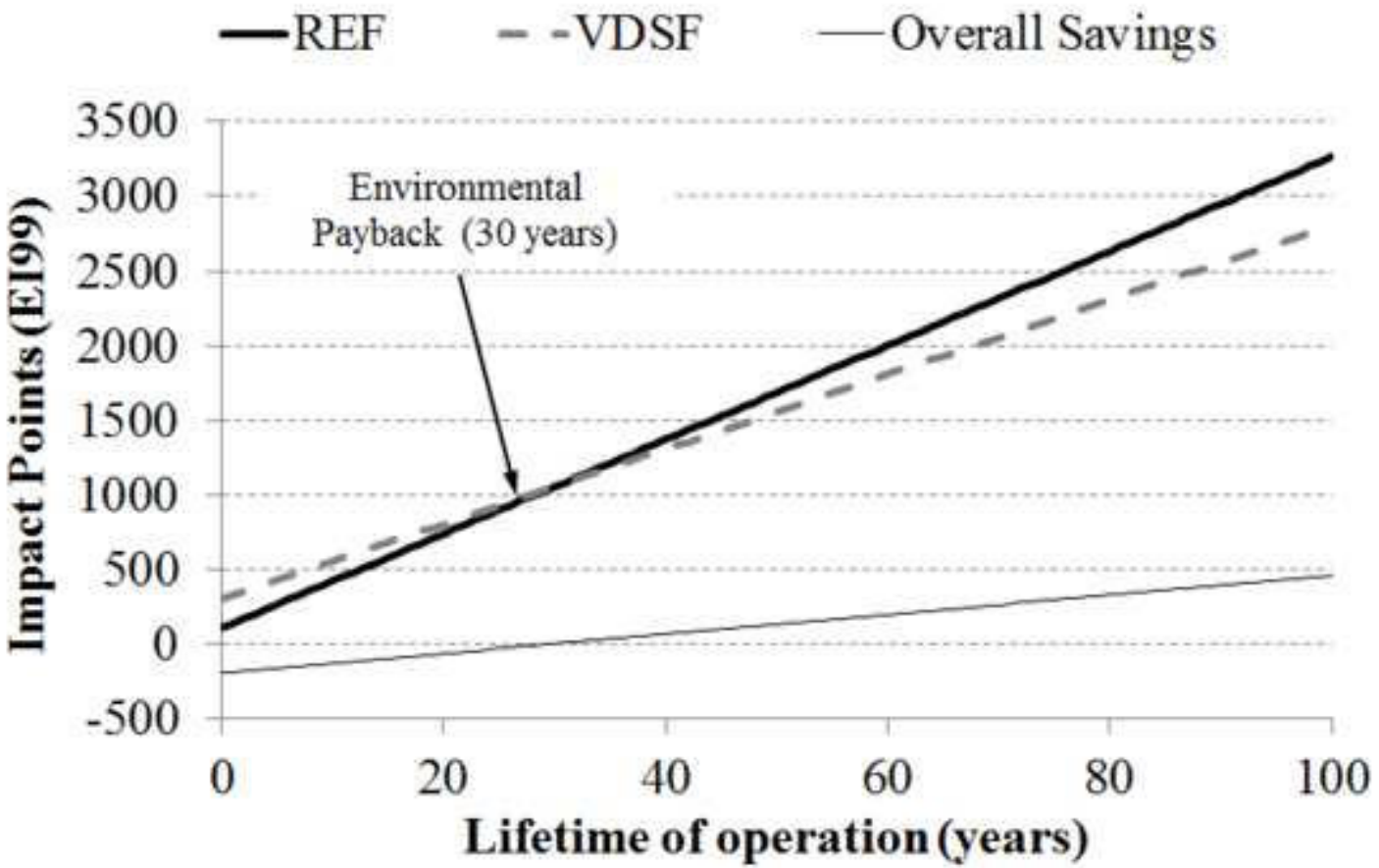

Figure 6

7 Numerical modelling of ventilated facades: A review

7.1 Introduction

As it was detailed in previous chapters, the thermal and energetic performance of the ventilated facade with PCM has been experimentally investigated. According to the experimental results during the cooling season, no net energy savings were registered due to the use of this prototype. Numerical simulation arises as an adequate tool to optimize the design and operation of this new system.

Thus, it leaded the PhD candidate to study, review and compare which methods have been used in the literature to study numerically the performance of ventilated double skin facades. The available literature on the field is specially focused on studying numerically the thermal performance of the DSF under different climate zones and different ways of implementation. Nevertheless, other than the numerical studies, an important effort has been done in the experimental field for better understanding the behaviour of these systems and to provide data and tools which might be used to validate the numerical models developed [65-69].

7.2 Contribution to the state-of-the-art

According to the literature, the numerical models which describe the thermal performance of ventilated facades can be grouped as analytical and lumped models [70,71], non-dimensional analysis [72], network models [73-75], control volume models [76-78], zonal approach [79], and Computational Fluid Dynamics (CFD) [80,81]. The following paper overviews the different typologies of modelling highlighting the strengths and weaknesses depending on the application and design requirements.

- A. de Gracia, A. Castell, L. Navarro, E. Oró, L.F. Cabeza. Thermal analysis of a ventilated facade with PCM for cooling applications. Renewable and Sustainable Energy Reviews doi.10.1016/j.rser.2013.02.029.

The paper analyses the existing numerical methods used to describe the thermal performance of ventilated facades and provides the important drawbacks from each study. Moreover, it points out the accuracy, application and computational effort required for each typology:

- Analytical and lumped models can provide specific information without consuming high computational resources. However, its application and accuracy are limited since they assume several hypotheses, such as constant wall temperatures.
- Dimensionless analysis can be useful to determine a specific parameter, such as the heat transfer through the walls. The main advantage of this methodology is the lack of computational effort. On the other hand, it requires numerous experimental measurements to develop the dimensionless correlations. Numerical tools, such as CFD, can also be used to build these correlations.
- The airflow network model is usually integrated with a thermal network, and without high computational requirements it can provide useful information about bulk flows.
- In the control volume approach, each skin of the DSF is divided into control volumes (approximately 1 m high), which are only coupled due to the presence of the air channel. This air channel is discretized orthogonally to the facade. This approach provides a good compromise between computational resources and accuracy.
- The zonal model has proved to provide information about the air flow, which is not possible using the lumped and control-volume models, but without having the accuracy neither the computational costs of CFD models.
- CFD is the unique way to solve some design aspects of ventilated facades, such as flow around venetian blinds, openings, and different shading systems. Its use in the building sector is limited because of problems related to the computing power and its integration with building energy simulation models (ES) is becoming an interesting topic. These coupled models can determine with higher accuracy the effect of ventilated facade in the thermal performance of a whole building system.

7.3 Journal paper

JOURNAL PUBLISHING AGREEMENT

Elsevier Ltd

YOUR ARTICLE DETAILS

Article:	Numerical modelling of ventilated facades: A review
Corresponding author:	Prof. Luisa F. Cabeza
E-mail address:	lcabeza@diei.udl.cat
Journal:	Renewable and Sustainable Energy Reviews
Our reference	RSER2458
PII:	S1364-0321(13)00131-7
DOI:	10.1016/j.rser.2013.02.029

Renewable and Sustainable Energy Reviews ▮ (▮▮▮▮) ▮▮▮–▮▮▮

Contents lists available at SciVerse ScienceDirect

Renewable and Sustainable Energy Reviews

journal homepage: www.elsevier.com/locate/rser

Numerical modelling of ventilated facades: A review

Alvaro De Gracia*, Albert Castell, Lidia Navarro, Eduard Oró, Luisa F. Cabeza

GREA Innovació Concurrent, Edifici CREA, Universitat de Lleida, Pere de Cabrera s/n, 25001-Lleida, Spain

ARTICLE INFO

Article history:
Received 11 June 2012
Received in revised form
11 February 2013
Accepted 18 February 2013

Keywords:
Review
Ventilated facades
Double skin facades (DSF)
Buildings Numerical modeling

ABSTRACT

The use of double skin facades (DSF) in the building sector and its thermal benefits have been widely studied numerically over the last 30 years. These modelling and simulations are based on different typologies, which have evolved altogether with the available computational resources. The models that have been used to study the thermal performance of DSF can be grouped as analytical and lumped models, non-dimensional analysis, network models, control volume, zonal approach, and computational fluid dynamics (CFD). This paper describes these different typologies of numerical modelling highlighting their benefits and limitations, and overviews the research produced using each typology.

Contents

1. Introduction

Nowadays, the building sector is consuming 40% of the global energy in the European Union, being two-thirds of this energy consumption due to the heating, ventilating and air conditioning (HVAC) systems. In order to reduce this high energy demand, the European directive on the energy performance of buildings (EPBD) suggests that all the EU member states should approve energetic policies to promote the inclusion of very low and even close to zero energy buildings [1].

The improvements in buildings envelopes have high potential in energy demand reduction and consequently in energy savings [2]. Within this context, the use of double skin facades (DSF) in the building sector has recently become more popular. Those facades, if well designed, can efficiently reduce the overall HVAC consumption in buildings by absorbing part of the solar radiation during winter and preventing overheating during warm periods [3]. Moreover, the use of ventilated DSF can improve the acoustic characteristics and day lighting inside the building.

Those constructive systems are based on a special type of envelope, where a second skin, usually a transparent glazing, is placed in front of a regular building facade. The air space in between (the channel) can be mechanically or naturally ventilated to improve the thermal performance of the building [4]. The DSF can work under different ventilation modes (Fig. 1a–c) or work as a Trombe wall (Fig. 1d), depending on the energetic requirements and weather conditions.

In addition, in the systems with external and internal glazing, an adjustable sunshade device is usually installed in the channel to prevent overheating during cooling periods [5]. Even though

* Corresponding author. Tel.: +34 973 3576; fax: +34 973 3575.
E-mail address: lcabeza@diei.udl.cat (A. De Gracia).

1364-0321/$ - see front matter © 2013 Published by Elsevier Ltd.
http://dx.doi.org/10.1016/j.rser.2013.02.029

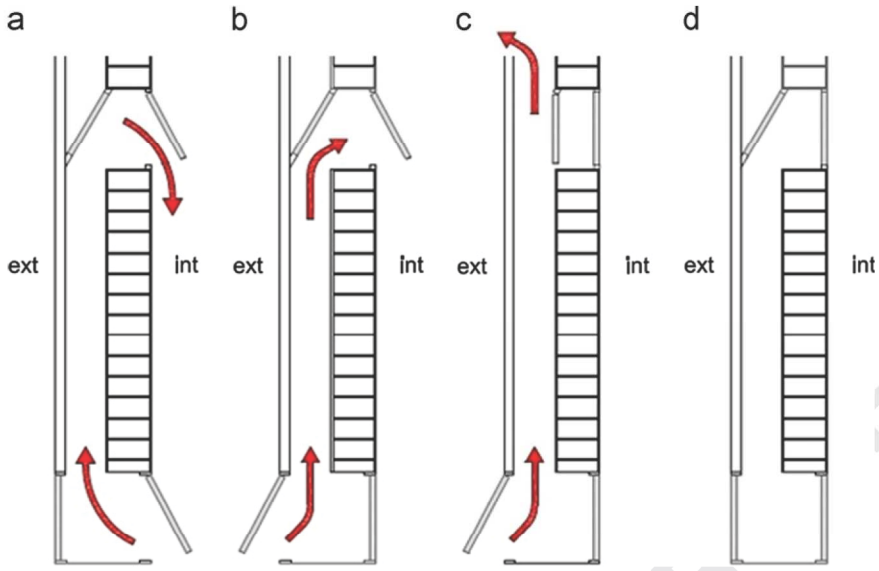

Fig. 1. Different operational modes of a ventilated DSF.

there are several different typologies of ventilated DSF, they are usually grouped under box window facade, shaft-box facade, corridor facade, and multi-story facade [6–8].

Ventilated facades and their thermal behaviour have been a topic of research over the last years. Shameri et al. [3] reviewed the literature related to DSF concluding that ventilation has been widely studied, while lack of research has been carried out regarding to the day lighting capacity of the envelope. The high fire hazard risk of this type of envelopes and the need of more research for better understanding of the DSF effects was also mentioned.

Moreover, Zhou and Chen [9] reviewed the potential of using DSF in the hot-summer and cold-winter zone in China, concluding that the implementation of this type of envelopes would be an efficient way to meet the task of sustainable commercial buildings design in China, if controlled shading devices are applied.

The available literature on the field is specially focused on studying numerically the thermal performance of the DSF under different climate zones and different ways of implementation. Nevertheless, other than the numerical studies, important effort has been done in the experimental field for better understanding the behaviour of these systems and to provide data and tools which might be used to validate the numerical models developed [10–14].

Numerical models are becoming essential in the design phase of these complex constructive systems. Models used to study numerically the thermal performance of the DSF systems can be grouped as analytical and lumped models, non-dimensional analysis, network models, control volume models, zonal approach, and computational fluid dynamics (CFD). The main goal of this paper is to overview the different typologies of numerical models and to describe the thermal response of these systems.

2. Analytical and lumped models

Analytical and lumped models can generally provide specific useful information in the design phase of the DSF without consuming high computational resources. However, several hypothesis must be assumed to solve the analytical models, while the lumped models assume constant temperature at each facade and cavity of the DSF.

The first numerical models which were developed to study numerically the behaviour of a DSF correspond to simple one-dimensional analytical models which solve the first principle using empirical correlations. In [15] the Trombe wall is treated as a solar flat plate collector taking into account its particularities, concluding that the most important factor in the performance of the Trombe wall is the transmissivity of the cover. Holmes [16] analysed and optimized in 1997 some of the design parameters of a naturally ventilated glazed facade using an analytical model which assumes linear vertical temperature gradient. The thermal transmittance in steady state and the flow rate due to natural convection in the air gap were studied in systems with one or two glazed layers with different emissivities.

It is well known that flow characteristics of DSF channel play a key role in the performance of the system. Grabe [17] developed and validated a simple simulation algorithm based on energy transport and Bernoulli equations to study the thermal behaviour and flow characteristics of DSF. The model proves the sensitivity and the difficulty of modelling flow resistances in the air channel.

Ciampi et al. [18] presented an analytical method based on the electrical analogy to calculate the electrical energy savings in buildings due to the use of ventilated facades in Southern Europe climates during summer. The model was used to analyse two particular cases. In the first case, inner masonry wall was given and the authors optimized the air duct and the outer facing. On the other hand, in the second case, the outer facing was fixed and, air duct and inner masonry were parameterized. It was concluded that in all cases the energy demand decreased with the air duct width and solar radiation. It was stated that the use of well-designed ventilated facades in buildings can reduce the electricity consumption for summer cooling by more than 40%.

A physical model also based on the thermal resistance network was proposed by Ong [19] to analyse the thermal performance of a solar chimney, similar to the Trombe wall. Steady-state heat transfer equations were solved using a matrix-inversion solution procedure. In this simple model the temperatures at all surfaces were assumed uniform, and air inlet temperature was supposed to be equal to the room temperature. Empirical correlations available from the literature were used to calculate convection and radiation heat transfer coefficients in the model, which proved good agreement with experimental data from Hirunlabh et al. [20].

Park et al. [21,22] optimized the energy performance, the visual comfort, and the thermal comfort of a DSF by using a motorized louver slat in the cavity and ventilation openings. Here, a two-dimensional lumped simulation model was developed under different operational modes. This numerical model, instead of using

Please cite this article as: De Gracia A, et al. Numerical modelling of ventilated facades: A review. Renewable and Sustainable Energy Reviews (2013), http://dx.doi.org/10.1016/j.rser.2013.02.029

empirical correlations available in the literature, was calibrated based on a parameter estimation technique using in situ measured experimental data. It was demonstrated that in lumped models based on descriptions of physical processes and augmented by calibration parameters to deal with the assumptions (surface temperatures, constant convective heat transfer coefficients, etc.), the calibration process plays an important role in the performance of the model and improves the accuracy of the models in comparison to experimental data.

3. Non-dimensional analysis

Balocco used non-dimensional analysis to determine the thermal performance of a naturally [23] and mechanically [24] ventilated facade. This methodology applies the Buckingham theorem to create correlations depending on non-dimensional numbers, so the same parameters might describe the process at different scales.

For the naturally ventilated DSF [23], 14 non-dimensional numbers with physical meaning were used to create a correlation based on experimental data, and to determine the heat flux transferred to the inner environment throughout the wall. On the other hand, 12 non-dimensional parameters were used to describe the thermal performance of the mechanically ventilated facade [24]. Both correlations proved to be valid for a wide range of conditions and were validated using experimental data and CFD simulation results. The non-dimensional models assume constant thermo-physical properties, except for air density, and they are presented as basic tools to evaluate some specific parameters which might be useful to design ventilated facades without using high complex simulation programs.

4. Airflow network modelling

Hensen et al. [25] stated that the airflow network method treat every building component and relevant HVAC fluid flows systems as a network of nodes representing rooms, parts of rooms, and system components, with internodal connections representing the distributed flow paths associated with cracks, doors, pipes, pumps, ducts, fans, and the like. Conservation of mass for the inlet and outlet flows of each node leads to a set of simultaneous and non-linear equations, which are integrated over time to characterize the flows. This airflow network modelling can provide fast useful information about bulk flows without consuming high computational resources. This method uses pressure differences and discharge coefficients for simple cross ventilation and network flow analysis where multiple inlets and outlets and internal flow branching occurs [26]. However if details about the nature of the flow field are required, CFD simulation must be used.

The airflow network model is usually integrated with a thermal network, which solves the heat balance in each node [9]. The coupling between the thermal and airflow model will be further discussed in the present paper. Tanimoto and Kimura [27] studied a DSF with venetian blinds using thermal and airflow networks (Fig. 2). Good agreement between the calculated pressures differences and temperatures and the experimental data was found.

Moreover, when the network modelling is used to analyse the thermal performance of a DSF integrated into a building, a thermal model of the building must be included in the algorithm altogether with the airflow model and the thermal model of the DSF [28]. The airflow model used in the DSF must take into account the buoyancy effect caused by thermal gradient along the channel and wind effect which may create pressure differences between the inlet and outlet. Stec and van Passen [29] used the network model

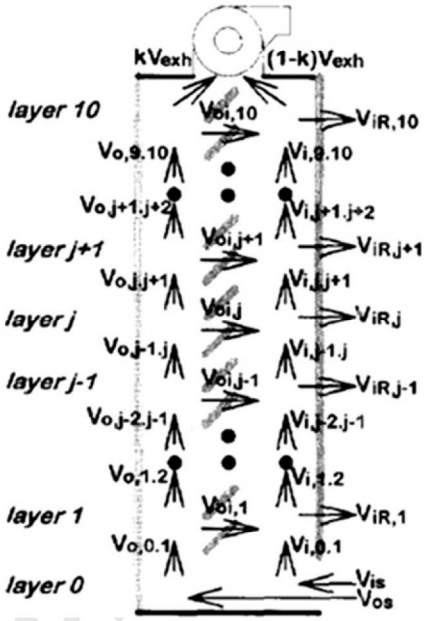

Fig. 2. Airflow network model applied to a ventilated facade with an integrated roll screen [27].

to settle down that to design a building with DSF, the integration of the HVAC system should be together with the facades. The authors developed a simulation program using Simulink to compare the thermal behaviour and the economic costs of different facades and HVAC solutions. DSF with external shading was chosen as the most promising technology for Dutch weather conditions. In addition, the same software was used to highlight the benefits of using plants instead of blinds in the DSF for shading and solar absorption purposes [30]. The study showed that temperature at all locations is reduced, as well as the cooling loads, when plants are used in the cavity. Moreover, the thermal performance of a DSF in hot and humid climates were modelled by Haase et al. [31] using thermal building simulation (TRNSYS) linked to a nodal airflow network (COMIS). The model was validated with experimental data, and was used to evaluate the impact of different factors in the cooling energy consumption of the building, such as orientation, window to wall ratio, and glazing types.

Fallahi et al. [32] described numerically an innovative design of DSF integrating passive thermal mass in the air channel. The airflow inside the channel was assumed one-dimensional and vertical, so no airflow modelling was needed and the given airflow rate was directly applied to reckon the convective heat transfer coefficients. On the other hand, when the facade is naturally ventilated, the nodal unidirectional airflow network method is applied. The authors used the numerical model to compare the annual heating and cooling loads of the new system against traditional DSF with and without thermal mass walls. The results showed that the use of the new system can reduce the cooling load in a 27% in comparison to a traditional DSF. It was also highlighted that the use of any of the ventilated facades skin (inner or outer wall) as a mass component reduces the cooling load, but increases the energy consumption during the winter period. This is because the thermal mass increases the stack effect inside the cavity.

The natural ventilation and thermal performance of DSF have been deeply studied using the software package TAS for the thermal analysis of buildings. In the TAS program the airflow network model is coupled with an energy simulation algorithm which includes a 2D CFD package. Gratia and De Herde [33] analysed the parameters that influence the greenhouse effect (Fig. 3) in a DSF cavity (solar radiation level, orientation and shading devices, opaque walls proportion, wind

Please cite this article as: De Gracia A, et al. Numerical modelling of ventilated facades: A review. Renewable and Sustainable Energy Reviews (2013), http://dx.doi.org/10.1016/j.rser.2013.02.029

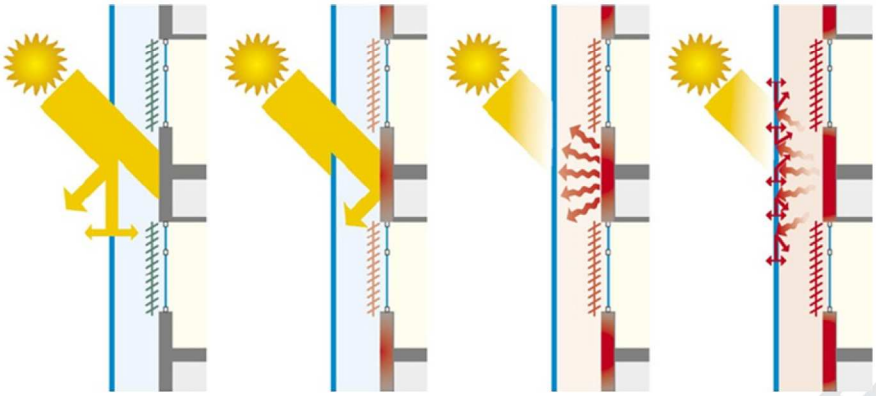

Fig. 3. Greenhouse effect in a DSF [33].

speed, colour of shading devices, depth of the cavity, glazing type, and openings). The authors concluded that the greenhouse effect must be minimized when no natural cooling strategies are used. On the other hand if those strategies are applied, the greenhouse effect is favourable when the DSF is south oriented. Similarly, the importance of the dynamic use of DSF was shown [34], as well as the crucial need of using control systems depending on the climatic conditions to program the use of shading devices and the day and night ventilation. Otherwise the DSF could worsen the performance of the whole building.

The position and colour of the shading devices used in a DSF of an office building were also studied using the TAS software [35]. Moreover, the energy demand during the heating and cooling periods of a building with and without DSF with different levels of insulations were compared [36], concluding that the orientation and use of heating and cooling natural strategies, the insulation level, and the internal gains have greater impact on the thermal performance of a building rather than the presence of a DSF. Hien et al. [37] used the TAS software to calculate the energy consumption, thermal comfort and condensations of single and double skin facade. The study demonstrated that under hot and humid weather conditions, naturally ventilated DSF are effective enough and the use of mechanical ventilation would provide negligible improvements. During the night, a fan must be employed to remove and prevent moisture condensation in the air channel.

The natural ventilation in office buildings with multi-storey DSF were studied by Gratia and De Herde [38–40] also using the TAS software. The authors provided guidelines related to the size and orientation of the openings in order to achieve a ventilation rate of 4 ACH under different wind conditions. Moreover, ventilation due to the stack effect and wind pressure was analysed to avoid overheating of the air gap. The authors concluded that cross-ventilation is less effective than the single-sided ventilation [40]. However it needs opening sizes 15–20 times smaller for similar air flow rates.

The building energy simulation program EnergyPlus has been also used to simulate the energy performance of DSF systems. The air cavity of the DSF can be divided as several zones and each zone is associated with an airflow network model. Chan et al. [41] analysed the optical and thermal impact of using different types of glasses in a DSF located in Hong Kong. These authors stated that the configuration of a DSF system with a single clear glass as an inner pane and a double reflective glazing as the outer pane is the most suitable solution under these environmental conditions. Even though a cooling energy demand reduction of 26% can be achieved, the high investment and maintenance costs of the DSF makes the system economically infeasible in Hong Kong. Furthermore, Hashemi et al. [42] validated a numerical model based on EnergyPlus using field measurements made on a hot arid climate during summer and winter periods for a DSF of an office high-rise building in Tehran. They concluded that night ventilation in the building is essential during summer to prevent increased cooling loads. From the simulation study it was demonstrated that both heating and cooling loads were reduced when a DSF is used.

5. Control volume approach

In the control volume approach, each skin of the DSF is divided into control volumes (approximately 1 m high), which are only coupled due to the presence of the air channel. This air channel is discretized orthogonally to the facade as shown on Fig. 4, so the mass flow rate of each control volume is equal to the mass flow rate at the inlet [9]. Moreover, the thermal gradient in the vertical direction is taken into account using this methodology. Faggembau et al. [43,44] implemented this approach using the AGLA code [45] to study numerically the thermal performance of a DSF and validated its algorithm with analytical solutions where possible and experimental measurements. The numerical model proved that the use of curtains inside the air channel instead of inside the building reduces the heat gains and that Low-ε coating reduces overheating during summer for facades with blinds inside the channel.

Following the same technique, Saelens et al. [46,47] studied the annual energy performance of an office building with different multiple-skin facades implementing the control volume method in TRNSYS (Fig. 5). The modelling environment consists of four models which are the facades, the office zone, the heating and cooling system, and the building energy management system. The energetic performance of three different multiple-skin facades, airflow window, DSF, and supply window (Fig. 6), and two traditional cladding systems, exterior and interior shading devices, were analysed numerically. The authors also highlighted the importance of using control strategies such as controlling the airflow rate and the recovery of air returning from the DSF in order to improve the energy efficiency of all facade systems. Moreover, Saelens et al. [48] demonstrated with experimental data and a sensitivity numerical study that the assumption of an inlet temperature equal to the exterior or interior air temperature is not valid. The inlet temperature must be estimated depending on the heating and cooling with the bounding surfaces and the heating due to solar radiation.

6. Zonal approach

The zonal approach modelling was developed by Jiru and Haghighat [49] and was applied to evaluate the thermal

Please cite this article as: De Gracia A, et al. Numerical modelling of ventilated facades: A review. Renewable and Sustainable Energy Reviews (2013), http://dx.doi.org/10.1016/j.rser.2013.02.029

performance of a DSF with venetian blinds. This methodology is an intermediate approach between the extremes of the lumped model and CFD, since DSF can be divided into a number of control volumes (2D or 3D), usually larger than the cells used in CFD models, so the system of algebraic equations to solve is smaller and much easier to solve in comparison to CFD methodology. An sketch of the zonal approach for a mechanically ventilated DSF with venetian blinds in the air channel is shown in Fig. 7.

The zonal model [49] was validated against experimental results and proves to provide information which is not possible for the lumped and the control volume approach models, moreover the described method does not need the computational requirements as CFD does. Finally, the model is used to study how the temperature difference between inlet and outlet varies depending on the inlet flow rate, the height of the DSF, and the presence or absence of the venetian blinds.

7. Numerical solution of partial differential equations and computational fluid dynamics (CFD)

The numerical methods for solving partial differential equations (PDEs) are based on replacing the differential equations by algebraic equations. The three classical choices for the numerical solution of PDEs are the finite difference method (FDM), the finite element method (FEM) and the finite volume method (FVM).

In the case of the popular finite difference method, this is done by replacing the differential quantities by sufficiently small differences [50]. Akbari and Borgers used the fully implicit finite difference model to study the free convective laminar [51] and turbulent [52] flows between parallel vertical plates. Empirical correlations were obtained from the model to predict the induced flow rate, the total height and the heat transfer rate between walls and fluid. Moreover, the convective laminar heat transfer between

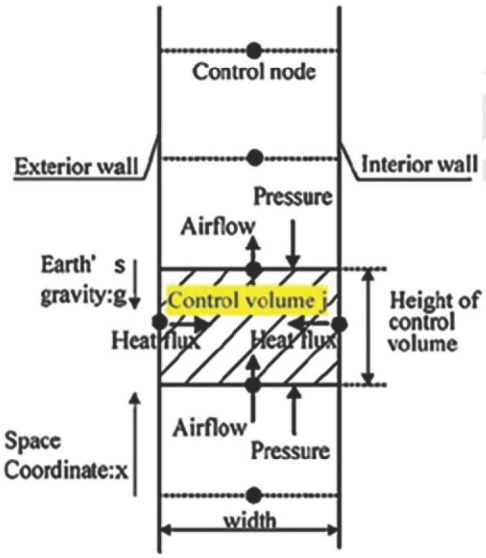

Fig. 4. Control volume discretization of the air channel of a DSF system [43].

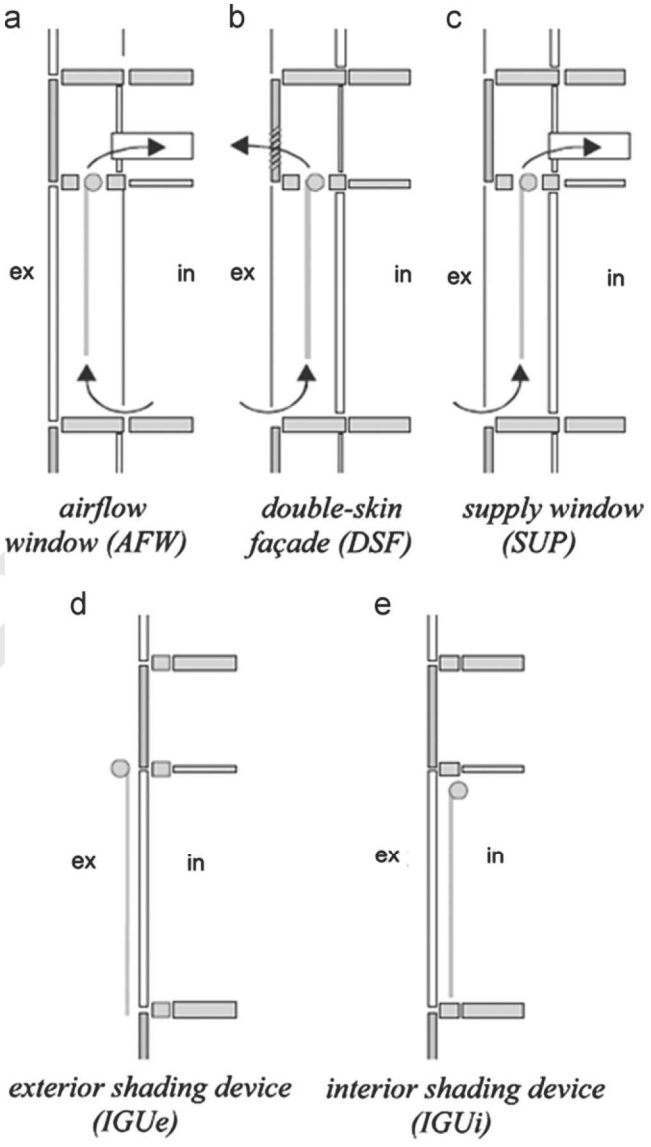

Fig. 6. Schematic representation of the multiple skin facades and the traditional solutions [47].

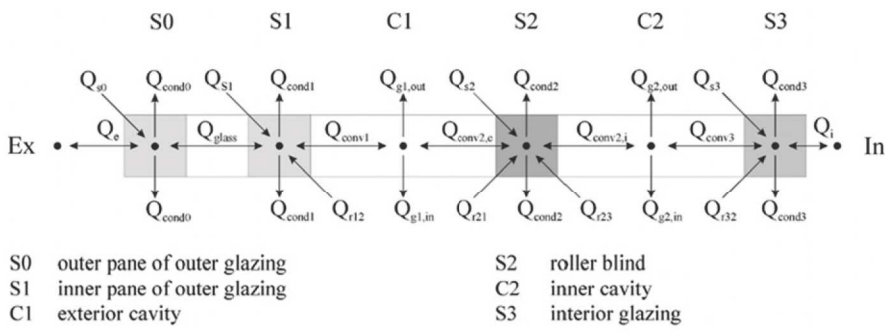

Fig. 5. Control volume discretization of a ventilated facade with lowered roller blind (Q is the heat flux; Q_s is the absorbed solar energy; Q_c is the convective heat transfer; Q_{cond} is the conductive heat transfer; Q_r is the radiation heat transfer) [46].

Please cite this article as: De Gracia A, et al. Numerical modelling of ventilated facades: A review. Renewable and Sustainable Energy Reviews (2013), http://dx.doi.org/10.1016/j.rser.2013.02.029

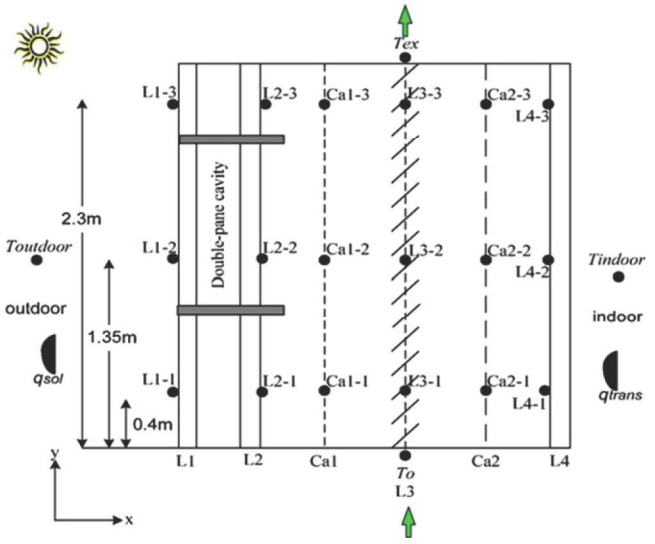

Fig. 7. Mechanically ventilated DSF: L1 is the exterior glass of the double-pane; L2 is the interior glass of the double-pane; L3 is the venetian blinds; L4 is the interior glass of the ventilated DSF; Ca1 is the outer cavity; and Ca2 is the inner cavity, T_0 is the air temperature at the inlet, T_{ex} is the air temperature at the exit, T_{indoor} is the room air temperature, $T_{outdoor}$ the outside air temperature, q_{sol} is the total solar radiation, q_{trans} is the transmitted solar radiation, ● is the thermocouple and ◖ is the pyranometer [49].

the air channel of a Trombe wall and its surfaces have been numerically investigated by Jubran et al. [53]. The numerical analysis included a conventional Trombe wall and a modified one with a tilt angle in the outer glass wall, concluding that the modified version gives better thermal performance.

Aside from using this methodology to determine the convective heat transfer coefficient, the finite differences method has been used to compare different types of DSF. Shen et al. [54] studied numerically the thermal performance of a classical and a composite Trombe wall. The authors developed a simulation model based on finite differences method and compared the results to the type 36 of TRNSYS software [55]. The model presented better agreement with experimental data rather than the type 36 since it does not assume constant discharge coefficients. In addition, Zalewski et al. [56] developed a one-dimensional model based on finite differences to describe the thermal behaviour of four different types of solar walls. The model was validated using experimental data and was used to compare the efficiency in solar heat storage of classical, composite, and insulated Trombe walls, and non-ventilated solar walls. Moreover, the supply in summertime of the different solar walls was also numerically compared. It was shown that the classical Trombe wall is the constructive system that maximizes the heat absorption, however it is difficult to control the heat supplied during summer which may produce overheating. On the other hand, the use of composite solar walls reduces drastically this possible overheating during summer periods. Furthermore, a factorial plan was carried out in the paper to conclude that to maximize efficiency of a composite solar wall, the storage wall should not be very thick and its absorption coefficient should be as high as possible.

In addition, the heat losses of a single and double skin facade office buildings were compared during winter in Istanbul [57]. A numerical model based on two steps (inter-space temperature and finite difference method) was used to point out that the use of DSF would reduce in a 40% the heat losses during winter.

Finally the thermal modelling of DSF with integrated photovoltaics (PV) has been addressed using finite difference method. Mei et al. [58] developed a numerical model to analyse an integrated ventilated PV facade. This model was implemented with TRNSYS building model, and was validated experimentally with measurements of a building in free floating conditions. Moreover, Charron and Athienitis [59] studied different configurations and the use of fins. It was concluded that even though the use of PV modules inside a cavity of a DSF reduces the electricity generation of the PV in a 21% due to the outer skin reflects part of the solar radiation, its efficiency increases about a 25% because of the heat rejected by the fans in the cavity.

Moreover, the finite element method was used by Agnoletto et al. [60] to solve the coupled conduction, convection, and long-wave radiation problem in a building envelope with DSF. Both inside and outside ambient temperatures were assumed constant, while the solar radiation varied in a sinusoidal form. The model determined the temperature distribution at each relevant surface, the air temperature and velocity distribution in the channel, the heat fluxes and the solar transmitted energy to the inside.

The finite volume method was used by Fedorov and Viskanta [61] to model the convective heat transfer coefficients in an asymmetrically heated vertical channel due to turbulent natural flow. The authors used a low Reynolds number k–ε turbulence model, which was experimentally validated and used to provide empirical correlations.

The finite volume method was also used to study numerically the DSF by many researchers. This method, developed by Patankar [62], discretizes the governing equations (Navier–Stokes and energy conservation) dividing the physical space into a finite number of control volumes. Yedder et al. [63] analysed numerically the natural convection in a Trombe wall solar collector using a constant heat flux boundary condition at the solar radiation receiving surface. After model validation it was concluded that the aspect ratio has a small influence on the heat transfer, while other parameters such as orifice position, channel width and size, have high influence in the thermal performance of the envelope. Mootz and Bezian [64] studied the influence of channel depth in the convective heat transfer. Two different options were introduced to solve the channel depth variation, changing or maintaining the total thickness of the wall, hence varying or not the insulation thickness. The results extracted from this numerical study concluded that if the thickness of the wall is maintained, the best panel performance during recovery periods requires a maximum channel spacing, while this channel must be minimized during non-recovery periods, since less insulation is used and hence there are more heat losses to the environment. On the other hand, large channel spacing proved to be the most efficient in both recovery and non-recovery periods when the thickness of the wall can be modified. Moreover, Balocco [65] presented a simple steady model to demonstrate that natural convection effect is affected by the ratio between channel width and height, since it affects the stack effect and the wall frictional resistance.

Hossegen et al. [66] and Seferis et al. [67] used the transient simulation program ESP-r, which is based on the finite volume technique, to study numerically the performance of DSF. Hossegen et al. [66] used this commercial software to study whether a double-skin should be applied to the east facade of a building in Norway. They concluded that the use of DSF reduces the heating energy demand in a 20%. However, it is not interesting from an economical point of view since the electrical energy savings will not defend the additional costs the DSF constitute. Furthermore, Seferis et al. [67] validated experimentally the model showing good agreement except for night periods during summer. The authors used the model to point out the improvements in the thermal behaviour of the facade due to the addition of a radiant barrier layer.

The CFD technique has been widely used for air flow simulation in the channel of a ventilated DSF. The air flow model consisted of a system of governing equation representing continuity, momentum,

Please cite this article as: De Gracia A, et al. Numerical modelling of ventilated facades: A review. Renewable and Sustainable Energy Reviews (2013), http://dx.doi.org/10.1016/j.rser.2013.02.029

turbulence, enthalpy, and concentration [68] solved for all nodes of a two-or three-dimensional grid in order to provide detailed information about the nature flow field. This numerical approach uses weather the FDM or the FVM to solve these equations. Hensen et al. [25] stated that even though the CFD approach can be applied to any thermofluid investigation, in the building physics domain, there are several problems to address, such as the computing power, the nature of the flow fields, the assessment of the complex, and the occupant-dependent boundary conditions. These limitations led to CFD studies being restricted to steady-state cases, very short simulation periods or the study of the convective heat transfer across the DSF surfaces and provide empirical correlations [69–72], where the aspect ratio of each node must be small enough so the grid can capture boundary layer effects [9].

Pasut and De Clari [73] have discussed which factors are important in the simulation of a naturally ventilated facade using the CFD technique, and which factors can be neglected since they only increase the computational cost of the simulation. A sensitivity analysis shows that the thermal conductivity and heat capacity of the air could be treated as a constant, since their values are calculated as functions of temperature, they only increase the execution time without providing significant improvement in the results. Moreover k-ε RNG turbulent model is suggested in comparison to k–ω models, due to its better agreement with experimental data. The authors have also highlighted that for natural ventilated DSF the velocity fieldd is almost bidirectional, hence 3D models are not needed.

Xamán et al. [70] used a two-dimensional steady state numerical model to describe the natural convection effect of a tall rectangular cavity in laminar and turbulent regimes (air channel of a DSF). Four different turbulence models k–ε were compared against experimental data, demonstrating that the model proposed by Ince and Launder [74] predicted the measured results more accurately. Empirical correlations of overall convective Nusselt numbers are given for different aspect ratios [68]. Moreover, Coussirat et al. [75] analysed different models of turbulence and radiation to simulate the thermal performance of a double glazed facade using CFD. The model was validated against Manz experimental data [76], and the study concluded that for this configuration P-1 Radiation model, and Standard and RNG k–ε model showed the smallest error in all cases. A mesh sensitivity test was also carried out, observing a clear dependence on the mesh density.

Validation of the numerical results using experimental data or analytical solutions must be done whatever which typology of modelling is used to describe the thermal performance of the DSF system. However, since CFD technique allows to calculate temperature, pressure and velocity maps, there are few experimental data which can be used to validate CFD models. Ding et al. [77] used reduced scale model experiments and CFD analysis to study the natural ventilation of a DSF with a thermal storage space called solar chimney. The experimental model was reproduced as 1/25 of the full-scale building. Here a solar chimney was used to strength the stack effect, ensuring natural convection and minimizing the effect of wind. The area of the openings was optimized depending on the airflow and pressure differences. Moreover, Gosselin et al. [78] presented a new computational method to describe the heat transfer and air flow in a dual-airflow window. The method consists of four steps and was validated with experimental tests on a full-scale dual-airflow window system. First, CFD is used without including radiation in the model, second a separated code calculates surface to surface radiation and solar radiation. The output from this second step is introduced in another CFD simulation as heat sources or sinks. Finally an average between temperature profiles of CFD models with and without radiations is done.

Even though some authors have developed their own CFD code to study the thermal performance of the DSF systems [79], commercial CFD packages have been widely used. An spectral optical model combined with CFD was implemented using Flovent to analyse the thermal behaviour of a DSF [76]. The model was validated with experimental data, extracted from a test element provided with approximately 60 sensors. It was concluded that the sequence alteration of a given set of layers in a glass double facade or the ventilation properties of the facade can vary drastically the solar energy transmittance. The same model was used by Manz et al. [80] to show that the change in the orientation of the forced flow relative to the gravitational field, influences the total solar energy gain, and hence cannot be modelled using a piston-flow model, but using CFD. Moreover Pérez-Grande et al. [81] used Fluent CFD package to study the effect of the glass properties on the thermal performance of a double-glazed facade. Total heat flux gains through the facades with different combinations of outer and inner glasses were compared. Naturally and mechanically ventilated facades were also evaluated using the model concluding that the selection of the glasses is a key point in the design of the double glassed facades, since the thermal loads into the buildings can vary an order of magnitude. Furthermore, Patania et al. [82] compared the thermal performance of three different opaque ventilated facades using Fluent CFD package. The parametric study included the analysis of different solar radiation intensity, inlet velocity and temperature. This study showed that the electrical energy savings during summer periods of an opaque ventilated facade can achieve 40%, and that the most important thermo-physic characteristics that affects the behaviour of the system is the thermal diffusivity of the external layer, standing that the lower is the diffusivity, the better energy performance of the ventilated facade. It was also remarked that the velocity profiles along the cavity are symmetric and two boundary layers are developed along both sides. Guardo et al. [83] also used Fluent package to study which parameters affect the most the reduction of solar load gain in a DSF. The numerical study concluded that the optical properties of the glass have a critical importance in the design of DSF, replacing the internal glazing for a low-emissivity glass reduces the solar load by half. Meanwhile a reduction of 55% of the transmissivity of the external glazing can provide 40% of solar load reductions. Finally, Wong et al. [84] used the Fluent CFD solver engine to evaluate the impact of using DSF in a high rise office building of 18 storeys. Their results indicate that DSF can be used to introduce natural ventilation to the high-rise buildings in the tropics.

As it was previously said, CFD simulation can provide information about the nature flow field, this is why this approach is the only way to solve some details in the design of a DSF, such as flow around venetian blinds [85–87], openings [88], and different shading systems (Fig. 8) [89]. Moreover, Safer et al. [86] assessed the modelling of a forced ventilated DSF with a venetian blind. 2D and 3D models were carried out to parameterize the air outlet position, the slat tilt angle, and the position of the blinds. Here, an homogeneous porous media model was used to reduce the number of meshes. The authors concluded that the slat tilt angle is important when the blind is in the centre of the channel and the facade is externally ventilated. Furthermore, for cases of external ventilation, it was found that the blinds have to be placed close to the inner surface to maximize the air flow and hence the heat transfer coefficients. Xu and Yang [87] coupled an optical model, an interface heat balance model, and the CFD model to study the natural ventilation in a DSF with venetian blinds. The numerical results were validated using the experimental data from Manz [75]. Moreover, Sanjuan et al. [88] developed a 3D CFD model to analyse the fluid dynamics and thermal performance of an open joint ventilated facade (Fig. 9), and to compare its behaviour against a conventional sealed ventilated facade. The results pointed out that while in a conventional ventilated facade the natural convection effect produces a loop in the air gap (where the air near the heated

Please cite this article as: De Gracia A, et al. Numerical modelling of ventilated facades: A review. Renewable and Sustainable Energy Reviews (2013), http://dx.doi.org/10.1016/j.rser.2013.02.029

surface ascends and the air near the cooled descends), in the open joint ventilated facade, the air can come in and out in every opening, which reduces the convective flow. In this study it was concluded that the use of an open joint ventilated facade lowered the temperatures in the air gap, producing a reduction of 26% in the heat gains during the summer period. However, this temperature reductions lead to increase the heat losses 50% during winter time.

Even though CFD can provide useful information about the airflow occurring in the DSF, the complete thermal and airflow description of these systems requires a coupled model including the modelling of optics (spectral method), the thermodynamics and fluid dynamics of the air chamber and room space (CFD), and a building energy simulation tool. An important effort has been done

Manz and Frank [90] developed a coupled model which is economical in terms of computing time. The model was used to highlight the natural night-time ventilation. Furthermore, Baldinelli [89] studied numerically a glass DSF with a movable shading device using an optical, CFD, and building energy models. Simulations under 2D approaches were validated with experimental data showing that the use of 2D instead of 3D approach give an almost negligible additional error. The model was used to compare the studied DSF against traditional constructive systems in the north of Italy such as glassed and opaque facades, showing significant improvements in the building energy behaviour (reducing the heating load in winter and minimizing the cooling load in summer) especially when forced convection is used in the air chamber.

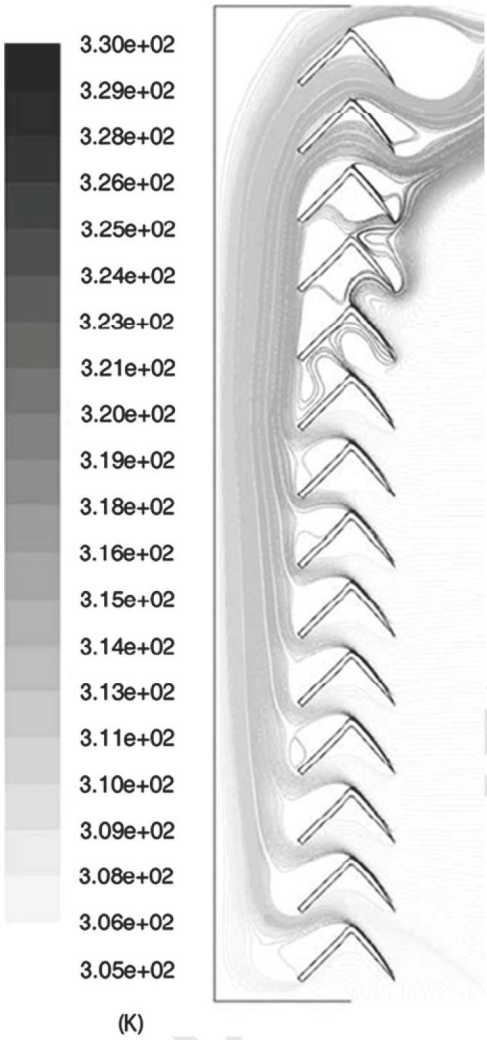

Fig. 8. Temperature air streamlines (K) around the shading system proposed by Baldinelli [89].

8. Integration between building energy and airflow models

The integration of building energy simulation (ES) and airflow model, usually CFD, can provide complementary information of the building performance. Moreover, the coupling simulation could better enhance the boundary conditions assumed for both, the thermal and airflow models. This coupled modelling is not only interesting for the numerical simulation of DSF but for any thermal zone of the building, as well.

According to Srebric et al. [91] there are three main discontinuities between ES and CFD: the time-scale, the modelling, and the speed discontinuity. The first discontinuity is produced because ES has a characteristic time-scale of hours while CFD has a few seconds. The modelling discontinuity appears since the air temperature is spatially averaged in the ES models and represented as a field distribution in CFD. In addition, the speed discontinuity reflexes the differences in the computing time needed for each model. Zhai et al. [92] describe some efficient approaches to bridge these discontinuities, such as static and dynamic coupling strategies. The static coupling involves one-step or two-step exchange of information between ES and CFD as seen in Fig. 10. The static coupling is appropriate in the cases where ES, CFD, or both are not very sensitive to the exchanged variables such as convective heat transfer

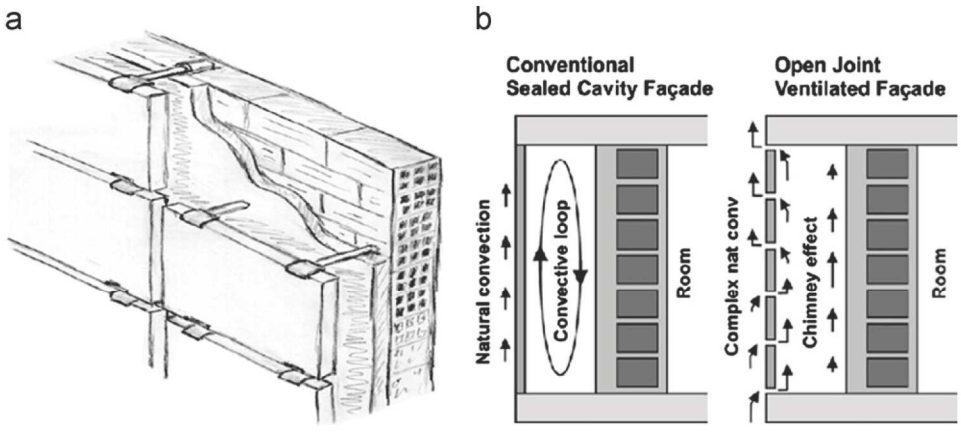

Fig. 9. (a) Sketch of an open-joint ventilated façade. (b) Differences in heat transfer processes between a conventional sealed cavity facade and an open joint ventilated facade. [88].

Please cite this article as: De Gracia A, et al. Numerical modelling of ventilated facades: A review. Renewable and Sustainable Energy Reviews (2013), http://dx.doi.org/10.1016/j.rser.2013.02.029

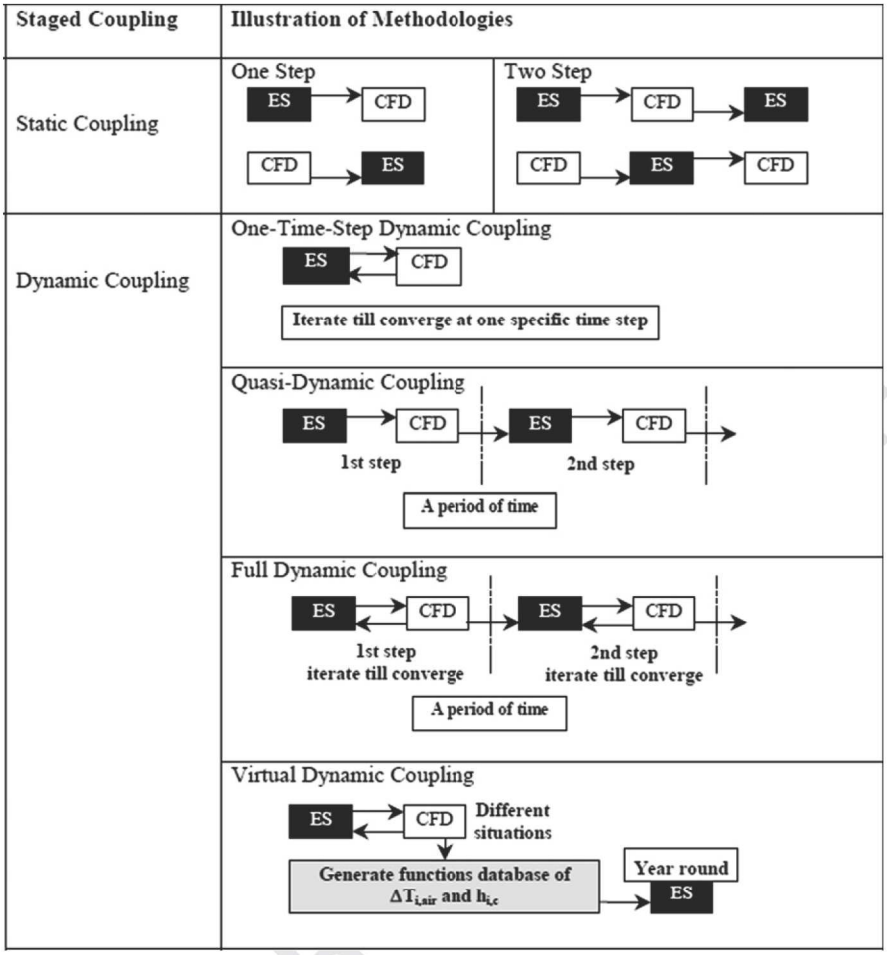

Fig. 10. Illustration of the staged coupling strategies (the arrow from CFD to ES indicates the transfer of thermal air distribution and convective heat transfer coefficient, while the arrow from ES to CFD indicates the transfer of surface temperatures and $Q_{heat\_extraction}$).

coefficients or thermal air distributions. On the other hand, dynamic coupling involves coupling between the two models at every time-step. In the one-time-step dynamic coupling and the full dynamic coupling, the iteration between ES and CFD is performed until convergence, which supposes a higher computational cost. Quasi-dynamic coupling requires less computational effort and is advised when the time-step is small and virtual dynamic coupling, as proposed by Chen and van der Kooi [93] is the most suitable coupling method for a whole year energy analysis.

Zhai and Chen [94] have developed a coupled program (EnergyPlus and MIT-CFD) incorporating different coupling strategies and the numerical results are validated in four different experimental facilities. The authors conclude that even though the coupled simulation took much longer computing time than energy simulation alone, the numerical results are more accurate, especially in the calculation and assumption of convective heat transfer coefficients.

9. Conclusions

The use of double skin facades (DSF) in the building sector has become popular and has been widely studied. Computer numerical simulation is one of the most powerful techniques in the design process of these systems. This paper overviews the existing numerical methods used to predict the thermal performance of DSF under different environmental conditions. The main conclusions which can be extracted from this study are summarised as follows:

- Several hypotheses must be assumed to solve the analytical and lumped models. However, they can generally provide specific useful information without consuming high computational resources.
- Dimensionless analysis is presented as a basic tool to calculate heat transfer through the walls of a DSF without using simulation programs of different complexity levels. Even though the dimensionless studies presented in this paper are based on experimental measurements, numerical tools, such as CFD, can also be useful to develop dimensionless correlations which describe the thermal performance of the system.
- The airflow network model can provide fast useful information about bulk flows without consuming high computational resources, and is usually integrated with a thermal network, and a building energy model.
- The control volume approach is based on one-dimensional discretization (in the indoor–outdoor direction for the solid layers, and in the flow direction for the air channel). This approach provides a good compromise between computational resources and accuracy.
- The zonal model has proved to provide information which is not possible for the lumped and the control-volume models.
- Computational fluid dynamics simulation is the unique way to solve some details in the design of a DSF, such as flow around venetian blinds, openings, and different shading systems.

Please cite this article as: De Gracia A, et al. Numerical modelling of ventilated facades: A review. Renewable and Sustainable Energy Reviews (2013), http://dx.doi.org/10.1016/j.rser.2013.02.029

Its use in the building sector is limited because of problems related to the computing power, the nature of the flow fields, the assessment of the complex, and the occupant-dependent boundary conditions. When using this numerical approach to model a ventilated facade, k–ε RNG turbulence model is recommended, and 3D models are not necessary since velocity field is almost bidirectional.

- The integration of building energy simulation (ES) and airflow model using CFD can provide more accurate prediction to study the thermal performance of a DSF or a whole building system.
- The different discontinuities between the ES and the CFD can be addressed using different coupling strategies, with different computational costs. Virtual dynamic coupling is the most suitable coupling method for a whole year energy analysis, while the static coupling is recommended in the cases where ES, CFD, or both are not very sensitive to the exchanged variables such as convective heat transfer coefficients or thermal air distributions.
- CFD simulation might be used to build numerical correlations which describe some specific parameters such as convective heat transfer coefficients. These correlations might be used by engineers or architects in simplified models during the design phase of the DSF.

Most of the models presented were validated against experimental results. However, further research is required to compare all the models with the same experimental test in order to evaluate accuracy and consumption of computational resources. Moreover, the researchers of this study want to highlight the potential and the importance of developing coupled models, which are able to use detailed information from CFD in an overall energy simulation model describing the thermal performance of a whole building.

Acknowledgements

The work was partially funded by the Spanish government (ENE2011-28269-C03-01) and the European Union (COST Action COST TU0802). The authors would like to thank the Catalan Government for the quality accreditation given to their research group (2009 SGR 534).

References

[1] Directive 2010/31/eu of the European parliament and of the council of 19 May 2010 on the energy performance of buildings; 2010. Available from: ⟨http://www.epbd-ca.eu⟩.
[2] Cabeza LF, Castell A, Medrano M, Martorell I, Pérez G, Fernández I. Experimental study on the performance of insulation materials in Mediterranean construction. Energy and Buildings 2010;42:630–6.
[3] Shameri MA, Alghoul MA, Sopian K, Fauzi M, Zain M, Elayeb O. Perspectives of double skin façade systems in buildings and energy saving. Renewable and Sustainable Energy Reviews 2011;15:1468–75.
[4] Safer N, Woloszyn M, Roux JJ. Three-dimensional simulation with a CFD tool of the airflow phenomena in single floor double-skin façade equipped with a Venetian blind. Solar Energy 2005;79:193–203.
[5] Ding W, Hasemi Y, Yamada T. Natural ventilation performance of a double-skin façade with a solar chimney. Energy and Buildings 2005;37:411–8.
[6] Wang PC. Natural ventilation in double-skin façade design for office buildings in hot and humid climate. PhD thesis. University of New South Wales, Australia, December; 2008.
[7] Faggembauu D. Heat transfer and fluid-dynamics in double and single skin facades. PhD thesis. Universitat Politècnica de Catalunya, Spain, December; 2006.
[8] Poirazis H. Double skin façades for office buildings. Report EBD-R-04/3. Lund University; 2004. T.
[9] Zhou J, Chen Y. A review on applying ventilated double-skin façade to buildings in hot-summer and cold-winter zone in China. Renewable and Sustainable Energy Reviews 2010;14:1321–8.
[10] Zalewski L, Chantant M, Lassue S, Duthoit B. Experimental thermal study of a solar wall of composite type. Energy and Buildings 1997;25:7–18.
[11] Torcellini P, Pless S. Trombe walls in low-energy buildings: practical experiences. In: VII World renewable energy congress, Denver; 2004.
[12] Pasquay T. Natural ventilation in high-rise buildings with double facades, saving or waste of energy. Energy and Buildings 2004;36:381–9.
[13] Gavan V, Woloszyn M, Kuznik F, Roux JJ. Experimental study of a mechanically ventilated double-skin façade with venetian sun-shading device: a full investigation in controlled environment. Solar Energy 2010;84:183–95.
[14] Huckermann V, Kuchen E, Leão M, Leão É. Empirical thermal comfort evaluation of single and double skin façades. Building and Environment 2010;45:976–82.
[15] Khadir Nasri. A model of a Trombe wall. Renewable Energy 1991;1:533–41.
[16] Holmes MJ. Optimization of the thermal performance of mechanically and naturally ventilated glazed facades. Renewable Energy 1994;5:1091–8.
[17] von Grabe J. A prediction tool for the temperature field of double facades. Energy and Buildings 2002;34:891–9.
[18] Ciampi M, Leccese F, Tuoni G. Ventilated facades energy performance in summer cooling of buildings. Solar Energy 2003;75:491–502.
[19] Ong KS. A mathematical model of a solar chimney. Renewable Energy 2003;28:1047–60.
[20] Hirunlabh J, Kongduang W, Namprakai P, Khedari J. Study of natural ventilation of houses by a metallic solar wall under tropical climate. Renewable Energy 1999;18:109–19.
[21] Park C, Augenbroe G, Messadi T, Thitisawat M, Sadegh N. Calibration of a lumped simulation model for double-skin façade systems. Energy and Buildings 2004;36:1117–30.
[22] Park C, Augenbroe G, Sadegh N, Thitisawat M, Messadi T. Real-time optimization of a double-skin façade based on lumped modeling and occupant preference. Energy and Buildings 2004;39:939–48.
[23] Balocco C. A non-dimensional analysis of a ventilated double façade energy performance. Energy and Buildings 2004;36:35–40.
[24] Balocco C, Colombari M. Thermal behavior of interactive mechanically ventilated double glazed façade: non-dimensional analysis. Energy and Buildings 2006;38:1–7.
[25] Hensen J, Bartak M, Drkal F. Modeling and simulation of a double-skin façade system. ASHRAE Transactions 2002;108:1251–9.
[26] Aynsley R. A resistance approach to analysis of natural ventilation airflow networks. Journal of Wind Engineering and Industrial Aerodynamics 1997;67&68:711–9.
[27] Tanimoto J, Kimura K. Simulation study on an air flow window system with an integrated roll screen. Energy and Buildings 1997;26:317–25.
[28] Stec W, Van Paassen D. Defining the performance of the double skin façade with the use of the simulation model. In: Eighth international IBPSA conference, Eindhoven; 2003.
[29] Stec W, Van Paassen D. Symbiosis of the double skin façade with the HVAC system. Energy and Buildings 2005;37:461–9.
[30] Stec W, Van Paassen D, Maziarz A. Modelling the double skin façade with plants. Energy and Buildings 2005;37:419–27.
[31] Haase M, Marques da Silva F, Amato A. Simulation of ventilated facades in hot and humid climates. Energy and Buildings 2009;41:361–73.
[32] Fallahi A, Haghighat F, Elsadi H. Energy performance assessment of double-skin façade with thermal mass. Energy and Buildings 2010;42:1499–509.
[33] Gratia E, De Herde A. Greenhouse effect in doublé-skin facade. Energy and Buildings 2007;39:199–211.
[34] Gratia E, De Herde A. Optimal operation of a south double-skin facade. Energy and Buildings 2004;36:41–60.
[35] Gratia E, De Herde A. The most efficient position of shading devices in a double-skin facade. Energy and Buildings 2007;39:364–73.
[36] Gratia E, De Herde A. Are energy consumptions decreased with the addition of a double-skin. Energy and Buildings 2007;39:605–19.
[37] Hien WN, Liping W, Chandra AN, Pandey AR, Xiaolin W. Effects of double glazed façade on energy consumption, thermal comfort and condensation for a typical office building in Singapore. Energy and Buildings 2005;37:563–72.
[38] Gratia E, De Herde A. Guidelines for improving natural daytime ventilation in an office building with a double-skin facade. Solar Energy 2007;81:435–48.
[39] Gratia E, De Herde A. Natural ventilation in a double-skin facade. Energy and Buildings 2004;36:137–46.
[40] Gratia E, De Herde A. Is day natural ventilation still possible in office buildings with a double-skin façade? Building and Environment 2004;39:399–409.
[41] Chan ALS, Chow TT, Fong KF, Lin Z. Investigation on energy performance of double skin façade in Hong Kong. Energy and Buildings 2009;41:1135–42.
[42] Hashemi N, Fayaz R, Sarshar M. Thermal behavior of a ventilated double skin façade in hot arid climate. Energy and Buildings 2012;42:1823–32.
[43] Faggembau D, Costa M, Soria M, Oliva A. Numerical analysis of the thermal behaviour of ventilated glazed facades in Mediterranean climates. Part I: Development and validation of a numerical model. Solar Energy 2003;75:217–28.
[44] Faggembau D, Costa M, Soria M, Oliva A. Numerical analysis of the thermal behaviour of ventilated glazed facades in Mediterranean climates. Part II: Applications and analysis of results. Solar Energy 2003;75:229–39.
[45] Costa M, Acebes O, Sen F, Platzer W, Haller A, Indetzki M, et al. Analysis of multifunctional ventilated facades. An European Joule Project. In: Proceedings of Eurosun conference, Copenhagen; 2000.
[46] Saelens D, Carmeliet J, Hens H. Energy performance assessment of multiple-skin facades. HVAC&R Research 2003;9:167–85.
[47] Saelens D, Roels S, Hens H. Strategies to improve the energy performance of multiple-skin facades. Building and Environment 2008;43:638–50.

Please cite this article as: De Gracia A, et al. Numerical modelling of ventilated facades: A review. Renewable and Sustainable Energy Reviews (2013), http://dx.doi.org/10.1016/j.rser.2013.02.029

[48] Saelens D, Roels S, Hens H. The inlet temperature as a boundary condition for multiple-skin facade modelling. Energy and Buildings 2004;36:825–35.
[49] Jiru TE, Haghighat F. Modeling ventilated double skin façade—A zonal approach. Energy and Buildings 2008;40:1567–76.
[50] Çengel Y. Heat transfer. A practical approach. McGraw-Hill; 1998.
[51] Akbari H, Borgers TR. Free convective laminar flow within the Trombe wall channel. Solar Energy 1979;22:165–74.
[52] Borgers TR, Akbari H. Free convective turbulent flow within the trombe wall channel. Solar Energy 1984;33:253–64.
[53] Jubran BA, Hamdan MA, Manfalouti W. Modelling free convection in a Trombe wall. Renewable Energy 1991;1:351–60.
[54] Shen J, Lassue S, Zalewski L, Huang D. Numerical study on thermal behavior of classical or composite Trombe solar walls. Energy and Buildings 2007;39:962–74.
[55] Solar Laboratory of energy (USA). Manuals of TRNSYS. University of Wisconsin-Madison, USA; 1994.
[56] Zalewski L, Lassue S, Duthoit B, Butez M. Study of solar walls—validating a simulation model. Building and Environment 2002;37:109–21.
[57] Yilmaz Z, Çetintas F. Double skin façade's effects on heat losses of office buildings in Istanbul. Energy and Buildings 2005;37:691–7.
[58] Mei Li, Infield D, Eicker U, Fux V. Thermal modelling of a building with an integrated ventilated PV façade. Energy and Buildings 2003;35:605–17.
[59] Charron R, Athienitis AK. Optimization of the performance of double-façades with integrated photovoltaic panels and motorized blinds. Solar Energy 2006;80:482–91.
[60] Agnoletto L, Cortella G, Manzan M. Finite element termal analysis of special building components. Energy and Buildings 1995;22:115–23.
[61] Fedorov AG, Viskanta R. Turbulent natural convection heat transfer in an asymmetrically heated, vertical parallel-plate channel. International Journal of Heat and Mass Transfer 1997;40:3849–60.
[62] Patankar S. Numerical heat transfer. Hempisphere Publications; 1980.
[63] Yedder RB, Du ZG, Bilgen E. Numerical study of laminar natural convection in composite Trombe wall systems. Solar & Wind Technology 1990;7:675–83.
[64] Mootz F, Bezian JJ. Numerical study of a ventilated facade panel. Solar Energy 1996;57:29–36.
[65] Balocco C. A simple model to study ventilated facades energy performance. Energy and Buildings 2002;34:469–75.
[66] Hosseggen R, Wachenfeldt BB, Hanssen SO. Building simulation as an assisting tool in decision making Case study: With or without a double-skin façade? Energy and Buildings 2008;40:821–7.
[67] Seferis P, Strachan P, Dimoudi A, Androutsopoulos A. Investigation of the performance of a ventilated wall. Energy and Buildings 2001;43:2167–78.
[68] Gan Guohui. A parametric study of Trombe walls for passive cooling of buildings. Energy and Buildings 1998;27:37–43.
[69] Manz Heinrich. Numerical simulation of heat transfer by natural convection in cavities of facade elements. Energy and Buildings 2003;35:305–11.
[70] Xamán J, Álvarez G, Lira L, Estrada C. Numerical study of heat transfer by laminar and turbulent natural convection in tall cavities of façade elements. Energy and Buildings 2005;37:787–94.
[71] Yilmaz T, Fraser S. Turbulent natural convection in a vertical parallel-plate channel with asymmetric heating. International Journal of Heat and Mass Transfer 2007;50:2612–23.
[72] Pappas A, Zhai Z. Numerical investigation on thermal performance and correlations of double skin façade with buoyancy-driven airflow. Energy and Buildings 2008;40:466–75.
[73] Pasut W, De Carli M. Evaluation of various CFD modelling strategies in predicting airflow and temperature in a naturally ventilated doublé skin façade. Applied Thermal Engineering 2012;37:267–74.
[74] Ince N, Launder B. On the computation of buoyancy-driven turbulent flows in rectangular enclosures. International Journal of Heat Fluid Flow 1989;10:110–7.
[75] Coussirat M, Guardo A, Jou E, Egusquiza E, Cuerva E, Alavedra P. Performance and influence of numerical sub-models on the CFD simulation of free and forced convection in double-glazed ventilated façades. Energy and Buildings 2008;40:1781–9.
[76] Manz H. Total solar energy transmittance of glass double façades with free convection. Energy and Buildings 2004;36:127–36.
[77] Ding W, Hasemi Y, Yamada T. Natural ventilation performance of a doublé-skin façade with a solar chimney. Energy and Buildings 2005;37:411–8.
[78] Gosselin JR, Chen Q. A computational method for calculating heat transfer and airflow through a dual-airflow window. Energy and Buildings 2008;40:452–8.
[79] Onishi J, Soeda H, Mizuno M. Numerical study on a low energy architecture based upon distributed heat storage system. Renewable Energy 2001;22:61–6.
[80] Manz H, Schaelin A, Simmler H. Airflow patterns and thermal behavior of mechanically ventilated glass double façades. Building and Environment 2004;39:1023–33.
[81] Pérez-Grande I, Meseguer J, Alonso G. Influence of glass properties on the performance of double-glazed facades. Applied Thermal Engineering 2005;25:3163–75.
[82] Patania F, Gagliano A, Nocera F, Ferlito A, Galesi A. Thermofluid-dynamic analysis of ventilated facades. Energy and Buildings 2010;42:1148–55.
[83] Guardo A, Coussirat M, Egusquiza E, Alavedra P, Castilla RA. CFD approach to evaluate the influence of construction and operation parameters on the performance of active transparent façades in Mediterranean climates. Energy and Buildings 2009;41:534–42.
[84] Wong PC, Prasad D, Behnia M. A new type of double-skin façade configuration for the hot and humid climate. Energy and Buildings 2008;40:1941–5.
[85] Jiru TE, Tau Y, Haghighat F. Airflow and heat transfer in double skin facades. Energy and Buildings 2011;43:2760–6.
[86] Safer N, Woloszyn M, Roux JJ. Three-dimensional simulation with a CFS tool of the airflow phenomena in single floor double-skin facade equipped with a venetian blind. Solar Energy 2005;79:193–203.
[87] Xu X, Yang Z. Natural ventilation in the double skin facade with venetian blind. Energy and Buildings 2008;40:1498–504.
[88] Sanjuan C, Suárez MJ, González M, Pistono J, Blanco E. Energy performance of an open-joint ventilated façade compared with a conventional sealed cavity façade. Solar Energy 2011;85:1851–63.
[89] Baldinelli G. Double skin façades for warm climate regions: Analysis of a solution with an integrated movable shading system. Building and Environment 2009;44:1107–18.
[90] Manz H, Frank Th. Thermal simulation of buildings with double-skin façades. Energy and Buildings 2005;37:1114–21.
[91] Srebric J, Chen Q, Glicksman LG. A coupled airflow-and-energy simulation program for indoor thermal environmental studies. ASHRAE Transactions 2000;106:465–76.
[92] Zhai Z, Chen Q, Haves P, Klems JH. On approaches to couple energy simulation and computational fluid dynamics programs. Building and Environment 2002;37:857–64.
[93] Chen Q, van der Kooi J. ACCURACY—a computer program for combined problems of energy analysis, indoor airflow, and air quality. ASHRAE Transactions 1988;94:196–214.
[94] Zhai ZJ, Chen QY. Performance of coupled building energy and CFD simulations. Energy and Buildings 2005;37:333–44.

Please cite this article as: De Gracia A, et al. Numerical modelling of ventilated facades: A review. Renewable and Sustainable Energy Reviews (2013), http://dx.doi.org/10.1016/j.rser.2013.02.029

8 A correlation of the convective heat transfer coefficient between an air flow and a phase change material plate

8.1 Introduction

The use of PCM in the building sector has been widely studied [82], both experimentally [28] and numerically [83]. The PCM can be integrated in building envelopes in order to increase its thermal energy storage capacity [18,51], in heat exchangers which might be included in the building ventilation system [84], or in special applications such as ventilated facades [76,85,86].

This study is focused on heat exchangers made of PCM plates. The heat transfer coefficient between the parallel PCM plates and the air flow is critical in the design phase of these systems since it defines the time needed to melt or solidify the PCM and the power of the heating or cooling supply. In the literature, the existing heat transfer correlations for the flow between parallel plates are for two cases: "constant and equal wall temperatures", and "constant and equal wall heat fluxes". According to Liu et al. [87], the case of "constant and equal wall temperature" is more appropriate to model the convective heat transfer occurring between a forced flow and a PCM solid, since the wall temperatures are almost constant during the phase change. However, thermal gradients can occur in the PCM wall, especially in heat exchangers with long PCM slabs, which makes the assumption of "constant and equal wall temperature" not valid.

8.2 Contribution to the state-of-the-art

A new correlation is built to determine the heat transfer coefficient between an air flow and a plate made of PCM. The correlation has two terms: one of them represents the evolution of the Nusselt number for a plate without phase change, the other one is a perturbation on the Nusselt number due to the phase change, and is presented in the following paper:

- A. de Gracia, D. David, A. Castell, L.F. Cabeza, J. Virgone. A correlation of the convective heat transfer coefficient between an air flow and a phase change material plate. Applied Thermal Engineering 51 (2013) 1245-1254.

The present study addressed for the first time the issue of forced convective heat transfer along PCM plates, and how the phase change process of the flat plates affects the evolution of the Nusselt number.

This Nusselt variation depends on the thermal boundary conditions at the surface of the plates. For a phase stabilized material (material which does not change phase within the designed thermal gradient, PSM) plate, this evolution is gradual and homogeneous all along the plate. Therefore, the heat transfer coefficient increases gradually until the final temperature is reached. On the other hand, for the PCM plate, it can be observed the formation of 5 distinct zones (Figure 19):

- First zone: the phase change has not started yet and the PCM is still in the solid phase.
- Second zone: this is the first part of the phase change, when the specific heat Cp increases with the temperature.
- Third zone: this is the second part of the phase change, when the specific heat Cp decreases with the temperature.
- Fourth zone: the phase change is finished. The PCM is in the liquid state, but it has not reached the thermal equilibrium.
- Fifth zone: the heating process is finished. The PCM is in the liquid state at steady state.

Thus, the first major difference between PCM and PSM plates is the apparition of the fifth zone near the leading edge. At this location, the plate is in thermal equilibrium with the air flow, hence there is no heat flux at the surface, and the convection heat transfer value has no effect on the system behaviour. The thermal boundary layer starts at the fourth zone. The starting point of the thermal boundary layer induces high values of the heat transfer coefficient.

The study uses de design of experiments methodology to build two original dimensionless empirical correlations, for a PCM and PSM plate. These correlations will be suitable for the simulation of sensible and latent heat storage systems, in a wide valid range of the different non-dimensional numbers. The use of these correlations instead of the existing ones from the literature provides a strong improvement in the accuracy of the model. Moreover, its use could save computational costs compared to the use of CFD simulations.

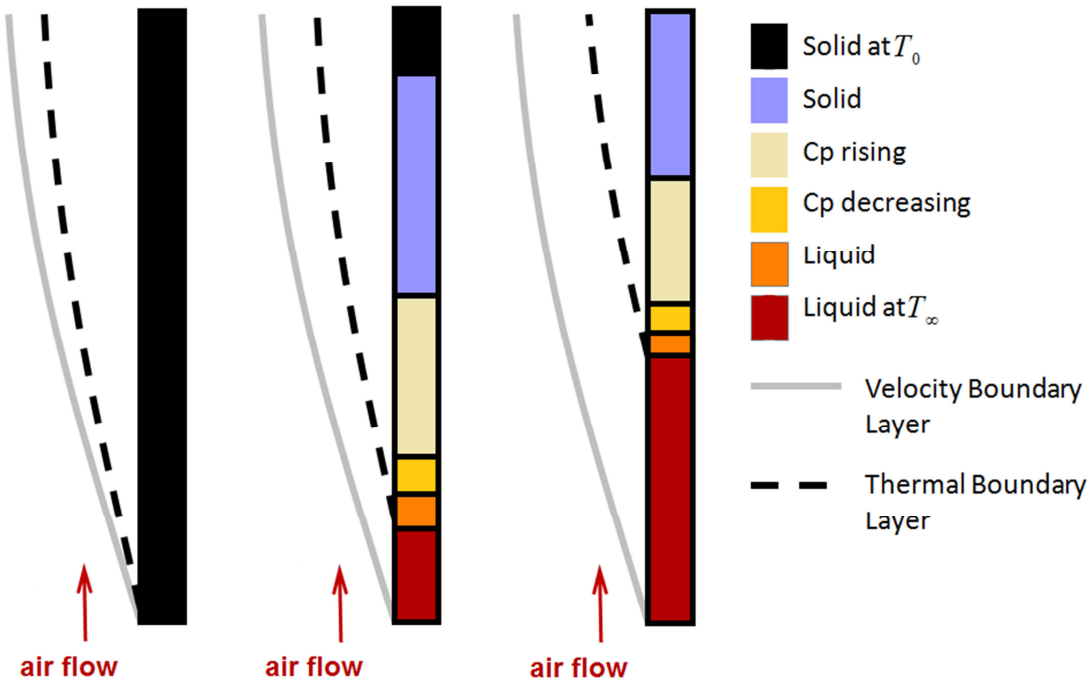

Figure 19. Evolution of the temperature repartition in the plate and its effect on the thermal boundary layer

8.3 Journal paper

Applied Thermal Engineering 51 (2013) 1245–1254

Contents lists available at SciVerse ScienceDirect

Applied Thermal Engineering

journal homepage: www.elsevier.com/locate/apthermeng

A correlation of the convective heat transfer coefficient between an air flow and a phase change material plate

Alvaro de Gracia [a,b], Damien David [b], Albert Castell [a], Luisa F. Cabeza [a,*], Joseph Virgone [b]

[a] GREA Innovació Concurrent, Universitat de Lleida, Edifici CREA, Pere de Cabrera s/n, 25001 Lleida, Spain
[b] CETHIL, UMR 5008, INSA-Lyon, Université Lyon1, Bât. Sadi Carnot, 9 rue de la Physique, 69621 Villeurbanne, France

Applied Thermal Engineering 51 (2013) 1245–1254

Contents lists available at SciVerse ScienceDirect

Applied Thermal Engineering

journal homepage: www.elsevier.com/locate/apthermeng

A correlation of the convective heat transfer coefficient between an air flow and a phase change material plate

Alvaro de Gracia [a,b], Damien David [b], Albert Castell [a], Luisa F. Cabeza [a,*], Joseph Virgone [b]

[a] GREA Innovació Concurrent, Universitat de Lleida, Edifici CREA, Pere de Cabrera s/n, 25001 Lleida, Spain
[b] CETHIL, UMR 5008, INSA-Lyon, Université Lyon1, Bât. Sadi Carnot, 9 rue de la Physique, 69621 Villeurbanne, France

HIGHLIGHTS

- Convective heat transfer of an air flow over a *PCM* plate is analyzed numerically.
- A numerical correlation is given from the CFD results.
- The phase change is addressed as perturbation in the Nusselt of a solid flat plate.
- The CFD simulations indicate movement in the thermal boundary layer.
- The numerical correlation was compared against CFD, showing good agreement.

ARTICLE INFO

Article history:
Received 6 March 2012
Accepted 28 November 2012
Available online 7 December 2012

Keywords:
Convective heat transfer coefficient
Correlation
Phase change material
Heat storage system
Transient forced convection
Numerical simulation

ABSTRACT

This paper provides a new correlation to determine the heat transfer coefficient between an air flow and a plate made of phase change material (*PCM*). This correlation was built for the simulation of heat storage units containing *PCM* plates subjected to an inlet temperature step. The presented correlation has the following form: $Nu_{x,t}^{PCM} = Nu^{PSM} \cdot f^{PCM}$. The first term Nu^{PSM} is for a plate made of traditional material. The term f^{PCM} is a perturbation due to the phase change in the plate. Each term depends on 5 non-dimensional parameters. One of them represents the advance in the total heating or cooling process, in order to take into account the transient evolution of the convective coefficient. The correlations are built using the Least Squares Method, from series of CDF simulation data. The shape of the perturbation f^{PCM} reveals a complex evolution of the temperature repartition in the *PCM* plate. Finally, a nodal model of the plate has been developed in order to test the provided new correlation and other correlations available in the literature. The results obtained with the present correlation show better agreements with the CFD results, which make this correlation suitable for the simulation of *PCM* heat storage systems.

1. Introduction

An efficient utilization of renewable energies in buildings could not be possible without appropriate energy storage systems. Indeed, the availability of these energies does not always coincide in time with the demand. Hence energy storage systems present a growing interest among research communities.

One possible way to store a high amount of energy in a small volume is the use of phase change materials (*PCM*). Dincer and Rosen [1] highlighted that the solid–liquid phase change presents high energy density and does not present volume expansion problems. The latent heat which is needed for the material melting/solidification enables to store a great amount of energy within a narrow temperature range. Paksoy [2] has studied several thermo-physical properties of various *PCM* for a correct selection of the material depending on the application.

The use of *PCM* in the building sector has been widely studied [3], both experimentally [4] and numerically [5]. The *PCM* can be integrated in composite walls [6], in heat exchangers which are included in the building ventilation system [7], or in ventilated facades [8,9].

Several studies have analyzed the thermal performance of different heat exchangers with *PCM*. Nomura et al. [10] evaluated experimentally a direct-contact heat exchanger with *PCM* and the rate of heat storage depending on the temperature of the heat transfer fluid and its flow rate. Kurnia et al. [11] studied numerically various U-tube configurations for a thermal energy storage unit with *PCM*. The results demonstrated that the use of the festoon

* Corresponding author. Tel.: +34 973 00 35 77; fax: +34 973003575.
E-mail address: lcabeza@diei.udl.cat (L.F. Cabeza).

1359-4311/$ – see front matter © 2012 Elsevier Ltd. All rights reserved.
http://dx.doi.org/10.1016/j.applthermaleng.2012.11.045

channel design yields improved heat transfer rate. Ye et al. [12] analyzed the effects of different cavity volume fractions of *PCM* in the heat transfer performance of a latent thermal unit. The numerical results from a CFD package were experimentally validated and correlations are proposed for volume expansion ration and time to finish thermal energy storage process as function of the *PCM* cavity volume fraction.

This study is focused on heat exchangers made of *PCM* plates. The air flowing between the parallel plates exchanges heat with the *PCM*. The performances of such systems are evaluated with building simulations. Those simulations require simple and accurate models of the heat exchangers, such as nodal models, in which the heat transfer between the air flow and the plate is modeled by the convective coefficient.

In the literature, the existing heat transfer correlations for the flow between parallel plates are for two cases: "constant and equal wall temperatures", and "constant and equal wall heat fluxes". According to Liu et al. [13], the case of "constant and equal wall temperature" is more appropriate to model the convective heat transfer occurring between a forced flow and a *PCM* solid, since the wall temperatures are almost constant during the phase change. However, thermal gradients can occur in the *PCM* wall, especially in heat exchangers with long *PCM* slabs, which makes the assumption of "constant and equal wall temperature" not valid.

Therefore, no correlation has been built for the specific case of an air flow over *PCM* plates, so there was no optimal choice of the convective coefficient values in *PCM* heat exchangers. Wei et al. [14] obtained the Nusselt number from the experimental value in a plate heat exchanger (PHE). Moreover, Dolado et al. [15] used the correlation from Gnielinski [16] for internal forced convective coefficient while Hed and Bellander [17] used the Reynolds–Colburn analogy [18]. However their simulation results might be affected by erroneous convective heat transfer coefficient values. Indeed, David et al. [19,20] simulated the thermal behavior of a composite *PCM* wall using different correlations to model the natural convection heat transfer over the wall. They spotted discrepancies in the simulation results.

In this study, a new correlation is built to determine the heat transfer coefficient between an air flow and a plate made of *PCM*. The correlation has two terms: one of them is for a plate without phase change, the other one is a perturbation on the Nusselt number due to the phase change. The methodology for the production of the two terms of the correlation is explained in Section 2. Details about the geometry and the thermal excitation of the system are also given in this section. The two terms of the correlation are built in Sections 3 and 4. The new correlation is finally implemented in a nodal model of *PCM* plates in Section 5. Nodal simulation results with new provided correlation and with other correlations available in the literature are compared to CFD results.

2. Methodology

2.1. Shape of the correlation

The correlation which is built in this paper has the form of Eq. (1), where $Nu_{x,t}^{PCM} = h \cdot x/k$ is the local Nusselt number at the ordinate x:

$$Nu_{x,t}^{PCM} = Nu^{PSM} \cdot f^{PCM} \tag{1}$$

The first term Nu^{PSM} is calculated for the heating/cooling process of a plate made of a traditional material which has the same thermo-physical properties of the *PCM* in the solid state. Since no phase change occurs in this plate, it is designated as the Phase Stabilized Material (*PSM*) plate.

The second term f^{PCM} describes the perturbation on the Nusselt number due to the phase change in the wall. Thus, the formalism which is chosen for the expression of $Nu_{x,t}^{PSM}$ enables to isolate phase change effects on the convective heat transfer through the term f^{PCM}.

For each term of the correlation, a list of 5 specific non-dimensional parameters has been defined. The dependency of Nu^{PSM} and f^{PCM} on those parameters are determined from series of computational fluid dynamics (CFD) simulations. The term Nu^{PSM} was obtained first from simulation results without phase change in the plate. The term f^{PCM} was calculated from simulations with phase change in the plate, by dividing the computed Nusselt number $Nu_{x,t}^{PSM}$ by Nu^{PSM}.

2.2. Geometry of the system

The system which concerns this study is a pile of *PCM* plates separated by air channels (Fig. 1a). The air flow between the plates is ensured by a homogeneous velocity inlet at the entrance of the channel. The heat storage/release starts with an inlet temperature step.

The geometry of the system has been simplified according to some hypotheses, in order to reduce the computational cost of the CDF simulations. First, it is assumed that the plates are sufficiently wide to get a 2-dimensional thermal behavior of the system. Then, since the geometry is periodic, only one channel surrounded by two

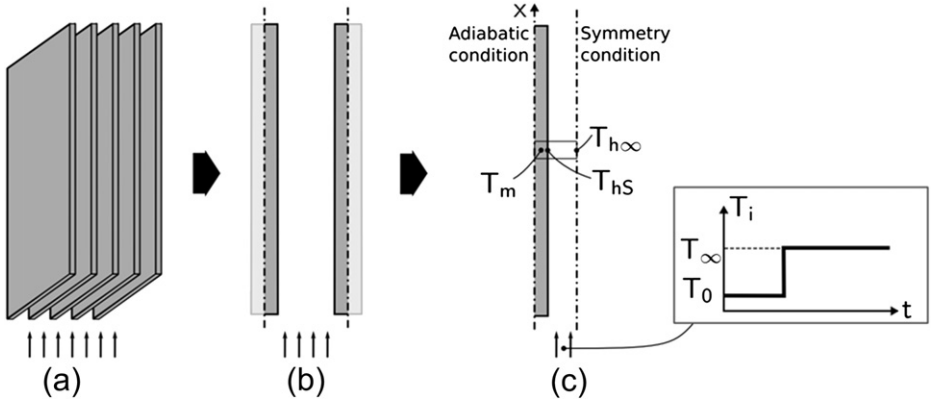

Fig. 1. Simplification of the heat exchanger geometry for the model: (a) actual geometry of the heat exchanger, (b) Simplified geometry using the hypothesis of a periodic system and a 2D flow, (c) Geometry of the model, using the hypothesis of independent boundary layers.

half plates can be considered. The system represented in Fig. 1b is obtained after performing these simplifications.

Moreover, it is assumed that the thermal and velocity boundary layers are thinner than the half-width of the air channel. Since there is no mixing between the boundary layers on the two sides of the channel, only a half-channel can be considered. Even if this type of geometry does not optimize the heat transfer between the plates and the channel, it can be justified in a technical point of view because it reduces the pressure drop along the storage system. The final geometry of the model is represented in Fig. 1c. For the simulations, the plate was 4 m high and the half-channel was 7.5 cm wide.

At the beginning of the simulations, the temperature is homogeneous at T_0 in all the system, and there is a steady flow in the fluid volume due to the homogeneous inlet velocity u_∞. At $t = 0$, the inlet temperature becomes equal to T_∞. Simulations are run until the plate temperature reaches the thermal equilibrium at T_∞. During the simulations, the half plate mid-temperature T_m, the mid-channel temperature $T_{h\infty}$, the plate surface temperature T_{hS} and heat flux density φ_{hS} are recorded at different heights and times in order to compute the heat transfer coefficients $h = \varphi_{hS}/(T_{hS} - T_{h\infty})$ and the non-dimensional parameters used in the correlations.

2.3. Numerical model

The simulations have been performed with the commercial software Star-CCM+. First, a comparative study between the different fluid models proposed by the software has been carried out. Those models have been tested for a stationary forced turbulent flow along an isothermal surface. The simulation results have then been compared to the empirical correlations from Bejan [21], which are valid for Prandtl number between 0.5 and 5:

$$\frac{h}{\rho \cdot Cp \cdot u_\infty} = \frac{\frac{1}{2}\cdot C_{f,x}}{0.9 + \left(\frac{1}{2}\cdot C_{f,x}\right)^{0.5} \cdot (13.2 \cdot \mathrm{Pr} - 10.25)} \tag{2}$$

where the drag coefficient $C_{f,x}$ is given either by:

$$\frac{1}{2}\cdot C_{f,x} = 0.0296\left(\frac{u_\infty \cdot x}{\upsilon}\right)^{-1/5} \tag{3}$$

or by:

$$C_{f,x} = 0.37\left[\log\left(\frac{u_\infty \cdot x}{\upsilon}\right)\right]^{-2.584} \tag{4}$$

The previous correlations are valid for Reynolds number varying between 10^5–10^7 (Eq. (3)) and from 10^5–10^9 (Eq. (4)).

The best agreement with the correlations was obtained with the Segregated implicit AMG SIMPLE solver and the "realizable" $k-\varepsilon$ turbulence model.

Hereafter, a mesh independent study was performed in order to reduce the duration of the transient simulations needed for this study. The resulting mesh consisted in 4400 rectangular cells, with a mesh refinement at the vicinity of the plate in order to capture the temperature and velocity gradients in the boundary layer.

A comparison between the final flow model and the correlations from Bejan [21] is shown in Fig. 2 for different values of the inlet velocity. The results of this comparison show only a slight deviation at the starting area of the plate. This deviation is due to the presence of the laminar zone. In this zone, neither the correlation from Bejan, nor for the $k-\varepsilon$ turbulence model are adapted.

The solid model is a finite volume model with 1334 rectangular cells. The specific heat of the solid and liquid phases is equal to Cp.

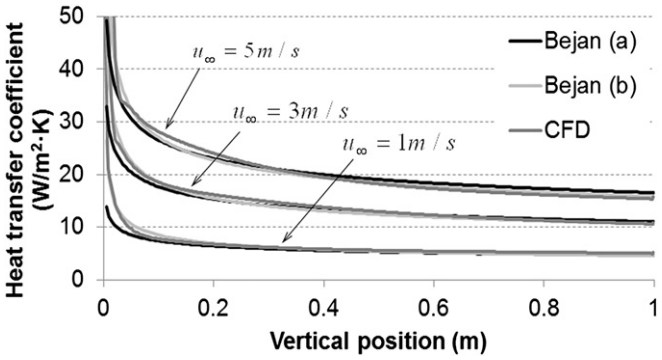

Fig. 2. Fluid model validation using empirical correlation available in literature [15].

The phase change was taken into account through an equivalent heat capacity [22]. During the melting or solidification, the temperature dependence of the *PCM* specific heat has a triangle shape centered on T_{PCM} (Fig. 3). This methodology was studied by Farid [23] and was found to be successful in describing the heat transfer in phase change materials.

3. Empirical correlation without the effect of phase change

3.1. Significant parameters

Five parameters were selected to build the correlation for a phase stabilized material wall:

$$Nu^{PSM} = Nu^{PSM}(\mathrm{Re}_x, \theta_x, A, B, C) \tag{5}$$

Those parameters intend to characterize:

- The flow regime
- The advance in the heating/cooling process
- The thermal and geometrical properties of the plate.

The first parameter is the local Reynolds number Re_x. It is an image of the flow regime. It is covered in the range $[1 \cdot 10^5; 2 \cdot 10^6]$ for a transitional and turbulent flow:

$$\mathrm{Re}_x = \frac{u_\infty \cdot x}{\upsilon} \tag{6}$$

The second parameter θ_x represents the progression of the plate heating/cooling process, at the height x. Since there are

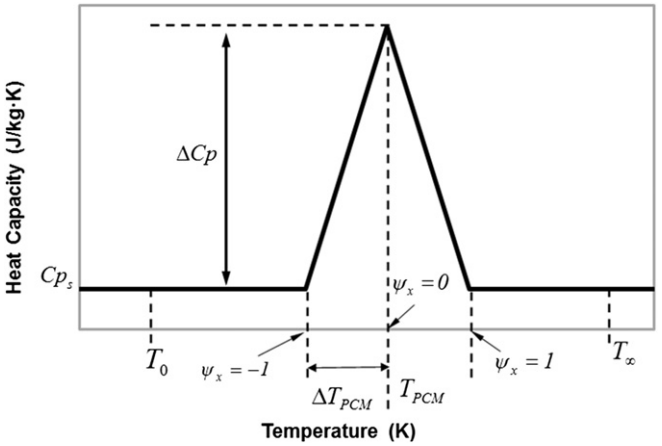

Fig. 3. Temperature dependency of the effective specific heat of the phase change material.

Table 1
Minimum and maximum values of the used parameters.

	Min. value	Max. value
u_∞ [m s^{-1}]	2	12
ρ_s [kg m^{-3}]	750	2200
Cp_s [J kg^{-1} K^{-1}]	500	4000
e [m]	0.002	0.02
k_s [W m^{-1} K^{-1}]	0.1	2.5

temperature gradients across the plate thickness, it is based on the temperature at the middle of the half plate T_m (Fig. 1c). The definition of θ_x is given in Eq. (7). It is equal to zero all over the plate at the beginning of the simulation and it is equal to one all over the plate at the end of the simulation.

$$\theta_x = \frac{T_m(x) - T_0}{T_\infty - T_0} \tag{7}$$

Even if θ_x is defined in the range [0; 1], the Nusselt correlation was built from simulation results with $\theta_x \in [0.05; 0.95]$. Indeed, when θ_x approaches one, the convective coefficient is undefined because the plate and the air flow have the same temperature.

The remaining parameters A, B and C take into account the thermal and geometrical characteristics of the plate. A is the volume specific heat ratio between the plate and the air:

$$A = \frac{\rho_s \cdot Cp_s}{\rho_s \cdot Cp} \tag{8}$$

B is the ratio between an estimation of the velocity boundary layer thickness $\delta_x = 5\sqrt{\upsilon x/u_\infty}$, and the thickness of the plate e:

$$B = \frac{\delta_x}{e} \tag{9}$$

C is the thermal conductivity ratio between the plate and the air:

$$C = \frac{k_s}{k} \tag{10}$$

Maximum and minimum values of the different physical quantities are shown in Table 1. They were chosen according to Cabeza et al. [24]. Using the parameters from Table 1, the valid ranges of Re_x, θ_x, A, B, and C are summarized in Table 2.

3.2. Formulation of the Nusselt number

The structure of the correlation is presented in Eq. (11). The dimensionless number θ_x is implemented in the form $(\theta_x + 1)^a$ because at the beginning of the transient process ($\theta_x = 0$), the heat transfer coefficient is neither equal to zero, nor equal to infinity:

$$Nu_{x,t}^{PSM} = \alpha_0 \cdot \mathrm{Re}_x^{\alpha_1} \cdot (\theta_x + 1)^{\alpha_2} \cdot A^{\alpha_3} \cdot B^{\alpha_4} \cdot C^{\alpha_5} \tag{11}$$

The software Design-Expert V8 for design of experiment (DOE) defined a set of 31 different simulations to be carried out for the determination of the five constants α_i. The results of those simulation were then introduced in the R 2.14 statistical software, which calculated the α_i using a Least Squares Method.

Table 2
Valid range of the dimensionless groups used.

	Min. value	Max. value
Re_x	$1 \cdot 10^5$	$2 \cdot 10^6$
θ_x	0.05	0.95
A	307.8	7222
B	0.125	14.05
C	4.17	104.2

Table 3
Standard deviation and p-value of the estimated parameters used in the Nu_{PSM} correlation.

	Standard deviation σ	p-value
α_0	0.102	$<2 \cdot 10^{-16}$
α_1	0.007	$<2 \cdot 10^{-16}$
α_2	0.024	$1.78 \cdot 10^{-10}$
α_3	0.004	0.725
α_4	0.007	0.182
α_5	0.004	0.728

3.3. Results

The correlation obtained after using the Least Squares Method is given in Eq. (12). The average deviation between the simulated Nusselt numbers and the Nusselt values calculated from the correlation is 2.4%.

$$Nu_{x,t}^{PSM} = 0.036 \cdot \frac{\mathrm{Re}_x^{0.78} \cdot (\theta_x + 1)^{0.18}}{A^{0.002} \cdot B^{0.01} \cdot C^{0.002}} \tag{12}$$

Moreover, the standard deviation and p-value of each estimated parameter (α_i) are shown in Table 3 (based on Eq. (12)). Since the p-value of the estimated parameters α_3, α_4 and α_5 are higher than 0.05, the variation of the parameters A, B and C is not significant to the Nusselt number. The authors propose to use an empirical correlation which depends only on Re_x and θ_x. This new correlation presents an average deviation of 2.5% from the numerical results, with standards deviations of the estimated parameter α_0 of 0.093, α_1 of 0.007 and α_2 of 0.024 (based on Eq. (13)).

$$Nu_{x,t}^{PSM} = 0.037 \cdot \mathrm{Re}_x^{0.78} \cdot (\theta_x + 1)^{0.18} \tag{13}$$

4. Nusselt perturbation due to the phase change

4.1. Significant parameters

A set of 5 dimensionless numbers were defined to describe the phase change perturbation f^{PCM} on the Nusselt evolution:

$$f^{PCM} = \frac{Nu_{x,t}^{PCM}}{Nu^{PSM}} = f^{PCM}(\mathrm{Re}_x, St, S_{Cp}, P, \psi_{PCM}) \tag{14}$$

Those parameters intend to characterize:

- The flow regime
- The thermal behavior of the *PCM* during the phase change
- The advance in the melting/solidification process.

The three parameters St, S_{cp} and P describe the properties of the plate material during the phase change. They characterize the temperature dependency of the *PCM* effective heat capacity (Cp curve) shown in Fig. 3.

St is the Stefan number based on the temperature difference $T_\infty - T_0$. The effect of this parameter on the Cp curve is shown in Fig. 4a.

$$St = \frac{Cp_s(T_\infty - T_0)}{\Delta H_{fusion}} \tag{15}$$

The parameter S_{Cp} is defined in Eq. (16) as the ratio between the increase of specific heat at the phase change temperature and the

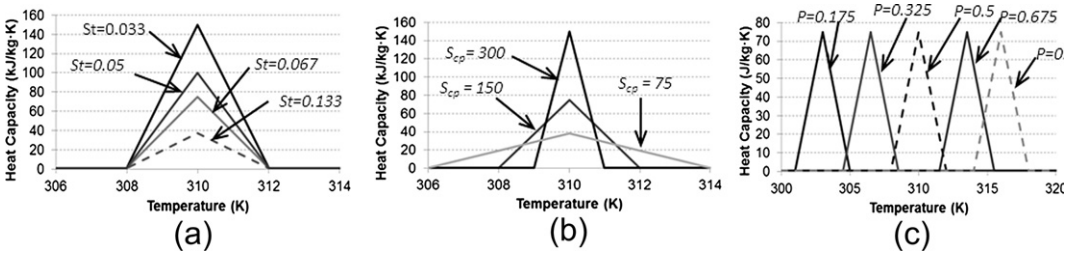

Fig. 4. Variation of the specific heat curve with (a) *St*, (b) S_{Cp} and (c) *P*.

specific heat in the solid or liquid region (see Fig. 3). Fig. 4b shows the variation of the *Cp* curve when S_{Cp} varies (constant *St*).

$$S_{Cp} = \frac{\Delta Cp}{Cp_s} \tag{16}$$

P fixes the position of the phase change temperature T_{PCM} in the overall process of heating or cooling [T_0; T_∞]. It is defined in Eq. (17). Fig. 4c shows the effect of *P* on *Cp* curves.

$$P = \frac{T_{PCM} - T_0}{T_\infty - T_0} \tag{17}$$

The last dimensionless number ψ_x characterizes the advance in the melting/solidification process at the height *x*. Similarly to the parameter θ_x, it is based on the temperature at the middle of the half plate T_m. The expression of ψ_x is given by Eq. (18). It has to be multiplied by −1 when used in a fusion process.

$$\psi_x = \frac{T_m(x) - T_{PCM}}{\Delta T_{PCM}} \tag{18}$$

Notice that ψ_x is equal to zero when the specific heat of the plate is maximum, at $T_m(x) = T_{PCM}$. It is equal to −1 at the beginning of the fusion/solidification process and it is equal to 1 at the end of the phase change (Fig. 3). The bounds of ψ_x depend on the initial and final temperatures T_0 and T_∞.

The studied ranges of the previous parameters are shown in Table 4.

4.2. Simulation results

Table 5 summarizes the set of numerical simulations which have been performed to determine f^{PCM}. The numerical results were analyzed through the evolutions of f^{PCM} over ψ_x.

The curves $f^{PCM}(\psi_x)$ for simulations C1–C14 are shown in Fig. 5. For $\psi_x \le -1$, the phase change has not started yet, hence there is no perturbation on the Nusselt number and $f^{PCM} = 1$. During the increasing part of the specific heat curves ($-1 \le \psi_x \le 0$), the phase change has no effect on the Nusselt number, and the perturbation remains equal to 1. The value of f^{PCM} starts to deviate when the plate reaches the temperature T_{PCM}. First, it can be observed an increase of f^{PCM} when $\psi_x > 0$ until $\psi_x = \psi_{cr}$. Finally, f^{PCM} stabilizes at a maximum value f_∞.

From Fig. 5a, it can be seen that the maximum perturbation f_∞ decreases when the Stefan number *St* increases. Thus, the higher is the latent heat, the higher is the phase change perturbation on the convection coefficient.

Fig. 5b shows that the maximum perturbation increases with *P*. The perturbation on the convective heat transfer coefficient will be higher if the phase change occurs at the beginning of the heating/cooling process.

Finally, from Fig. 5c and d, it can be observed that the flow regime (through the Reynolds number) and the width of the phase change temperature range (through the parameter S_{Cp}) have only slight effects on the perturbation curves.

Moreover, Fig. 6 compares the perturbation evolutions for a melting and a solidification process. The curves are identical, therefore the same dimensionless model can be used to describe a heating or a cooling process.

4.3. Formulation of the phase change perturbation

Given the description of the perturbation curves provided in the last section, the function $f^{PCM}(\psi_x)$ can be expressed as a piecewise function given by Eq. (19) (Fig. 7).

$$f^{PCM}(\psi_x)\begin{cases} 1 & \text{for } \psi_x < 0 \\ \dfrac{(f_\infty - 1)}{\psi_{cr}^2}\cdot\psi_x^2 + 1 & \text{for } 0 \le \psi_x < \psi_{cr} \\ f_\infty & \text{for } \psi_x \ge \psi_{cr} \end{cases} \tag{19}$$

The values of f_∞ and ψ_{cr} depend on the parameters Re_x, *St*, S_{cp} and *P* (Eqs. (20) and (21)). They are defined from the simulation results by using a Least Squares Method.

$$f_\infty = \alpha_0 \cdot St^{\alpha_1} \cdot P^{\alpha_2} \cdot S_{Cp}^{\alpha_3} \cdot \mathrm{Re}^{\alpha_4} \tag{20}$$

$$\psi_{cr} = \alpha_0 \cdot St^{\alpha_1} \cdot P^{\alpha_2} \cdot S_{Cp}^{\alpha_3} \cdot \mathrm{Re}^{\alpha_4} \tag{21}$$

Table 4
Valid range of the parameters used in the correlation for f^{PCM}.

	Min. value	Max. value
St	0.033	0.14
P	0.175	0.8
S_{Cp}	72	300

Table 5
Set of numerical simulations carried out to define the phase change.

Case	*Re*	*St*	*S*	*P*
C1	10^6	0.034	291.8	0.5
C2	10^6	0.07	145.4	0.5
C3	10^6	0.07	145.4	0.175
C4	10^6	0.07	291.8	0.5
C5	10^6	0.07	72.9	0.5
C6	10^6	0.07	205.3	0.5
C7	10^6	0.14	72.2	0.5
C8	10^6	0.51	194.2	0.5
C9	$4.1 \cdot 10^5$	0.07	145.4	0.325
C10	$8.2 \cdot 10^5$	0.07	145.4	0.325
C11	10^6	0.07	145.4	0.325
C12	$1.6 \cdot 10^6$	0.07	145.4	0.325
C13	10^6	0.07	145.4	0.675
C14	10^6	0.07	145.4	0.8

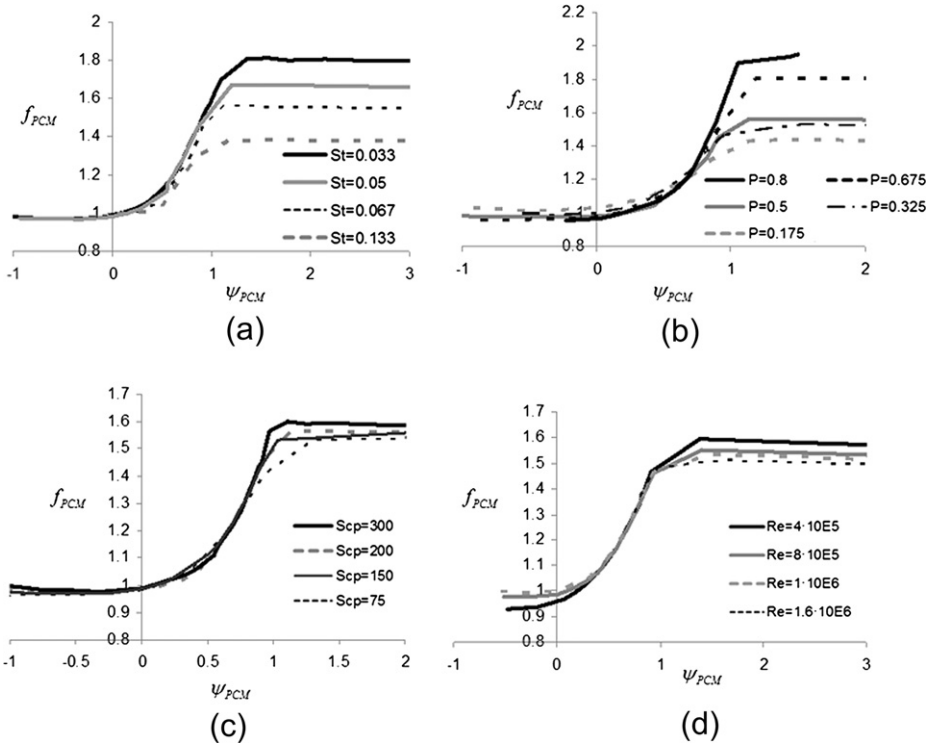

Fig. 5. Effect on the perturbation in the Nusselt evolution due to variation of (a) *St*, (b) *P*, (c) S_{Cp} and (d) *Re*.

The correlation in Eq. (22) calculates the value of the maximum perturbation f_∞ with an average error of 2.51% compared to the CFD results. Reynolds number and S_{Cp} are not significant in the correlation since its *p*-value are 0.636 and 0.550, respectively (based on Eq. (22)). The authors propose a new correlation (Eq. (23)) without these two dimensionless numbers. This new correlation presents an average error of 2.84% with the numerical results with standards deviations of the estimated parameter α_0 of 0.140, α_1 of 0.050 and α_2 of 0.034 (based on Eq. (23)).

$$f_\infty = 1.69 \cdot \frac{P^{0.15}}{St^{0.22} \cdot \mathrm{Re}^{0.026} \cdot S_{Cp}^{0.033}} \tag{22}$$

$$f_\infty = 1.08 \cdot \frac{P^{0.14}}{St^{0.19}} \tag{23}$$

Furthermore, a correlation for ψ_{cr} is provided by Eq. (24). Again, the Reynolds number and the parameter S_{Cp} are not significant to determine ψ_{cr} (*p*-value of 0.308 and 0.854, respectively). The use of Eq. (25) instead of Eq. (24) only increases the average error from 2.35% to 2.71%. The standard deviation of the estimated parameter α_0 is 0.116, of α_1 is 0.042 and of α_2 is 0.028 (based on Eq. (25)).

$$\psi_{cr} = 0.65 \cdot \frac{P^{0.10} \cdot \mathrm{Re}^{0.0082} \cdot S_{Cp}^{0.039}}{St^{0.095}} \tag{24}$$

$$\psi_{cr} = 0.8 \cdot \frac{P^{0.10}}{St^{0.13}} \tag{25}$$

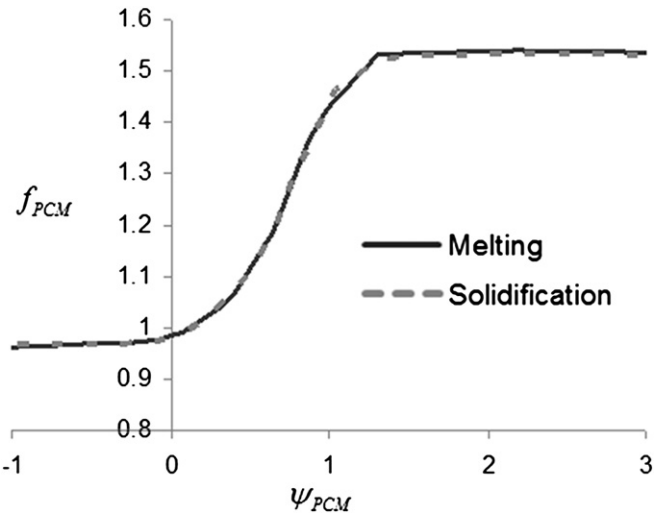

Fig. 6. Comparison of the perturbation of the Nusselt number due to solidification and melting process (simulation C2).

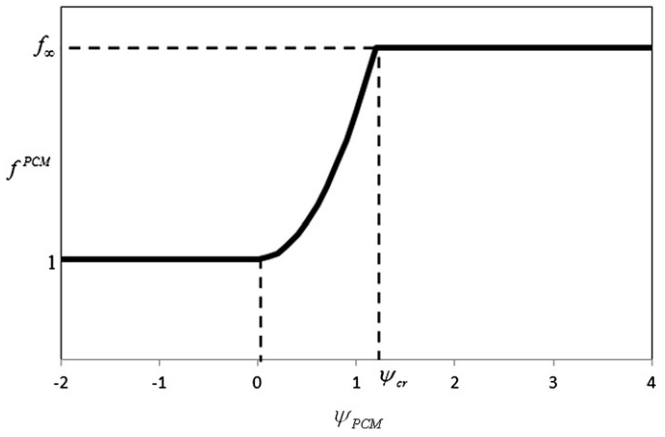

Fig. 7. Shape of the perturbation in the Nusselt evolution due to the phase change.

4.4. Discussion

The particular shape of the curves $f^{PCM}(\psi_x)$ can be understood by analyzing the temperature repartitions in the plate during the cooling and heating processes. For this purpose, Fig. 8 contains schematic representations of the plate temperature repartition at the beginning and at the middle of a heating process. The two sketches on the left are for a *PSM* plate while the two sketches on the right stands for a *PCM* plate. The velocity boundary layer and the repartition of the heat transfer coefficient are represented on each schema.

The initial conditions are identical for both types of plate: the *PCM* is solid at the temperature T_0. Since the air flow is due to external forces, it is not affected by the thermal response of the plate. Hence, the velocity repartition in the fluid is identical for both types of plates and it does not evolve during the heating process.

Nusselt variations are due to evolutions of the thermal boundary conditions at the surface of the plates. For the *PSM* plate, this evolution is gradual and homogeneous all along the plate. The heat transfer coefficient increases gradually all along the plate until the final temperature is reached.

On the other hand, for the *PCM* plate, we observe the formation of 5 distinct zones. From the top of the plate (last scheme on Fig. 8):

- First zone: the phase change has not started yet and the *PCM* is still in the solid phase.
- Second zone: this is the first part of the phase change, when the specific heat *Cp* increases with the temperature.
- Third zone: this is the second part of the phase change, when the specific heat *Cp* decreases with the temperature.
- Fourth zone: the phase change is finished. The *PCM* is in the liquid state, but it has not reached the thermal equilibrium at T_∞.
- Fifth zone: the heating process is finished. The *PCM* is in the liquid state at the temperature T_∞.

Thus, the first major difference between *PCM* and *PSM* plates is the apparition of the fifth zone near the leading edge. At this location, the plate is in thermal equilibrium with the air flow, hence there is no heat flux at the surface, and the convection heat transfer value has no effect on the system behavior.

The thermal boundary layer starts at the fourth zone. The starting point of the thermal boundary layer induces high values of the heat transfer coefficient. Therefore, the perturbation value is higher in this zone. Since the liquid phase receives heat from the air flow at a high rate, the temperature progression between the end of phase change and the final temperature is fast. Hence, this zone is relatively narrow compared to the other ones.

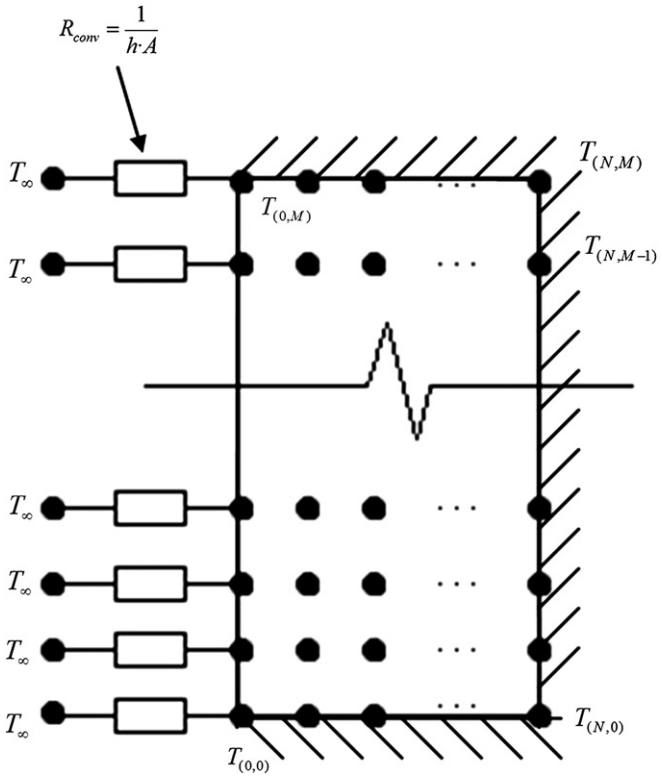

Fig. 9. Sketch of the nodal model.

The phase change occurs in second and third zones. The same amount of heat must be stored in the plate during the first (*Cp* rising) and second (*Cp* decreasing) part of the phase change. However, since the heat transfer rate is higher during the second part, the third zone is narrower.

During the simulation, the sequence of the different zones is shifted toward the upper part of the plate. The last zone which corresponds to the thermal equilibrium grows until it covers the whole wall.

5. Assessment of the present correlations

The purpose of the correlations developed in this study is to use them in simplified models of latent heat storage systems. These

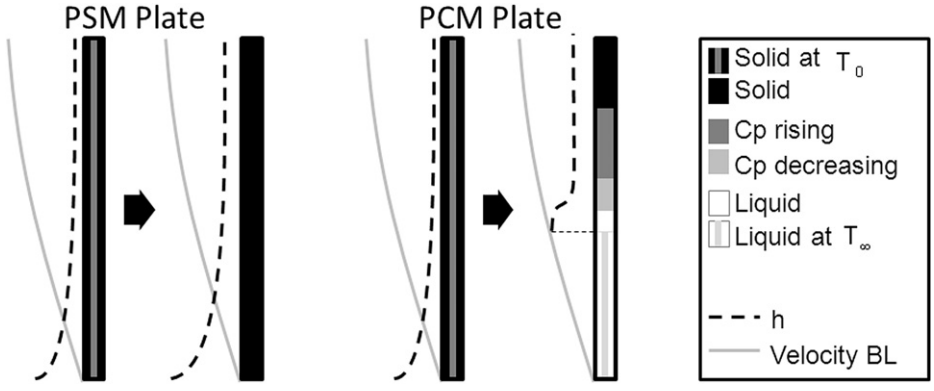

Fig. 8. The evolution of the temperature repartition in the plate and its effect on the convection coefficient. On the left: phase stabilized plate. On the right, phase change material plate.

Table 6
Physical and geometrical variables input in the numerical model.

Physical and geometrical input	Value
ΔH_{PCM} [kJ kg^{-1}]	150
ΔCp [kJ kg^{-1} K^{-1}]	75
Cp_s [J kg^{-1} K^{-1}]	512.3
ρ_s [kg m^{-3}]	2200
k_s [W m^{-2} K^{-1}]	2.5
$e/2$ [m]	0.006
L [m]	4

models include finite volume models for the plates, which are connected to the air flows through convective heat transfer coefficients.

In this section, a nodal model of a half-channel is developed. Simulations are performed with different correlations for the convective heat transfer coefficient. The simulation results are compared to CFD results in order to evaluate the improvement due to the use of the correlation built in this study.

5.1. Finite volume model

The energy equation is solved using a fully implicit finite volume method [25]. The transient two-dimensional heat transfer in a *PCM* plate (Eq. (26)) is completed by initial and boundary conditions (Eq. (27)–(31)). L is the height of the plate, $e/2$ is the half-width of the plate. A sketch of the nodal model is presented in Fig. 9.

$$\frac{\partial H_{PCM}}{\partial t} = k_s\left(\frac{\partial^2 T}{\partial x^2}+\frac{\partial^2 T}{\partial y^2}\right) \quad \text{with } \partial H_{PCM} = \rho_s Cp(T)\partial T \tag{26}$$

$$\text{(i)} \quad t = 0 \quad T_0 \tag{27}$$

$$\text{(ii)} \quad x = 0 \quad \frac{\partial T}{\partial x} = 0 \tag{28}$$

$$\text{(iii)} \quad x = L \quad \frac{\partial T}{\partial x} = 0 \tag{29}$$

$$\text{(iv)} \quad y = 0 \quad -k_s\frac{\partial T}{\partial x} = h\cdot\left(T_\infty - T_{surf,x}\right) \tag{30}$$

$$\text{(v)} \quad y = e/2 \quad \frac{\partial T}{\partial x} = 0 \tag{31}$$

A mesh independence study was carried out for the control volume numerical model. A mesh of 400 nodes is used with 40 and 10 nodes in the x and y direction. The system of algebraic linear equations extracted from the finite volume method was solved using the Gauss Seidel iterative algorithm with a time step of 1 s.

The geometric and thermo-physical properties of the plate simulated with the nodal model are gathered in Table 6. The *PCM* plate is heated from 300 K to 320 K. The melting process starts at 308 K and finishes at 312 K. The temperature T_{PCM} is 310 K.

5.2. Simulation results

One of the main interests in simulating *PCM* exchangers is to predict the time needed to complete the heating or cooling processes of the plates. As it was previously discussed, the transient evolution of the convective heat transfer coefficient is not explicitly expressed through time, but through the dimensionless parameters θ_x and ψ_x, which represent the advances in the heating/cooling and fusion/solidification process. In this section, all the results are presented as functions of time.

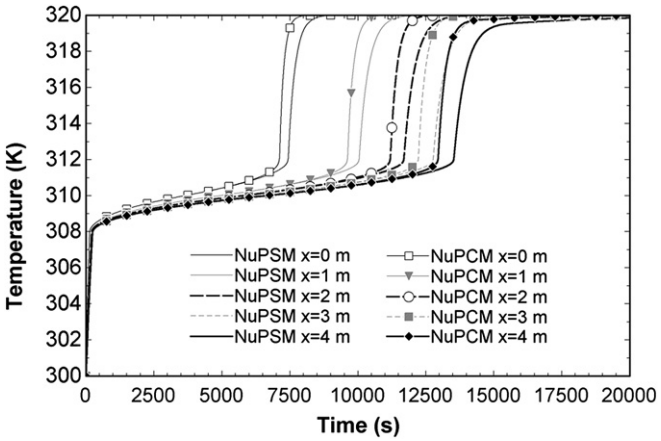

Fig. 10. Evolution of the temperature at the middle of the half *PCM* plate, at different heights. Comparison between the correlations with and without *PCM* perturbation.

Fig. 10 presents the difference in the thermal evolution of the central node at different heights, when the numerical model uses the given base empirical correlation, Nu^{PSM} (Eq. (13)) or the correlation Nu^{PCM} which takes into account the perturbation due to the phase change f^{PCM} (Eqs. (19), (23) and (25)).

As it was expected, no differences were found before the phase change temperature peak (310 K), since the perturbation only acts with positives values of ψ_x (Eq. (21)). After the peak, the incidence in the thermal evolution of the *PCM* plate due to perturbation is significant and grows along the height of the plate. The time needed to melt the node at $x = 4$ m is reduced around 5% from the time of the overall process when the perturbation due to phase change is used.

Time evolutions of the convective heat transfer coefficient, with and without the perturbation, are presented in Fig. 11. As it was previously mentioned, there is no difference between the models before the phase change peak. However, after the phase change peak two distinct behaviors are observed. For the simulations which use the *PCM* perturbation on h, the heat transfer coefficient grows gradually and reaches a plateau at $\psi_x = \psi_{cr}$. For the other simulations, the results show a slight jump of the h coefficient after the phase change is finished. This is due to a fast evolution of the parameter θ_x in the liquid phase.

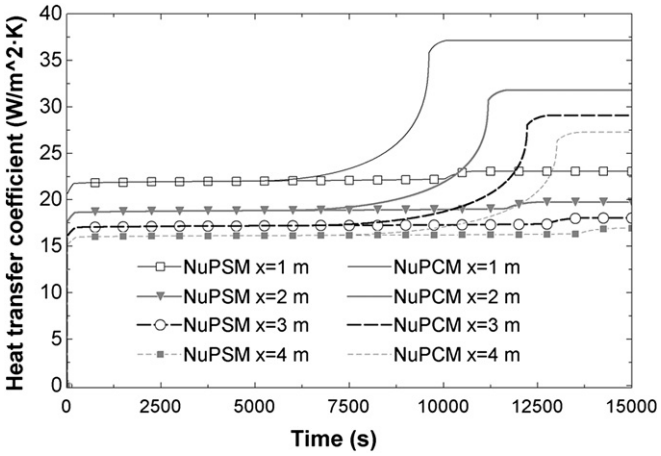

Fig. 11. Evolution of the heat transfer coefficient at different heights of the *PCM* plate. Comparison between the correlations with and without *PCM* perturbation.

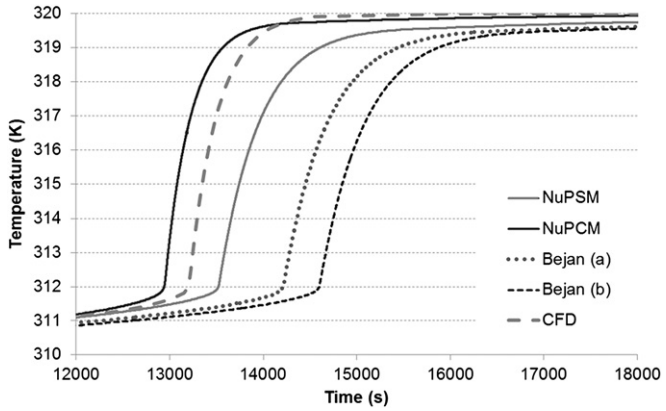

Fig. 12. Evolution of the temperature at the top of the *PCM* plate. Comparison between CFD results and nodal model results with different empirical correlations.

Table 7
Correlation comparison of the time needed to cover the 95% of the heating process.

Empirical correlation	Time to achieve 319 K (s)	Error in comparison to CFD (%)
Nu_{PSM}	14,550	5.4
Nu_{PCM}	13,530	2
Bejan (a)	15,380	11.5
Bejan (b)	15,825	14.7

The thermal load of a *PCM* wall is finished when the top part of the plate has reached the final temperature T_∞. Fig. 12 shows the time evolution of the temperature at the central node at the top of the half plate, for different simulations using different correlations of the heat transfer coefficient. The results are compared to the CDF results. It can be seen that the empirical correlation provided in this work presents better agreement with the CFD results in comparison to the correlation provided by Bejan [21], especially the model which considers the perturbation in the Nusselt number due to the phase change.

Table 7 presents the time needed for each correlation to cover the 95% of the overall heating process (319 K) in the analyzed node and compares this time against the time needed in the CFD model (13,800 s). It is important to highlight that the model which uses the perturbations not only finish the phase change earlier (3h 36 min40 s from 3 h46 min40 s) but it achieves steady state conditions earlier by increasing the heat transfer coefficient at the studied positions.

6. Conclusions

The present study assessed for the first time the issue of forced convective heat transfer along *PCM* plates. Its major achievements are not only practical, with the production of accurate correlations for latent heat storage systems, but also theoretical, with the first analysis of how the temperature repartitions in *PCM* plates during heat storage processes, affects the convective heat transfer coefficients.

From the practical point of view, the correlations for a *PCM* plate, and the correlation for the *PSM* plate are original. These correlations will be suitable for the simulation of sensible and latent heat storage systems, in a wide valid range of the different non-dimensional numbers. The use of these correlations in a nodal model will save computational costs compared to the use of computational fluid dynamics simulations.

On the theoretical point of view, the series of simulations which have been performed enabled the authors to have a first understanding of how the plate material phase change affects the convective heat transfer. They clearly showed the presence of a zone, at the bottom of the plate, in which the wall material is in thermal equilibrium with the flow. The presence of this zone delays the starting point of the thermal boundary layer, which leads to heat transfer enhancement at this location.

Obviously, the present study does not pretend to cover the whole subject of forced convection along *PCM* plates. The correlation will have to be compared to experimental results in the future. And a theoretical analysis of the Navier Stokes equations might be necessary to provide further interpretations of the plate behavior near a flow with time-dependent temperature.

Acknowledgements

This work was supported by the “Corporación Tecnológica de Andalucía” by means of the project “MECLIDE-Soluciones estructurales con materiales especiales para la climatización diferida de edificios” with the collaboration of DETEA. The work was partially funded by the Spanish Government (ENE2011-22722 and ULLE10-4E-1305) and the European Union (COST Action COST TU0802). The authors would like to thank the Catalan Government for the quality accreditation given to their research group (2009 SGR 534).

References

[1] I. Dincer, M.A. Rosen, Thermal Energy Storage, Systems and Applications, John Wiley & Sons, Chinchester, United Kingdom, 2002.
[2] H.Ö. Paksoy, Thermal Energy Storage for Sustainable Energy Consumption. Fundamentals, Case Studies and Design, In: NATO Science Series, Springer, Adana, Turkey, 2007.
[3] H. Mehling, L.F. Cabeza, Heat and Cold Storage with PCM. An up to Date Introduction into Basics and Applications, Springer-Verlag, Berlin Heidelberg, Garching, Germany, 2008.
[4] F. Kuznik, J. Virgone, K. Johannes, In-situ study of thermal comfort enhancement in a renovated building equipped with phase change material wallboard, Renewable Energy 36 (2011) 1458–1462.
[5] F. Kuznik, J. Virgone, K. Johannes, Development and validation of a new TRNSYS type for the simulation of external building walls containing PCM, Energy and Buildings 45 (2010) 1004–1009.
[6] A. Castell, I. Martorell, M. Medrano, G. Pérez, L.F. Cabeza, Experimental study of using PCM in brick constructive solutions for passive cooling, Energy and Buildings 42 (2010) 534–540.
[7] J. Borderon, J. Virgone, R. Cantin, K. Kuznik, Full-scale Study of a Building Equipped with a Multi-layer Rack Latent Heat Thermal Energy Store System, In: HVAC&R, vol. 17(4), Taylor and Francis, 2011, p. 566–576.
[8] D. Faggembauu, M. Costa, M. Soria, A. Oliva, Numerical analysis of the thermal behaviour of ventilated glazed facades in Mediterranean climates. Part I: development and validation of a numerical model, Solar Energy 75 (2003) 217–228.
[9] D. Faggembauu, M. Costa, M. Soria, A. Oliva, Numerical analysis of the thermal behaviour of ventilated glazed facades in Mediterranean climates. Part II: applications and analysis of results, Solar Energy 75 (2003) 229–239.
[10] T. Nomura, M. Tsuobta, T. Oya, N. Okinaka, T. Akiyama, Heat storage in direct-contact heat exchanger with phase change material, Applied Thermal Engineering 50 (2013) 26–34.
[11] J. Kurnia, A. Sasmito, S. Jangam, A. Mujumdar, Improved design for heat transfer performance of a novel phase change material (PCM) thermal energy storage (TES), Applied Thermal Engineering 50 (2013) 896–907.
[12] W. Ye, D. Zhu, N. Wang, Fluid flow and heat transfer in a latent thermal energy unit with different phase change materials (PCM) cavity volume factions, Applied Thermal Engineering 42 (2012) 49–57.
[13] M. Liu, W. Saman, F. Bruno, Validation of a mathematical model for encapsulated phase change material flat slabs for cooling applications, Applied Thermal Engineering 31 (2011) 2340–2347.
[14] J. Wei, Y. Kawaguchi, S. Hirano, H. Takeuchi, Study on a PCM heat storage system for rapid heat supply, Applied Thermal Engineering 25 (2005) 2903–2920.
[15] P. Dolado, A. Lazaro, J.M. Marin, B. Zalba, Characterization of melting and solidification in a real scale PCM-air heat exchanger: numerical model and experimental validation, Energy Conversion and Management 52 (2011) 1890–1907.
[16] V. Gnielinski, New equations for heat and mass transfer in turbulent pipe and channel flow, International Journal of Chemical Engineering 16 (1976) 359–368.

[17] G. Hed, R. Bellander, Mathematical modelling of PCM air heat exchanger, Energy and Buildings 38 (2006) 82–89.
[18] J.P. Holman, Heat Transfer, eighth ed., McGraw-Hill Companies, New York, USA, 1998.
[19] D. David, F. Kuznik, J. Roux, Numerical study of the influence of the convective heat transfer on the dynamical behavior of a phase change material wall, Applied Thermal Engineering 31 (2011) 3117–3124.
[20] D. David, Étude Experimental study of the natural convection in the vicinity of walls containing phase change materials PhD. Centre de Thermique de Lyon, France, 2010 (in French).
[21] A. Bejan, Convection Heat Transfer, second ed., John Wiley & Sons, Carpentersville, USA, 1995.
[22] P. Lamberg, R. Lehtiniemi, A.M. Henell, Numerical and experimental investigation of melting and freezing processes in phase change material storage, International Journal of Thermal Sciences 43 (2004) 277–287.
[23] M.M. Farid, A new approach in the calculation of heat transfer with phase change, in: 9th International Congress on Energy and Environment, Miami, 1989. p. 1–19.
[24] L.F. Cabeza, A. Castell, C. Barreneche, A. de Gracia, A.I. Fernández, Materials used as PCM in thermal energy storage in buildings: a review, Renewable and Sustainable Energy Reviews 15 (2011) 1675–1695.
[25] S. Patankar, Numerical Heat Transfer and Fluid Flow, Hemisphere Publications, Washington, USA, 1980.

Glossary

A: dimensionless number used in the Nusselt correlation
B: dimensionless number used in the Nusselt correlation
C: dimensionless number used in the Nusselt correlation
$C_{f,x}$: local skin-friction coefficient, dimensionless
Cp: specific heat, J kg^{-1} K^{-1}
e: thickness of the solid plate, m
f^{PCM}: perturbation in the Nusselt correlation due to phase change, dimensionless
St: Stefan number
H_{PCM}: enthalpy of the *PCM*, kJ kg^{-1}
h: convective heat transfer coefficient, W m^{-2} K^{-1}
k: thermal conductivity, W m^{-1} K^{-1}
L: total height of the plate, m
Nu^{PSM}: Nusselt number of an air flow over a phase stabilized material
$Nu_{x,t}^{PCM}$: Nusselt number of an air flow over a phase change material
P: dimensionless number used in the perturbation correlation
PCM: phase change material
PSM: phase stabilized material
Pr: Prandlt number
Re: Reynolds number
S_{Cp}: dimensionless number used in the perturbation correlation
T_0: initial temperature, K
T_∞: air flow temperature inlet, K
T_{hS}: plate surface temperature, K
$T_{h\infty}$: fluid mid-channel temperature, K
$T_{m(x)}$: temperature at the center of the plate at a certain height (x), K
T_{PCM}: phase change temperature, K
t: time, s
u_∞: air flow velocity inlet m s^{-1}
x: position parallel to the flow direction, m
y: position perpendicular to the flow direction, m

Greek symbols
ΔCp: increment in the specific heat due to phase change, kJ kg^{-1} K^{-1}
ΔT_{PCM}: half temperature phase change range, K
α_i: constants used in the empirical correlation
δ_x: thermal boundary layer thickness, m
φ_{hS}: heat flux density, W m^{-2}
ρ_s: density of the solid plate, kg m^{-3}
σ: standard deviation
ψ_x: dimensionless number used in the perturbation correlation
υ_{air}: air kinematic viscosity, m^2 s^{-1}

9 Numerical analysis of a ventilated facade with PCM

9.1 Introduction

As it was previously stated, the new type of ventilated facade with PCM in its air chamber has been tested experimentally during both winter [85] and summer [86] periods. From the experimental campaign, important net electrical energy savings were registered due to the use of this system during the winter period. On the other hand, no net savings were achieved during the summer season due to an excessive use of mechanical ventilation during night time.

The aim of this study is to optimize the operational schedule of the fans under different summer weather conditions, during the solidification and melting processes of the PCM. An own developed numerical model, based on control volume approach, was validated against experimental data. This typology of numerical model provides a good compromise between computational resources and accuracy [88].

The different weather conditions analysed in this work were grouped as severe and mild summer. The authors have discerned between these two periods for the thermal analysis of the whole system because it is very important to ensure that the PCM can be completely solidified every cycle. The PCM used in this application (Sp-22) can be fully solidified only when the outer temperature during the night time drops enough time below 17.5 ºC.

9.2 Contribution to the state-of-the-art

The own developed numerical tool was used to optimize the use of fans during the solidification process of the PCM (night time) and during the cooling supply, and is presented in the following paper:

- A. de Gracia, L. Navarro, A. Castell, L.F. Cabeza. Numerical analysis of a ventilated facade with PCM. Applied Thermal Engineering, submitted ATE-D-2013-….

A full solidification of the PCM could be only achieved during the mild summer period. Under these weather conditions, the system optimizes its performance when solidifying the PCM from 4:00 to 7:00 hrs. (Figure 20). Moreover, the cooling supply achieves its maximum (5.52 MJ/day) in the case when the system starts the melting period at 11:00 and finishes at 15:00. If the electrical energy consumption of the fans is taken into account, the net electrical energy supplied by the ventilated facade with PCM is 2.49 MJ/day.

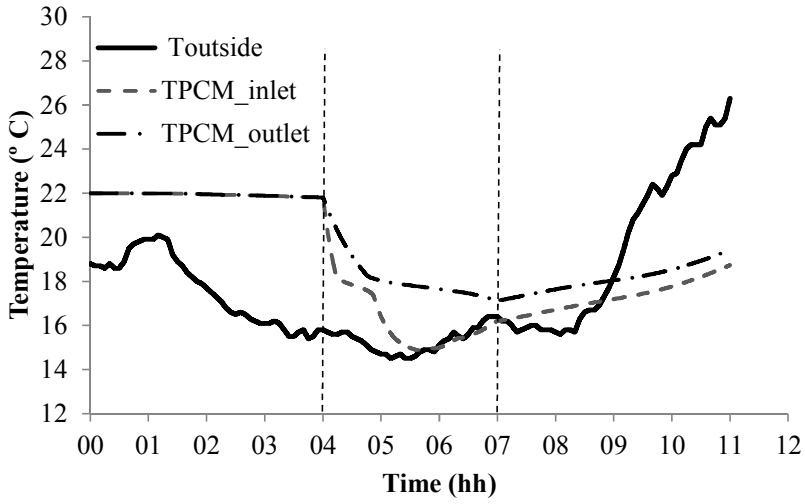

Figure 20. Thermal evolution of the PCM during the solidification process

In addition, the exposure to heat gains reduces dramatically the cooling capacity of the system when supplying the cold stored after 11:00 hrs. The use of a metallic structure to hold the glass and the insulating panels reduces strongly the thermal resistance of the outer skin. The energetic performance of a ventilated facade with wooden structure has been also evaluated numerically. The improvement on the thermal resistance of the outer skin allows the system to give a net energy supply of 4.02 MJ/day, which is 61.6 % higher than the maximum achieved by the facade with the metallic structure.

On the other hand, during the severe summer period the outer temperature hardly ever drops below 17.5 ºC during night time, which combined with the high hysteresis detected in the PCM (melts at 21.5 ºC and solidifies at 18 ºC), makes almost impossible to solidify completely the PCM. The system if providing mechanical ventilation from 1:00 to 7:00 hrs is only able to solidify 32.25 % of the PCM, which leaded the authors to study the possibility of increasing the mass flow rate pumped by the fans by a factor f, with increasing proportionally the electrical power needed ($120 \cdot f$ W). The numerical results demonstrated that for a certain desired portion of solidified PCM, it is recommended to increase the power of mechanical ventilation during less time of consumption, in order to maximize the storage efficiency.

The present numerical study and previous experimental work [86] demonstrated that the hysteresis registered in the SP-22 limits strongly the potential of the system in solidifying the PCM, especially during the sever summer period. Therefore, other materials without hysteresis should be tested in the future.

9.3 Journal paper

Elsevier Editorial System(tm) for Applied Thermal Engineering
Manuscript Draft

Manuscript Number:

Title: Numerical analysis of a ventilated facade with PCM

Article Type: Research Paper

Keywords: Ventilated facade; phase change materials (PCM); numerical simulation; buildings

Corresponding Author: Prof. Luisa F. Cabeza, PhD

Corresponding Author's Institution: Universitat de Lleida

First Author: Alvaro de Gracia, Engineer

Order of Authors: Alvaro de Gracia, Engineer; Lidia Navarro, Engineer; Albert Castell, PhD; Luisa F. Cabeza, PhD

Numerical analysis of a ventilated facade with PCM

Alvaro de Gracia, Lidia Navarro, Albert Castell, Luisa F. Cabeza
GREA Innovació Concurrent, Universitat de Lleida, Edifici CREA, Universitat de Lleida, Pere de Cabrera s/n, 25001, Spain Phone: +34-973003576 E-mail: lcabeza@diei.udl.cat

ABSTRACT

A new type of ventilated facade (VF) with macro-encapsulated phase change material (PCM) in its air cavity is presented in this paper. Two identical house-like cubicles located in Puigverd de Lleida (Spain) were monitored during 2012, and in one of them, the VF with PCM was implemented in the south wall. The versatility of the facade allows the system to reduce both heating and cooling loads. During winter, the PCM increases the heat storage capacity of the system exposed to solar radiation and during summer the system can be used as a cold storage unit or as a night free cooling device. From the experimental winter campaign, important net electrical energy savings were registered due to the use of the VF. On the other hand, no net energy savings were achieved during summer due to excessive use of mechanical ventilation. In this paper, an own developed numerical model, based on finite control volume approach, was validated against experimental data and it is used to optimize the operational schedule of both solidification and melting processes in order to achieve net electrical energy savings. During the mild summer period the system presents a net energy supply of 2.49 MJ/day. This value would be increased by 61.6 % if a wooden structure would have been used instead of the current metallic structure. Moreover, the high hysteresis of the PCM limits strongly the potential of the system in supplying cooling during the severe summer period.

Keywords: Ventilated facade, phase change materials (PCM), numerical simulation, buildings

1. Introduction

Ventilated facades have been recently introduced in the building sector to match the energetic restrictions required by the European Directive 2010/31/EU [1]. They are also a suitable constructive system to improve the energetic efficiency of refurbished buildings [2]. These constructive systems are special types of envelopes, where a second skin is placed in front of a regular building facade, creating an air space in between, named channel [3].

The thermal performance of these systems has been experimentally studied [4,5]. However, the high costs of these special envelopes have caused that numerical studies have been more abundant in the literature. The existing numerical methods used to predict the thermal behavior of the different ventilated facades have been reviewed by de Gracia et al. [6] and can be grouped as analytical and lumped models [7,8], non-dimensional analysis [9], network models [10-12], control volume [13-15], zonal approach [16], and computational fluid dynamics [17,18].

In this paper, a control volume approach is used to optimize numerically the energetic performance of a ventilated facade with macro-encapsulated phase change material (PCM) in its air chamber. The control volume approach provides a good compromise between computational resources and accuracy, and it is presented as an adequate tool to study the overall thermal performance of a ventilated facade [6].

PCM have been intensively studied for building applications [19,20] . In this study the PCM is tested in a ventilated facade for cooling applications. During this period, the outer skin was covered with an insulating panel to prevent solar radiation inside the cavity. The operating principle of the system during the summer period is to solidify the PCM during the night time and to use it as a cooling supply during the peak load hours. However, the system did not show any net electrical energy savings due to extensive use of mechanical ventilation [21]. The numerical model presented in this paper is validated against experimental data obtained in that facility and it is used to optimize the operational schedule of both, the solidification and the melting process of the PCM, as well as to determine the potential of the system in providing a cooling supply under severe and mild summer conditions.

2. Experimental set-up

The experimental set-up used to evaluate the thermal performance of a ventilated facade with PCM during summer period consists of two identical house-like cubicles with the same inner dimensions (2.4 m x 2.4 m x 5.1 m). The only difference between the two cubicles is that one of them is equipped in the south wall with a ventilated facade with PCM inside its air chamber, while the other cubicle keeps the basic constructive system. Both cubicles, reference (REF) and ventilated facade (VF) are shown in Figure 1.

The ventilated facade presents an air channel of 15 cm thick which represents 0.36 m^2 of channel area ($A_{channel}$). The inner layer is based on the alveolar brick constructive system while the outer envelope is made by a metallic structure which holds the glass layer. An extra outer

layer of expanded polyurethane panels was placed to cover the transparent glazing during the summer period since solar radiation inside the cavity for cooling purposes must be avoided.

Six automatized gates were installed at the different openings of the channel in order to control the operational mode of the facade. These gates are controlled by ST450N linear spindle actuators. Moreover, three fans (FCL 133 Airtecnics), of 40 W each, were placed at the inlet of the air channel to provide mechanical ventilation when needed. The system which controls the fans and gates is programmed in a Microchip 18F45J10, and allows the system to operate under the following modes:

(i) PCM solidification period (Figure 2a): During the night time, the air enters to the channel from the outer environment, solidifies the PCM and is pumped outdoors. This mode uses the fans (mechanical ventilation) to ensure the complete solidification of all the PCM.

(ii) Storage period (Figure 2b): The ventilated facade is closed after the PCM is solidified and before the cooling supply is required, therefore the coldness from the night is stored until it is needed at warmer hours of the day.

(iii) PCM melting period (Figure 2c): The cold stored in the PCM is pumped by the fans to the inner environment to satisfy the cooling demand.

The PCM used inside the air channel was the macro-encapsulated salt hydrate SP-22 from Rubitherm. The selection of this PCM (melting and solidification temperature at 21.5 ºC and 18 ºC, respectively) allows the ventilated facade to be used as a cold storage system in summer and as a heating supply in winter. 112 macro-encapsulated CSM panels were installed inside the cavity, creating 14 channels as shown in Figure 3.

Both cubicles were fully instrumented and data was registered at 5 min intervals to evaluate their thermal performance.

The physical properties of the materials used in the model are detailed in Table 1. The thermal transmittance in steady state of the outer skin is calculated using the electrical analogy [22]. This value is increased strongly to 3.05 $W/m^2 \cdot K$, due to the metallic structure. More detailed information about the constructive system can be found in de Gracia et al. [21].

3. Methodology

3.1. Numerical modelling

The numerical model solves the energy equation using a fully implicit finite control volume method in the two dimensional Cartesian coordinates system [23].

Heat transfer in PCM, glass, alveolar brick and polyurethane panels during the three different periods (Figure 2a, 2b and 2c) is governed by the heat conduction equation:

$$\frac{\partial H}{\partial t} = k\frac{\partial^2 T}{\partial x^2} + k\frac{\partial^2 T}{\partial y^2} \qquad \text{(Eq.1)}$$

Heat transfer during mechanical air ventilation is governed by the following equation:

$$\frac{\partial H}{\partial t} + v_y \frac{\partial H}{\partial y} = k\left(\frac{\partial^2 T}{\partial x^2} + \frac{\partial^2 T}{\partial y^2}\right) \qquad \text{(Eq.2)}$$

The set of governing equations (1)-(2) is completed by the following initial and boundary conditions (Figure 4):

(i)	t = 0	$T = T_0$	(Eq.3)
(ii)	x = 0	$-k_{OS}\frac{\partial T}{\partial x} = h_{out}\cdot\left(T_{out} - T_{w\_out}\right)$	(Eq.4)
(iii)	x = L_1	$-k_{OS}\frac{\partial T}{\partial x} = h_1\cdot\left(T_{air} - T_{w1}\right)$	(Eq.5)
(iv)	x = L_2	$-k_{alv}\frac{\partial T}{\partial x} = h_2\cdot\left(T_{air} - T_{w2}\right)$	(Eq.6)
(v)	x = L_3	$-k_{alv}\frac{\partial T}{\partial x} = h_{\text{int}}\cdot\left(T_{w\_\text{int}} - T_{\text{int}}\right)$	(Eq.7)
(vi)	y = 0	$\frac{\partial T}{\partial y} = 0$	(Eq.8)
(vii)	y = H	$\frac{\partial T}{\partial y} = 0$	(Eq.9)
(viii)	z = 0	$-k_{PCM}\frac{\partial T}{\partial x} = h_3\cdot\left(T_{air} - T_{w3}\right)$	(Eq.10)
(ix)	z = e_{PCM}	$-k_{PCM}\frac{\partial T}{\partial x} = h_4\cdot\left(T_{air} - T_{w4}\right)$	(Eq.11)

The finite difference equations are obtained by discretizing equations (1) and (2) over each control volume.

Moreover, the radiosity method is used to calculate the solar and thermal radiation balance. On top of the solar radiation incident to the outer skin, the thermal radiation between the outer skin and the sky, and between the PCM, alveolar brick and outer skin are considered:

$$j_i = \varepsilon_i \cdot \sigma \cdot T_i^4 + (1 - \varepsilon_i) g_i \quad \text{(Eq.12)}$$

$$g_i = \sum_{n=1}^{k} F_{i,k} \cdot j_k \quad \text{(Eq.13)}$$

The following assumptions have been made to simplify the analysis:

(i) The thermal radiation between surfaces is considered one-dimensional (x).

(ii) The temperature of the air at the inlet of the channel is considered equal to the outer temperature during the PCM solidification period.

(iii) The temperature of the air at the inlet of the channel is considered equal to the inner temperature during the PCM melting period.

(iv) The heat transfer coefficients between the facade and the inner and outer environments (h_{in} and h_{out}) are assumed constant and equal to 7 and 20 $W/m^2 \cdot K$ according to the Spanish standards [24].

(v) The PCM is homogeneous and isotropic.

(vi) The phase change was taken into account through an equivalent heat capacity [25]. During the melting or solidification, the temperature dependence on the PCM specific heat has a triangle shape centered on T_{PCM}. This methodology was studied by Farid [26] and was found to be successful in describing the heat transfer in phase change materials.

(vii) During the storage period, the movement of the air inside the air channel due to the natural convection effect is not modeled. However, the empirical correlation from Jakob [27] is used to calculate the heat transfer coefficient between the air and the adjacent surfaces during this period.

(viii) The atmosphere (sky) is considered as a blackbody at a temperature equal to $T_{sky} = 0.0552 \cdot T_{out}^{1.5}$ [28].

Empirical correlations of Nusselt number were used to calculate the different convective heat transfer coefficients during forced convection periods:

(i) Heat transfer coefficient between the outer skin, the alveolar brick layer and the air channel (h_1 and h_2): $\overline{Nu} = C \cdot \mathrm{Re}^n \cdot \mathrm{Pr}^m$, C=0.0296, m=0.08 and n=0.33 [22].

(ii) The heat transfer coefficients between the air flow and the PCM layers (h_3 and h_4) were calculated using the correlation proposed by de Gracia et al. [29]. This

correlation takes into account the perturbation in the Nusselt evolution due to the phase change of a solid flat plate.

A mesh independent study was performed in order to reduce the duration of the transient simulations needed for the study. In the resulting mesh the number of nodes taken in the x-direction was: 16 nodes in outer skin, 20 for the PCM panels, and 20 for the alveolar brick layer. Moreover, in the y-direction 8 nodes were used.

The system of algebraic linear equations extracted from the finite differences method was solved using Gauss Seidel iterative method with a time step of 5 seconds.

3.2. Code validation with experimental data

Experimental data was used to test the accuracy of the numerical solutions and validate the model. The following tests were simulated and compared against measured experimental data:

(i) PCM solidification period: The PCM inside the channel is initially at 19 ºC. A cold air flow is pumped from the outside (around 10 ºC) in order to solidify the PCM. Figure 5 shows the experimental and numerical thermal profiles of the PCM at the inlet and outlet of the channel. The numerical model presents an average relative error of 1.85 % in predicting the PCM thermal evolution during its solidification process.

(ii) Storage period: The PCM is in the solid state and is being heated by the outer heat gains (external convection and solar radiation). Figure 6 shows the experimental and numerical thermal profiles of the PCM at the inlet and outlet of the channel. During this period, the model presents an average relative error of 0.84% in predicting the PCM temperature.

(iii) PCM melting period: The PCM inside the channel is initially at 5.5 ºC. A hot air flow is pumped by the fans from the inner environment (28 ºC) and melts the PCM. Figure 7 shows the thermal evolution of the PCM at the inlet and outlet of the channel. The average relative error between the numerical results and the measured experimental data is 2.7%. Moreover, since the thermal evolution of the air at the inlet and outlet of the channel is critical to determine the cooling rate of the system, Figure 8 compares the air temperature at different heights of the channel during the cooling discharge (average relative error of 3.75%).

3.3 Description of the parametric analysis

As it was previously said, the developed numerical model is used to optimize the use of fans during the PCM solidification period in order to register net electrical energy savings due to the use of the ventilated facade with PCM.

The different weather conditions analyzed in this work were grouped as severe and mild summer. The authors have discerned between these two periods for the thermal analysis of the whole system because it is very important to ensure that the PCM can be completely solidified every cycle. The PCM can be fully solidified only when the outer temperature during the night time drops enough time below 17.5 ºC. Standard severe and mild summer days in the Mediterranean climate were chosen to make this optimization, and are shown in Figure 9 and Figure 10. The mild summer conditions represent the thermal oscillation and solar radiation registered in the experimental set-up (Puigverd de Lleida, Spain) the 8th of September 2012, while the severe summer weather conditions were measured the 10th of August 2012.

The parametric study under mild winter conditions consists of different steps:

(i) The whole system is at 22 ºC at 01:00 a.m. This is justified because in the real programming of this application, the channel is opened and subjected to natural convection cooling before the PCM solidification period. Since the air temperature at this time was around 20 ºC, the authors considered a thermal lag of 2 ºC between the PCM, alveolar brick and outer skin, and the outer air which is circulating naturally though the facade.

(ii) The PCM solidification period starts (t_i) between 1:00 and 04:00 as it is shown in Table 2.

(iii) The PCM solidification period ends (t_e) between 02:00 and 08:00. After this step, the facade closes its openings until 11:00 (storage period).

The aim of this parametric study is to evaluate which is the optimal timing (instant and duration) of the PCM solidification period (use of fans) in order to achieve a full solidification of the PCM and to determine its temperature at 11:00, when the PCM melting period could be demanded.

Once the solidification period of the PCM will be optimized, the numerical code will be used to quantify the cooling supply and net energy savings from the system for different defined

melting periods and durations. The PCM melting period starts (t_i) between 11:00 and 14:00 and finishes between 2 and 5 hours later.

The study of the energetic performance of the ventilated facade under severe winter conditions will be focused on the potential of the system in solidifying the PCM. In this part, the mass flow rate pumped by the fans is multiplied by a factor (f) of 1.5, 2, 2.5, 3, 3.5 and 4, increasing proportionally the electrical power needed ($120 \cdot f$ W).

4. Results and discussion

4.1 Mild summer period

The percentage of PCM which has been solidified during the PCM solidification period (based on the enthalpy of fusion released), and its temperature at 11:00 are shown in Table 2 for each analyzed case. The important hysteresis of this PCM (SP-22) affects strongly the thermal performance of the whole system, since it needs outer temperatures below 17.5 ºC to be able to solidify the PCM. On the other hand the melting occurs at 21.5 ºC. This important hysteresis makes that only cases in which the PCM has been fully solidified are taken as possible solutions.

As it can be seen in Table 2, although in 5 cases the PCM is fully solidified, there are only two cases ("h" and "k") in which mechanical ventilation is minimized (only used 3 hours). The only difference between them is whether the fans start to pump air from the outer environment at 03:00 or at 04:00. From these two cases, "k" is found to be slightly better because of the temperature of the PCM before the PCM melting period. In addition, the authors want to highlight that case "j" solidifies the 94.5% of the PCM during only 2 hours of mechanical ventilation, however, as it was previously stated, only fully solidified PCM cases will be selected.

Moreover, Figure 11 shows the thermal evolution of the PCM at the inlet and outlet of the channel for case "k". The whole system starts at 22 ºC and decreases slightly its temperature due to heat losses to the environment until 04:00, when the PCM solidification period is programmed to start. It can be seen that even though the PCM at the inlet only needs 1 hour to be fully solidified, at the outlet of the channel, the PCM has just finished its solidification process after the 3 hours of mechanical ventilation. After this time (07:00), the whole system is

subjected to heat gains from the outer environment due to natural convection and solar radiation, and increases its temperature until 11:00, when a cooling supply could be demanded.

The cooling supplied by the system when operating under different time schedules is presented in Table 3. All cases presented are based on the k scenario of the solidification process. The cooling supply achieves its maximum (5.52 MJ/day) when the system starts the melting period at 11:00 until 15:00. If the electrical energy consumption of the fans (120 W) is taken into account, the net energy supplied by the ventilated facade with PCM under mild summer conditions is 2.49 MJ/day. The cooling supply must finish when the thermal gradient between the air at the inlet and outlet of the channel is below $\Delta T_{\min}$ (Eq. 14). After this moment the system is consuming more energy from the fans than it is supplying with the cold air. This can be easily seen in all the cases with 4 and 5 hours of melting period, when the excessive use of fans have reduced the net energy supply and even supply negative energy balances in some cases. Table 3 also shows the maximum net energy supply by the system, if the melting period would have finished before the thermal gradient was below $\Delta T_{\min}$. The authors want to highlight that if the system had been controlled every minute instead of hourly, the cooling supply would have been increased, however, this improvement does not exceed 3.5%.

$$\Delta T_{\min} = \frac{\dot{W}_{fans}}{\dot{m} \cdot C_{Pair}} \qquad \text{(Eq.14)}$$

Moreover, even though the system can start its melting period after 11:00, the exposure to heat gains reduces dramatically the cooling capacity of the system. The use of a metallic structure to hold the glass and the insulating panels reduces strongly the thermal resistance of the outer skin. Therefore, the researchers of this study want to test an alternative structure for the system. The energetic performance of a ventilated facade with wooden structure is shown in Figure 12. The thermal transmittance in steady state of this new outer skin is 0.827 $W/m^2 \cdot K$. The reduction of this value affects strongly the cooling supply potential of the ventilated facade. This new structure not only allows the system to pump cold air to the inner environment during 5 hours, but it provides useful cooling supply when the melting period starts at 14:00, as well. The maximum net energy supply is produced from 11:00 to 16:00 (case “d”), providing 4.02 MJ/day, and being 61.6% higher than the maximum achieved by the facade with the metallic structure. Other materials with similar thermal conductivity than wood and adequate mechanical properties, such as plastic, must be also considered in the design phase of this ventilated facade.

4.2 Severe summer period

From the experimental data registered in a previous work [21], during the severe summer period the outer temperature hardly ever drops below 17 ºC during the night time, which combined with the high hysteresis detected in the PCM (melts at 21.5 ºC and solidifies at 18 ºC), makes impossible to solidify completely the PCM, as shown in Figure 13. The system, when providing mechanical ventilation from 01:00 to 07:00, is only able to solidify 32.25 % of the PCM, which led the authors to study the possibility of increasing the mass flow rate pumped by the fans by a factor f.

As it can be seen in Figure 13, the outer temperature is only below 18 ºC (phase change peak) during the last 3 hours (from 04:00 to 07:00). In order to take advantage of the low outer temperatures, the authors have analyzed the energetic performance of the system operating at different powers during 1, 2 or 3 hours and finishing always the solidification period at 07:00. In addition to the portion of PCM solidified during the night-time (p) for each power of mechanical ventilation and duration of the solidification process, Figure 14 also presents the storage efficiency (ε) for each case, as defined in Eq. 15:

$$\varepsilon = \frac{m_{PCM} \cdot H_f \cdot p}{W_{fans}} \qquad \text{(Eq. 15)}$$

As seen in Figure 14, the storage efficiency is only above 1 in a few cases, when the solidification period only lasts 1 hour and the power of the fans is multiplied by a factor of 2.5 to 4. However, the portion of PCM solidified is limited, being its maximum 58% in the case when the power factor f is 4. On the other hand, in the cases with 3 hours of solidification period the system can solidify 88% of the PCM but with a low storage efficiency of 0.55. From the presented results it can be demonstrated that in order to provide the same amount of PCM solidified and maximize the storage efficiency, it is advisable to increase the power of mechanical ventilation during less time.

The numerical results show low values of storage efficiency, as well as the impossibility of fully solidify the PCM, which agree with the experimental measurements [21]. Both studies demonstrated that the high hysteresis of the PCM affects dramatically the potential of the system in solidifying it during the severe summer season, and hence to be able to supply cooling during the daytime.

5. Conclusions

This paper studied numerically the thermal performance of an opaque ventilated facade with macro-encapsulated PCM in its air cavity for cooling purposes.

A mathematical model based on the control volume approach has been developed and validated against experimental data. The numerical tool is used to optimize the use of fans during the PCM solidification period, since its excessive use could suppress any net electrical energy savings due to the use of this system.

In this study the different weather conditions were grouped as severe and mild summer. During the mild season, the outer temperature drops below the phase change temperature during enough time, so the system can fully solidify the PCM. An optimal combination under the mild conditions to solidify the PCM with the minimum hours of mechanical ventilation is found when the system starts to pump air from the outer environment at 04:00 a.m. during 3 hours. Moreover, the cooling supplied by the system achieves its maximum (5.46 MJ/day) in the case when the melting period starts at 11:00 until 15:00. The ventilated facade provides a net energy supply of 2.49 MJ/day when the electrical energy consumed by the fans is taken into account.

Moreover, even though the system can start its melting period after 11:00, the exposure to heat gains reduces dramatically its cooling capacity. These heat gains can be strongly reduced if a wooden or plastic structure is used instead of the current metallic one. The numerical results demonstrated that the use of the wooden structure would increase the duration of the cooling supply to 5 hours and the maximum net energy supply would be 61.6 % higher than the one achieved with the metallic structure.

On the other hand, during the sever summer period the outer temperature hardly ever drops below 17 ºC, which combined with the high hysteresis detected in the PCM makes it difficult to solidify completely the PCM. The authors have evaluated the storage efficiency and the portion of PCM which has been solidified when increasing the mass flow rate pumped by the fans with a factor f which varied between 1.5 and 4. From the numerical results, for a certain desired portion of PCM solidified, it is recommended to increase the power of mechanical ventilation during less time of operation, in order to maximize storage efficiency.

The numerical model which describes the energetic performance of the ventilated facade during the summer season could be implemented in TRNSYS as a new type. The inclusion of the

developed model into an overall building simulation could be useful to determine annual savings, as well as the efficiency of different control strategies.

The present numerical study and previous experimental work [21] demonstrated that hysteresis registered in the SP-22 limits strongly the potential of the system in solidifying the PCM, especially during the sever summer period. Therefore, other materials without hysteresis should be tested in the future.

Acknowledgments

This work was supported by the "Corporación Tecnológica de Andalucía" by means of the project "MECLIDE-Soluciones estructurales con materiales especiales para la climatización diferida de edificios" with the collaboration of DETEA. The work partially funded by the Spanish government (ENE2011-28269-C03-01 and ULLE10-4E-1305) and the European Union (COST Action COST TU0802), with the collaboration of the City Hall of Puigverd de Lleida. The authors would like to thank the Catalan Government for the quality accreditation given to their research group (2009 SGR 534).

References

[1] Directive 2010/31/EU of the European parliament and of the council of 19 May 2010 on the energy performance of buildings. Available from: http://www.epbd-ca.eu.
[2] M.A. Shameri, M.A. Alghoul, K. Sopian, M. Fauzi, M. Zain, O. Elayeb, Perspectives of double skin façade systems in buildings and energy saving, Renew Sust Energ Rev 15 (2011) 1468-1475.
[3] N. Safer, M. Woloszyn, J.J. Roux, Three-dimensional simulation with a CFD tool of the airflow phenomena in single floor double-skin façade equipped with a Venetian blind, Sol Energy 79 (2005) 193-203.
[4] V. Gavan, M. Woloszyn, F. Kuznik, J.J. Roux, Experimental study of a mechanically ventilated double-skin façade with venetian sun-shading device: A full scale investigation in controlled environment, Sol Energy 84 (2010) 183-195.
[5] T. Pasquay, Natural ventilation in high-rise buildings with double facades, saving or waste of energy, Energ Buildings 36 (2004) 381-389.
[6] A. de Gracia, A. Castell, L. Navarro, E. Oró, L.F. Cabeza, Numerical modelling of ventilated facades: A review, Renew Sust Energ Rev (2013) doi.10.1016/j.rser.2013.02.029

[7] J. von Grabe, A prediction tool for the temperature field of double facades, Energ Buildings 34 (2002) 891-899.
[8] C. Park, G. Augenbroe, T. Messadi, M. Thitisawat, N. Sadegh, Calibration of a lumped simulation model for double-skin façade systems, Energ Buildings 36 (2004) 1117-1130.
[9] C. Balocco, M.Colombari, Thermal behavior of interactive mechanically ventilated double glazed façade: Non-dimensional analysis, Energ Buildings 36 (2006) 1-7.
[10] J. Hensen, M. Bartak, F. Drkal, Modeling and simulation of a double-skin façade system, ASHRAE Tran 108 (2002)1251-1259.
[11] W. Stec, D. van Paassen, Symbiosis of the double skin façade with the HVAC system, Energ Buildings 37 (2005) 461-469.
[12] E. Gratia, A. De Herde, Optimal operation of a south double-skin façade, Energ Buildings 36 (2004) 41-60.
[13] D. Faggembau, M. Costa, M. Soria, A. Oliva, Numerical analysis of the thermal behaviour of ventilated glazed facades in Mediterranean climates. Part I: development and validation of a numerical model, Sol Energy 75 (2003) 217-228.
[14] D. Saelens, J. Carmeliet, H. Hens, Energy Performance Assessment of Multiple-Skin Facades, HVAC&R Res 9 (2003)167-185.
[15] P. Seferis, P. Strachan, A. Dimoudi, A. Androutsopoulos, Investigation of the performance of a ventilated wall, Energ Buildings 43 (2001) 2167-2178.
[16] T.E. Jiru, F. Haghighat, Modeling ventilated double skin façade – A zonal approach, Energ Buildings 40 (2008) 1567-1576.
[17] H. Manz, A. Schaelin, H. Simmler, Airflow patterns and thermal behavior of mechanically ventilated glass double façades, Build Environ 39 (2004) 1023-1033.
[18] W. Pasut, M. De Carli, Evaluation of various CFD modelling strategies in predicting airflow and temperature in a naturally ventilated double skin façade, Appl Therm Eng 37 (2012) 267-274.
[19] A. de Gracia, L. Navarro, A. Castell, A. Ruiz-Pardo, S. Álvarez, L.F. Cabeza, Thermal analysis of a ventilated facade with PCM for cooling applications, Energ Buildings, in press.
[20] L. F. Cabeza, A. Castell, C. Barreneche, A. de Gracia, A.I. Fernández, Materials used as PCM in thermal energy storage in buildings: A review, Renew Sust Energ Rev 15 (2011) 1675-1695.
[21] A.M. Khudhair, M.M. Farid, A review on energy conservation in building applications with thermal storage by latent heat using phase change materials, Energ Convers Manage 45 (2004) 263-275.
[22] Y.A Çengel, Heat and Mass transfer, McGraw-Hill Education, India, 2007.
[23] S. Patankar, Numerical Heat Transfer, Hemisphere Publications, 1980.

[24] Ministerio de Economía y Competitividad. Código técnico de la edificación. Documento Básico HE. Ahorro de Energía, 2010.
[25] P. Lamberg, R. Lehtiniemi, A.M.Henell, Numerical and experimental investigation of melting and freezing processes in phase change material storage, Int J Therm Sci 43 (2004) 277-287.
[26] M.M. Farid, A new approach in the calculation of heat transfer with phase change, 9th International Congress on Energy and Environment, Miami, 1989. p. 1-19.
[27] M. Jakob, Free convection through enclosed gas layers, Trans. ASME (1946) 68:189-194.
[28] W.C. Swinbank, Q.J. Roy, Long-wave radiation from clear skies, Q J Roy Meteor Soc (1936) 89:339.
[29] A. de Gracia, D. David, A.Castell, L.F. Cabeza, J. Virgone, A correlation of the convective heat transfer coefficient between an air flow and a phase change material plate, Appl Therm Eng 51 (2013) 1245-1254.

Nomenclature

Cp	Specific heat J kg^{-1} K^{-1}
e	Thickness m
ε	Emissivity
f	Mass flow rate factor
g	Incoming radiosity W m^{-2}
h	Heat transfer coefficient W m^{-2} K^{-1}
H	Total volumetric enthalpy J m^{-3}
j	Outgoing radiosity W m^{-2}
k	Thermal conductivity W m^{-1} K^{-1}
L	Distance m
$\dot{m}$	Mass flow rate kg s^{-1}
Nu	Nusselt number
p	Portion of PCM solidified
Pr	Prandtl number
Re	Reynolds number
ρ	Density kg m^{-3}
t	time s
T	Temperature K
σ	Stephan-Boltzmann constant (5.67×10^{-8} W m^{-2} K^{-4})
$\dot{W}$	Power of the mechanical ventilation W

Subscript

air	Air channel
alv	Alveolar brick layer
e	End
i	Initial
in	Inside
OS	Outer skin
out	Outside
w	Wall

Figure Captions

Table 1 Thermo-physical properties of the used materials

	Outer skin	Alveolar brick	PCM
k	0.15	0.28	0.6
C_p	1000	1000	$C_p(T)$
ε	0.3 out 0.92 in	0.2	0.77
ρ	882	1500	570

Table 2 Case description and numerical results for the solidification period

Case	t_i	t_e	Use of fans (h)	% H	PCM outlet Temperature at 11:00 (^{0}C)
a	01:00	03:00	2	28.75	-
b	01:00	04:00	3	76.25	-
c	01:00	05:00	4	98.75	-
d	02:00	04:00	2	68.75	-
e	02:00	05:00	3	96.5	-
f	02:00	06:00	4	100	19.28
g	03:00	05:00	2	84.75	-
h	03:00	06:00	3	100	19.42
i	03:00	07:00	4	100	19.16
j	04:00	06:00	2	94.5	-
k	04:00	07:00	3	100	19.38
l	04:00	08:00	4	100	18.98

Table 3 Case description and numerical results for the melting period

case	t_i	t_e	Cooling supply (MJ/day)	Time supply (h)	Net energy supply (MJ/day)	Time excess (h)	Max net energy supply (MJ/day)
a	11:00	13:00	3.71	2	1.55	0	1.55
b	11:00	14:00	4.82	3	2.23	0	2.23
c	11:00	15:00	5.52	4	2.49	0.09	2.50
d	11:00	16:00	5.46	5	2.00	1.09	2.50
e	12:00	14:00	3.12	2	0.96	0	0.96
f	12:00	15:00	4.06	3	1.47	0	1.47
g	12:00	16:00	4.55	4	1.52	0.4	1.59
h	12:00	17:00	4.21	5	0.76	1.4	1.59
i	13:00	15:00	2.62	2	0.46	0	0.46
j	13:00	16:00	3.41	3	0.82	0	0.82
k	13:00	17:00	3.64	4	0.62	0.72	0.85
l	13:00	18:00	3.14	5	-0.32	1.72	0.85
m	14:00	16:00	2.20	2	0.04	0	0.04
n	14:00	17:00	2.84	3	0.25	0.05	0.25
o	14:00	18:00	2.76	4	-0.27	1.05	0.25
p	14:00	19:00	2.26	5	-1.20	2.05	0.25

Figure(s)
Click here to download high resolution image

Figure 1

Figure(s)
Click here to download high resolution image

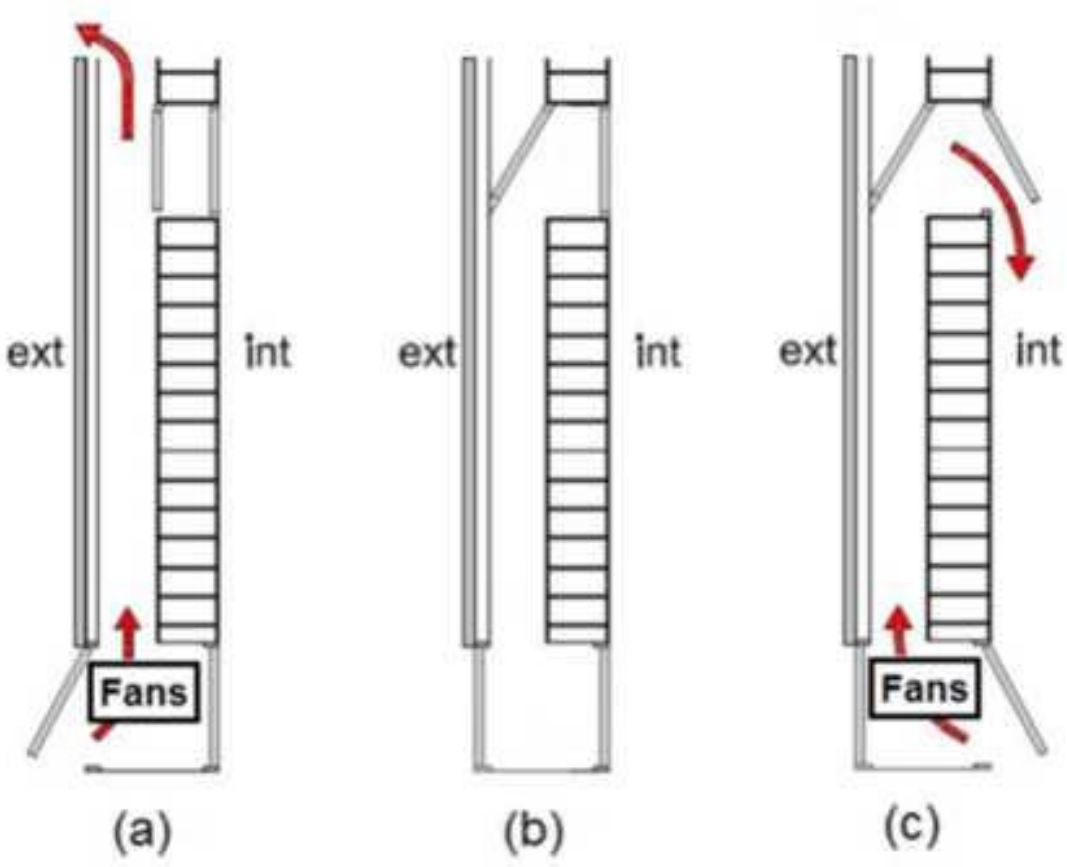

Figure 2

Figure(s)
Click here to download high resolution image

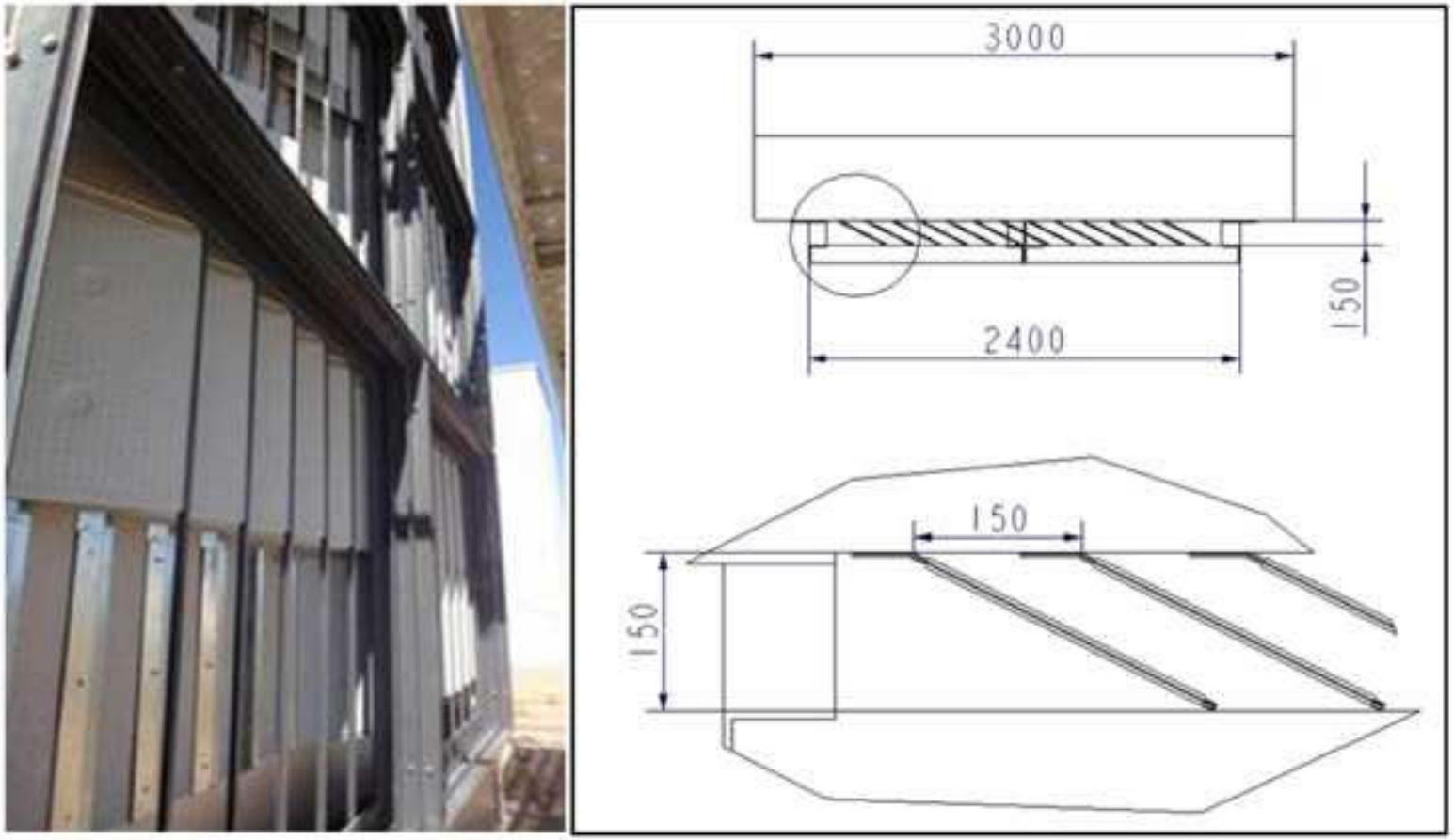

Figure 3

Figure(s)
Click here to download high resolution image

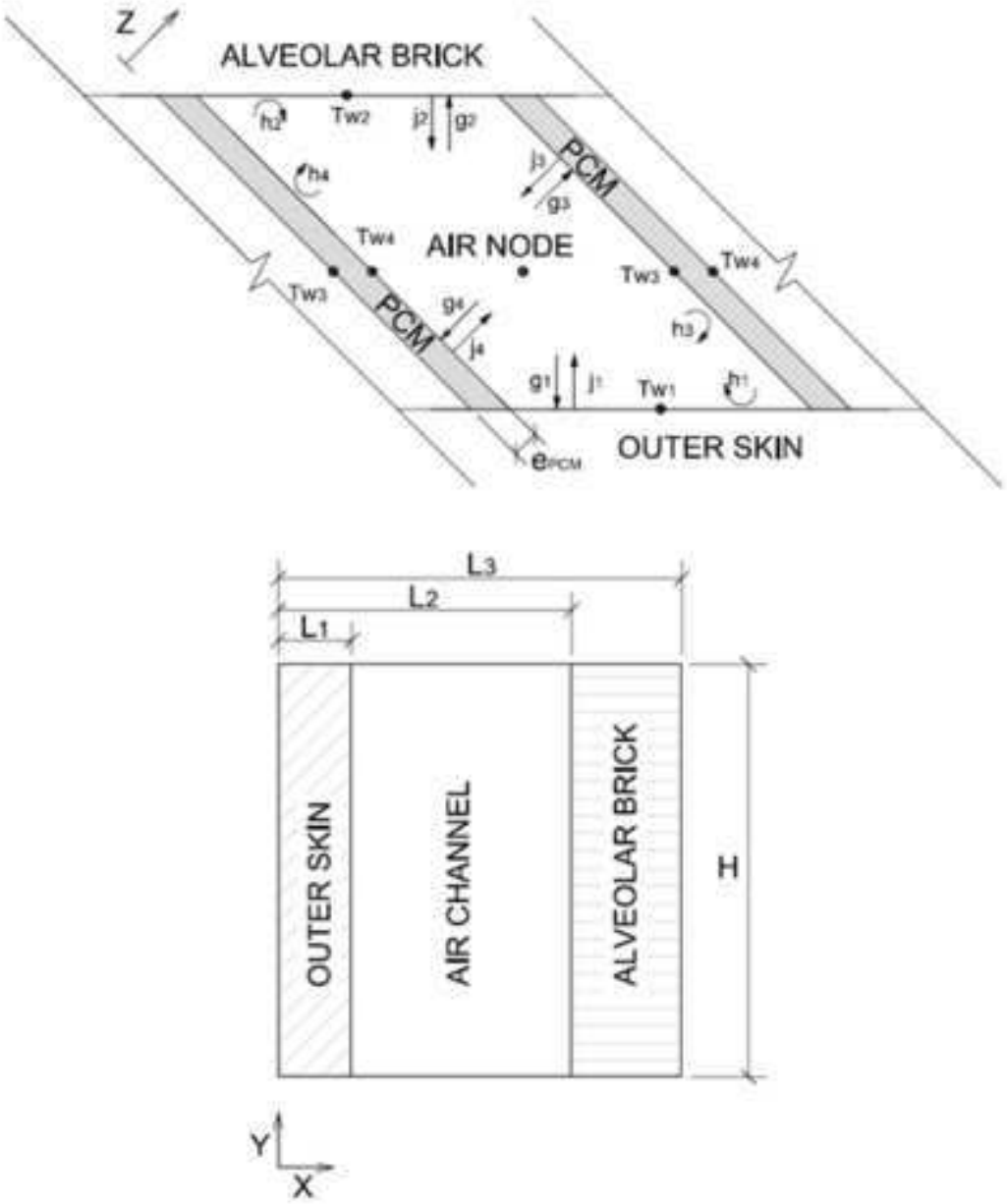

Figure 4

Figure(s)
Click here to download high resolution image

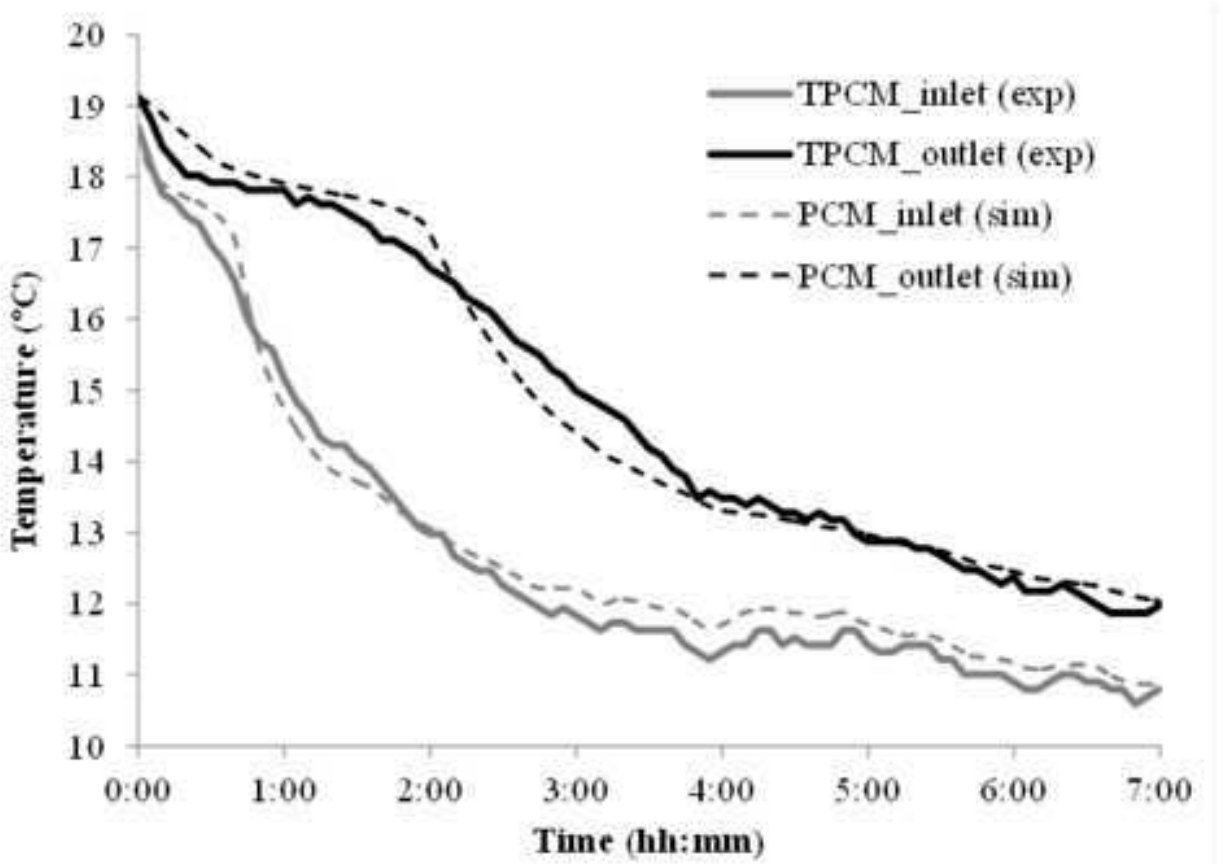

Figure 5

Figure(s)
Click here to download high resolution image

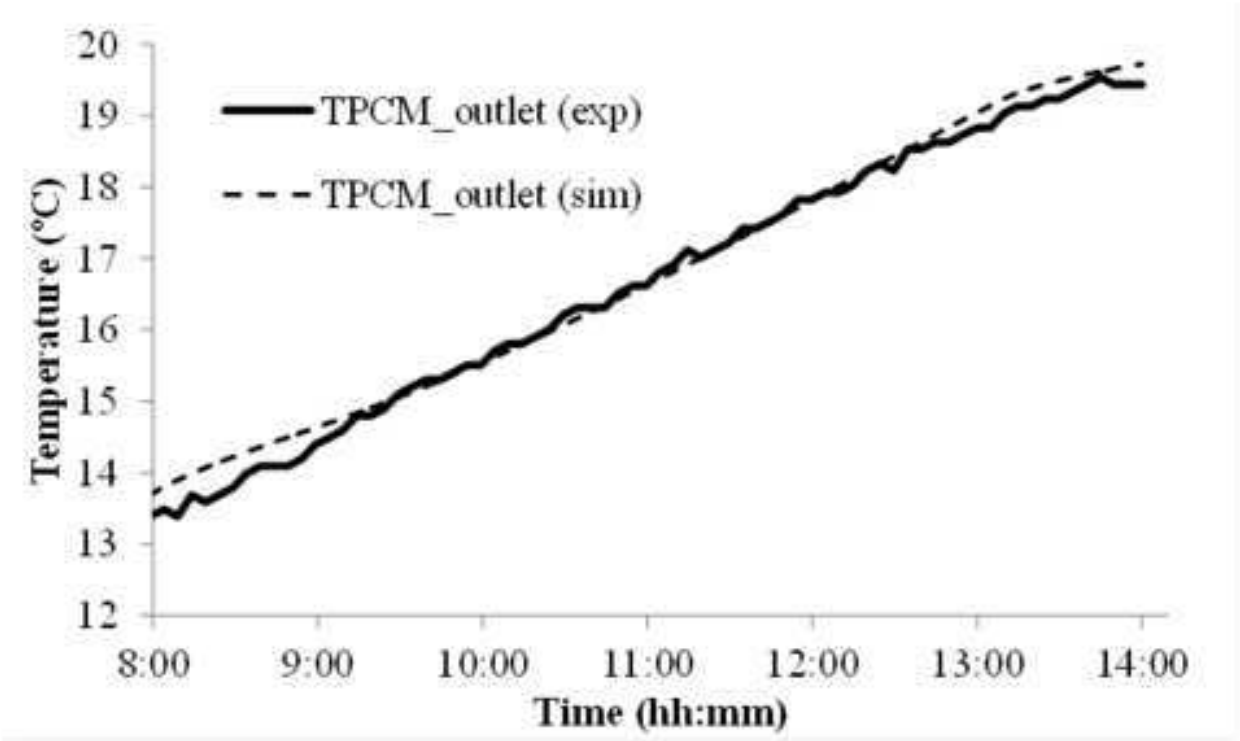

Figure 6

Figure(s)
Click here to download high resolution image

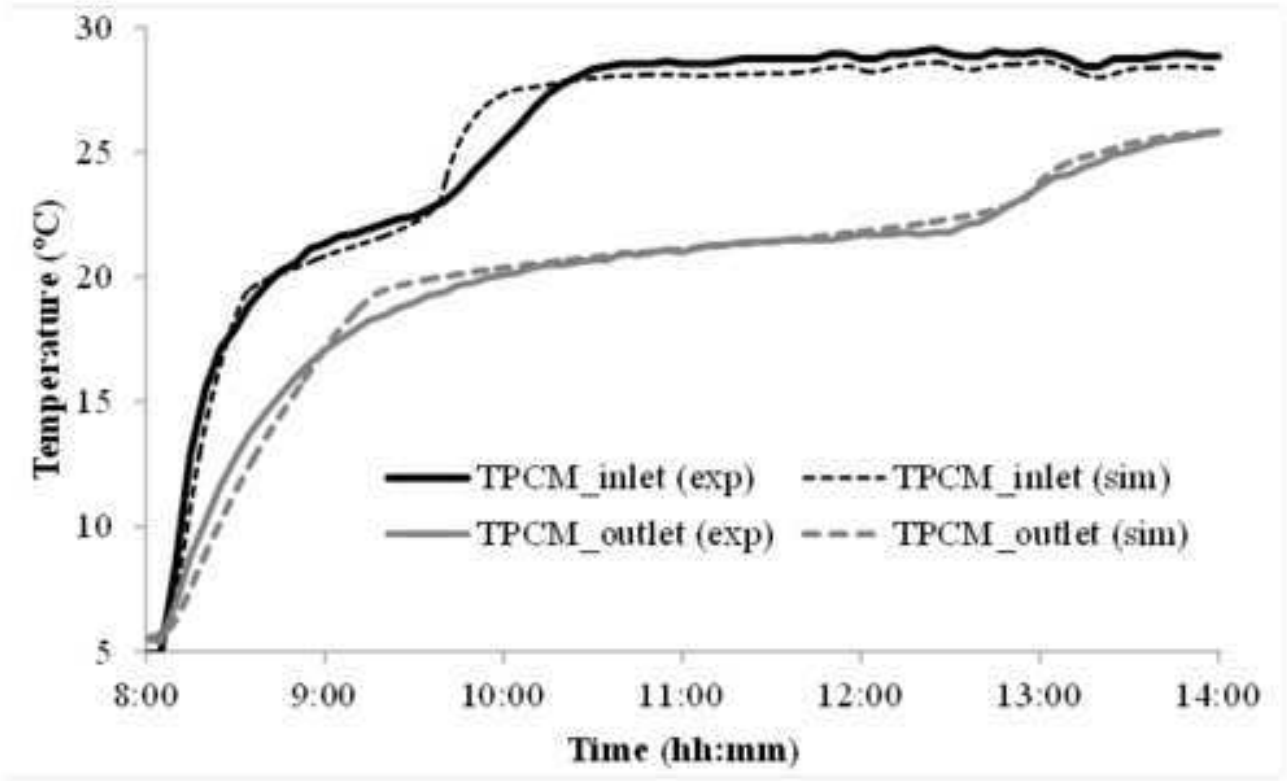

Figure 7

Figure(s)
Click here to download high resolution image

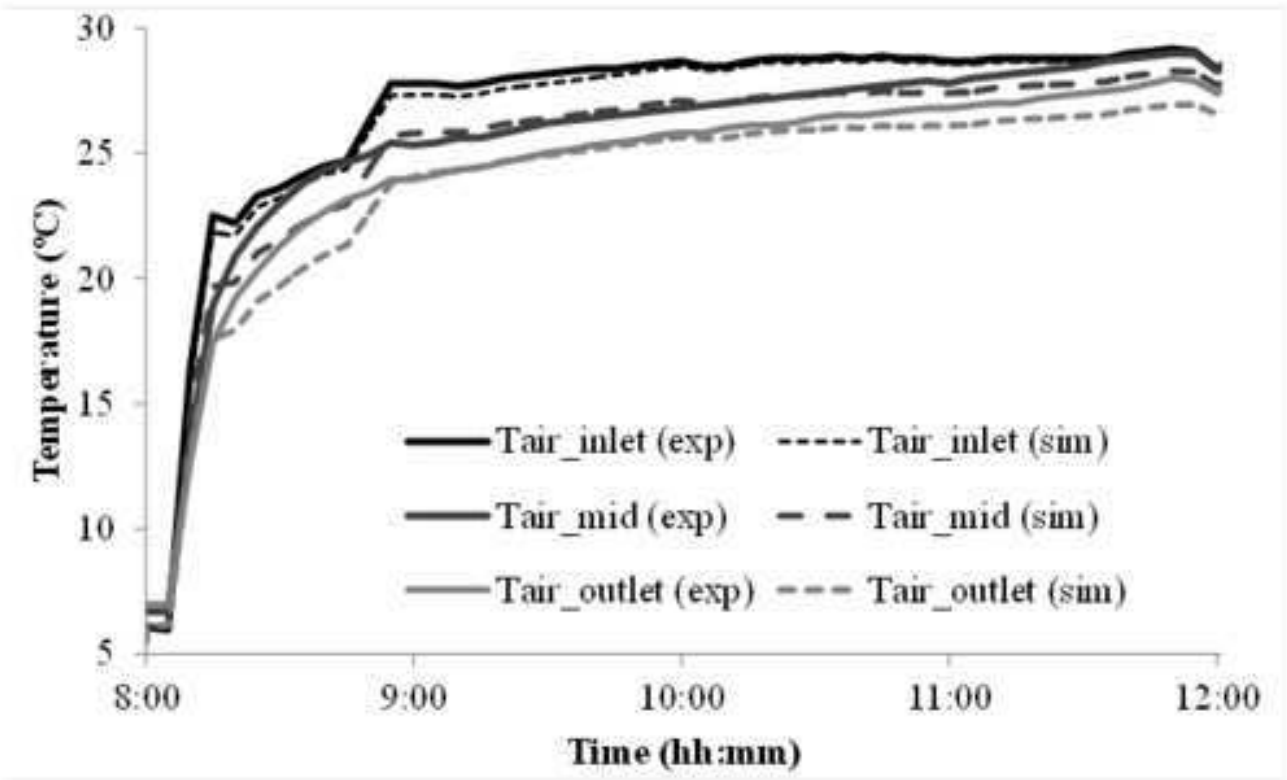

Figure 8

Figure(s)
Click here to download high resolution image

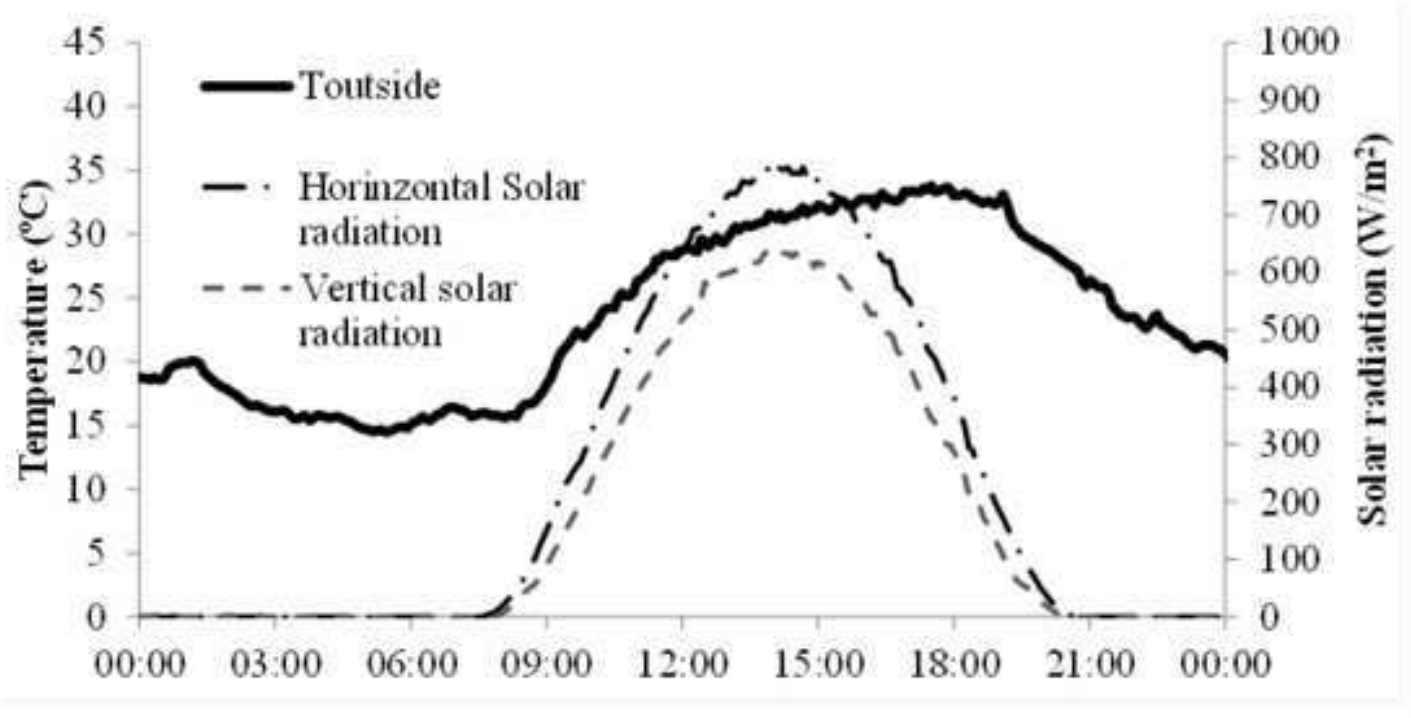

Figure 9

Figure(s)
Click here to download high resolution image

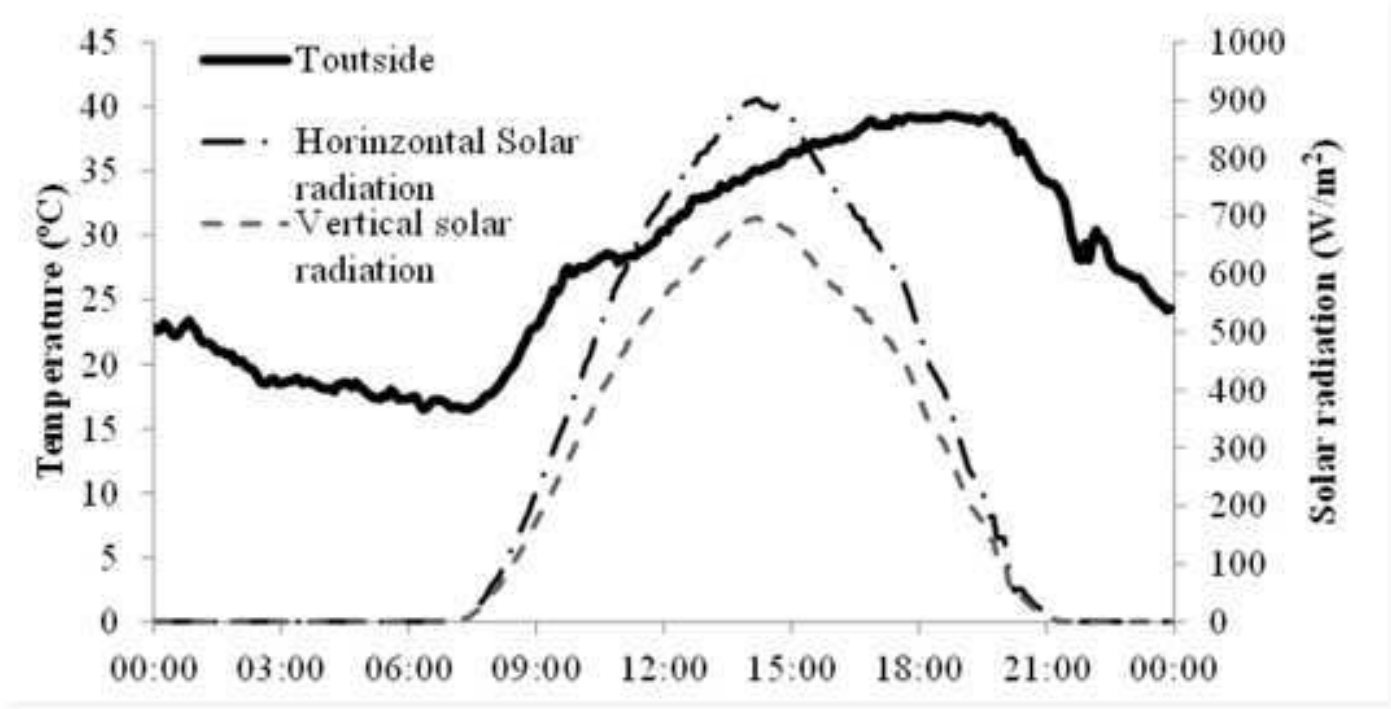

Figure 10

Figure(s)
Click here to download high resolution image

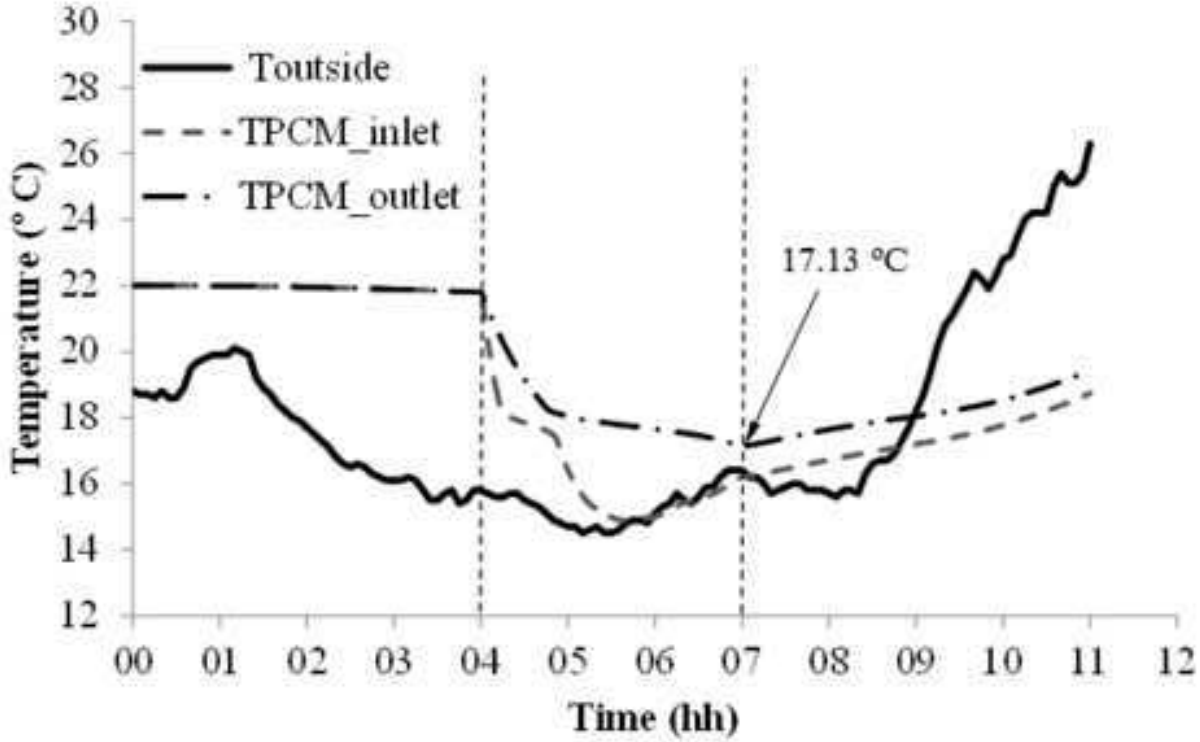

Figure 11

Figure(s)
Click here to download high resolution image

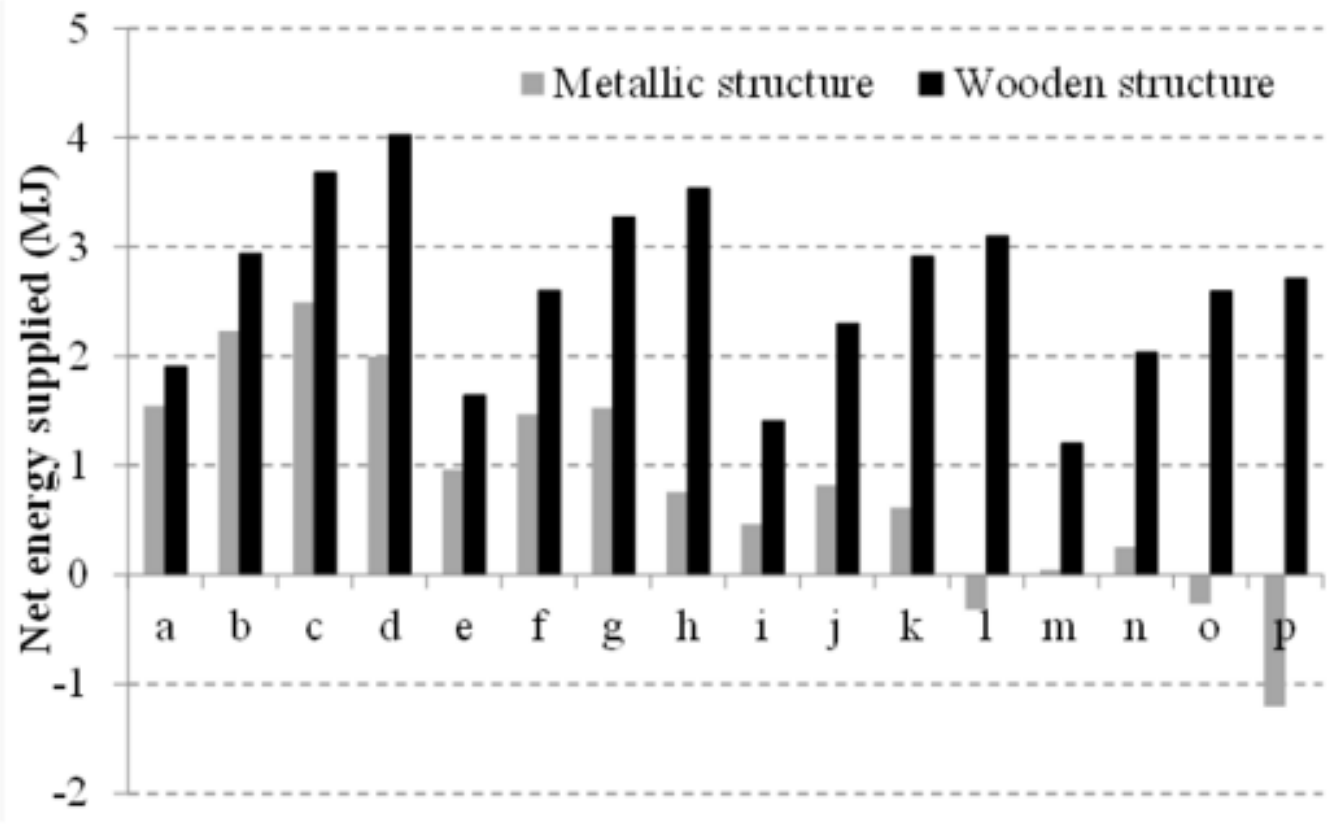

Figure 12

Figure(s)
Click here to download high resolution image

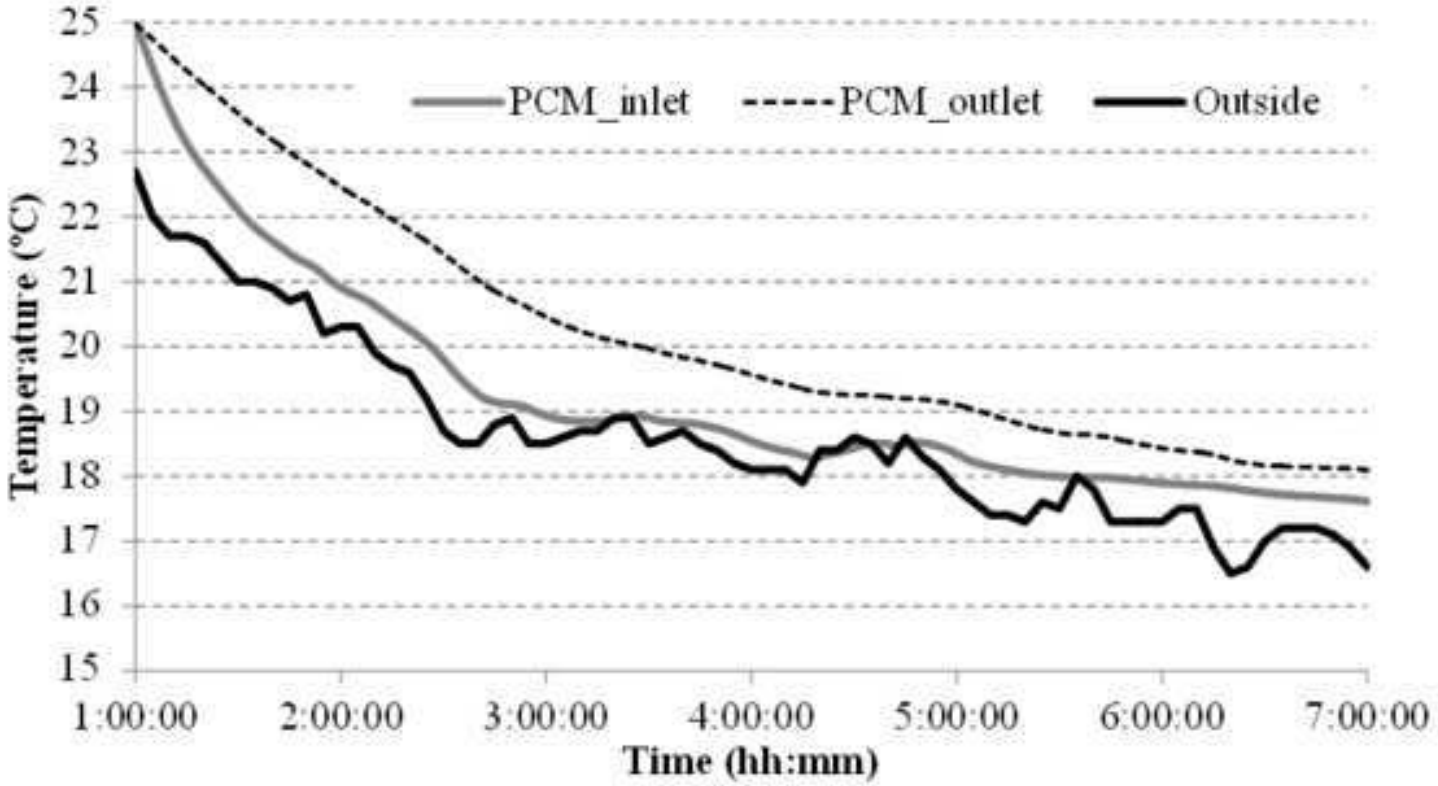

Figure 13

Figure(s)
Click here to download high resolution image

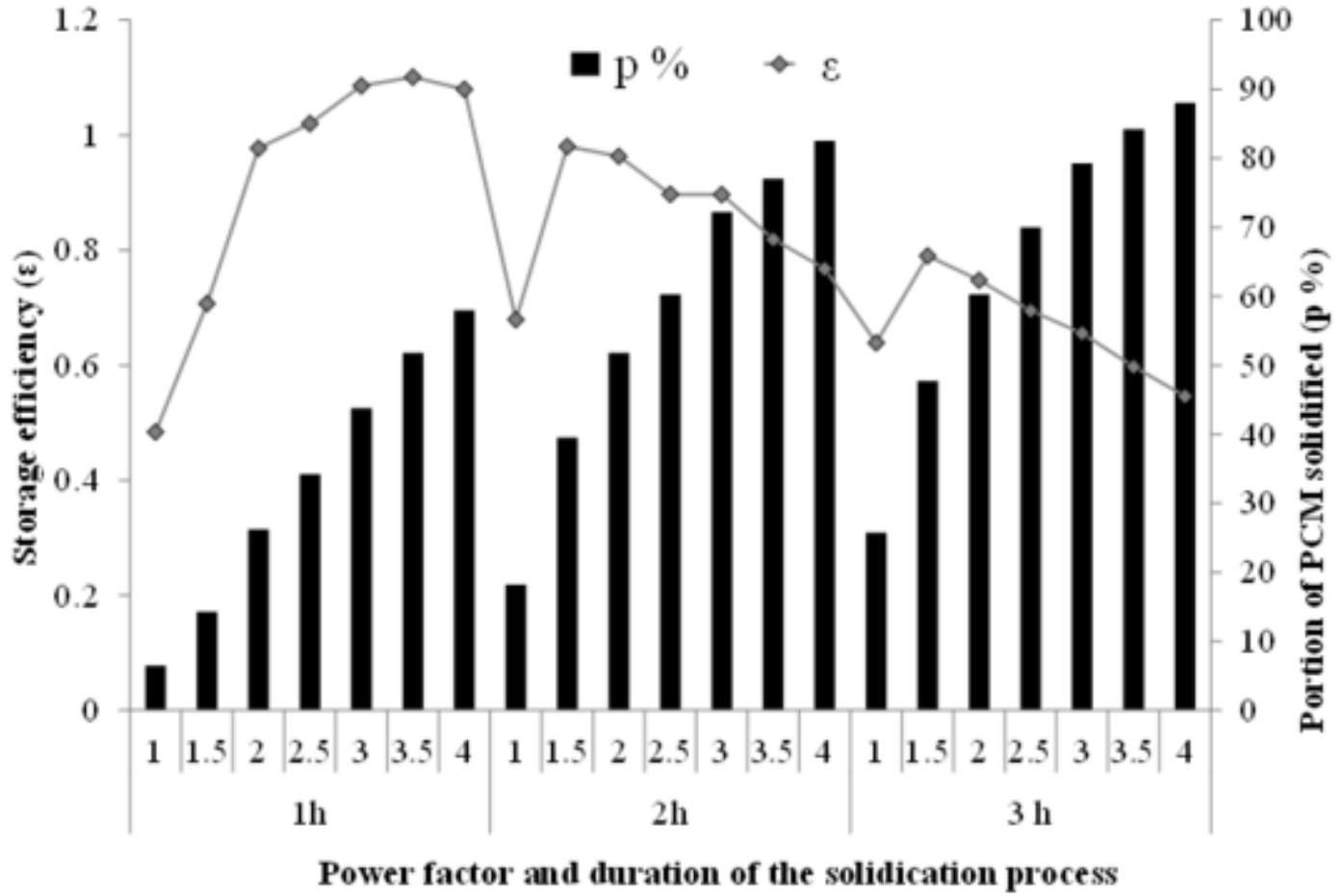

Figure 14

10 Conclusions and recommendations for future work

10.1 Conclusions of the thesis

This PhD thesis analyses the thermal performance of an innovative type of ventilated double skin facade which contains macro-encapsulated panels of PCM in its air chamber. The versatility of this new VDSF allows the system to reduce both heating and cooling loads of a building. During the winter period the VDSF acts as a solar collector and supplies to the inner environment the heat stored in the PCM from the solar radiation. On the other hand, during the summer season, it can be used as a cold storage system and also to provide night free cooling.

The major achievements of this PhD are the following:

- The experimental measurements have demonstrated the potential of this new ventilated facade with PCM to reduce both heating and cooling loads.
- The LCA study showed that the use of this new system in a building reduces its environmental impact throughout its whole life span.
- A new Nusselt correlation was developed to describe the heat transfer between a PCM flat plate and an air flow. This correlation takes into account the effect of the phase change in the evolution of the Nusselt number.
- A numerical tool was developed and validated against experimental results. This numerical model can be used to optimize the operational schedule and to design ventilated facades with PCM under different weather conditions and energetic requirements.

The main conclusions that came out from the experimental part of the thesis are listed below:

- The experimental results demonstrated the high potential of this new VDSF in reducing the electrical energy consumption of the HVAC systems of a building during the winter season. These savings depend strongly on the mode of operation and the weather conditions, being under severe winter conditions

between 19% and 26% depending on the HVAC set point (21 ºC and 19 ºC, respectively). Moreover, with and appropriate operational schedule the system could achieve net energy savings of 86.2% during the mild winter season.

- The measured electrical energy consumption of the heat pumps and fans demonstrated that the use of mechanical ventilation in this system during winter is unnecessary unless a fast heating supply is needed.
- The injection efficiency during winter is around 40% when the system supplies heat to the inner environment during the sunny hours. On the other hand, this value is significantly reduced (to 19%) when the use of the solar energy (heating supply) does not match with its production.
- The high hysteresis of the SP-22 makes that the latent heat provides almost no thermal benefits during winter, since its phase change temperature during the solidification process is very low (18 ºC) to be used in this facade.
- The experimental results during the summer period highlighted the potential of the night free cooling effect in reducing the cooling loads of a building. This operation mode could inject air at a temperature below the set point under both severe and mild summer conditions (34.9 MJ/day and 42.8 MJ/day, respectively).
- The set of experiments under summer conditions demonstrated that the cold storage system is almost useless unless the PCM has been fully solidified during the night period. The hysteresis of the PCM makes the full solidification difficult, especially under severe summer conditions.
- During the cooling season, the system can prevent successfully the overheating effect between the PCM solidification and melting periods, being the air inside the cavity even lower than the outer environmental temperature during the peak load. Therefore, the cubicle is exposed to less heat gains through this envelope, which produces a reduction in the energy consumed by the heat pump during the period.
- No net electrical energy savings were registered due to the use of the VDSF with PCM during the summer period. The excessive use of fans during the solidification process must be reduced. Moreover, there is a necessity of

improving the thermal resistance of the outer skin by supressing, when possible, the thermal bridges occurring through the metallic structural frame.

In addition, the environmental impact of using this VF in a building has been evaluated using the LCA methodology. The main conclusions extracted from the environmental study are the following:

- The LCA study demonstrated that the use of this particular ventilated facade reduces by 7.7 % the overall environmental impact, considering a building lifetime of 50 years. Moreover, the environmental payback of the system is 30 years.
- Since 56 % of the environmental impact produced during the manufacturing/dismantling phase is due to the structural steel, important environmental savings would be achieved with a wooden structure. The environmental payback of the system with a wooden structure would be reduced to 6 years.

An extensive literature review about the different numerical typologies used to describe the thermal performance of a ventilated facade has been done. The different methodologies were grouped as: analytical and lumped models, dimensionless analysis, airflow network model, control volume approach, zonal model, and CFD. From the review it can be concluded that:

- The control volume approach provides a good compromise between computational resources and accuracy. Moreover, it is presented as an adequate tool to study the overall thermal performance of a ventilated facade.
- Computational fluid dynamics simulation is the most accurate technique to solve some details in the design of a ventilated facade. However, its use in the building sector is limited because of problems related to the computing power, the nature of the flow fields, and the occupant-dependent boundary conditions. CFD simulation might be used to build numerical correlations which describe some specific parameters such as convective heat transfer coefficients. These

correlations might be used by engineers or architects in simplified models during the design phase of the VDSF.

- The potential and the importance of developing coupled models, which are able to use detailed information from CFD in an overall energy simulation model describing the thermal performance of a whole building.

Furthermore, an original Nusselt correlation for latent heat storage systems is developed. This correlation describes the convective heat transfer between a PCM flat plate and an air flow and demonstrated that:

- The effect of the phase change affects the Nusselt evolution since the starting point of the thermal boundary layer is not fixed.
- The use of this correlation instead of the existing ones from the literature provides a strong improvement in the accuracy of the model. Moreover, the use of this correlation could save computational costs compared to the use of CFD simulations.

Finally, a numerical investigation has been conducted to optimize the energetic performance of the system for cooling purposes. The numerical study concluded that:

- During the mild season, the outer temperature drops below the phase change temperature during enough time to fully solidify the PCM.
- An optimal combination under the mild conditions to solidify the PCM with the minimum hours of mechanical ventilation is found when the system starts to pump air from the outer environment at 4:00 a.m. during 3 hours. Moreover, the cooling supplied by the system achieves its maximum (5.46 MJ/day) in the case when the melting period starts at 11:00 until 15:00 hrs. The ventilated facade provides a net energy supply of 2.49 MJ/day when the electrical energy consumed by the fans is taken into account.
- If the cooling is supplied after 11:00 hrs., the exposure to heat gains reduces dramatically the cooling capacity of the system. These heat gains can be strongly reduced if a wooden or plastic structure is used instead of the current metallic

one. The numerical results demonstrated that the use of the wooden structure would increase the duration of the cooling supply to 5 hours and the maximum net energy supply would be 61.6 % higher than the one achieved with the metallic structure.

- During the severe summer period, the provided mechanical ventilation must be intensively used during few night hours. For a certain desired portion of solidified PCM, it is recommended to increase the power of mechanical ventilation during less time of consumption, in order to maximize storage efficiency.

10.2 Recommendations for future work

The experimental and numerical studies have proven the potential of a new typology of ventilated facade to reduce both heating and cooling loads. However, some design aspects could be addressed to improve the thermal performance of this system. The hysteresis observed in the used PCM limits strongly the use of the stored latent heat for heating purposes and makes its solidification difficult during the cooling season. Therefore other materials without hysteresis should be tested in the future to overcome these limitations.

Moreover, the use of another structure with better thermal resistance, instead of the current metallic one, could limit the heat losses to the outer environment and hence increase the storage efficiency during both winter and summer periods.

The net electrical energy savings would have been even higher if a thermal control system had been used being programmed depending on the energy demand, production and storage.

The numerical model which describes the energetic performance of the ventilated facade during the summer season could be implemented in TRNSYS as a new type. The inclusion of the developed model into an overall building simulation could be useful to determine annual savings, as well as the efficiency of different control strategies

The current morphology of the facade and its openings to the building, make the introduction of the prototype into the market difficult. Nevertheless, the operational principle of this ventilated facade with PCM with its studied design requirements could be used and implemented in a new active system independently installed from the building. This system could be easily implemented in the actual HVAC building systems.

References

[1] International Energy Agency. Energy Technology Perspectives 2012. Pathways to a Clean Energy System. France, 2012.

[2] L.F. Cabeza, A. Castell, M. Medrano, I. Martorell, G. Pérez, I. Fernández. Experimental study on the performance of insulation materials in Mediterranean construction. Energy and Buildings 42 (2010) 630-6.

[3] J. Zhou, Y. Chen. A review on applying ventilated double-skin façade to buildings in hot-summer and cold-winter zone in China. Renewable and Sustainable Energy Reviews 14 (2010) 1321-1328.

[4] M.A. Shameri, M.A. Alghoul, K. Sopian, M. Fauzi, M. Zain, O. Elayeb. Perspectives of double skin façade systems in buildings and energy saving. Renewable and Sustainable Energy Reviews 15 (2011) 1468-1475.

[5] N. Safer, M. Woloszyn, J.J. Roux. Three-dimensional simulation with a CFD tool of the airflow phenomena in single floor double-skin facade equipped with a venetian blind. Solar Energy 79 (2005) 193-203.

[6] H. Poirazis. Double Skin Façades for Office Buildings. Report EBD-R-04/3. Technical report, Division of Energy and Building Design. Lund University, 2004.

[7] D. Saelens, S. Roels, H. Hens. Strategies to improve the energy performance of multiple-skin facades. Building and Environment 43 (2008) 638-50.

[8] A. Ruiz-Pardo. Ahorro energético mediante el uso de elementos de doble envolvente transparente-opaco “Energy savings through the use of double transparent-opaque envelopes”. PhD Thesis. Universidad de Sevilla, 2008.

[9] G. Baldinelli. Double skin facades for warm climate regions: analysis of a solution with an integrated movable shading system. Energy and Buildings 36 (2004) 1107-18.

[10] L. Mei, D. Infield, U. Eicker, V. Fux. Thermal modelling of a building with an integrated ventilated PV façade. Energy and Buildings 35 (2003) 605-617.

[11] C. Sanjuan, M.J. Suárez, M. González, J. Pistono, E. Blanco. Energy performance of an open-joint ventilated façade compared with a conventional sealed cavity façade. Solar Energy 85 (2011) 1851-1863.

[12] O. Aschehoug, M. Perino. Expert Guide – Part 2 Responsive Building Elements. IEA ECBCS Annex 44 Integrating Environmentally Responsive Elements in Buildings, 2009.

[13] D. Faggembauu. Heat transfer and fluid-dynamics in double and single skin facades. Phd Thesis. Universitat Politècnica de Catalunya, 2006.

[14] P. Arce, M. Medrano, A. Gil, E. Oró, L.F. Cabeza. Overview of thermal energy storage (TES) potential energy savings and climate change mitigation in Spain and Europe. Applied Energy 88 (2011) 2764-2774.

[15] I. Dincer, M.A. Rosen. Thermal energy storage, systems and application. John Wiley & Sons, Chichester, United Kingdom (2002).

[16] R.Parameshwaran, S. Kalaiselvam, S. Harikrishnan, A. Elayaperumal. Sustainable thermal energy storage technologies for buildings: A review. Renewable and Sustainable Energy Reviews 16 (2012) 2394-2433.

[17] B. Todorovic, B. Maric. The influence of double facades on building heat losses and cooling loads. Faculty of Mechanical Engineering, Belgrade University. Technical Report, 2002.

[18] A. Castell, I. Martorell, M. Medrano, G. Pérez, L.F. Cabeza. Experimental study of using PCM in brick constructive solutions for passive cooling. Energy and Buildings 42 (2010) 534-540.

[19] A. de Gracia, A. Castell, M. Medrano, L.F. Cabeza. Dynamic thermal performance of alveolar brick construction system. Energy Conservation and Management 52 (2011) 2495-2500.

[20] E. Gratia, A. De Herde. The most efficient position of shading devices in a double-skin façade. Energy and Buildings 39 (2007) 364-73.

[21] A. Viljoen, J. Dubile, M. Wilson, M. Fontoynont. Investigations for improving the daylighting potential of double-skinned office buildings. Solar Energy 59 (1997) 179-94.

[22] E. Gratia, A. De Herde. Natural cooling strategies efficiency in an office building with a double skin façades. Energy and Buildings 36 (2004) 1139-52.

[23] A. de Gracia, E. Oró, M.M. Farid, L.F. Cabeza. Thermal analysis of including phase change material in a domestic hot water cylinder. Applied Thermal Engineering 31 (2011) 3938-3945.

[24] Y. Hamada, J. Fukai. Latent heat thermal energy storage tanks for space heating of buildings: comparison between calculations and experiments. Energy Conversion and Management 46 (2005) 3221-35.

[25] F. Agyenim, N. Hewitt. The development of a finned phase change material (PCM) storage system to take advantage of off-peak electricity tariff for improvement in cost of heat pump operation. Energy and Buildings 42 (2010) 1552-60.

[26] A.I. Fernández, M. Martínez, M. segarra, I. Martorell, L.F. Cabeza. Selection of materials with potential in sensible thermal energy storage. Solar Energy Materials & Solar Cells 94 (2010) 1723-1729.

[27] A. Castell. Analysis and implementation of thermal energy storage using phase change materials for cooling applications. PhD Thesis. Universitat de Lleida, 2008.

[28] F. Kuznik, J. Virgone, K. Johannes, In-situ study of thermal comfort enhancement in a renovated building equipped with phase change material wallboard, Renewable Energy 36 (2011) 1458–1462.

[29] A.M. Khudhair, M.M. Farid. A review on energy conservation in building applications with thermal storage by latent heat using phase change materials, Energy Conversion and Management 45 (2004) 263–275.

[30] V.V. Tyagi, D. Buddhi. PCM thermal storage in buildings: a state of art. Renewable ans Sustainable Energy Reviews 11 (2007) 1146-1166.

[31] X. Xu, Y. Zhang, K. Lin, H. Di, R. Yang. Modeling and simulation on the thermal performance of shape-stabilized phase change material floor used in passive solar buildings. Energy and Buildings 37 (2005) 1084-1091.

[32] B. Zalba, J.M. Marin, L.F. Cabeza, M. Harald. Free cooling of buildings with phase change materials. International Journal of Refrigeration 27 (2004) 839-849.

[33] P. Dolado, A. Lazaro, J.M.Marin, B. Zalba. Characterization of melting and solidification in a real scale PCM-air heat exchanger: Numerical model and experimental validation. Energy Conversion and Management 52 (2011) 1890-1907.

[34] S.M. Vakilaltojjar, W. Saman. Analysis and modeling of a phase change storage system for air conditioning applications. Applied Thermal Engineering 21 (2001) 249-263.

[35] G. Hed, R. Bellander. Mathematical modeling of PCM air heat exchanger. Energy and Buildings 38 (2006) 82-9.

[36] U. Stritih, V. Butala. Energy saving in building with PCM cold storage. International Journal of Energy Research 31 (2007) 1532-1544.

[37] U.Stritih, V. Butala. Experimental investigation of energy saving in buildings with PCM cold storage. International Journal of Refrigeration 33 (2010) 1676-1683.

[38] W. Saman, F. Bruno, E. Halawa. Thermal performance of PCM thermal storage unit for a roof integrated solar heating system. Solar Energy 78 (2005) 341-9.

[39] V. Butala, U. Stritih. Experimental investigation of PCM cold storage. Energy and Buildings 41 (2009) 354-359.

[40] L.F. Cabeza, A. Castell, C. Barreneche, A. de Gracia, A.I. Fernández. Materials used as PCM in thermal energy storage in buildings: a review. Renewable and Sustainable Energy Reviews 15 (2011) 1675-1695.

[41] B. Zalba, J.M. Marín, L.F. Cabeza, H. Mehling. Review on thermal energy storage with phase change: materials, heat transfer analysis and applications. Applied Thermal Engineering 23 (2003) 251-283.

[42] A. Abhat. Low temperature latent heat thermal energy storage. Heat storage materials. Solar Energy 30 (1983) 313-32.

[43] J. Paris, M. Falardeau, C. Villeneuve. Thermal storage by latent heat: a viable option for energy conservation in buildings. Energy Sources 15 (1993) 85-93.

[44] J. Cot-Gores, A. Castell, L.F. Cabeza. Thermochemical energy storage and conversion: A-state-of-the-art review of the experimental research under practical conditions. Renewable and Sustainable Energy Reviews 16 (2012) 5207-5224.

[45] L.E. Bourdeau. Study of two passive solar systems containing phase change materials for thermal storage. In: Proceedings of the fifth national passive solar conference, Amherst, Newark, DE: American Solar Energy Society (1980) 297-301.

[46] A.A. Ghoneim, S.A. Klein, J.A. Duffie. Analysis of collector-storage building walls using phase change materials. Solar Energy 47 (1991) 237-42.

[47] U. Stritih, P. Novak. Thermal storage of solar energy in the wall for building ventilation. IEA, ECES IA Annex 17, Advanced Thermal Energy Storage Techniques Feasibility Studies and Demonstration Projects, 2nd Workshop. Lubjana, 2002.

[48] C. Eiamworawutthikul, J. Strohbehn, C. Harman. Investigation of Phase-Change Thermal Storage in Passive Solar Design for Light-Construction Building in the Southeastern Climate Region. A Research Program to Promote Energy Conservation and the Use of Renewable Energy.

[49] M. Costa, O. Aceves, F. Sen, W. Platzer, A. Haller, M. Indetzki, T. Ojanen. Analysis of Multi-Functional Ventilated Facades. An European Joule Project (http://erg.ucd.ie/enerbuild/restricted/pdf/multi_functional.pdf).

[50] D. Heim. Whole year analysis of TIM-PCM solar thermal storage wall. SimBuild 2004, IBPSA-USA National Conference Boulder, CO.

[51] M.M. Farid, S. Behzadi. Energy storage for efficient energy utilization in buildings, in: 1st International High Performance Buildings Conference 12-15 July. Purdue University, USA; 2010.

[52] Directive 2010/31/eu of the European parliament and of the council of 19 May 2010 on the energy performance of buildings. Available from: http://www.epbd-ca.eu.

[53] L. Xu, T. Ojima, Field experiments on natural energy utilization in a residential house with a double skin façade system. Building and Environment 42 (2007) 2014-2023.

[54] H. Manz, T. Frank. Thermal simulation of buildings with double-skin façades. Energy and Buildings 37 (2005) 1114-1121.

[55] W. Ding, Y. Hasemi, T.Yamada. Natural ventilation performance of a double-skin façade with a solar chimney. Energy and Buildings 37 (2005) 37:411-8.

[56] T. Ramesh, R. Prakash, K.K. Shukla. Life cycle energy analysis of a residential building with different envelopes and climates in Indian context. Applied Energy 89 (2012) 193-202.

[57] A. Dodoo, L. Gustavsson, R. Sathre. Effect of thermal mass on life cycle primary energy balances of a concrete- and a wood-frame building. Applied Energy 92 (2012) 462-472.

[58] F. Ardente, M. Beccale, M. Cellura, M. Mistretta. Building energy performance: A LCA case study of kenaf-fibres insulation board. Energy and Buildings 40 (2008) 1-10.

[59] A.M. Papadoppoulos, E. Giama. Environmental performance evaluation of thermal insulation materials and its impact on the building. Building and Environment 42 (2007) 2178–2187.

[60] A. Castell, K. Menoufi, A. de Gracia, L. Rincón, D. Boer, L.F. Cabeza. Life Cycle Assessment of alevolar brick construction system incorporating phase change materials (PCMs). Applied Energy 101 (2013) 600-608.

[61] A. de Gracia, L. Rincón, A. Castell, M. Jiménez, D. Boer, M. Medrano, L.F. Cabeza. Life cycle assessment of inclusion of phase change materials (PCM) in experimental buildings. Energy and Buildings 42 (2010) 1517-1523.

[62] K. Menoufi, A. Castell, L. Navarro, G. Pérez, D. Boer, L.F. Cabeza L.F. Evaluation of the environmental impact of experimental cubicles using Life Cycle

Assessment: A highlight on the manufacturing phase. Applied Energy 92 (2012) 534-544.

[63] PRé-Consultants. The Eco-indicator 99. A damage oriented method for life cycle impact assessment. Methodology report and manual for designers. Technical Report, PRé Consultants, Amersfoort. The Netherlands, 2000.

[64] The ecoinvent Center. A competence centre of ETH; PSI;Empa & ART; http://www.ecoinvent.ch/. Ecoinvent data v2.1.

[65] L. Zalewski, M. Chantant, S. Lassue, B. Duthoit. Experimental thermal study of a solar wall of composite type. Energy and Buildings 25 (1997) 7-18.

[66] P. Torcellini, S. Pless. Trombe walls in low-energy buildings: Practical experiences. VII World Renewable Energy Congress, Denver; 2004.

[67] T. Pasquay. Natural ventilation in high-rise buildings with double facades, saving or waste of energy. Energy and Buildings 36 (2004) 381-389.

[68] V. Gavan, M. Woloszyn, F. Kuznik, J.J. Roux. Experimental study of a mechanically ventilated double –skin façade with venetian sun-shading device: A full investigation in controlled environment. Solar Energy 84 (2010) 183-195.

[69] V. Huckermann, E. Kuchen, M. Leão, É. Leão. Empirical thermal comfort evaluation of single and double skin façades. Building and Environment 45 (2010) 976-982.

[70] J. von Grabe. A prediction tool for the temperature field of double facades. Energy and Buildings 34 (2002) 891-899.

[71] C. Park, G. Augenbroe, T. Messadi, M. Thitisawat, N. Sadegh. Calibration of a lumped simulation model for double-skin façade systems. Energy and Buildings 36 (2004) 1117-1130.

[72] C. Balocco, M.Colombari. Thermal behavior of interactive mechanically ventilated double glazed façade: Non-dimensional analysis. Energy and Buildings 36 (2006) 1-7.

[73] J. Hensen, M. Bartak, F. Drkal. Modeling and simulation of a double-skin façade system. ASHRAE Transactions 108 (2002)1251-1259.

[74] W. Stec, D. van Paassen. Symbiosis of the double skin façade with the HVAC system. Energy and Buildings 37 (2005) 461-469.

[75] E. Gratia, A. De Herde. Optimal operation of a south double-skin façade. Energy and Buildings 36 (2004) 41-60.

[76] D. Faggembau, M. Costa, M. Soria, A. Oliva. Numerical analysis of the thermal behaviour of ventilated glazed facades in Mediterranean climates. Part I: development and validation of a numerical model. Solar Energy 75 (2003) 217-228.

[77] D. Saelens, J. Carmeliet, H. Hens. Energy Performance Assessment of Multiple-Skin Facades. HVAC&R Researcj 9 (2003)167-185.

[78] P. Seferis, P. Strachan, A. Dimoudi, A. Androutsopoulos. Investigation of the performance of a ventilated wall. Energy and Buildings 43 (2001) 2167-2178.

[79] T.E. Jiru, F. Haghighat. Modeling ventilated double skin façade – A zonal approach. Energy and Buildings 40 (2008) 1567-1576.

[80] H. Manz, A. Schaelin, H. Simmler. Airflow patterns and thermal behavior of mechanically ventilated glass double façades. Building and Environment 39 (2004) 1023-1033.

[81] W. Pasut, M. De Carli. Evaluation of various CFD modelling strategies in predicting airflow and temperature in a naturally ventilated double skin façade. Applied Thermal Engineering 37 (2012) 267-274.

[82] H. Mehling, L.F. Cabeza. Heat and Cold Storage with PCM. An up to Date Introduction into Basics and Applications, Springer-Verlag, Berlin Heidelberg, Harching, Germany, 2008.

[83] F. Kuznik, J. Virgone, K. Johannes. Development and validation of a new TRNSYS type for the simulation of external building walls containing PCM. Energy and Buildings 45 (2010) 1004-1009.

[84] J. Borderon, J. Virgone, R. Cantin, K. Kuznik. Full-scale Study of a Building Equipped with a Multi-layer Rack Latent Heat Thermal Energy Store System. HVAC&R 17(2011) 566-576.

[85] A. de Gracia, L. Navarro, A. Castell, A. Ruiz-Pardo, S. Álvarez, L.F. Cabeza. Experimental study of a ventilated facade with PCM during winter period. Energy and Buildings 58 (2013) 324-332.

[86] A. de Gracia, L. Navarro, A. Castell, A. Ruiz-Pardo, S. Álvarez, L.F. Cabeza. Thermal analysis of a ventilated facade with PCM for cooling applications. Energy and Buildings under review

[87] M. Liu, W. Saman, F. Bruno. Validation of a mathematical model for encapsulated phase change material flat slabs for cooling applications. Applied Thermal Engineering 31 (2011) 2340-2347.

[88] A. de Gracia, A. Castell, L. Navarro, E. Oró, L.F. Cabeza, Numerical modelling of ventilated facades: A review, Renewable and Sustainable Energy Reviews (2013) doi.10.1016/j.rser.2013.02.029.